

**Chemical-genetic  
interrogation of small  
molecule mechanism of  
action in *S. cerevisiae***

*Michaela Spitzer*

Doctor of Philosophy  
University of Edinburgh  
September 28, 2011

---

## Declaration

---

I declare that this thesis was composed by myself and that the work contained therein is my own, except where explicitly stated otherwise in the text. This work has not been submitted for any other degree or professional qualification.

*(Michaela Spitzer)*

---

## Preface

---

The work described in this thesis was carried out under the supervision of Prof. Mike Tyers. I began my postgraduate studies in the Tyers lab at the University of Toronto in March 2005. I successfully reclassified into the PhD program in December 2006. In October/November 2007 I transferred to the University of Edinburgh because the Tyers lab relocated to the Wellcome Trust Center of Cell Biology in Edinburgh.

---

## Acknowledgements

---

I would like to thank Mike for introducing me to the fascinating world of discoveries and big visions that is research. At times it was overwhelming, but once things fell into place and (almost) everything made sense, it was satisfying yet challenging to be working in science.

I am very thankful that I had the chance to collaborate with the labs of Liz Patton and Gerry Wright. These collaborations enabled me to see how powerful chemical biology in *S. cerevisiae* can be when combined with screens in zebrafish and clinically relevant fungal pathogens. These projects widened my horizon and I came to appreciate the budding yeast even more.

I would like to thank everyone in the Tyers lab, past (Toronto) and present (Edinburgh), for interesting discussions, advice and encouragement. I am grateful for advice, time and comments from Juri Rappsilber, Liz, Christine and Jan while I was writing my thesis.

I want to thank my family for being supportive of my work even though they probably still don't know what exactly I am doing. A big thank you also goes out to all my friends in Berlin, Auckland, Toronto and here in Edinburgh, especially the non-scientist ones who were very understanding, interested in my work and supporting. I am sure a few of them now think of me every time they hear the word 'yeast'.

Relationships are complicated as it is. It gets even more difficult when you

work together. But I think we managed somehow and we definitely both learned a lot. So thank you Jan, for being so patient with me, especially in times when I was down. I value the time you took to answer all my questions related to statistics and cheminformatics. Thank you also for sharing your tricks of the computational trade.

---

## Abstract

---

The budding yeast *S. cerevisiae* is widely used as a model organism to study biological processes that are conserved among eukaryotes. Different genomic approaches have been applied successfully to interrogate the mode of action of small molecules and their combinations. In this thesis, these technologies were applied to different sets of chemical compounds in the context of two collaborative projects. In addition to insight into the mode of action of these molecules, novel approaches for analysis of chemical-genetic profiles to integrate GO annotation, genetic interactions and protein complex data have been developed.

The first project was motivated by a pressing need to design novel therapeutic strategies to combat infections caused by opportunistic fungal pathogens. Systematic screens of 1180 FDA approved drugs identified 148 small molecules that exhibit synergy in combination with fluconazole, a widely used anti-fungal drug (Wright lab, McMaster University, Canada). Genome-wide chemical-genetic profiles for 6 of these drugs revealed two different modes of action of synergy. Five of the compounds affected membrane integrity; these chemical-genetic interactions were supported by microscopy analysis and sorbitol rescue assays. The sixth compound targets a distinct membrane-associated pathway, sphingolipid biosynthesis. These results not only give insight into the mechanism of the synergistic interactions, they also provide starting points for the prediction of synergistic anti-fungal combinations with potential clinical applications.

The second project characterised compounds that affected melanocytes in a chemical screen in zebrafish (Patton lab, Edinburgh). Chemical-genetic screens in *S.cerevisiae* enabled us to show that melanocyte pigmentation reducing compounds do so by interfering with copper metabolism. Further, we found that defects in intracellular AP1 and AP3 trafficking pathways cause sensitivity to low copper conditions. Surprisingly, we observed that the widely-used MAP-kinase inhibitor U0126 affects copper metabolism. A nitrofuran compound was found to specifically promote melanocyte cell death in zebrafish. This enabled us to study off-target effects of these compounds that are used to treat trypanosome infections. Nifurtimox is a nitrofuran prodrug that is activated by pathogen-specific nitroreductases. Using yeast and zebrafish we were able to show that nitrofurans are also bioactivated by host-specific aldehyde dehydrogenases suggesting that a combination therapy with an aldehyde dehydrogenase inhibitor might reduce side effects associated with nifurtimox.

---

## Contents

---

<b>Preface</b>	<b>ii</b>
<b>Acknowledgements</b>	<b>iii</b>
<b>Abstract</b>	<b>v</b>
<b>List of Figures</b>	<b>xi</b>
<b>List of Tables</b>	<b>xiv</b>
<b>List of Abbreviations</b>	<b>xv</b>
<b>1 Introduction</b>	<b>1</b>
1.1 Chemical Biology . . . . .	2
1.2 Functional genomics tools in <i>S. cerevisiae</i> to interrogate mode of action of small molecules. . . . .	4
1.2.1 The yeast deletion set as a resource for chemical genomics	4
1.2.2 Haplo-insufficiency screens to identify drug targets . . . . .	6
1.2.3 Chemical-genetic profiles reveal drug target pathways . . . . .	7
1.2.4 Dosage-suppression . . . . .	8
1.2.5 Spontaneous drug-resistant mutants . . . . .	8
1.2.6 High-content screening . . . . .	9



1.2.7	Expression profiling . . . . .	9
1.2.8	Chemical-chemical interactions . . . . .	10
1.3	Challenges in drug discovery . . . . .	10
1.3.1	A short history of drug discovery . . . . .	10
1.3.2	Current approaches to drug discovery . . . . .	12
1.3.3	Organism-based drug discovery in the zebrafish . . . . .	14
1.3.4	Repurposing of drugs . . . . .	16
1.3.5	Multicomponent therapies . . . . .	23
1.4	Aims of this thesis . . . . .	30
<b>2</b>	<b>Materials and methods</b>	<b>31</b>
2.1	General materials and methods . . . . .	31
2.1.1	Yeast media . . . . .	31
2.1.2	Chemicals . . . . .	32
2.1.3	Buffers and solutions . . . . .	32
2.1.4	<i>S. cerevisiae</i> barcode microarrays . . . . .	33
2.2	Specific methods for Chapter 3 . . . . .	39
2.2.1	Fungal strains and culture conditions . . . . .	39
2.2.2	Compounds . . . . .	40
2.2.3	High-throughput screen of Prestwick library . . . . .	40
2.2.4	Data analysis of Prestwick library screen . . . . .	40
2.2.5	Determination of MIC . . . . .	41
2.2.6	Synergy assessment . . . . .	42
2.2.7	Chemical-genetic screens . . . . .	42
2.2.8	Validation of chemical-genetic interactions . . . . .	43
2.2.9	Sorbitol rescue assay . . . . .	43
2.2.10	<i>In vivo</i> imaging of effects of synergising compounds . . . . .	43
2.2.11	Insect larvae assays . . . . .	44
2.2.12	Computational analysis of gene-drug network interactions . . . . .	44
2.3	Specific methods for Chapter 4 . . . . .	45
2.3.1	Zebrafish methods . . . . .	45
2.3.2	Yeast methods . . . . .	47

<b>3</b>	<b>Interrogating the Mode of Action of Small Molecule Synergies in Yeast</b>	<b>49</b>
3.1	Introduction . . . . .	50
3.2	Results . . . . .	53
3.2.1	A high-throughput screen identifies 148 compounds that potentiate the action of fluconazole . . . . .	53
3.2.2	Synergy assessment and fungicidal activity . . . . .	63
3.2.3	Interrogation of the mode of action of drug synergies by genome-wide screens in <i>S. cerevisiae</i> . . . . .	69
3.2.4	Cell biological effects of synergistic drug combinations . . .	79
3.2.5	Integration of chemical-genetic interactions with genetic in- teraction networks . . . . .	85
3.2.6	Further characterisation of drug synergies . . . . .	89
3.2.7	Summary of Results . . . . .	95
3.3	Discussion . . . . .	96
3.3.1	New antifungal chemical space revealed by systematic screens for syncretic drug combinations . . . . .	96
3.3.2	Molecular mechanisms of synergism . . . . .	96
3.3.3	Species-specific synergistic effects . . . . .	98
3.3.4	Devising higher order drug combinations . . . . .	98
3.3.5	Therapeutic implications . . . . .	100
<b>4</b>	<b>Zebrafish and yeast</b>	<b>101</b>
4.1	Introduction . . . . .	102
4.1.1	Skin cancer . . . . .	102
4.1.2	Zebrafish as a model to study melanocyte biology . . . . .	104
4.1.3	A chemical screen identified compounds that affect melanocytes and pigmentation in <i>D. rerio</i> . . . . .	104
4.2	Results . . . . .	108
4.2.1	Chemical-genetic profiles in <i>S. cerevisiae</i> reveal potential copper-metabolism pathways . . . . .	108

4.2.2	The MEK inhibitor U0126 elicits an unexpected copper-metabolism phenotype . . . . .	114
4.2.3	Knockdown of trafficking proteins identified in yeast screens sensitises zebrafish to copper-dependent hypopigmentation . . . . .	118
4.2.4	Investigation of off-target effects of nitrofurans with zebrafish and yeast . . . . .	120
4.2.5	Mode of action of a compound that selectively kills melanocytes in <i>D. rerio</i> . . . . .	127
4.2.6	Summary of Results . . . . .	131
4.3	Discussion . . . . .	132
<b>5</b>	<b>Summary and Concluding Remarks</b>	<b>135</b>
5.1	Summary . . . . .	135
5.2	Concluding Remarks . . . . .	135
<b>A</b>	<b>Development and implementation of methods for the analysis of chemogenomic profiles of small molecules</b>	<b>160</b>
A.1	Gene Ontology . . . . .	160
A.1.1	GO annotation data files . . . . .	163
A.2	Optimisation of chemical-genetic screens . . . . .	163
A.3	Quality control . . . . .	165
A.4	Data analysis procedure to calculate Z-scores . . . . .	167
A.5	Correlation between chemical-genetic screens . . . . .	168
A.6	Overview plots . . . . .	169
A.7	Testing for GO enrichment . . . . .	170
A.8	Z-scores for GO categories . . . . .	171
A.9	Evaluation of chemogenomic data on the level of protein complexes . . . . .	173
A.10	Physical and genetic interactions to interpret chemical-genetic interactions . . . . .	173
A.11	Follow-up experiments . . . . .	175
A.12	Concluding remarks . . . . .	177
<b>B</b>	<b>Structural clusters of 148 hit compounds</b>	<b>179</b>

---

## List of Figures

---

3.1	Visualisation of row effects in HTP screen data. . . . .	54
3.2	Data variation between screens. . . . .	55
3.3	Normalisation of high-throughput chemical screen data. . . . .	56
3.4	Scatterplots of the Prestwick Chemical library screens. . . . .	58
3.5	Activity of hit compounds from Prestwick Chemical library screens.	59
3.6	Overlap of hits between different fungal species. . . . .	60
3.7	Structural clusters among the 148 hit compounds. . . . .	61
3.8	Chemical structures and application classification of 17 compounds selected for synergy confirmation experiments . . . . .	64
3.9	Heatmap of drug interactions with fluconazole in each species. . .	65
3.10	Assessment of high throughput screen performance. . . . .	66
3.11	Heatmap of interactions between known antifungals and fluconazole.	68
3.12	Chemical structures of the six drugs chosen for detailed mode of action studies. . . . .	70
3.13	Sensitivity of heterozygous essential deletion strains to six different drugs. . . . .	70
3.14	Confirmation of hits from haplo-insufficiency screen. . . . .	72
3.15	Heatmap of haploid chemical-genetic profiles. . . . .	73
3.16	Haploid deletion strain sensitivity to different fluconazole concen- trations and different syncretic drugs. . . . .	74

3.17	Sensitivity of haploid deletion strains to six syncretic synergisers.	75
3.18	Haploid deletion strains sensitive to syncretic synergisers. . . . .	77
3.19	Microscopy to visualise the effects of syncretic drugs on membrane integrity. . . . .	80
3.20	Effects of clomiphene on membrane integrity. . . . .	81
3.21	Effects of tamoxifen on membrane integrity. . . . .	82
3.22	Effects of trifluoperazine on membrane integrity. . . . .	83
3.23	Presence of sorbitol rescues WT <i>S. cerevisiae</i> . . . . .	84
3.24	Integration of chemical-genetic and genetic networks. . . . .	86
3.25	Rationalization of synergistic interactions. . . . .	87
3.26	Chemical-genetic profiles of signature deletion strains in response to 11 psychoactive drugs. . . . .	89
3.27	Top predictions for synergisers based on profiles of signature deletion strains. . . . .	90
3.28	Synergistic activity of fluconazole with sertraline in an <i>in vivo</i> infection model. . . . .	93
3.29	Synergistic activity of fluconazole with sertraline against clinical isolates of <i>Candida</i> strains. . . . .	94
4.1	Phenotypic screen to identify compounds that affect melanocytes.	105
4.2	Compounds that are melanocytotoxic in zebrafish. . . . .	107
4.3	Boxplots of Z-scores for barcode arrays. . . . .	110
4.4	Chemical-genetic interactions of compounds that have an effect on copper metabolism. . . . .	112
4.5	Phenotype caused by U0126 treatment in the developing zebrafish embryo. . . . .	115
4.6	Novel target pathways for U0126, a MEK inhibitor. . . . .	117
4.7	Identification of gene-nutrient interactions in melanocyte pigmentation. . . . .	119
4.8	The 5-NO <sub>2</sub> moiety is required for nitrofuran activity in zebrafish and yeast. . . . .	121
4.9	Rescue of 5-nitrofuran toxicity by Aldh2 inhibitors. . . . .	123

4.10	Effect of NFN1 on aldehyde dehydrogenase gene deletions in <i>S. cerevisiae</i> . . . . .	124
4.11	Rescue of 5-nitrofurantoin toxicity by aldehyde dehydrogenase deletions in <i>S. cerevisiae</i> . . . . .	125
4.12	Sensitivity of haploid deletion strains to different concentrations of NFN1. . . . .	126
4.13	Haploid deletion strains sensitive to NFN1 treatment. . . . .	128
4.14	GO categories of deletion mutants affected by NFN1 treatment. . . . .	129
4.15	Spot dilution assay of <i>S. cerevisiae</i> strains deleted for genes involved in DNA damage repair pathways. . . . .	129
4.16	Confirmation of a subset of drug-gene interactions for NFN1. . . . .	130
4.17	Comparison of chemical-genetic profile of NFN1 with that of DNA damaging drugs. . . . .	131
A.1	Scatter plots of green versus red intensities of barcode array data. . . . .	164
A.2	Quality control plots for barcode microarrays. . . . .	166
A.3	Correlation between profiles of one compound screened at different concentrations. . . . .	168
A.4	Correlation coefficients for 60 profiles (30 different compounds). . . . .	169
A.5	Different methods to determine deletion strains sensitive or resistant to drug treatment. . . . .	171
A.6	Average Z-scores for GO categories in 60 chemical-genetic screens. . . . .	172
A.7	Z-scores for protein complexes in 60 chemical-genetic screens. . . . .	174
A.8	Integration of chemical-genetic profiles and genetic and physical interaction data. . . . .	176

---

## List of Tables

---

2.1	Washing steps for barcode microarrays. . . . .	38
3.1	Contingency table for data from primary high-throughput screen and results of confirmatory assays. . . . .	66
3.2	P-values for mean Z-scores of fluconazole-specific deletion strains in each of the chemical-genetic profiles as shown in Figure 3.16B. . . . .	76
3.3	P-values for the CGS and PPP simulations. . . . .	88
3.4	FICI values for combinations of sertraline and trifluoperazine with the ergosterol biosynthesis inhibitors terbinafine and ketoconazole in different species. . . . .	91
3.5	Analysis of interactions between syncretic drugs and higher order combinations with fluconazole. . . . .	92
3.6	MIC and FICI values for drug resistant <i>Candida</i> strains treated with combinations of fluconazole and sertraline. . . . .	95
4.1	Characterisation of small molecules that cause copper-metabolism phenotypes. . . . .	109
4.2	Genes in the GO categories shown in Figure 4.6B . . . . .	117
A.1	List of species databases that are members of the GO consortium. . . . .	161
A.2	Status of Gene Ontology as of September 4, 2009. . . . .	162

---

## List of Abbreviations

---

AMP	Adenosine monophosphate
ATP	Adenosine triphosphate
CAD	cationic amphiphilic drugs
CGS	Chemical genetic space
Cy3 dye	fluorescent cyanine dye (green)
Cy5 dye	fluorescent cyanine dye (red)
dH <sub>2</sub> O	Distilled water
DNA	Deoxyribonucleic acid
DMSO	Dimethyl sulfoxide
EMA	European Medicines Agency
FDA	U.S. Food and Drug Administration
FIC	Fractional inhibitory concentration
FICI	Fractional inhibitory concentration index
G418	Geneticin
GO	Gene ontology
HIV	Human immunodeficiency virus
HTP	High-throughput
IGF	insulin-like growth factor
L	Litre



MAD	Median absolute deviation
MDR	Multiple drug resistance
mL	Millilitre
MIC	Minimum inhibitory concentration
$\mu$ L	Microlitre
$\mu$ M	Micromolar
mM	Millimolar
MO	Morpholino antisense Oligonucleotide
NCGC	NIH Chemical Genomics Center
NIH	National Institutes of Health
NPC	NCGC Pharmaceutical Collection
OD	Optical density
ORF	Open reading frame
PDE-5	Phosphodiesterase-5
pf	post fertilisation
pg	picogram
PCR	Polymerase chain reaction
PPP	Parallel pathway permutation
RNA	Ribonucleic acid
RNAi	RNA interference
RT	Room temperature
rpm	Revolutions per minute
SC	Synthetic complete
SGA	Synthetic genetic array
SGAM	Synthetic genetic array mapping
UV	ultraviolet
WT	Wild-type

# CHAPTER 1

---

## Introduction

---

The discovery of small molecules that elicit a specific effect in the cell is of interest for different reasons. Small molecules can be useful tools to interrogate functional and mechanistic aspects of biological pathways. They can also be drug leads for the development of therapeutic agents. The last twenty years have seen increased efforts at this interface between biology and chemistry which ultimately resulted in a community of scientists who identify themselves as chemical biologists. The term “Chemical Biology“ came into wide use in the 1990s, but the origins of this discipline can be traced back right to the beginnings of biology and chemistry as distinct sciences in the 18th century. A number of journals are dedicated to the publication of papers that aim to understand and manipulate biological systems at the molecular level. The first of these journals, “Current Opinions in Chemical Biology“, was launched in 1997 by Elsevier. This was followed by “BMC Chemical Biology“ in 2001. Nature, ACS and Springer followed suit in 2005, 2006 and 2007, respectively. Wiley-Blackwell renamed their “Journal of Peptide Research“ into “Chemical Biology & Drug Design“ in 2006. There is still a debate if chemical biology really is a new field of study or if established fields like biochemistry, cell biology and pharmacology are simply being rebranded. Even though chemical biology integrates methodologies traditionally used in these fields, the current

multi-disciplinarity in science has allowed them to blend into a distinct discipline that is defined by the desire to understand and manipulate biological systems. Chemical biology has already succeeded in changing the way biologists view small molecules in two important ways. The definition of a compound's mode of action has been pushed towards greater accuracy. It also succeeded to highlight the importance of small molecules in biological pathways and their potential to manipulate biological systems.

One of the biggest challenges that chemical biologists face is the characterisation of the mode of action of small molecules. Genomic methods in yeast have been successfully applied to this problem (Section 1.2).

Drug discovery currently faces many challenges because target-based drug discovery has reached its limit, leading to fewer new drugs being approved each year by the U.S. Food and Drug Administration (FDA) in the last decades. Further, developing drug resistance renders drugs ineffective, increasing the need for new therapies. New approaches for drug discovery are urgently needed. One approach to overcome the limitations of *in vitro* chemical screens is the use of model organisms in high-throughput screens (Section 1.3.3). Other strategies to speed up the process of drug discovery include repurposing of already approved drugs (Section 1.3.4) as well as drug combinations to develop more effective and specific therapies (Section 1.3.5). Rational approaches for the discovery of effective drug combinations are being developed based on functional genomics experiments to interrogate biological systems.

## 1.1 Chemical Biology

Chemical Biology can be both, the use of chemistry to understand biological processes and nature inspiring developments that advance chemistry. One of the earliest examples of this approach must be the experiments on gases by Joseph Priestley in the 18th century. Priestley, who was a natural philosopher among other things, identified various gases including oxygen and nitrous oxide. He used mice in his experiments into the effects and chemistry of these gases (Morrison & Weiss, 2006). Another important contribution to chemical biology came from

Friedrich Wöhler (1800 - 1882) when he managed to synthesise urea. This proved that it is possible to synthesise biological compounds from inorganic substances (Morrison & Weiss, 2006). Cellular imaging became possible because of the development of chemical methods. Anna Atkins (1799 - 1871) who was a botanist and photographer also contributed to the development of imaging techniques. She grew up surrounded by scientists like Sir John Herschel and William Henry Fox Talbot, because her father, John George Children, a fellow of the Royal Society, was a British chemist, mineralogist and zoologist. Anna learned photography from Talbot and she made use of Herschel's cyanotype process for monochromatic colour photography to document botanical specimen (Morrison & Weiss, 2006). The technique that Anna developed revealed intricate details of her specimen. Her images are still displayed in art galleries like the J Paul Getty Museum<sup>1</sup>. Dyes continued to play an important role in the 19th and early 20th century. For example, the development of Rudolf Virchow's theory of cellular pathology relied on dyes to stain fine structures within the cell. Paul Ehrlich visualised bacteria with specific dyes and realised that this could be used to deliver toxins to bacteria to kill them. This led to his idea of the 'magic bullet'.

These are examples of how chemicals can be used to advance biology. Chemical biologists today are still interested in using small molecules to interrogate biological processes, such as mitosis (Mayer *et al.*, 1999), and to understand biological complexity of bacteria for example (reviewed in Falconer *et al.*, 2011). Probing biological systems with small molecules has many advantages over traditional genetic methods. Timing of compound treatment is a big advantage in several aspects. Most compounds act rapidly after addition, allowing the response to be observed by imaging and preventing cells from adapting to the perturbation as is the case with gene deletions. Further, in *in vivo* studies, the time point of drug treatment can be varied to study different aspects of development. Normally, compound treatment is reversible, allowing the study of lasting effects of compound exposure. The time and dose of compounds can be varied to suit the current assay. Different compounds can be easily combined to assess effects of treatment with multiple compounds and to identify compound interactions.

---

<sup>1</sup><http://www.getty.edu/art/gettyguide/artMakerDetails?maker=1542>

Compounds are also not limited to a specific strain or species. Their effect can easily be assessed in mutant strains and in other organisms. These molecular probes can also have therapeutic value. One disadvantage of small molecular probes compared to genetic methods is that not every protein can be targeted. Hopkins & Groom (2002) for example estimate that only 10% of the genome of different species are 'druggable'. Another hurdle that has to be taken is the interrogation of the mode of action of small molecules. The advent of functional genomics has played an important role in elucidating the mechanisms by which small molecules exert their action.

## **1.2 Functional genomics tools in *S. cerevisiae* to interrogate mode of action of small molecules.**

The availability of complete genome sequences was met with great expectations for drug discovery. The sequence of the human genome allows for novel approaches to understand and characterise diseases to develop new drugs. The genome sequences of pathogens offer the possibility to identify pathogen-specific drug targets for the development of antibiotic and antifungal therapies. Chemical genomics enables the development of new strategies for drug discovery. Rather than finding drugs for known protein targets, it is now possible to find compounds that elicit the desired effect and to then investigate the mode of action of that compound. Functional genomic approaches in the budding yeast *Saccharomyces cerevisiae* played an important role in the development and implementation of chemical genomic methods to elucidate the targets of known and novel compounds.

### **1.2.1 The yeast deletion set as a resource for chemical genomics**

The publication of the genome sequence of the budding yeast (Goffeau *et al.*, 1996) was soon followed by collaborative efforts to generate genome-wide collections of yeast deletion strains (Winzeler *et al.*, 1999; Giaever *et al.*, 2002). Each of the

6000 genes was individually replaced with the dominant drug resistance marker *kanMX* using a PCR-based gene deletion strategy. The aim of this effort by the *Saccharomyces* Genome Deletion Project was the assignment of functions to all open reading frames (ORFs) in the yeast genome through large-scale phenotypic analysis. The deletion project revealed that about 5000 genes are dispensable for growth in the budding yeast. Many genome-wide screens were conducted to interrogate the roles of these non-essential genes in various biological processes like bud site selection (Ni & Snyder, 2001), vacuolar protein sorting (Bonangelino *et al.*, 2002), telomere length maintenance (Askree *et al.*, 2004) and centromeric cohesion (Marston *et al.*, 2004). Tucker & Fields (2004) identified genes important for resistance against oxidative and chemical stress in liquid cultures in 96-well plates. In these screens, each deletion strain was assessed individually. It is also possible to conduct competitive growth assays with pooled deletion strains. Deletion strains in the collection are 'barcoded', enabling quantification of each strain in a culture of pooled deletion strains (Shoemaker *et al.*, 1996). These molecular tags are sets of 20 base-pairs that are unique to each deletion strain. Two such tags were placed up- and downstream of the drug resistance marker during deletion strain constructions. Strain abundance can be assessed with barcode microarrays that represent the barcodes of all deletion strains (Cook *et al.*, 2008). This approach allows the identification of deletion strains that are sensitive or confer resistance under specific growth conditions or in response to compound treatment (Giaever *et al.*, 2002). For example, this method was used to identify genes that are required for resistance to UV radiation (Birrell *et al.*, 2001) and to explore the molecular basis for off-target effects of psychoactive drugs (Ericson *et al.*, 2008). Large-scale profiling of the deletion sets against many different compounds and conditions revealed phenotypes for nearly all genes and provides a rich dataset to explore the function of genes as well as the mode of action of small molecules (Hillenmeyer *et al.*, 2008).

Competitive growth assays have several advantages compared to approaches that test each deletion strain individually on agar plates or in 96 well plate format. Screening of pooled deletion mutants is much more time- and resource-effective since the whole deletion set can be screened in culture volumes as low as 1 mL. For

chemical genomic screens this also means that the amount of compound needed is minimal. The pooled approach also greatly reduces experimental variance because all strains are screened simultaneously under the same conditions.

### 1.2.2 Haplo-insufficiency screens to identify drug targets

The functions of essential genes can be assessed with heterozygous deletion strains where only one copy of each gene is deleted. These strains have been used in drug-induced haploinsufficiency profiling aimed at identifying biological targets of small molecules (Giaever *et al.*, 1999; Lum *et al.*, 2004). The reasoning behind this approach is that lowering the dose of a gene encoding an essential drug target results in hypersensitivity to treatment with that drug. Giaever *et al.* (1999) performed proof of principle experiments with single deletion strains and with a pool of 223 heterozygous deletion mutants. First they showed that strains heterozygous for the known essential drug target genes *HIS3*, *ALG7*, *RNR2*, *TUB1/2* or *ERG11* show increased sensitivity to 3-amino-triazole, tunicamycin, hydroxyurea, benomyl and fluconazole, respectively. They then succeeded in identifying *alg7/ALG7* as one of three strains that were highly sensitive to tunicamycin treatment from a pool of 223 heterozygous deletion strains. Lum *et al.* (2004) screened 78 compounds against pools of 3503 heterozygous deletion strains to characterise the cellular effects of these medically relevant small molecules. The majority of compounds yielded 10 or less strains with drug-specific sensitivities. Analysis of the results confirmed known targets for many compounds and suggested novel targets for well described compounds. For example, the vasodilator molsidomine sensitised the *erg7/ERG7* strain and one of its metabolites was confirmed to inhibit ergosterol biosynthesis at the lanosterol synthase step in the budding yeast. The metabolite also inhibited lanosterol synthase purified from rat liver which could explain the cholesterol lowering effects of molsidomine that have been reported (Chassoux, 1989). In another study, 81 psychoactive drugs were found to inhibit yeast growth and were examined for their effects on biological processes using the heterozygous deletion set (Ericson *et al.*, 2008). The results provided insights into side-effects associated with drug treatment. Interestingly, Lum *et al.* (2004)

and Ericson *et al.* (2008) identified *neo1/NEO1* strains as sensitive to various antidepressive drugs. *NEO1* encodes an aminophospholipid translocase (flippase) and Spitzer *et al.* (2011) subsequently showed that cationic amphiphilic drugs, like the antidepressiva, cause membrane perturbation probably by intercalating into one of the two layers. These and other studies (Giaever *et al.*, 2004; Hillenmeyer *et al.*, 2008) confirm the utility of the heterozygous deletion set to identify biological targets of small molecules and provide a rich data set that can be used to uncover pathways affected by the compounds that were screened.

It is important to keep in mind that not all compounds inhibit the function of an essential protein in the cell. In the case of compounds that target several non-essential proteins or cause damage to cellular structures (DNA or cell membranes, for example), induced haploinsufficiency profiling will not be able to identify the direct target.

### **1.2.3 Chemical-genetic profiles reveal drug target pathways**

Competitive growth assays with the haploid or homozygous deletion sets typically yield larger numbers of sensitive strains than the haploinsufficiency screens. The result of such a screen is called the chemical-genetic profile of a compound. Drug-hypersensitivity of a deletion strain is a chemical-genetic interaction, analogous to genetic interactions that have been explored to characterise the function of all yeast genes (Costanzo *et al.*, 2010). The deletion set has been used in systematic screens to identify the functional interactions of genes (Tong *et al.*, 2004). These genetic interactions, such as synthetic lethality, can also be used to link bioactive compounds to their cellular target pathways (Parsons *et al.*, 2004; Parsons *et al.*, 2006). Integration of genetic and chemical-genetic interactions revealed that there is an overlap between the chemical-genetic profiles of compounds and the genetic interactions of their protein targets. However, this overlap is not complete, reflecting the fact that drugs do not simply mimic deletion of the target gene and that they have additional effects in the cell. Drug treatment also sensitises strains deleted in proteins involved in general stress response, drug metabolism and drug



transport.

In the same way that genes with similar functions display a similar spectrum of genetic interactions, compounds with similar mode of actions were found to share similar chemical-genetic profiles, allowing clustering and classification of compounds based on these profiles (Parsons *et al.*, 2006).

#### 1.2.4 Dosage-suppression

Increased dosage of a target protein can confer resistance to drug treatment. Drug targets have been successfully identified based on the dosage-dependent suppression of drug toxicity. Traditionally, wild type yeast is transformed with a random genomic library and resistance of the resultant transformants to drug treatment is assessed. The drug targets of cycloheximide (Fried & Warner, 1982), tunicamycin (Rine *et al.*, 1983), ketoconazole (Launhardt *et al.*, 1988) and sorafenib (Vahlensieck *et al.*, 1994) were identified with this technique.

Advances in genome-wide techniques and the creation of genome-wide overexpression libraries enabled systematic overexpression screens. The method developed by Luesch *et al.* (2005) used a yeast genomic library, but for the resistance screens transformants were arrayed in 384-well format. This allowed comparison of screen results for different compounds allowing identification of general and specific suppressors. Other approaches monitor the abundance of transformants using microarrays to identify genes that confer resistance to drug treatment (Butcher *et al.*, 2006; Abruzzi *et al.*, 2007; Hoon *et al.*, 2008).

#### 1.2.5 Spontaneous drug-resistant mutants

Chemical-genomic approaches discussed so far all involve reverse-genetic approaches. Random mutagenesis and subsequent selection of mutants resistant to a compound is a forward genetic approach that has also been used to identify targets of compounds. For example, Kitamura *et al.* (2009) identified  $\beta$ -1,6-glucan synthase as the target of a compound that selectively targets the fungal cell wall by analysis of a resistant *S. cerevisiae* mutant.

There are different strategies for the identification of the mutations responsible

for drug resistance. Dominant mutations can be mapped by creating a genomic DNA library from a resistant mutant that is transformed into wild type yeast and transformants that show resistance are isolated. Mapping of recessive mutations is usually done by transforming the resistant mutant with a genomic library from a wild type strain followed by identification of transformants that are not resistant anymore, involving replica plating steps. Ho *et al.* (2009) developed a method for more efficient mapping of resistant mutations. They created a molecular barcoded yeast ORF library that can be transformed into resistant mutants and allows rapid fitness assessment of all transformants to be done simultaneously.

The deletion set can also be used for rapid mapping of drug resistance mutations. A method called synthetic genetic array mapping (SGAM) has been described (Jorgensen *et al.*, 2002) where every deletion strain can be considered a marker along the genome of *S. cerevisiae*. Mating of a resistant mutant to the whole deletion collection would reveal the chromosomal location of the suppressor allele because it is impossible to obtain strains that carry the resistance allele and the deletion marker when they are linked.

### **1.2.6 High-content screening**

Intracellular changes in response to compound treatment can be monitored by fluorescence microscopy. Ohnuki *et al.* (2010) derived 500 morphological parameters from yeast after treatment with compound and the obtained parameters were compared to those of deletion mutants to identify the molecular target of the drugs. The authors successfully recovered known targets of four different drugs. The effect of drugs on mammalian cells has been assessed in this way, too (Perlman *et al.*, 2004; Young *et al.*, 2008).

### **1.2.7 Expression profiling**

Changes in gene expression in response to small molecule treatment have been used to characterise the effects of small molecules on cells (Hughes *et al.*, 2000). Comparing gene expression profiles of deletion mutants with gene expression in response to drug treatment allowed for Erg2 to be identified as the drug target of

the topical anaesthetic dyclonine. Cytosolic aldehyde dehydrogenase (Ald6) was identified as the target of compounds that suppress the toxicity of FK506 in yeast (Butcher & Schreiber, 2004). The use of expression profiling in various species for the interrogation of drug target pathways, a drug's specificity and pathways downstream of the drug target has been reviewed in Butcher & Schreiber (2005). The "Connectivity Map" is an approach to use gene expression profiles of human cells treated with small molecules to identify functional connections among diseases (Lamb *et al.*, 2006).

### 1.2.8 Chemical-chemical interactions

The biological activity of compounds can be profiled by testing for chemical-chemical interactions with a set of compounds with known mode of action. Farha & Brown (2010) combined 186 bioactive compounds with 14 known antibiotics and identified promising synergistic interactions with the known antibiotics. They were also able to generate hypotheses about the potential mode of action for many compounds and confirmed these predictions for two compounds. Eight compounds that were promiscuously synergistic were found to be membrane-active.

This approach is easily transferrable to other species because genome-wide libraries are not required.

## 1.3 Challenges in drug discovery

### 1.3.1 A short history of drug discovery

Herbal potions and wound dressing have been used for a very long time. Ancient Egyptian medicine dates back to 3300 BC and was well documented. The Egyptian Ebers Papyrus (1550 BC) is the most comprehensive record of Egyptian medicine known today. It was bought by Georg Ebers in 1872/73 in Thebes and is currently kept at the library of the University of Leipzig<sup>2</sup>. Chinese and Ancient Greek medicine also have very long traditions. Traditional Chinese medicine

---

<sup>2</sup>[http://www.ub.uni-leipzig.de/site.php?page=die\\_ubl/sosa/scholl4](http://www.ub.uni-leipzig.de/site.php?page=die_ubl/sosa/scholl4)

looks back on over 2000 years of history and includes herbal medicine, acupuncture, massage and diet. The first Greek medical school opened 700 BC and this is where the practice of observing patients has been established. Hippocrates is considered the "Father of Medicine" and the Hippocratic Oath for physicians is still in use today.

Despite such a long history of medicine, only a handful of drugs were available at the beginning of the 20th century. These included cocaine and morphine that were used as local anaesthetics, aspirin for pain and fever relief, digitalis for the treatment of heart conditions, antipyrine, a painkiller, and quinine to treat malaria. These drugs have been discovered based on observations resulting from accidental exposure of animals or humans to small molecules. William Withering learned about the use of digitalis to treat congestive heart failure from an old folk herbalist. He succeeded in isolating digitalis as the active ingredient in the late 18th century (Hauptman & Kelly, 1999). These discoveries provided scientists with the knowledge that there are bioactive compounds. The discovery of the causes of infectious diseases by Louis Pasteur and Robert Koch was also a key development to advance medicine. Later, Louis Pasteur also discovered the principle of immunisation.

The early 20th century saw the first systematic attempts to find drugs. Paul Ehrlich synthesised and tested 900 arsenical compounds on mice infected with trypanosomes which eventually led to the discovery of the syphilis treatment salvarsan in 1909, the first man made antibiotic. Ehrlich also postulated that parasites have 'chemoreceptors' that are unique to them and that they could be exploited to treat diseases by delivering toxins with 'magic bullets'. The year 1929 saw the discovery of the  $\beta$ -lactam antibiotic penicillin by Alexander Fleming. While studying staphylococcal variants he noticed that one of his petri dishes was contaminated with mould and in the vicinity of the fungus, the *Staphylococcus* colonies were transparent, an indicator of bacterial lysis (Fleming, 1929). It would take another decade before penicillin was used in hospitals. Following the success of penicillin, many companies focused on the discovery of antibiotics (Drews, 2000) and the 1950s saw the discovery of non-lactam antibiotics (Fischbach *et al.*, 2009).

The first cancer chemotherapeutics and antipsychotics were also discovered in the 1950s. AIDS had a big influence on the drug development and research in the field of immunology in the 1980s. In addition, this was the time when resistance to drugs first emerged, motivating further research. The growing understanding of human physiology and disease led to rational drug design. Robotics and automation as well as advances in combinatorial chemistry allowed for large chemical libraries to be screened for bioactivity by pharmaceutical companies.

### 1.3.2 Current approaches to drug discovery

There are several approaches in drug discovery that are based on existing drugs. Therapies can be developed that re-optimize drugs that are already used to treat a specific disease. A method that is widely used is the combination of known drugs. Many diseases are multi-factorial involving several genetic and environmental factors and could therefore be treated more effectively with drug combinations (Reich & Lander, 2001; Loktionov, 2003; Kaplan & Junien, 2000). There is also less potential for drug resistance to develop. Treatments for HIV, cancer and bacterial infections are often combinations of drugs. The concept of drug combinations is explored in more detail in Section 1.3.5. Drug replacement or drug rotation is another approach to stem the tide of drug resistance. This method was successfully used in Malawi, where chloroquine was replaced nationwide by sulfadoxine-pyrimethamine because the prevalence of chloroquine resistant *Plasmodium falciparum* was about 85% (Kublin *et al.*, 2003; Laufer *et al.*, 2006). Eight years later, in 2000, this value was only 13% and chloroquine can now be used again to treat malaria. Ideally, it would be used in combination with other drugs to prevent the re-emergence of resistant strains. There are also many drugs that were abandoned due to unwanted side-effects. These could be reconsidered and their dosing or formulation modified to reduce side effects. As shown in Chapter 4, it is also possible to devise drug combinations to minimize side effects of an otherwise effective drug.

Repurposing of known drugs is a very time and cost effective way to discover new treatments for diseases. Different approaches and resources as well as

advantages of drug repurposing are described in detail in Section 1.3.4.

The discovery of new compounds with bioactivity has mostly been applied in the context of target-based approaches to drug design that are still widely used. The advances in robotics and automation as well as combinatorial chemistry enabled screens of large synthetic chemical libraries against purified target proteins to identify compounds that modulate the activity of the protein in the desired way. Increasingly, libraries of natural products and extracts from plants or microorganisms are used in screens as well. These screens can also be done *in silico* if the structure of the protein target is known. The structures of large chemical libraries can be used by cheminformatics docking algorithms. For example, *in silico* drug discovery in the context of neglected diseases is reviewed in Ekins *et al.* (2011).

The exact number of unique proteins that are targeted by FDA approved drugs has been debated (Overington *et al.*, 2006; they stated the number as 324). It is clear however, that it is definitely much smaller than the number of genes. The advent of functional genomics advances the understanding of disease and enables the identification of new potential drug targets (Hartwell *et al.*, 1997). The concept of synthetic lethality is applied to target discovery in cancer (reviewed in Chan & Giaccia, 2011). RNAi screens have been successfully used to identify pathways that can be targeted in combination therapies to treat cancer (Bauer *et al.*, 2010; Seyhan *et al.*, 2011). Further, *in vivo* screens could be integrated with the target-based approach to identify new targets for drug discovery (Sams-Dodd, 2005; Section 1.3.3).

There has been a steady decline in the number of new drugs approved by the FDA in the last two decades despite increased spending on research and development. In addition, very few new drug classes have been discovered in the last decades to treat infections, for example (Fischbach *et al.*, 2009). Emerging resistance increases the need for new therapies (Clatworthy, 2007). Organism-based drug discovery (Section 1.3.3), drug repurposing (Section 1.3.4) and combinations of drugs (Section 1.3.5) are three strategies to bring much needed innovation into the field of drug discovery to meet these demands for new drugs.

### 1.3.3 Organism-based drug discovery in the zebrafish

Many of the limitations of target-based drug discovery can be overcome by screening chemical libraries in model organisms. Such screens would assess compound activity in the physiological context and subsequent tests for effectiveness, side effects, toxicity and pharmacokinetics of hit compounds are not necessary because the effect of small molecules on a whole organism is observed during screening. The use of model organisms allows the discovery of new pathways and proteins that can be targeted to treat diseases. The range of observable phenotypes can also be expanded to include development, physiology and behaviour. Model organisms that have been used in high-throughput chemical screens are the nematode *Caenorhabditis elegans*, the fruitfly *Drosophila melanogaster* and the zebrafish *Danio rerio* (reviewed in Giacomotto & Ségalat, 2010). Kwok *et al.* (2006) screened 14,000 compounds in *C. elegans* and identified over 300 compounds that caused various phenotypes. They also investigated the mode of action of a compound that resembles a class of widely prescribed anti-hypertension drugs. A genetic suppressor screen in *C. elegans* allowed them to identify L-type calcium channels as the target of this compound. *Drosophila* was shown to be amenable to chemical screens and antiepileptic drug candidates have been identified by Stilwell *et al.* (2006).

Zebrafish is a useful model to study human diseases because it is much more similar to mammals with respect to its anatomy and physiology than the invertebrates *C. elegans* and *D. melanogaster*. It is also probably best established as a tool for high throughput screens (Patton & Zon, 2001; Taylor *et al.*, 2010). Pioneering work by George Streisinger revealed the potential of zebrafish for genetic screens (Streisinger, 1981). The first large-scale genetic screens in this vertebrate identified many genes that are essential during development of zebrafish embryos (Driever *et al.*, 1996; Haffter *et al.*, 1996). The screens also resulted in phenotypes that resemble human genetic disease conditions and validated zebrafish as a model for biological processes in vertebrates. These high-throughput studies were feasible because the generation time of zebrafish is fairly short (only 3-4 months), they have a large progeny size of 100 to 200 eggs, and recessive mutations can

be recovered within two generations. The assessment of phenotypes is possible because the transparent zebrafish embryos develop outside the mother and at 6 days post fertilisation most of the organs and tissues are fully developed and clearly visible. The ease of waterborne treatment makes the zebrafish amenable to high-throughput chemical screens. Compounds can simply be added to the media and are absorbed through skin and gills. The small size of the embryos allows for screens to be conducted in 96- or 384-well plates with several embryos per well. The embryos are able to survive for days on the nutrients in the yolk sac. The zebrafish is now established as a vertebrate model for drug discovery screens (MacRae & Peterson, 2003; Langheinrich, 2003; Zon & Peterson, 2005; Peal *et al.*, 2010; Taylor *et al.*, 2010).

The first chemical high-throughput screen in zebrafish was conducted by Peterson *et al.* (2000). Following compound treatment, embryos were analysed for phenotypes relating to the central nervous system, the cardiovascular system, the ear and the skin with a dissecting microscope. Screening of only 1100 compound yielded modifiers of all four systems. Milan *et al.* (2003) screened a small set of 100 compounds for effects on the cardiovascular system. In their 96-multi-well set-up they used automated fluorescence microscopy to monitor the heart rate of embryos expressing GFP in the myocardium. A screen for cell cycle inhibitors emphasised the importance of organism-based screening. From a library of over 16,000 compounds (DIVERSet from Chembridge), Murphey *et al.* (2006) identified 14 compounds that were not found previously to have an effect on cell cycle even though these compounds were screened for mitotic effects in mammalian cell lines several times (for example in Haggarty, 2000). In addition, 7 of these newly identified compounds showed activity in the developing embryos only. Murphey and colleagues went on to show that 3 of these compounds were inactive *in vitro* because of the presence of serum that is used to culture cell lines. The remaining 4 compounds are most likely activated by embryo metabolism.

Zebrafish can also be used in behaviour-based screens because touch, sight and behavioural responses can easily be monitored. The Peterson lab was able to find new psychoactive compounds and to identify their molecular targets using a high-throughput approach in zebrafish (Kokel *et al.*, 2010). The movement of zebrafish



embryos in response to light and touch stimuli was converted into behavioural barcodes amenable to computational analysis. Compounds with similar mode of action elicited similar patterns of behaviour and therefore clustered together based on their barcodes.

Zebrafish strains that model human disease conditions can be used in screens to identify potential drug leads. Compounds that suppress the cardiovascular phenotype in a zebrafish mutant were readily identified by Peterson *et al.* (2004). Even diseases without known target pathways for which zebrafish models exist are amenable to this approach. Zebrafish has also successfully been used to study the progression of infections with *Mycobacterium marinum* (Davis *et al.*, 2002) and *Salmonella typhimurium* (Van der Sar *et al.*, 2003). These infection models could eventually be used for *in vivo* identification of novel antimicrobial compounds in the host-pathogen context (Mukhopadhyay & Peterson, 2006).

These examples show that it is possible to assess the effect of 1000s of compounds in high-content screens in zebrafish. The drug discovery assays that can be conducted in zebrafish include drug discovery for diseases for which models exist in zebrafish like various cancers, infectious and vascular diseases. It is also possible to screen for neuroactive compounds. Further, organism-based drug screens can also uncover pro-drugs that rely on metabolism to be activated that would be missed in *in vitro* screens.

### 1.3.4 Repurposing of drugs

A drug discovery strategy that has garnered considerable interest in the scientific community over last few years is the repurposing or repositioning of drugs (Ashburn & Thor, 2004; Chong & Sullivan, 2007; Boguski *et al.*, 2009). As the Scottish pharmacologist and Nobel laureate James W. Black famously put it "The most fruitful basis for the discovery of a new drug is to start with an old drug". Amy Patterson, NIH Associate Director for Science Policy pointed out recently that most drugs fail during the last stages of development, not because they are toxic, but because of lack of efficacy. She further said that the estimated success rate of repurposed drugs is 30%.

While there are numerous examples of serendipitous discoveries of new uses for known drugs, the last five years saw an increase in systematic screens to uncover new therapeutic uses for old drugs. Repurposing of existing drugs is a very attractive approach since it is faster and less costly than the usual route of drug discovery because bioavailability and biosafety profiles already exist and pharmacokinetics are known as well. Further, chemical optimisation, manufacturing and formulation have been worked out already. The possibility to identify new therapies rapidly, means that this approach is suited to tackle emerging diseases like flu or resistant pathogens. Lower costs associated with this strategy makes it applicable to neglected diseases (Section 1.3.4)

The 'promiscuous nature' of drugs is one factor that makes the concept of drug repurposing work. A single drug often interacts with multiple pathways or proteins in the cell, which can lead to undesired side-effects (Keiser *et al.*, 2009). However, drugs that are found to be safe in human, may prove to have multiple therapeutic uses. This is known as the 'known compound-new target' approach. The success of drug repurposing is also based on the fact that target proteins or pathways might actually play a critical role in more than one disease, thus allowing for drugs with a specific target to be used in a new indication.

### **Approaches for the discovery of new indications for old drugs**

There are numerous repurposed drugs that are marketed for new therapeutic indications already and examples are given in Ashburn & Thor (2004) as well as Chong & Sullivan (2007, supplementary materials). Most of these new indications for old drugs have been discovered by chance. Systematic approaches based on large-scale screens are feasible now because various chemical libraries of known drugs are available (see below). There are several examples of screens to identify therapies for rare and neglected diseases (Section 1.3.4). Neuroprotective properties of  $\beta$ -lactam antibiotics were revealed in a screen of 1,040 FDA-approved drugs (Rothstein *et al.*, 2005). Ceftriaxone was one of the 15  $\beta$ -lactams that were identified as active and when administered to animals it causes increased expression and activity of glutamate transporters which play an important role in

glutamate toxicity. In a mouse model of amyotrophic lateral sclerosis, ceftriaxone delayed loss of neurons and muscle strength, and lead to increased survival. In another screen, Balgi *et al.* (2009) assessed the effect of more than 3500 approved and off-patent compounds on mTORC1. They succeeded in identifying inhibitors of mTORC1 which is indicated in diseases like tuberous sclerosis, diabetes, cardiovascular disease and cancer.

Boguski *et al.* (2009) predict that the use of post marketing surveillance information (managed by the FDA in the USA and EMA in Europe) as well as data mining of hospital records will play an important role in the identification, assessment and understanding of beneficial drug side effects which might lead to new indications for known drugs (Keiser *et al.*, 2009). Many such knowledge-based drug repositioning approaches have been developed and have been reviewed by Dudley *et al.* (2011) and Ekins *et al.* (2011).

### **Chemical libraries for systematic drug repositioning screens**

There are several chemical libraries that consist of approved drugs and bioactive compounds. The LOPAC1280 Library of Pharmacologically Active Compounds is available from Sigma-Aldrich<sup>3</sup> and consists of 1,280 marketed drugs and pharmaceutically relevant compounds that represent all major drug classes. The SPECTRUM Collection<sup>4</sup> is available from MicroSource and contains 2,000 compounds that are marketed drugs, natural products and other bioactive compounds. The library contains 1,000 off-patent drugs and recent 'blockbuster' drugs. The majority of these drugs are approved in the US (800) whereas the other 200 drugs are in use in Europe and Japan. 580 natural products were selected based on structure and chemical class. The remaining 420 compounds represent non-drug enzyme inhibitors, membrane active compounds, cellular toxins and receptor blockers that have either been dropped or did not reach development. Widely used herbicides and pesticides are also included. The Prestwick chemical library<sup>5</sup> contains 1,120 bioactive compounds most of which are off-patent drugs (90%) and some

---

<sup>3</sup>[www.sigmaaldrich.com/chemistry/drug-discovery/validation-libraries/lopac1280-navigator.html](http://www.sigmaaldrich.com/chemistry/drug-discovery/validation-libraries/lopac1280-navigator.html)

<sup>4</sup>[www.msdiscovery.com/spectrum.html](http://www.msdiscovery.com/spectrum.html)

<sup>5</sup>[www.prestwickchemical.com](http://www.prestwickchemical.com)

are bioactive alkaloids or related substances.

There are two attempts to create collections of all chemicals that have been used in medicine, including approved drugs and the so-called 'fallen angels', drugs that were dropped by pharma companies because of lack of efficacy in clinical trials. The Johns Hopkins Clinical Compound Library (JHCCL) is an ongoing project run by the Johns Hopkins Clinical Compound Screening Initiative<sup>6</sup> aimed at providing resources for effective drug repurposing. The initiative was launched as a collaboration in 2002 between Johns Hopkins Pharmacology and the Malaria Research Institute at the Johns Hopkins Bloomberg School of Public Health. Currently, the compound collection contains 3,100 existing drugs and the goal is to collect all 11,000 drugs ever used in medicine. In 2007 this number was 8,850 (Chong & Sullivan, 2007) and the sources of compounds were described as follows: 2,933 unique drugs approved by the FDA since 1938, drugs from the FDA Orange Book (in 2006 there were 1,107), drugs from the Physician Desk reference (888 as of 2006) and another 7,057 compounds that have either been approved abroad or were abandoned after phase II clinical trials in the US. There are many compounds that passed toxicology assessments but were ultimately not effective enough to be approved. These pipeline drugs are a valuable resource for drug repurposing efforts. The final list of 8,850 compounds excludes antiseptics, vaccines and therapeutic extracts.

The National Institutes of Health (NIH) Chemical Genomics Center (NCGC) created the NCGC Pharmaceutical Collection (NPC) as an informatics and a screening resource (Huang *et al.*, 2011). First, a comprehensive, non-redundant list of approved molecular entities was assembled. Through matching of compounds from various data sources, a list of 9,969 molecular entities was assembled. 4,034 molecular entities are currently approved by at least one regulatory agency world wide and 4,935 unique molecular entities are registered but not approved. The data sources included various FDA and World Health Organization drug lists as well as the European and the Japanese pharmacopeia. 7,631 of these compounds were considered amenable to high-throughput screening (2,750 approved and 4,881 registered molecular entities). Proteins and antibodies were

---

<sup>6</sup>[www.jhccsi.org](http://www.jhccsi.org)

excluded as well as molecules insoluble in DMSO and only compounds with more than 15 atoms and at least one carbon or nitrogen atom were included. The idea is to screen these compounds in as many assays as possible to identify potential drugs or drug leads. The results of all screens will be available publicly via PubChem<sup>7</sup> and the NPC browser. This will allow the data to be used for drug repurposing and to define the activities of known bioactive small molecules. The NPC browser also allows for virtual screening and docking approaches of the collection.

### **Thalidomide, its fall and rise**

Thalidomide, was prescribed in the 1950s to treat morning sickness in pregnant women (Ashburn & Thor, 2004). The drug was banned just a few years later because it led to severe skeletal birth defects. In 1964, it was used by a physician as a last resort to treat a critically ill patient with inflammatory condition erythema nodosum laprosum (ENL). Surprisingly, the patient was soon healed of his sores and was pain free. Thalidomide was approved as a treatment for ENL in 1998 and is still the only drug to treat ENL. In the 1990s it was discovered that thalidomide had anti-angiogenic properties (D'Amato *et al.*, 1994) and today this drug's main use is in cancer treatment, primarily multiple myeloma.

### **Sildenafil, a PDE-5 inhibitor with many therapeutic indications**

Another example where a new indication was discovered accidentally is sildenafil (Viagra<sup>®</sup>). Pfizer had originally developed sildenafil to treat angina. The compound inhibits phosphodiesterase-5 (PDE-5) which relaxes coronary arteries and allows greater coronary blood flow. The drug did not prove effective in a trial in the early 1990s, but persistent and unusually strong erections were reported as side effects by several volunteers. Since PDE-5 had been identified as a key enzyme in mediating erections (Ignarro *et al.*, 1990), a few small scale trials were soon followed by a large scale trial (3700 patients in Morales *et al.*, 1998). They all confirmed sildenafil to be an effective treatment of erectile dysfunction. Con-

---

<sup>7</sup><http://pubchem.ncbi.nlm.nih.gov/>

cerns about the safety of the drug for patients with (suspected) heart disease were voiced soon after its release as Viagra<sup>®</sup>.

Pleiotropic effects of PDE-5 inhibitors like sildenafil were soon discovered (Gross, 2010). Several papers have demonstrated potential for sildenafil to treat cardiovascular conditions. It was shown to have cardioprotective properties in rabbits (Ockaili *et al.*, 2002) and it was successfully used in mice to treat cardiac hypertrophy and remodelling which frequently lead to heart failure (Takimoto *et al.*, 2005). In 2005 it was approved for the treatment of pulmonary arterial hypertension. Sildenafil also has therapeutic potential for improving vascular function in diabetic patients (Mammi *et al.*, 2011). Das *et al.* (2010) observed enhanced antitumour activity of the chemotherapeutic doxorubicin in combination with sildenafil while sildenafil also reduced the toxicity of doxorubicin. Recently, sildenafil has been described as a multidrug resistance modulating drug that enhances the sensitivity of cancer cells to standard chemotherapeutics (Shi *et al.*, 2011). It has also been described as a lead compound in antimalarial drug design in a molecular docking study (Howard *et al.*, 2011).

Sildenafil is an example of a drug with various therapeutic indications because its target, phosphodiesterase-5, is important in many biological processes.

### **A new role for metformin as anticancer drug**

Metformin is probably the world's most widely prescribed anti-diabetic drug. It is of the biguanide class and is used to treat type 2 diabetes. Several retrospective analyses as well as *in vitro* and *in vivo* studies have reported that metformin may also have anti-cancer properties (reviewed in Chong & Chabner, 2009; Sahra *et al.*, 2010). Intriguingly, Hirsch *et al.* (2009) showed that metformin selectively kills cancer stem cells *in vitro* and *in vivo* and the combination of doxorubicin effectively wiped out tumours and prevented recurrence in mouse studies.

The effect of metformin for the treatment of diabetes is two-fold. Metformin has been shown to facilitate the trafficking of glucose transporters in several tissues which improves glucose uptake (Kozka & Holman, 1993). The drug also partially inhibits complex 1 of the mitochondrial respiratory chain (Owen *et al.*,

2000) resulting in lower ATP levels in the cells. This in turn activates AMP kinase, which is a major sensor of the energy status of the cell (Zhou *et al.*, 2001). Once activated, AMPK phosphorylates and therefore inactivates the transcriptional activator TORC2 which leads to decreased expression of genes involved in gluconeogenesis (Koo *et al.*, 2005). The inhibition of gluconeogenesis is thought to be the basis for the therapeutic effect of metformin in diabetes.

The effect of metformin against breast cancer cells has been shown to depend on AMPK (Zakikhani *et al.*, 2006; Zhuang & Miskimins, 2008). Metabolic reprogramming is one of the hallmarks of cancer. The metabolic switch from oxidative phosphorylation to glycolysis is known as the Warburg effect (Kim & Dang, 2006) and enables cancer cells to adapt to a hypoxic environment. Metabolic states and adaptation are probably important for understanding how metformin affects cancer cell proliferation. Perturbation of the balance between AMP and ATP and activation of the AMPK pathway induces stress that is similar to metabolic stress. Depending on cell type, this leads to apoptosis, autophagy or cell cycle arrest.

Like sildenafil, metformin shows how one target pathway can be important for the treatment of two diseases, in this case diabetes and cancer.

### **Application of drug repurposing to orphan diseases**

Over 6000 diseases have been classified as rare or orphan diseases by the NIH. Due to low prevalence and/or limited commercial potential, only about 5% of orphan diseases can be treated with 350 drugs and biological products that are available for rare diseases (Sardana *et al.*, 2011). Since cost is an important factor in drug development, repurposing of drugs was early on seen as an opportunity to find therapies for orphan diseases. In one of the first drug-repurposing screens, Chong *et al.* (2006) identified 87 drugs from the Johns Hopkins Clinical Compounds Library (it contained 2500 drugs then) that inhibited growth of the human malaria parasite *Plasmodium falciparum*. The antihistamine astemizole was found to be highly effective against 3 different *P. falciparum* strains and in two mouse models of malaria. The same library was screened by Gloeckner *et al.* (2010) to find new

therapies for the neglected tropical disease Onchocerciasis, or river blindness, which is caused by the nematode *Onchocerca volvulus* and affects over 37 million people in third world countries. Closantel, a veterinary anthelmintic showed potent and specific activity against *O. volvulus* larvae.

The cost-effective option of drug repurposing will hopefully boost the development of safe and effective therapies for rare and neglected diseases.

### 1.3.5 Multicomponent therapies

The idea of drug combinations is not new. In fact, traditional Chinese medicine, the Egyptian Ebers Papyrus (1550 BC) and other historical approaches to medicine relied on mixtures of herbs and herbal extracts. In the late 19th century, investigators in Western medicine became interested in interactions between purified compounds. The British physician and pharmacologist Thomas Richard Fraser described the interaction between physostigma and atropia in 1871. In the early 20th century Siegfried Walter Loewe, a German pharmacologist, endocrinologists and clinical chemists, quantified the effects of drug combinations (Loewe, 1928). His work later resulted in the definition of Loewe additivity as a reference model for drug interactions (Loewe, 1953). This model is based on the assumption that a compound should only have additive interactions with itself. The biologist Chester Ittner Bliss taught himself statistics which he used to develop, among other things, the Bliss independence model to assess drug interactions (Bliss, 1939). This method assumes the relative effect of a drug at a specific concentration to be independent of the presence of another drug. These two models were the basis for many more methods that were devised subsequently to classify synergistic drug combinations. These models have been discussed in Greco *et al.* (1995) in the context of the debate about the definition of synergy.

#### **Inspired by nature: effective combinations of natural compounds**

There are examples in nature where mixtures of compounds result in maximal activity. For example, medicinal plants that produce the antimicrobial agent berberine were shown to also produce an inhibitor of multi-drug resistance pumps



(Stermitz *et al.*, 2000). The MDR inhibitor has no apparent activity on its own, but this combination effectively overcomes bacterial resistance against berberine. The larvae of beewolf digger wasps are constantly threatened by pathogenic bacteria and fungi. Kroiss *et al.* (2010) discovered that the wasps protect their larvae with a 'cocktail' of nine antibiotics that is being produced by symbiotic bacteria (*Streptomyces* spp.) that the wasps cultivate on their antennae. Snake venoms are combinations of many different proteins and microbials also produce a multitude of bioactive compounds to defend themselves against other microbial species.

### **Tackling the complexity of cellular networks with drug combinations**

The complexity of cellular networks as well as the multifactorial nature of many diseases suggest that multi-component therapies might be more effective than single agents. They contain many features such as cross talk, feedback and feed-forward loops which systems biology is only beginning to unravel. Living systems are characterised by an intrinsic robustness that needs to be studied to be able to develop drugs that can control such a complex system (Kitano, 2007). Biological networks and their structure have been studied extensively (Watts & Strogatz, 1998; Jeong *et al.*, 2000) and theoretical considerations have resulted in the conclusion that weak links are just as important in biological networks as strong links (Csermely, 2004). Drug discovery has focussed on targeting essential proteins that correspond to strong links in a network. Csermely *et al.* (2005) subsequently suggested that partial inhibition of a surprisingly small number of cellular targets can have stronger effects than complete inhibition of a single target. This was confirmed for the transcriptional regulatory networks of *S. cerevisiae* and *E. coli* where weak inhibition of 3-5 nodes had a greater impact than complete deletion of a single node (Ágoston *et al.*, 2005). The interest in drug combinations has grown in recent years. For example, the company CombinatoRx (now Zalicus) was founded with the aim to identify synergistic combinations of approved drugs that are effective therapies (Borisy *et al.*, 2003). Different experimental and modelling approaches were developed in the research community to find multi-target

drugs for specific diseases. There are many potential advantages of drug combinations including a reduction in side effects and reduced host toxicity. In addition, the combination of compounds might induce effects that cannot be obtained with a single drug resulting in higher efficacy against a disease. Attacking a system on multiple fronts also lowers the risk of resistance and might help fight heterozygous populations of tumour or pathogen cells. One important thing to keep in mind is the fact that normal cells are affected by compound treatment as well and therapeutic synergy is based on the selective toxicity against cancer or pathogen cells relative to host cells. Therapeutic regimens might also have to be optimised to improve the results of combination therapy (Berenbaum, 1990).

Drugs that were developed separately to treat a disease have been combined based on clinical observations because they are more effective than treatment with either agent alone. These drug combinations have been called 'congruous' (Keith *et al.*, 2005). Successful examples of such 'congruous' drug combinations are: Combivir<sup>®</sup> by GlaxoSmithKline for HIV treatment, Advair<sup>®</sup> by GlaxoSmithKline to treat asthma and Advicor<sup>®</sup> by Kos Pharmaceuticals to treat hypercholesterolaemia.

Devising higher order drug combinations is also of interest and has been attempted by combining drugs that are already used to treat the target disease. Berenbaum *et al.* (1983) compared the effect of double and triple antibiotic drug combinations against *Pseudomonas maltophilia* and observed that triple combinations usually resulted in synergy, even if the organism was resistant to one of the drugs. First trials comparing two- and three-drug combinations in chemotherapy generated inconclusive results about whether the higher-order drug combinations are more effective (Pirker, 2002). Many clinical trials currently compare the efficacy of two- and three-drug regimens.

While clinical observations have led to a number of successful drug combinations, interactions with drugs that are not normally used to treat the target disease are unlikely to be discovered. These combinations, where one of the active ingredients was not developed to treat the target disease, have been termed 'syncretic' drug combinations. Therefore, approaches for *de novo* discovery of synergistic drug combinations are needed to explore the space of syncretic drug

combinations.

### **Different mechanisms of drug interactions**

The combination of two drugs might be synergistic because one compound facilitates the action of the other one by affecting multi drug resistance pumps or drug metabolism. The aforementioned berberine-combination produced by plants is a good example of this type of drug interaction. The antibiotic Augmentin<sup>®</sup> is another example. This drug combines the  $\beta$ -lactam antibiotic amoxicillin with the  $\beta$ -lactamase inhibitor clavulanate to prevent the degradation of amoxicillin.

Two drugs that target the same pathway or even the same protein can also increase pharmaceutical efficacy when combined. An example are the DNA damaging chemotherapeutic agents mitomycin C and doxorubicin (Shuhendler *et al.*, 2007). Synergy has also been observed between the two microtubule inhibitors discodermolide and paclitaxel (Honore *et al.*, 2004).

Combination treatment with compounds that have separate targets can result in synergistic drug interactions. These targets can be in the same cell or in different tissues. Yeh *et al.* (2006) systematically explored the interactions between 21 antibiotics and found, that protein synthesis inhibitors synergised with inhibitors of folic acid biosynthesis and with inhibitors of DNA synthesis. Metformin suppresses gluconeogenesis in the liver and also improves glucose uptake in peripheral tissues. This drug is often combined with glyburide (Glucovance<sup>®</sup>) which leads to increased insulin secretion from the pancreas or rosiglitazone (Avandamet<sup>®</sup>) which improves insulin sensitivity. The different actions of the compound pairs in different tissues lead to improved glucose homeostasis to treat type 2 diabetes more effectively.

There are drug combinations where one component confines the action of the other component to specific cells. In Section 4.2.4 (Ishizaki, Zhou *et al.*, submitted), the combination of nifurtimox with an aldehyde dehydrogenase inhibitor has been suggested to reduce the side-effects of nifurtimox by inhibiting the bioactivation of nifurtimox in host cells. Similarly, the effects of levodopa are confined to the brain to treat Parkinson's disease. It is given in combination with carbidopa

(the combination is called Sinemet<sup>®</sup>) which cannot cross the blood brain barrier and therefore prevents levodopa to be converted to dopamine everywhere in the body but the brain preventing unwanted side-effects of dopamine.

It is important to be aware of drug interactions that lead to unwanted effects as is the case with contra-indicated drugs. These adverse effects are normally only discovered in retrospective because complex drug interactions are hard to predict and can often only be observed empirically. Tatonetti *et al.* (2011) describe an unwanted synergistic effect of the anti-depressant paroxetine and the lipid-lowering agent pravastatin on glucose levels in the blood of patients. Both drugs are widely prescribed and many patients are comedicated with both drugs to treat depression and hypercholesterolemia. Using electronic medical records, the authors evaluated changes in blood glucose levels in response to treatment with these drugs. Each drug on their own did not cause any changes to blood glucose levels whereas comedication resulted in an increase of glucose levels from 110 mg/dL to 128.6 mg/dL. This increase was even larger when diabetic patients were included in the analysis. Glucose levels changed from 115.2 mg/dL to 163.2 mg/dL.

Jia *et al.* (2009) have assembled a comprehensive list of drug interactions reported in the literature. The authors also attempted to classify these interactions based on their mechanism of interaction.

### **Systematic screens to identify effective drug combinations**

A pragmatic approach to identify drug combination is their empirical discovery through high-throughput screening of compound combinations in disease model assays. However, the sheer number of possible combinations renders this approach intractable. Even a small library of 1000 compounds results in nearly half a million possible combinations.

One way to reduce the screening space is the use of an 'anchor drug'. Combination therapies to treat rheumatoid arthritis were designed around 'anchor drugs', compounds with low toxicity and rapid, sustained action. Other drug(s) can then be added sequentially, allowing drug combinations to be tailored to each

patient. Sulphasalazine and methotrexate have been described as good 'anchor drugs' to treat rheumatoid arthritis (Farr & Bacon, 1995; Pincus, 2003). Such an 'anchor drug' can be used in combination screens using chemical libraries to identify agents that synergise with this drug. This reduces the combinatorial space to be screened greatly. Zhang *et al.* (2007) identified microbial metabolites that synergise with the antifungal agent ketoconazole. They screened 20,000 microbial extracts in combination with ketoconazole and then purified six natural product compounds from the 12 extracts that were hits. Ejim *et al.* (2011) screened the antibiotic minocycline in combination with previously approved drugs and identified 41, 35 and 6 drug combinations that showed synergy in the model organism *Escherichia coli* and the bacterial pathogens *Staphylococcus aureus* and *Pseudomonas aeruginosa*, respectively. Fluconazole was used as an anchor drug to find effective antifungal combination therapies (Spitzer *et al.*, 2011). 148 previously approved drugs were found to synergise with fluconazole in the budding yeast and three different pathogenic fungi. Spectinomycin was successfully used as an 'anchor drug' by Ramón-García *et al.* (2011) to identify synergistic drug combinations for tuberculosis therapies. All these screens were done at a single concentration and hits were confirmed with concentration matrices to assess the drug interactions further.

A more thorough approach to discover synergistic drug combinations between previously approved drugs was taken by Borisy *et al.* (2003). They set up a high-throughput screen where each drug combination was assessed in a 6x6 matrix. Screening efforts were kept to a minimum by pooling drugs that did not show activity on their own. Synergistic drug combinations against fluconazole-resistant *C. albicans* were identified as well as anti-inflammatory drug combinations. The most promising discovery came from a screen of 100,000 drug combinations against human tumour cells. The antipsychotic chlorpromazine and the antiparasitic agent pentamidine were identified and subsequently shown to act highly synergistic to prevent tumour growth in mice. The drug combination was patented by CombinatoRx in 2003 and Lee *et al.* (2007) reported that chlorpromazine treatment results in mitotic arrest and causes monopolar spindles whereas pentamidine causes chromosomal segregation defects and delayed

progression through mitosis. The combination was also shown to synergise with microtubule-binding agents in three-way combinations.

### **Computational approaches to identify effective drug combinations**

A lot of data is available on cellular responses to drug treatments like gene expression profiles, chemical-genetic profiles and others. It is desirable to use computational methods to assess the effect of treatment with drug combinations to predict effective multicomponent therapies, or at least to reduce the space of possible drug combinations to test experimentally. Nelander *et al.*, (2008) derived a model of regulatory interactions in breast cancer cells based on results of combinatorial perturbation experiments. Read-outs included growth phenotype as well as molecular states of proteins. They correctly recovered known regulatory couplings and feed-back loops and the authors suggest that models can be built to predict the effects of drug combinations to optimise existing combination therapies and to discover new ones. A similar approach was taken by Iadevaia *et al.* (2010). The authors designed optimal drug combinations against a breast cancer cell line by focussing on the insulin-like growth (IGF) factor signalling network. Data on protein phosphorylation after IGF-1 stimulation for mass action modelling was used to predict drug combinations that minimised phosphorylation of other proteins in the network. They confirmed their prediction that simultaneous inhibition of MAPK and PI3K/AKT pathway decreases viability of cancer cells.

Another approach, Medicinal Algorithmic Combinatorial Screen, uses optimisation strategies based on search algorithms to enrich for activity of drug cocktails against cancer cell lines (Zinner *et al.*, 2009). By cycling between experimental evaluation of drug combinations and rule-based creation of new combinations of any size, a three-way drug combination was rapidly identified as most active from a pool of 19 drugs.

Jansen *et al.*, 2009, used chemical genetic profiles to generate a list of 18 compounds that were predicted to synergise with fluconazole of which 11 and 10 combinations were confirmed to be synergistic against *S. cerevisiae* and *C. albicans*, respectively.

RNA interference (RNAi) screens in mammalian cells have also been used to devise synergistic drug combinations. Bauer *et al.* (2010) identified gene products that increase sensitivity to paclitaxel in breast cancer cells when they are targeted with RNAi. Known drugs that target the top hits from the RNAi screen were then tested in combination with paclitaxel and found to be synergistic in 2D and 3D cultures and in paclitaxel-resistant cell lines. A similar approach was taken by Seyhan *et al.* (2011). Breast cancer cells were screened against an RNAi library in the presence of neratinib. Various biological pathways were identified and treatment of cells with combinations of neratinib and paclitaxel or cytarabine resulted in synergistic effects in both cases.

## 1.4 Aims of this thesis

The overall aim of this thesis is the application of yeast functional genomic approaches to interrogate the mode of action of small molecules that were identified in drug discovery screens in pathogenic fungi and zebrafish. First, I will characterise known drugs that showed synergistic interactions with the antifungal fluconazole in a high-throughput screen to reveal mechanisms of synergy. Second, I will present experiments in the budding yeast that complement experimental approaches in zebrafish to understand the effects of small molecules on zebrafish melanocytes. I also developed and implemented different approaches to analyse chemical genomics data that was generated in the context of these projects.

## 2.1 General materials and methods

### 2.1.1 Yeast media

Tyers lab Extra YPD media (XY)

10 g Bacto yeast extract

20 g Bacto peptone

0.1 g Adenine

0.2 g Tryptophane

Synthetic complete media (SC)

1.7 g yeast nitrogen base without amino acids or ammonium sulphate

2 g amino acid master mix

5 g ammonium sulphate or 1 g L-glutamic acid potassium salt (if adding G418 to media later)

Media was brought up to a volume of 900 mL with dH<sub>2</sub>O and autoclaved. 100 mL 20% glucose was added before use for a final sugar concentration of 2%. To pour plates, 20 g Bacto agar was added to the medium before autoclaving. Glucose



was added before pouring plates.

### **2.1.2 Chemicals**

Most chemicals were ordered from Sigma Aldrich. Chemicals were dissolved in DMSO and aliquots of mM stock solutions stored at  $-20^{\circ}\text{C}$ . Fluconazole was the only exception in that it was dissolved in distilled water and stored at room temperature.

### **Maybridge drugs**

Many of the drugs in Chapter 4 were from the Maybridge Screening Collection. For follow up experiments, 25 mg these drugs were ordered via Thermo Fisher Scientific. They were dissolved in DMSO and aliquots stored at  $-20^{\circ}\text{C}$ .

### **2.1.3 Buffers and solutions**

Winston-Hoffman Lysis buffer

2% Triton X-100, 1% SDS, 100mM NaCl, 10mM Tris.Cl pH8.0, 1mM EDTA  
pH8.0

SSPE

3M NaCl  
0.2M  $\text{NaH}_2\text{PO}_4$   
20mM EDTA

Triton X-100

10 mL of TRITON X-100 were poured (very slowly) into beaker with 70 ml water and stir bar. Solution was stirred until the TRITON X-100 dissolved completely.

Ammonium acetate, 4 M

Made with distilled water, adjusted to pH 7.0

Sodium acetate

Made with distilled water, adjusted to pH 5.2.

TE

10 mM Tris, pH 7.5

1 mM EDTA

#### 2.1.4 *S. cerevisiae* barcode microarrays

##### Materials

- Microarrays - were printed by the Samuel Lunenfeld Research Institute Microarray Laboratory in Toronto, Canada<sup>1</sup>.
- Lifter slips from Thermo Scientific
- Stabilisation and Drying Solution from Agilent

##### Primers used for the barcode microarrays

D2-cy3 Cy3-CGAGCTCGAATTCATCGAT

D2-cy5 Cy5-CGAGCTCGAATTCATCGAT

U2-Cy3 Cy3-GTCGACCTGCAGCGTACG

U2-Cy5 Cy5-GTCGACCTGCAGCGTACG

D1 CGGTGTCGGTCTCGTAG

U1 GATGTCCACGAGGTCTCT

D2 ATCGATGAATTCGAGCTCG

U2 CGTACGCTGCAGGTCGAC

##### Summary of chemical-genetic screening protocol

Deletion pools were subjected to compound treatment, and cell pellets were frozen down for pool composition analysis by barcode microarray. For barcode microarrays, genomic DNA was extracted from drug treated as well as solvent treated cell pellets. Barcode tags were amplified by PCR using common fluorescently labelled UP and DN primers (OPERON Biotechnologies, Germany). The PCR products for experimental and control samples were competitively hybridised to spotted

---

<sup>1</sup><http://www.mshri.on.ca/microarray/>

barcode microarrays (Cook *et al.*, 2008) and spot intensities were analysed to identify sensitive and resistant deletion strains.

### **Generation of deletion pool**

The *S. cerevisiae* deletion collections (MATa and heterozygous deletion strains for essential genes) were obtained from Research Genetics (Germany). Haploid and heterozygous essential deletion pools were generated by pinning the corresponding frozen collections onto XY plates containing glucose and 200 mg/L of G418. After 2 days colonies were condensed to 384 format on XY plates containing glucose. Cells were then scraped into 15% glycerol after another two days of growth. Aliquots of the deletion pool were stored at -80°C.

### **DNA extraction**

Genomic DNA for barcode microarrays was isolated following a protocol modified from the Boeke lab:

1. For drug screens we normally use 2-5 ODU which will give 50  $\mu\text{L}$  of DNA with a concentration of 300-600ng/ $\mu\text{L}$ .
2. Spin cells down at 3600 rpm for 1 min and discard liquid.
3. Add 200  $\mu\text{L}$  volume of glass beads ( 600 $\mu\text{m}$ ), 200  $\mu\text{L}$  of Winston-Hoffman Lysis buffer and 200  $\mu\text{L}$  of phenol/chloroform to each tube.
4. Vortex tubes for 10 minutes at RT. The table vortex works well if tubes are taped onto it. Vortex on setting 7. Briefly spin down the glass beads and liquids from the wall of the tubes.
5. Add 450  $\mu\text{L}$  of 1X TE to each tube and mix well.
6. Spin at 14,000rpm for 4 minutes.
7. Transfer aqueous phase ( 600  $\mu\text{L}$ ) into a new tube with 300  $\mu\text{L}$  of phenol/chloroform. Vortex for 5 minutes.
8. Spin as in step 5.
9. Transfer aqueous phase ( 550  $\mu\text{L}$ ) into a new tube with 300  $\mu\text{L}$  of chloroform (chloroform: isoamyl alcohol: 24:1). Vortex for 5 minutes.

10. Spin as above and transfer the aqueous phase ( 500  $\mu$ L) into a new tube and add 10  $\mu$ L of RNaseA (10mg/ml). Incubate at 37°C for 30 minutes.
11. After incubation, add 300  $\mu$ L phenol/chloroform. Vortex for 5 minutes.
12. Spin tubes at 14,000 rpm for 4 minutes.
13. Transfer aqueous phase ( 400  $\mu$ L) into a new tube containing 300  $\mu$ L chloroform. Vortex for 5 minutes and spin as above.
14. Transfer aqueous phase ( 300  $\mu$ L) into a new tube (normal 1.5 mL Eppendorf tube) and precipitate with 7.5  $\mu$ L of Ammonium Acetate (4M, pH7.0) and 750  $\mu$ L of 100% ethanol. Mix well by inversion.
15. Spin at 14,000rpm for 10 minutes at 4°C.
16. Wash DNA pellet with 70% ethanol.
17. Dry DNA pellet and resuspend in 50  $\mu$ L of TE.
18. After quantification dilute to 50 ng/ $\mu$ L for microarrays.

The DTAB/CTAB (dodecyl- and cetyltrimethylammonium bromide) based method for gDNA isolation was found to not be suitable for DNA extraction for microarray barcode extraction. The PCR reaction to amplify and label the barcodes was not as efficient as with DNA extracted following the protocol above which resulted in low hybridisation intensity.

### Generation of labelled DNA probe

Four PCR reactions are required per microarray since (nearly) every deletion strain has two barcodes, the UP- and the DOWN-tag. These were amplified separately for control and experimental using the U1/U2 and D1/D2 primer pairs, respectively. An example of the four reactions is as follows:

Control	UP-tag	Primers U1 and U2-Cy5
	DOWN-tag	Primers D1 and D2-Cy5
Experimental	UP-tag	Primers U1 and U2-Cy3
	DOWN-tag	Primers D1 and D2-Cy3

Generally, control samples were labelled with Cy5 and experimental samples with Cy3. Dye-swap experiments were also conducted to assess dye bias.

A PCR master mix in the following proportions was made and kept on ice:

10x PCR buffer (-Mg)	5 $\mu$ L
50 mM MgCl <sub>2</sub>	1.5 $\mu$ L
2 mM dNTPs	5 $\mu$ L
ddH <sub>2</sub> O	30.3 $\mu$ L
Taq	0.2 $\mu$ L
<hr/>	
Total volume	42 $\mu$ L

These volumes were multiplied by the number of arrays, with 4 reactions per microarray. For each reaction, the following was added to 0.2 mL PCR tubes (with the primer and gDNA combinations as in the table above):

Master mix	42 $\mu$ L
Labelled primer (25 $\mu$ M)	2 $\mu$ L
Unlabelled primer (25 $\mu$ M)	2 $\mu$ L
gDNA (25 ng/ $\mu$ L)	4 $\mu$ L

The following PCR conditions were used for amplification and labelling of barcode sequences:

94°C	3 min
94°C	30 sec )
50°C	30 sec ) <i>x38</i>
72°C	30 sec )
72°C	5 min
4°C	forever

After completion of the PCR program, 2  $\mu$ L of each PCR reaction were run on a 2% agarose gel to assess efficiency of the PCR reactions. The 4 PCR reaction for each microarray were then combined into one Eppendorf tube. The following mix of blocking primers and precipitating agents was added to this:

100 $\mu$ M U1	5 $\mu$ L
100 $\mu$ M D1	5 $\mu$ L
100 $\mu$ M U2block	5 $\mu$ L
100 $\mu$ M D2block	5 $\mu$ L
5 mg/ml linear acrylamide	1 $\mu$ L

The DNA mixture was then precipitated by addition of:

3 M NaOAc, pH 5.2	22.5 $\mu$ L
blocking primer mix	21 $\mu$ L
95% EtOH	550 $\mu$ L

Samples were placed at  $-20^{\circ}\text{C}$  for at least 1 hour.

### Hybridisation of barcode microarrays

Microscope slide boxes were used as chambers for the microarrays with glass slides as pedestals to place the microarrays onto. A small amount of chamber hybridisation buffer (DIG Easy Hybe) was added into these boxes. Microarray hybridisations were conducted following this protocol:

1. Spin samples at 14,000 rpm and  $4^{\circ}\text{C}$  for 30 minutes to pellet the labeled DNA. Wash once with 70% EtOH.
2. Dry briefly at room temperature (5 minutes).
3. Resuspend pellets in 5  $\mu$ l of ddH<sub>2</sub>O
4. Add resuspended sample to 50  $\mu$ L of DIG Easy Hybe.
5. Place the hybridisation buffer containing sample at  $95-100^{\circ}\text{C}$  for 2 min. Fast cool on ice for 5 minutes.
6. Maintain samples at  $50-55^{\circ}\text{C}$  covered from light until ready to add to arrays.
7. Take out arrays one at a time. Add sample to the array and use a large coverslip (24x60) to cover the surface. Be careful of bubbles. The working surface of the arrays is quite large. When you use a 24x60 coverslip, try to make the distance from the edges of the coverslip to the barcode or to the end of the slide about the same. This will allow complete coverage of the probe containing region. Immediately after completion, transfer the array

to the chamber and keep at 25°C. To prevent evaporation of the chamber hybridisation buffer, wrap the edges of the chamber in parafilm.

8. Hybridise overnight at 25°C (>12 hours).

### Washing of microarrays

Washes were prepared as shown in Table 2.1 below. One extra Falcon tube with solution 1 was prepared for each microarray. Falcon tubes with solution 1 were pre-warmed to 30°C. The Agilent stabilisation solution and acetonitrile were also kept at 30°C for 30-60 minutes before beginning the washing procedure (the stabilisation solution sometimes forms white precipitate while it is stored at RT). The coverslips were carefully removed one at a time for each array in the first wash. Washes were performed as indicated in Table 2.1.

	Solution	Temp	Procedure	Container
1	6x SSPE, 0.05% Triton X-100 - 15 mL SSPE - 250 $\mu$ L Triton - 34.75 mL ddH <sub>2</sub> O	30°C	5-10 dips	50 mL, in Falcon tube
2	2x SSPE, 0.05% Triton X-100 - 5 mL SSPE - 250 $\mu$ L Triton - 44.75 mL ddH <sub>2</sub> O	RT	5-10 dips	50 mL, in Falcon tube
3	0.2x SSPE, 0.05% Triton X-100 - 0.5 mL SSPE - 250 $\mu$ L Triton - 49.25 mL ddH <sub>2</sub> O	RT	5-10 dips	50 mL, in Falcon tube
4	0.2x SSPE - 2.5 mL SSPE - 247.5 mL ddH <sub>2</sub> O	RT	5-10 dips	250 mL in black staining box
5	Acetonitrile	RT	10 sec	50 mL, in Falcon tube
6	Agilent Antioxidation solution	RT	30 sec	50 mL, in Falcon tube

Table 2.1: Washing steps for barcode microarrays.

Microarrays were protected from light, scanned with a GenePix 4200AL and hybridisation intensities were analysed with GenePix Pro 6.0 software.

## Analysis of yeast barcode microarray data

Custom R scripts were written to store and analyse the barcode microarray data. The database interface packages DBI and RMySQL as well as data analysis R packages like gplots and limma were used to identify sensitive and resistant deletion strains from the barcode array data. Spots with low intensity as well as spots of low quality were excluded from further analysis. The intensities of duplicate spots on the arrays were averaged. Based on log<sub>2</sub> fold change ratios (drug treatment/solvent-only control), Z-scores were calculated for up and down barcode tags for each strain:  $Z = (x - \mu)/\sigma$  where  $\mu$  is the mean log<sub>2</sub> fold change of the whole array and  $\sigma$  the standard deviation. For each strain, the two Z-scores for up and down barcode tags were averaged to get the final Z-score. Raw data and Z-scores were stored in a custom MySQL database. Sensitive and resistant deletion strains were identified with standard procedures for Z-score and quantile-based statistics for microarray data (Quackenbush, 2002; Cheadle *et al.*, 2003).

## 2.2 Specific methods for Chapter 3

### 2.2.1 Fungal strains and culture conditions

The strains employed in this study were *Saccharomyces cerevisiae* BY4741, *Candida albicans* Caf2-1 (from M. Whiteway), *Cryptococcus neoformans* H99 and *Cryptococcus gattii* R265 (both from J.W. Kronstad) as well as the following fluconazole resistant strains: *Candida albicans* F-1-2008 (clinical isolate), *Candida albicans* F-07-2007 (clinical isolate), *Candida parapsilosis* ATCC 22019 and *Candida glabrata* (all from D. Yamamura). *S. cerevisiae* was grown on SC agar, *Candida* and *Cryptococcus* species were maintained on Sabauroud dextrose agar (Difco<sup>TM</sup>). *S. cerevisiae* and *Cryptococcus* strains were incubated at 30°C, while *Candida* strains were incubated at 37°C.



### 2.2.2 Compounds

Fluconazole (Sandoz, Quebec, Canada) was purchased as a 2 mg/mL solution in water, sodium chloride and hydrochloric acid and/or sodium hydroxide. Albendazole (Sigma, Oakville, Canada), amphotericin B (Sigma), azaperone (Prestwick Chemical, Delaware, USA), clofazimine (Sigma), clomiphene citrate (Sigma), daunorubicin HCL (Sigma), ebselen (Sigma), ellipticine (Sigma), hyamine (Sigma), kawain (Sigma), ketoconazole (Sigma), L-cycloserine (Sigma), lynestrenol (Prestwick Chemicals), mevinolin (Sigma), mitoxantrone dihydrochloride (Sigma), nitrofurantoin (Sigma), sertraline (Sigma), suloctidil (Sigma), tamoxifen citrate (Sigma), trifluoperazine dihydrochloride and zaprinast (Sigma) were purchased as standard powders. All stock solutions were prepared in 100% dimethyl sulfoxide (DMSO). Fluconazole was stored at room temperature while all other stock solutions were kept at -20°C.

### 2.2.3 High-throughput screen of Prestwick library

The Prestwick Chemical library ([www.prestwickchemical.com](http://www.prestwickchemical.com)) was screened in duplicate against *Candida albicans*, *Cryptococcus neoformans*, *Cryptococcus gattii* and *Saccharomyces cerevisiae* at a final concentration of 30  $\mu$ M. Screens were conducted in 384-well flat bottom microtitre plates in the presence and absence of 1/2 MIC fluconazole. Each plate included 32 high growth and 12 low growth control wells. Plates were incubated for 48 hours at 30°C or 37°C and OD<sub>600</sub> was determined for each well. These absorbance values were then corrected using the control values for each plate and percent residual activity was calculated for every compound in each screen.

### 2.2.4 Data analysis of Prestwick library screen

Replicate screens were examined using scatterplots to assess the correlation between replicate screens. Residual activity values were averaged between duplicate screens. Plate-wise normalisation was then conducted to remove column-, row- and plate-bias in the data. Application of robust median absolute deviation

(MAD; Chung *et al.*, 2008; Birmingham *et al.*, 2009) statistics to scatterplots of screen data in the presence of fluconazole versus Prestwick library alone allowed us to define hit compounds. Compounds that on their own did not affect growth below noise levels but were more than 2 MADs away from the diagonal of the with-versus-without-fluconazole scatterplot were identified as active. Within this group, compounds that caused more than 80% growth inhibition in the presence of fluconazole were defined as highly active.

### 2.2.5 Determination of MIC

Procedures for MIC determination were based on Clinical and Laboratory Standards Institute protocols<sup>2</sup>. Overnight cultures of the corresponding fungal strain were set up in SC media and then diluted in 0.85% NaCl to an OD<sub>530</sub> of 0.11, followed by a 1:100 dilution in 0.85% NaCl and finally a 1:20 dilution in SC media. Two-fold dilution series (0-128  $\mu\text{g}/\text{mL}$ ) of fluconazole and other drugs were set up and added to 200  $\mu\text{L}$  of the diluted culture in 96 well plates. After 48 hours of growth at 30°C or 37°C, OD<sub>600</sub> was measured with a microplate absorbance reader. The minimum inhibitory concentration (MIC) for fluconazole was defined as the lowest concentration causing 80% reduction in growth which corresponds to 2 on the azole MIC numerical scale. MIC for other drugs was set as the lowest concentration that inhibited growth completely. 6 different concentration combinations of compound and fluconazole were used for time kill MIC assays (compound at 1/4 MIC, compound at MIC, fluconazole at 1/4 MIC, fluconazole at MIC, fluconazole and compound both at 1/4 MIC, and fluconazole and compound both at MIC). Dilutions from each well were spotted at 0, 24 and 48 hours onto an SC agar plate. Colonies were counted after an 48 hour incubation. The definition of a fungicidal effect was  $>3 \cdot \log_{10}$  reduction in CFU/mL (99.9% killing) at synergistic concentrations after incubation for 24 hours.

---

<sup>2</sup>formerly the National Committee for Clinical Laboratory Standards; <http://www.clsi.org/documents>

## 2.2.6 Synergy assessment

Syncretic compounds and fluconazole were 2-fold serially diluted across rows and columns of a 96 well plate (0-128  $\mu\text{g}/\text{mL}$ ; except for daunorubicin, terbinafine, trifluoperazine and ellipticine which ranged from 0-64  $\mu\text{g}/\text{mL}$ ). The checkerboards were incubated with fungal cultures and  $\text{OD}_{600}$  was determined after 48 hours. The fractional inhibitory concentration index (FICI) of each drug combination was determined according to standard CLSI protocols (Eliopoulos & Moellering, 1991; Odds, 2003):

$$FICI = \frac{MIC_{Drug\ A\ in\ combination}}{MIC_{Drug\ A\ alone}} + \frac{MIC_{Drug\ B\ in\ combination}}{MIC_{Drug\ B\ alone}}$$

To probe chemical interactions between sertraline, trifluoperazine, L-cycloserine, suloctidil and tamoxifen, checkerboard assays were carried out between these 5 compounds in the absence and presence of 1/2 and 1/8 MIC fluconazole (16 and 4  $\mu\text{g}/\text{mL}$ , respectively).

## 2.2.7 Chemical-genetic screens

Concentrations that caused up to 30% growth inhibition in the deletion pools after 12 hours incubation with a starting  $\text{OD}_{600}$  of 0.025 were determined for clomiphene, L-cycloserine, sertraline, suloctidil, tamoxifen, trifluoperazine and fluconazole. For each of the synergising drugs, a 5 x 5 matrix of increasing concentrations of each drug (concentrations causing up to 25% growth inhibition) and fluconazole (0-8  $\mu\text{g}/\text{mL}$ , corresponding to growth inhibition of 0-25%) was set up in 10 mL cultures. Single drug dilution series with up to 30% growth inhibition as well as solvent-only controls (DMSO, water) were set up as well. The final DMSO concentration was 0.2% for all screens. Deletion pools were grown for about 10 generations, until saturation of the cultures. Cell pellets were frozen down for DNA extraction.

The microarray data for this project is available on ArrayExpress (E-MTAB-394).

## 2.2.8 Validation of chemical-genetic interactions

### Growth assays in 96 well format

Chemical-genetic interactions from barcode microarray experiments were confirmed with growth assays in 96-well flat-bottom polystyrene plates (Corning Incorporated, USA) on Sunrise shaker/readers (Tecan). Single gene deletion and wild type strains were grown in the presence of dilution series of clomiphene, L-cycloserine, sertraline, suloctidil, tamoxifen, trifluoperazine and fluconazole. OD<sub>600</sub> readings were taken every 15 minutes. All assays were done in XY medium with a starting OD of 0.0025. The final DMSO concentration was 2%. Log ratios between deletion and wild type strains were calculated from OD values at the time point where control wells have reached the end of log phase (with custom R scripts). Negative log-ratios indicate sensitivity of a deletion strain to a drug whereas positive ratios denote resistance.

### 2.2.9 Sorbitol rescue assay

Sorbitol rescue assays were done in 96-well plates using the Tecan Sunrise plate readers. 100 $\mu$ L cultures of BY4741 were set up in XY medium with 1M sorbitol (from 5 M stock) or with water as control. Drugs and solvent controls were added as indicated.

### 2.2.10 *In vivo* imaging of effects of synergising compounds

Drug concentrations that affected growth of *S. cerevisiae* significantly were used for imaging (64  $\mu$ g/mL for fluconazole, 128  $\mu$ g/mL for L-cycloserine and sertraline). Cells were grown to log phase, then drug was added and cultures were grown for another 1 or 3 hours (results were the same for both incubation times). Dyes used were Hoechst dye (Bisbenzimidazole H 33258, Sigma), Calcofluor White M2R (Fluorescent Brightener 28, Sigma), FM4-64 (N-(3-triethylammoniumpropyl)-4-(6-(4-(diethylamino)phenyl)hexatrienyl)pyridinium dibromide, Molecular Probes) and Mitotracker Green FM (Molecular Probes). For all dyes, cells were harvested by centrifugation at 12,000 rpm for 2 minutes. After washing and staining, cells

were mounted on slides with 1% low melt agarose for imaging. For DNA staining, cells were resuspended in 40  $\mu\text{L}$  YPD and 10  $\mu\text{L}$  of 200  $\mu\text{M}$  Hoechst dye (dissolved in  $\text{dH}_2\text{O}$ ), grown for 15 minutes at 30°C, washed once with  $\text{dH}_2\text{O}$  and resuspended in 15  $\mu\text{L}$   $\text{dH}_2\text{O}$  for slide mounting. Cells were resuspended in 198  $\mu\text{L}$  0.1 M Tris/HCl, pH 8 and 2  $\mu\text{L}$  of 3.5 mg/mL Calcofluor White M2R (in  $\text{dH}_2\text{O}$ , 1 drop of 5M NaOH was added to stock solution to aid solubility) for cell wall staining. Cells were then grown for 15 minutes at 30°C, washed once with  $\text{dH}_2\text{O}$ , resuspended in 15  $\mu\text{L}$   $\text{dH}_2\text{O}$  and mounted. For mitochondria labelling, cells were resuspended in pre-warmed, Mitotracker Green containing YPD (500nM). After 45 minutes incubation at 30°C, cells were washed with 200  $\mu\text{L}$  PBS and resuspended in 15  $\mu\text{L}$   $\text{dH}_2\text{O}$  for mounting. Vacuolar membranes were stained by resuspending cells in 40  $\mu\text{L}$  YPD with 1  $\mu\text{L}$  of FM4-64 (1 mg/mL, dissolved in DMSO). Cells were incubated for 15 minutes at 30°C, spun down, resuspended in 15  $\mu\text{L}$  PBS and mounted. Imaging was done on a Leica DMI 6000 B microscope with a Hamamatsu Orca ER-AG camera and Volocity 4 software. Images were deconvolved with AutoDeblur Gold CWF using 2-D blind deconvolution (10 iterations per image).

### **2.2.11 Insect larvae assays**

Per dish, ten weight matched (250-400 mg/worm) *G. mellonella* caterpillars were inoculated with *C. neoformans* H99. 24 hours later they were injected with sertraline and fluconazole combined, sertraline and fluconazole alone and/or control solutions (DMSO and PBS) (Mylonakis *et al.*, 2005). Over 7 days, caterpillars were examined visually for discolouration due to melanisation and for failure to respond to touch as an inviability endpoint. Experiments were performed in triplicate.

### **2.2.12 Computational analysis of gene-drug network interactions**

Analysis of genetic interactions between sets of genes sensitive to drug treatment was based on genetic interaction data acquired from BioGRID (Breitkreutz *et*

*al.*, 2008; BIOGRID release 2.62 from [www.thebiogrid.org](http://www.thebiogrid.org)). The visualisation of bipartite graphs and simulations were performed with an online tool available at [http://tyerslab.bio.ed.ac.uk/tools/genelookup\\_bipartite.php](http://tyerslab.bio.ed.ac.uk/tools/genelookup_bipartite.php).

Simulations based on chemical-genetic space (CGS) were done with a set of 1143 non-essential deletion strains that respond to various drug treatments (Hillenmeyer *et al.*, 2008). For each drug pair, control gene sets of the same size were picked at random and the number of genetic interactions between the sets was counted to generate a background distribution, which was used to calculate the p-value for each drug pair. For parallel pathway permutation (PPP) simulations, the chemical-genetic interactors of fluconazole and each of the synergistic drugs were pooled, randomly assigned to two groups and genetic interactions counted to obtain a background distribution for each drug pair. 10,000 simulations were run for the CGS and the PPP approaches.

## **2.3 Specific methods for Chapter 4**

### **2.3.1 Zebrafish methods**

#### **Phenotypic screen**

Embryos were acquired by pair breedings of wild-type AB, AB\* and TL zebrafish lines. Phenotypic screens with small molecules were done in 96-well microtiter plates. Each well contained two 4-hpf zebrafish embryos in 300  $\mu$ L E3 embryo medium. Compounds were added to a final concentration of 10  $\mu$ M in 1% DMSO. Compound libraries screened were the LOPAC Small Scale International Version (1280 compounds; from Sigma-Aldrich) and a set of 1570 bioactive compounds (a subset of the Maybridge screening collection from Fisher Scientific International; described in Spitzer *et al.*, in preparation). Embryos were imaged for phenotypic changes at several time points: 28-hpf, 36-hpf, 48-hpf and 56-hpf.

#### **Small molecule treatment**

CI-1040 was obtained from Richard Marais (London, UK) and PD0325901 was kindly provided by Hilary McLauchlan (University of Dundee, UK). Embryos at

different developmental stages were treated with neocuproine and U0126 at 10  $\mu$ M or 25  $\mu$ M and PD0325901 at 1  $\mu$ M or 2.5  $\mu$ M. Inhibition of MEK pathway activity during development was achieved by treating 4-hpf embryos with compounds continuously until 12 hpf; immediate effects were assessed by applying a single dose of compound from 10 hpf to 12 hpf.

### **Western blotting**

12-hpf Embryos were frozen (at  $-80^{\circ}\text{C}$ ). Lysis of samples was done in RIPA buffer [2M Tris pH 7.5, 5M NaCl, 1% NP40, Na-deoxycholate, 10% SDS, 0.5 M NaF, 1M  $\beta$ - glycosyl phosphate and protease-inhibitor cocktail tablet (Roche)]. Bradford assays were used to normalise samples which were then separated by SDS-PAGE, transferred to a Hybond-C Extra nitrocellulose membrane (Amersham Biosciences) and probed with rabbit [p44/42 MAPK (1:2000) and phospho-MEK1/2 (Ser217/221) (1:500) (Cell Signaling Technology)] or mouse [phospho-p44/42 MAPK (E10) (1:2000), alpha-tubulin B-5-1-2 (1:50,000) (Santa Cruz)] antibodies. Detection was carried out with with horseradish-peroxidase- conjugated secondary antibodies (Roche).

### **Electron microscopy**

Embryos were fixed with 2.5% glutaraldehyde, 2% paraformaldehyde in 100 mM cacodylate buffer (pH 7.2) with 2 mM  $\text{MgCl}_2$  and 0.1% picric acid. After a wash with 200mM cacodylate buffer, samples were fixed with 1% osmium tetroxide in 100mM cacodylate buffer (pH 7.0), then washed with distilled water, stained en bloc with 0.5% aqueous uranyl acetate, and dehydrated with ethanol. Samples were embedded in Agar 100 resin, sections were cut, stained (with lead citrate) and viewed on a transmission electron microscope (FEI Tecnai 12).

### **Morpholino oligonucleotides**

Gene Tools (USA) designed all four MOs. One MO was designed to block splicing of ap3s2, a zebrafish ortholog of the yeast gene APS3. The MO sequence for ap3s2-MO1 was: 5'- TGCAAAAGCCTCTCCATCACCTTCC-3'. Ac-

tivity of ap3s2-MO was confirmed by PCR with the following primers: AP3S2-F1 [5'-TCAACAACCATGGGAAACCC-3' (forward primer)] and AP3S2-R1 [5'-TGACTGCAGAAACGGCTCG-3' (reverse primer)]. Inclusion of intron 2 was determined by sequencing of the longer cDNA product. A second MO blocked translation of ap1s1, a zebrafish ortholog of the yeast gene APS1. The sequence for ap1s1-MO1 was: 5'-ACAGA- AGCATAAAGCGCATCATTTTC-3'. This MO has been previously verified by Western blotting of morphant embryo extracts with an antibody (Montpetit *et al.*, 2008). In addition, two splice-site MOs were used: ap3s2-MO2 (5'-TGCAGTTACGTTACCTGTATAAGA-3') and ap1s1-MO2 (5'-GACTAGCATAACCTACGTAAACACAC-3') (Montpetit *et al.*, 2008). Activity of ap3s2-MO2 activity was confirmed by PCR with primers AP3S2-F2 [5'-TGCAGCAGCAGATCATCAGGG-3' (forward primer)] and AP3S2-R2 [5'-GACTGTCAGTAATGG- CAAGAGG-3' (reverse primer)]. For each gene, results were consistent with both MOs, with increasing concentration of MO (5-10 pg) eliciting greater effects. 1 mM stock solutions were prepared for each MO with water. For Figure 5A, we injected 1-3 pg into each one-cell stage embryo. All MOs were labeled with a fluorescent tag to assess even MO distribution throughout the embryo. Changes in pigmentation were assessed by at least two individuals who scored the phenotypes blinded to the MO genotypes.

### 2.3.2 Yeast methods

#### Yeast chemical-genetic profiles

The MATa haploid and the essential heterozygous yeast deletion sets (Research Genetics, Germany) were used to generate chemical-genetic profiles. Deletion pools were created as described in Section 2.2.7. The growth-inhibition screens are slightly different from the screens described in Section 2.2.7. 5-mL deletion-pool cultures were set up with a starting OD<sub>600</sub> of 0.025. After a 2-h pre-growth period, compound or DMSO for solvent control samples was added. Compound concentrations were selected such that pool growth was inhibited by 20-30% compared to control cultures after 12 hours at 30°C. Cultures were then diluted to an OD<sub>600</sub> of 0.025 twice and fresh compound was added both times to allow for



competitive growth for a total of 20 generations. Each compound was screened at two concentrations. The final DMSO concentration was 0.4% in all cultures.

The microarray data is available at ArrayExpress (accession number E-TABM-922).

### **Assignment of GO biological process terms**

Rather than relying on fixed cut-offs to define GO biological processes that are enriched among the deletion mutants that were most affected by compound treatment, average Z-scores were determined for all biological processes with data for at least four genes. For each screen, we applied quartile-based statistics to identify significantly affected processes. Annotations were taken from Saccharomyces Genome Database (<http://www.yeastgenome.org>, release 02/07/2009).

---

# Interrogating the Mode of Action of Small Molecule Synergies in Yeast

---

Most of the work presented in this chapter has been published in:

- Michaela Spitzer<sup>1</sup>, Emma Griffiths<sup>1</sup>, Kim M. Blakely, Jan Wildenhain, Linda Ejim, Laura Rossi, Gianfranco De Pascale, Jasna Curak, Eric Brown, Mike Tyers, and Gerard D. Wright: Syncretic Drug Combinations Potentiate the Antifungal Fluconazole and Overcome Pathogen Resistance. *Molecular Systems Biology* (2011 Jun 21).

This project was carried out in collaboration with Gerry Wright's lab at MacMaster University in Hamilton, Canada. The McMaster lab screened the Prestwick library against four different fungal species. Emma Griffith and Kim Blakely carried out the follow-up experiments in all four species to confirm drug interactions. Emma also confirmed the synergy of sertraline with fluconazole in fluconazole-resistant *Candida* strains and in the *G. mellonella in vivo* infection model and she tested higher order combinations of synergising compounds. Microscopy images were taken by Laura Rossi, Jasna Curak and Gianfranco De

---

<sup>1</sup>The first two authors are joint first authors and contributed equally to this work.

Pascale. Jan Wildenhain implemented the chemical-genetic space and the parallel pathway permutation simulations. He also clustered the hit compounds based on their chemical structures.

The data analysis of the screen (normalisation, identification of hit compounds and overlap between the different species) as well as the analysis of the structural clusters among the hits were done by me. I selected a subset of hit compounds for the mode of action studies in *S. cerevisiae*, conducted the genome-wide screens, analysed the chemical-genetic data, confirmed chemical-genetic interactions and carried out the sorbitol rescue assay. I also worked on the integration of chemical-genetic interactions with genetic interaction networks with Jan. All figures were generated by me and all graphs and heatmaps were plotted with R, unless stated otherwise. All figures except for 4.1, 4.2, 4.7A & C, 4.11, 4.13 and 4.27 were either taken or adapted from the paper or the supplementary information of Spitzer *et al.* (2011) according to the creative commons share-alike licence.

### 3.1 Introduction

Systemic infections caused by invasive fungi present a major threat to critically ill patients (Gullo, 2009). In recent years, the frequency of fungal infections has increased dramatically. Between 1979 and 2000, the number of fungal bloodstream infections has increased by more than 200% in the United States (Pfaller & Diekema, 2007). Immune-compromised individuals, like cancer chemotherapy, HIV-infected and organ transplant patients, are especially susceptible to viral, bacterial and fungal infections that are normally defeated by a healthy immune system. The single most prevalent fungal pathogen among intensive care unit patients is *C. albicans*, accounting for 17% of infections (Gullo, 2009). Infections with other *Candida* species as well as the *Cryptococcus* and *Aspergillus* genera are also increasing, especially in immune-compromised patients (Clark & Hajjeh, 2002; Gullo, 2009). Significant morbidity and mortality are associated with invasive fungal infections but unfortunately therapeutic options are limited as compared to bacterial infections.

Unlike bacteria, fungal pathogens are eukaryotes which means that their

metabolism and cellular structures are more similar to mammalian host cells. The first scientific breakthrough was the discovery of polyene antifungals in the 1950s. Amphotericin B is still the front line fungicide even though it causes severe host toxicity because it non-specifically disrupts cell membrane integrity. Continued efforts to improve this drug resulted in a less toxic liposomal formulation of amphotericin B about ten years ago. The 1970s saw the development of the synthetic azoles that target fungal ergosterol biosynthesis by inhibiting lanosterol 14 $\alpha$ -demethylase, the gene product of *ERG11*, an essential cytochrome P450 enzyme (Groll *et al.*, 1998; Revankar *et al.*, 2004). Ketoconazole was the first azole to be approved for the treatment of systemic fungal infections in 1981. It was soon found to interact with many other drugs and to cause hepatic toxicity. The first-generation triazoles (fluconazole and itraconazole) were introduced in the early 1990s and represented a major improvement in the treatment of systemic fungal infections because they displayed a broader spectrum of antifungal activity. The azoles act by binding the heme Fe(III) of Erg11 which results in depletion of ergosterol, accumulation of toxic C-14 methyl sterols and cell membrane disruption. Even though the triazoles had an improved safety profile, their cross-reactivity towards human P450 enzymes also results in toxicity. A major clinical limitation is the fact that these drugs are fungistatic and clinical resistance emerges (Cannon *et al.*, 2009; Marie & White, 2009). Second-generation triazoles have been developed and their host toxicity is still being assessed. Voriconazole, posaconazole and ravuconazole are supposed to have greater potency and possess increased activity against resistant and newly emerging pathogens. Allylamines, like terbinafine, are compounds that also target the ergosterol biosynthesis pathway, but they inhibit squalene synthase. Their antifungal specificity is based on the fact that the fungal form of squalene synthase is much more sensitive to treatment than the mammalian one. The newest class of antifungal compounds are the echinocandins and they target one of the few structures that are fungus-specific, the cell wall. They were introduced ten years ago and inhibit  $\beta$ -(1,3)-D-glucan synthase, a cell wall biosynthesis enzyme. However, these drugs are limited in their antifungal spectrum. The dearth of safe and effective antifungal therapies and the threat posed by emerging clinical drug resistance make the development

of novel antifungal strategies a necessity.

Traditional single-agent therapies require fungal-specific targets that are essential for pathogen cell growth. The scarcity of essential drug targets is a major challenge in antifungal drug discovery. One factor contributing to this problem is the high degree of conservation of biochemical and molecular biological networks across all eukaryotes. Another reason is the extensive buffering found in biological networks. The systematic deletion of every single gene in the model yeast *S. cerevisiae* revealed that  $\sim 5000$  of its  $\sim 6000$  genes are actually dispensable for growth in nutrient-rich growth conditions (Winzeler *et al.*, 1999). This problem is aggravated by the fact that many of the essential genes can provide sufficient function at only a fraction of wild type dosage (Yan *et al.*, 2009). Genome-wide genetic screens in the budding yeast have revealed that almost all non-essential genes display synthetic genetic interactions (Tong *et al.*, 2001). This means that the deletion of non-essential genes becomes lethal in specific genetic backgrounds where another non-essential gene has been deleted. It has been estimated that the yeast genetic landscape is governed by more than 200,000 binary synthetic lethal interactions (Costanzo *et al.*, 2010).

The robust organisation of genetic networks as well as the success of combinatorial therapies suggests that systematic drug design approaches should focus on multicomponent drugs. Combinations of small molecule inhibitors of essential as well as non-essential targets have been shown to exhibit additive or even synergistic effects on cell viability (Sharom *et al.*, 2004; Ágoston *et al.*, 2005; Fitzgerald *et al.*, 2006; Lehár *et al.*, 2007; Lehár *et al.*, 2008). Fungal infections are often treated with ad hoc combinations of anti-infective drugs (Johnson & Perfect, 2010). This approach however, fails to exploit the complexity of the chemical-genetic space (Sharom *et al.*, 2004; Lehár *et al.*, 2008). Instead, unbiased screens for small molecule combinations that show unexpected interactions are needed to fully explore the chemical-genetic landscape. These have been referred to as syncretic combinations (Keith *et al.*, 2005). As described in Section 1.3.5, focused small molecule library screens (Borisy *et al.*, 2003; Zhang *et al.*, 2007; Zhai *et al.*, 2010) as well as computational approaches (Lehár *et al.*, 2007; Nelander *et al.*, 2008; Jansen *et al.*, 2009; Zinner *et al.*, 2009) have successfully identified com-

pounds that enhance the activity of known drugs in budding yeast and in cancer cell lines. Further, direct tests of synergistic compounds have yielded drug combinations that are active against pathogenic fungi, including the combination of fluconazole with chemical inhibitors of Hsp90, calcineurin or ARF (Cowen *et al.*, 2009; Singh *et al.*, 2009; Epp *et al.*, 2010) and the antibiotic polymyxin B (Zhai *et al.*, 2010).

The aim of the work described in this chapter was the identification of compounds that potentiate the action of the antifungal drug fluconazole.

## 3.2 Results

### 3.2.1 A high-throughput screen identifies 148 compounds that potentiate the action of fluconazole

The Prestwick Chemical library consists of 1120 bioactive compounds, 90% of which are off-patent drugs and 10% are bioactive alkaloids or related substances. This collection was used in cell-based high-throughput screens against the human pathogens *C. neoformans* (H99), *C. gattii* (R265) and *C. albicans* (Caf2-1) as well as the model yeast *S. cerevisiae* (BY4741). Screens were conducted in duplicate at a concentration of 30  $\mu\text{M}$  in the presence and absence of 1/2 MIC fluconazole to identify compounds that have minimal antifungal activity on their own but potentiate the anti-fungal action of fluconazole. Residual activity was determined for each compound in each of the eight screens by normalising final OD values for each drug against control wells within each plate.

#### Normalisation of HTP data

Systematic errors in HTP screen data are a well known problem and methods for the correction of biases have been developed for a range of applications, including microarrays (Quackenbush, 2002), *in vitro* screening of chemical libraries (Malo *et al.*, 2006) and RNA interference screens (Birmingham *et al.*, 2009). In the context of cell-based small molecule screens, such as this one, edge effects are a valid concern (Lundholt *et al.*, 2003). This means that wells along the edge

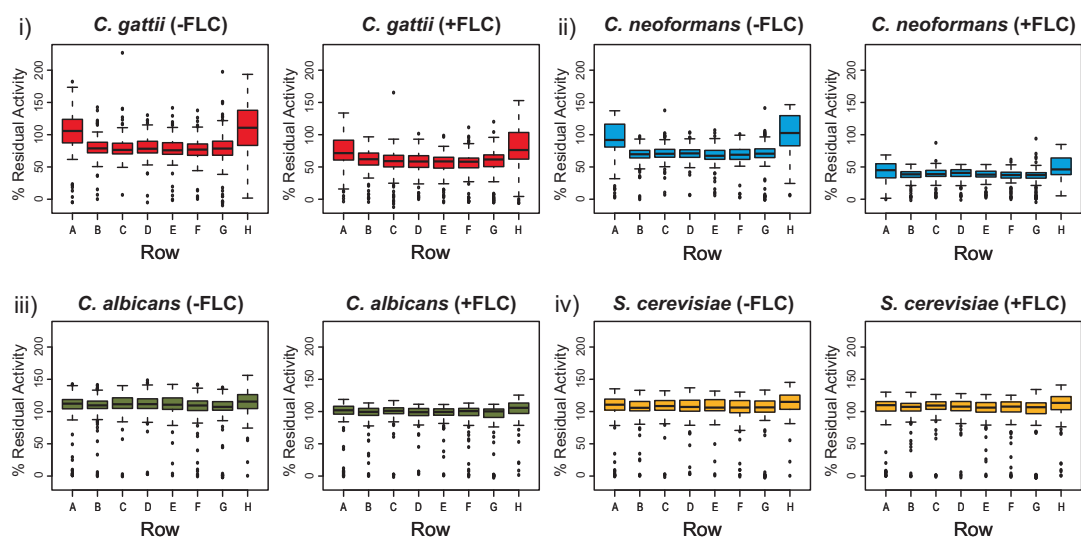


Figure 3.1: Visualisation of row effects in HTP screen data of (i) *C. gattii*, (ii) *C. neoformans*, (iii) *C. albicans* and (iv) *S. cerevisiae* screens with and without fluconazole. For each of the screens, data points for each row from all 14 plates are summarised by a boxplot to visualize the range and spread of values. The box represents the middle 50% of the data, the black line represents the median of the data and points outside the reach of the whiskers are considered outliers.

of a microtitre plate give higher or lower readings than the rest of the plate. A simple way to check screen data for these effects, is to compare the range of residual activities for each column and each row across all plates. Screen data was analysed per column and per row for each of the eight screens. There were no obvious column effects present in any of the screens (data not shown). In contrast, the data points in rows A and H showed a larger spread in all four *C. gattii* and *C. neoformans* screens than the other two screens (Figure 3.1 i,ii). In addition, the wells in these rows had higher residual activity values. A similar trend was observed in the *C. albicans* and *S. cerevisiae* screens, where the spread of all columns was similar, but rows A and H showed a slight increase in residual activity (Figure 3.1 iii, iv). A number of factors can be involved in the generation of such effects such as a bias of the span-8 pipettor used to set up the plates for screens, evaporation in the outer wells during incubation or uneven temperature across the plate during incubation. These effects were removed by correction of the row means towards the plate mean.

The identification of hit compounds is based on the comparison of screen results with and without fluconazole. In Figure 3.2A the raw data for each of

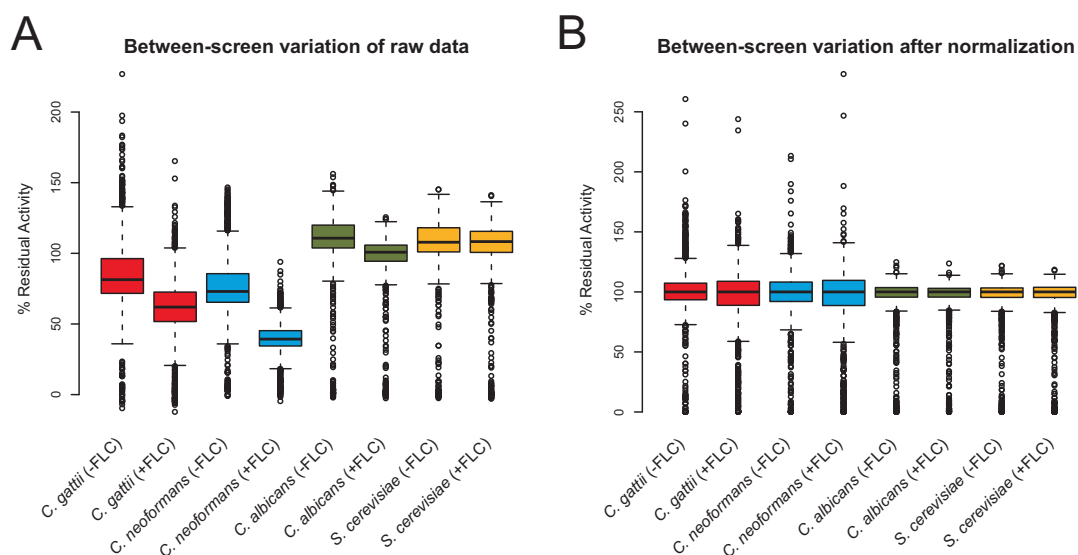


Figure 3.2: Data variation between screens. (A) Box plot summary of the raw % residual activity data for each of the eight screens. Values for screens of *C. gattii* and *C. neoformans* in the presence of fluconazole (boxplots 2 and 4) are much lower than those of the corresponding screens without fluconazole (boxplots 1 and 3). (B) Box plot summary of the % residual activity data after normalisation. Median is now 100 for all screens and the spread of the data is similar in each pair of screens (with and without fluconazole). This facilitates identification of hit compounds.

the screens was summarised by a boxplot. It is obvious that there is variability between the screens in different species. Differences in spread and values of the residual activity can clearly be seen. The outcome of data normalisation based on dividing the data for each plate by the corresponding plate median is shown in Figure 3.2B. The median residual activity is 100% in all screens now. The variation has been greatly reduced and is comparable between the two screens for each species.

To summarise the data normalisation, Figure 3.3 visualises the correction of plate to plate variation as well as row- and column-specific effects. In each of the plots, all 1120 compounds of the library are represented along the x-axis whereas the y-axis corresponds to residual activity as measured for the screen. Each row in Figure 3.3 corresponds to one of the four fungal species. The first and third plot in each row represent the raw data from screens without and with fluconazole whereas the second and fourth graph show the data after normalisation. Strong row effects were corrected in the first three screens (Figure 3.3 i-iii). Screens ii



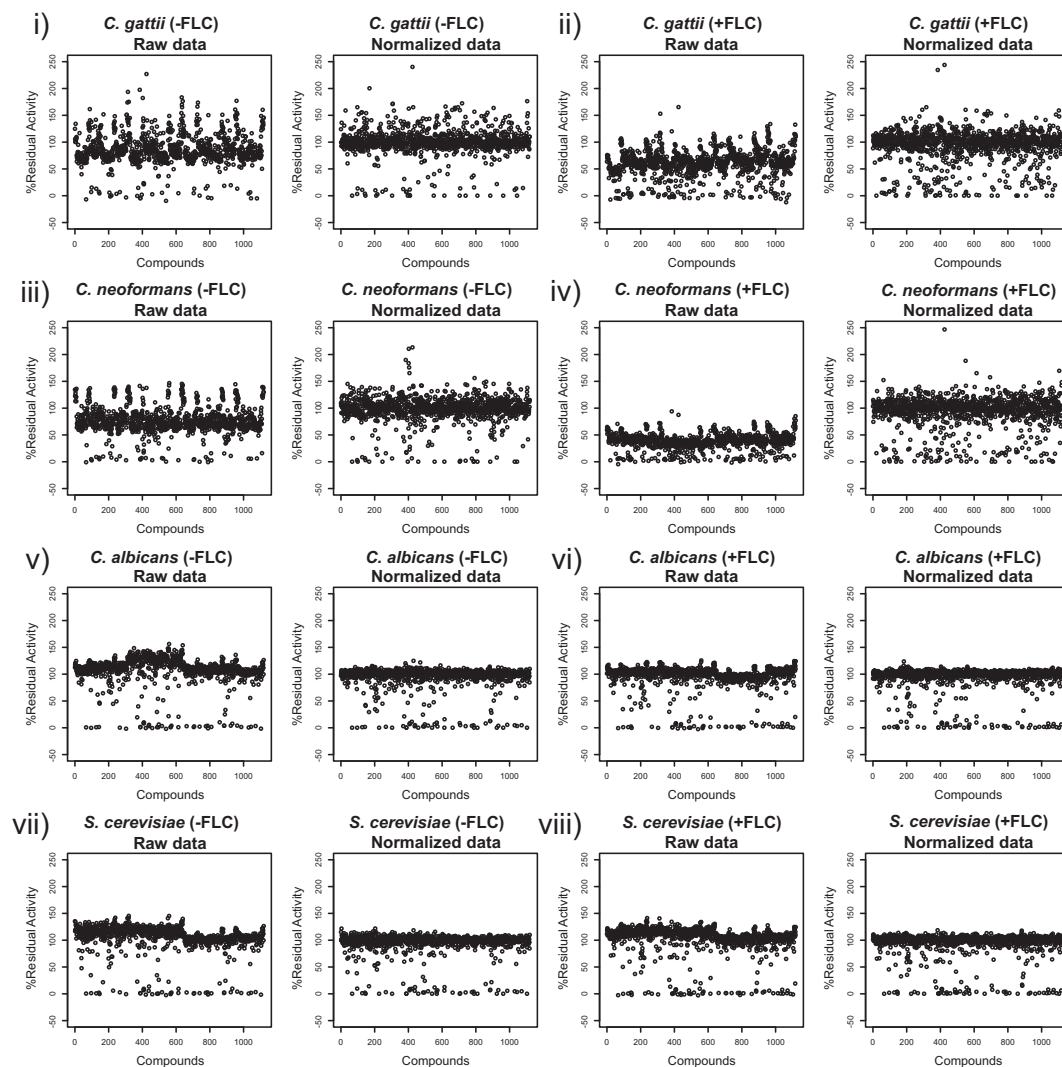


Figure 3.3: Normalisation of high-throughput chemical screen data. In the plots of raw data (first plot in each of the panels i - viii) variation between plates and spatial effects within plates can be seen. Variation between screens can also be seen when the left plot in panels i and ii as well as in panels iii and iv are compared. The effects of data normalisation can be seen in the plot on the right in each panel.

and iv displayed much lower residual activity values than any of the other screens. In screens v to viii, variation between plates was corrected. After normalisation, all screens have a median residual activity of 100%, indicating that the majority of compounds did not show significant activity. The screens in *C. albicans* and *S. cerevisiae* (Figure 3.3 v-viii) have slightly smaller standard deviations than the other two screens.

### Identification of hit compounds

A fluconazole-enhancing compound will inhibit yeast growth significantly more in the presence of 1/2 MIC fluconazole compared to single drug application. To identify such compounds, data from the screens with and without fluconazole was compared for each of the four fungal species (Figure 3.4).

The data was analysed for hit compounds using robust median absolute deviation (MAD; Chung *et al.*, 2008; Birmingham *et al.*, 2009) statistics. Since the data has been normalised and the median for each screen is 100, the diagonal was used as a model to define hits. Therefore, data points for drugs that do not affect growth of the fungal strains differentially in the screens with and without fluconazole will fall along the diagonal.

The scatter plots in Figure 3.4 revealed that most compounds did not affect growth in either condition whereas a few compounds abolished growth completely in both screens for each fungal strain (35-45 drugs in each species). Some compounds inhibited growth of the fungal strains equally in both conditions.

Potential fluconazole-interacting compounds will be more active in the screen with fluconazole (*y*-axis) and will therefore be found in the lower right corner of the scatter plots. Compounds that were at least 2 MADs below the diagonal were considered potential fluconazole-interacting drugs. These are shown as yellow and red filled circles in Figure 3.4. The red dots represent the most potent synergisers from the high throughput screen since these compounds inhibited growth by more than 80% in the presence of fluconazole compared to the effect of these drugs on their own.

In total, 148 bioactive compounds were identified in the four screens (Fig-

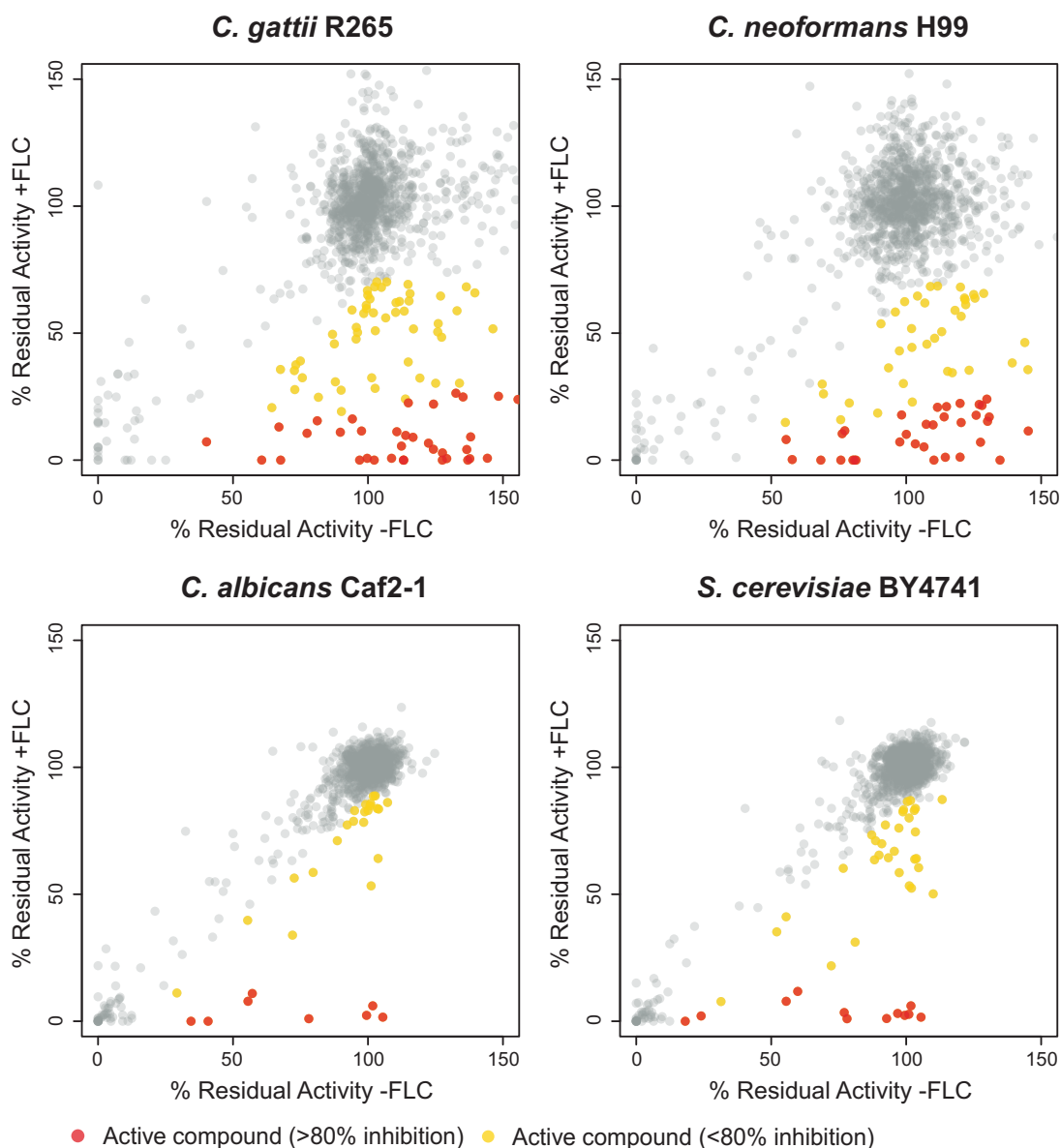


Figure 3.4: Scatterplots of the Prestwick Chemical library screens. For each of the four fungal species, residual growth percentage values for fungi treated with compounds alone (x-axis) and in the presence of fluconazole (y-axis) are plotted. In each plot, hit compounds are found below the diagonal, in the bottom right corner. Hits are marked in red (very strong inhibition in the presence of fluconazole) and yellow. Compounds above the diagonal are not marked because the screen is not suited to identify antagonistic drug interactions (see text).

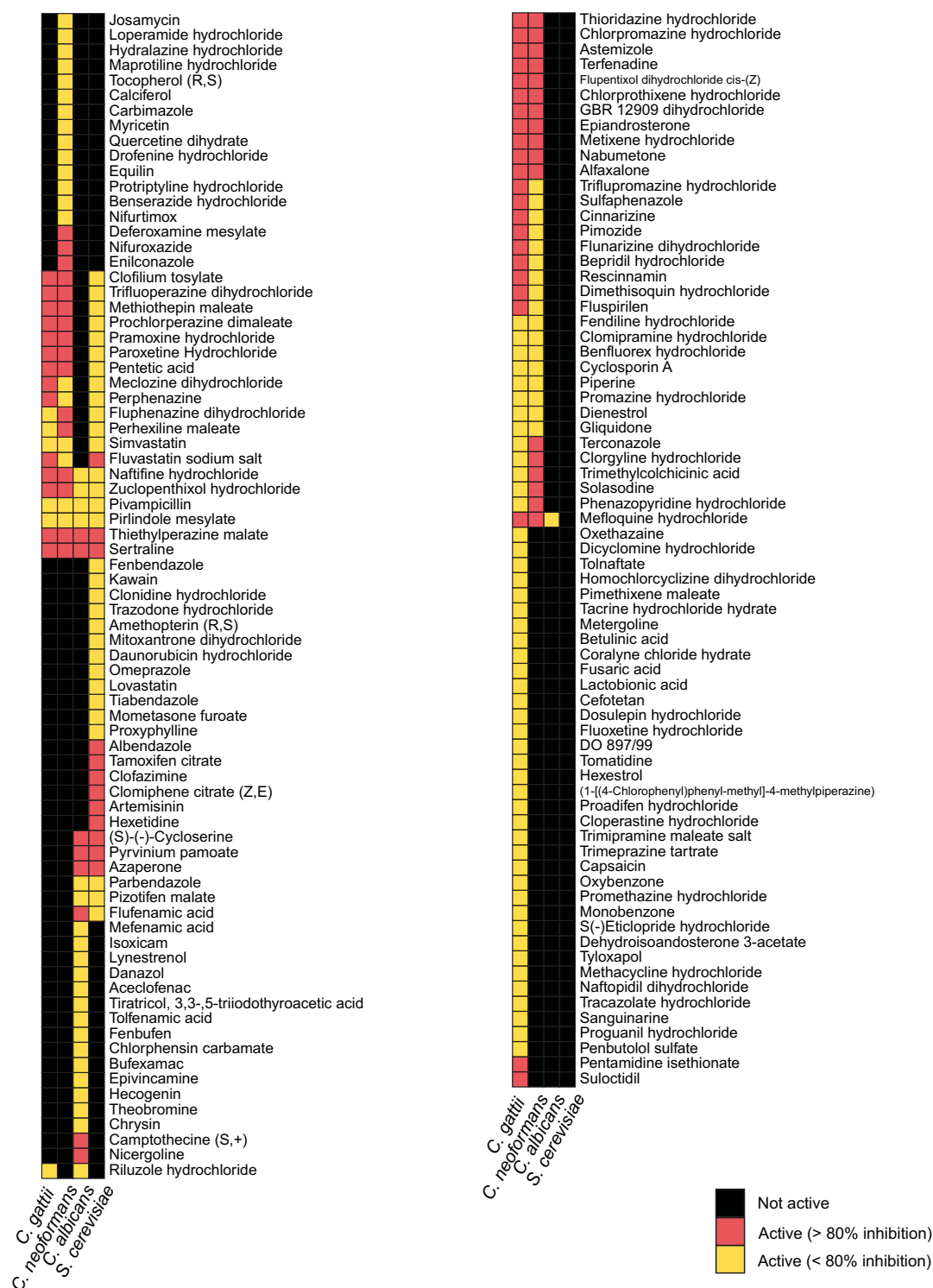


Figure 3.5: Activity of hit compounds from Prestwick Chemical library screens. 148 compounds showed activity in at least one of the four screens against *C. neoformans* (H99), *C. gattii* (R265), *C. albicans* (Caf2-1) and *S. cerevisiae* (BY4741). The colours correspond to level of activity in the screen: red indicates compounds with 80% increase in activity in combination with fluconazole as compared to effect of single drug and yellow are all compounds that are 2 MADs away, but exhibit less than 80% additional activity in the presence of fluconazole.

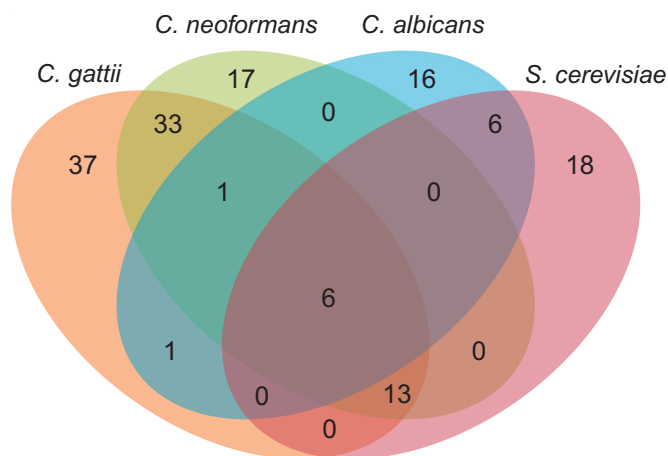


Figure 3.6: Overlap of hits between different fungal species.

ure 3.5). 91 compounds were active in *C. gattii* and 70 in *C. neoformans*. The screens in *C. albicans* and *S. cerevisiae* only revealed 30 and 43 synergistic combinations, respectively. Analysis of the overlap of hits between the different fungal strains as displayed in Figure 3.6 revealed a striking species- or genus-specificity of the compounds. Of the hits, only six compounds were active in all tested species: the antidepressant sertraline which is marketed as Zoloft®; the allylamine antifungal naftifine; the monoamine oxygenase inhibitor pirlindole which also has antidepressant activity; the antibiotic prodrug pivampicillin; the anti-nausea drug thiethylperazine which is marketed as Torecan; and, the antipsychotic drug zuclopenthixol. The latter two compounds belong to a large group of phenothiazine-derived drugs (Figure 3.7A) that are used as antipsychotics. Of all hits, 88 compounds showed activity in a single species or genus only. There is little overlap between *S. cerevisiae* and *C. albicans* (12 compounds), whereas *C. gattii* and *C. neoformans* share many hits (53 compounds). These two genera still have a considerable number of unique hits, 37 and 17 drugs, respectively.

The screen data was also analysed for potential antagonistic drugs. There was very little overlap between the four fungal strains, which does not reflect the degree of overlap that was observed for the fluconazole-interacting drugs. Of the 12, 9, 21 and 21 drugs that were classified as antagonistic in the *C. gattii*, *C. neoformans*, *C. albicans* and the *S. cerevisiae* screens, respectively, only two compounds are shared between *C. gattii* and *C. neoformans*, and one compound is shared between *C. neoformans* and *C. albicans*. In addition, three of these

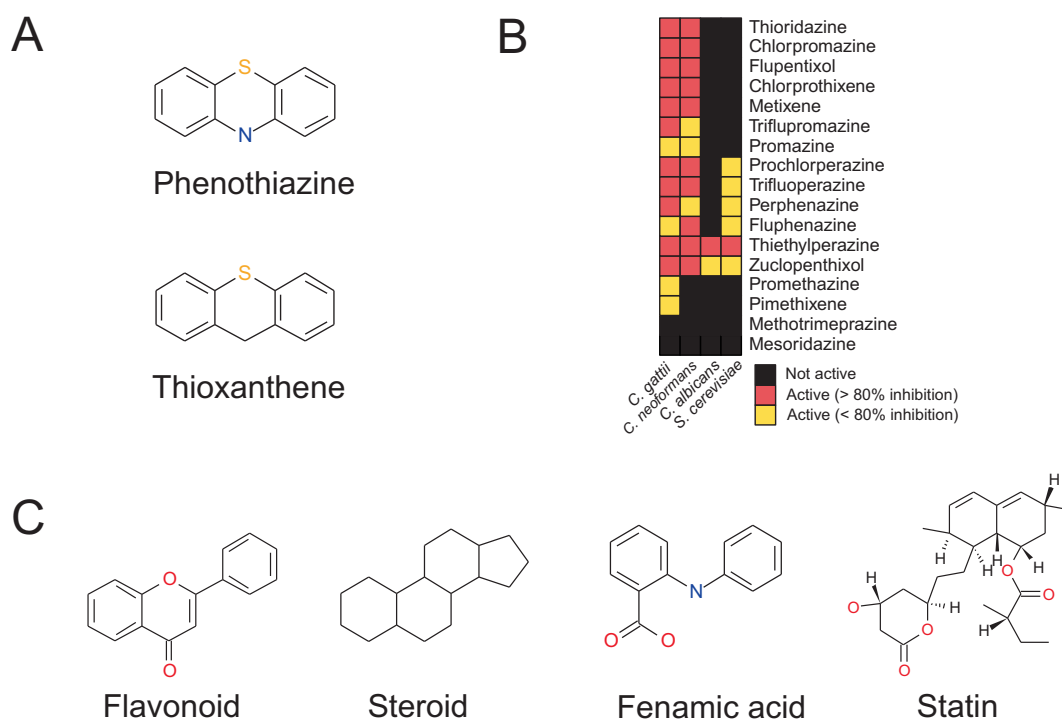


Figure 3.7: Structural clusters among the 148 hit compounds. (A) Backbone structure of phenothiazine and thioxathene compounds. (B) Activity of phenothiazine/thioxathene-derived compounds in different fungal species. (C) Backbone structure of other structural clusters of compounds. Structures (A) and (C) were drawn using Symyx Draw, now Accelrys Draw ([accelrys.com/resource-center/downloads/freeware](http://accelrys.com/resource-center/downloads/freeware)).

antagonistic compounds (clofazimine and kawain in *C. albicans* and suloctidil in *C. neoformans*) were tested against all four species (see Section 3.2.2) and they did not exhibit antagonistic interactions with fluconazole. In fact, suloctidil exhibits synergy with fluconazole in three of the tested fungal strains. This suggests that the screen set-up is not adequate to detect antagonistic drug interactions.

### Structurally distinct groups of compounds enhance activity of Fluconazole

The 148 compounds that potentiated the action of fluconazole are structurally very diverse and represent a wide range of therapeutic application classes including cardiovasculars, hormone modulators, dermatologicals, a variety of neuroleptic drugs, genitourinary tract anti-infectives and antiparasitics.

Clustering of all hit compounds based on their chemical structures revealed

several groups with similar structural features (Appendix). There were 37 clusters in total, 22 of which contained at least two compounds. One structural group that stood out were the tricyclic antipsychotics of the phenothiazine and thioxanthene type. They are spread across clusters 16 and 30 (Appendix). The backbone structure of these two compound classes are shown in Figure 3.7A. The Prestwick library contains 17 of these and 15 were active in the screen, especially against *C. gattii* and *C. neoformans* (Figure 3.7B). Li *et al.* (2008) have shown that derivatives of tricyclic phenothiazines inhibit fatty acid synthesis and disrupt lipid trafficking. Phenothiazine-derivatives have also been described to have antifungal activity which might at least partially be based on the lipophilic character of these compounds (reviewed in Pluta *et al.*, 2011). Another cluster comprises of three plant-derived flavonoids (cluster 1 in Appendix; backbone structure shown in Figure 3.7C). Flavones have been shown to have antifungal properties by Young *et al.*, 2007 and Rauha *et al.*, 2000. Further, 12 steroid-based compounds showed drug interactions with fluconazole (cluster 7; backbone structure shown in Figure 3.7C) as well as two synthetic estrogen compounds (cluster 22). It is possible that these compounds interfere with ergosterol biosynthesis and/or integrate into membranes, changing their composition and physical properties. Since fluconazole targets the fungal membrane, this could explain the observed drug interactions. Further, seven non-steroidal anti-inflammatory drugs showed activity in the screen (clusters 13, 20 and 22). Four of these are fenamic acid derivatives, the backbone structure of which is shown in Figure 3.7C. Three statins were also among the hits (clusters 27 and 28, backbone structure shown in Figure 3.7C). Synergy between azole antifungals and statins have been described before (Nyilasi *et al.*, 2010). Statins are fungal metabolites and are prescribed to lower cholesterol levels in the blood. Their antifungal activity and synergy with azoles are probably based on their effect on membrane fluidity. Statin-treated fungal cells have been shown to have lower levels of ergosterol and therefore exhibit decreased membrane fluidity (Gyetvai *et al.*, 2006). Various antimicrobial compounds with very different structures were also hits in the screens (Appendix). Known modes of action include binding to DNA, inhibition of translation or thiamine metabolism as well as targeting microtubules or cell

wall processes.

### 3.2.2 Synergy assessment and fungicidal activity

Enhancing drug interactions can be additive or synergistic. The high-throughput screen only generated a single data point per drug, so it is impossible to distinguish between these two types of interaction. To characterise the drug interactions for a subset of hit compounds and to assess the reliability of the high-throughput screen, standard concentration matrix (checkerboard) analysis was conducted in all four fungal species. Based on this data, fractional inhibitory concentration indices (FICIs) were calculated, which is the accepted method for drug interaction quantification in infectious diseases (Eliopoulos & Moellering, 1991; Odds, 2003).

12 of the 148 hit compounds were selected based on criteria of commercial availability, known mode of action and therapeutic importance to investigate the nature of their interaction with fluconazole further. The subset of containing albendazole, azaperone, clofazimine, clomiphene, L-cycloserine, kawain, lynestrenol, mitoxantrone, sertraline, suloctidil, tamoxifen, and trifluoperazine is representative of the structural diversity and the variety of therapeutic application classes present in the hit set (Figure 3.8).

To this collection, five known antifungal drugs were added which would allow us to explore potential interactions between antifungals: amphotericin B, ketoconazole, terbinafine, fenpropidin and caspofungin (Figure 3.8). Amphotericin B is a polyene macrolide that binds to ergosterol in the fungal membrane, effectively creating pores which results in leaky cells with depolarised membranes. Ketoconazole, terbinafine and fenpropidin (an agricultural fungicide) are ergosterol biosynthesis inhibitors. Terbinafine is actually a clinically relevant allylamine analogue of naftifine, one of the six compounds that showed activity in all four screens. Caspofungin is the first drug of the new class of echinocandins which target the fungal cell wall by inhibiting  $\beta$ -(1,3)-D-glucan synthase.



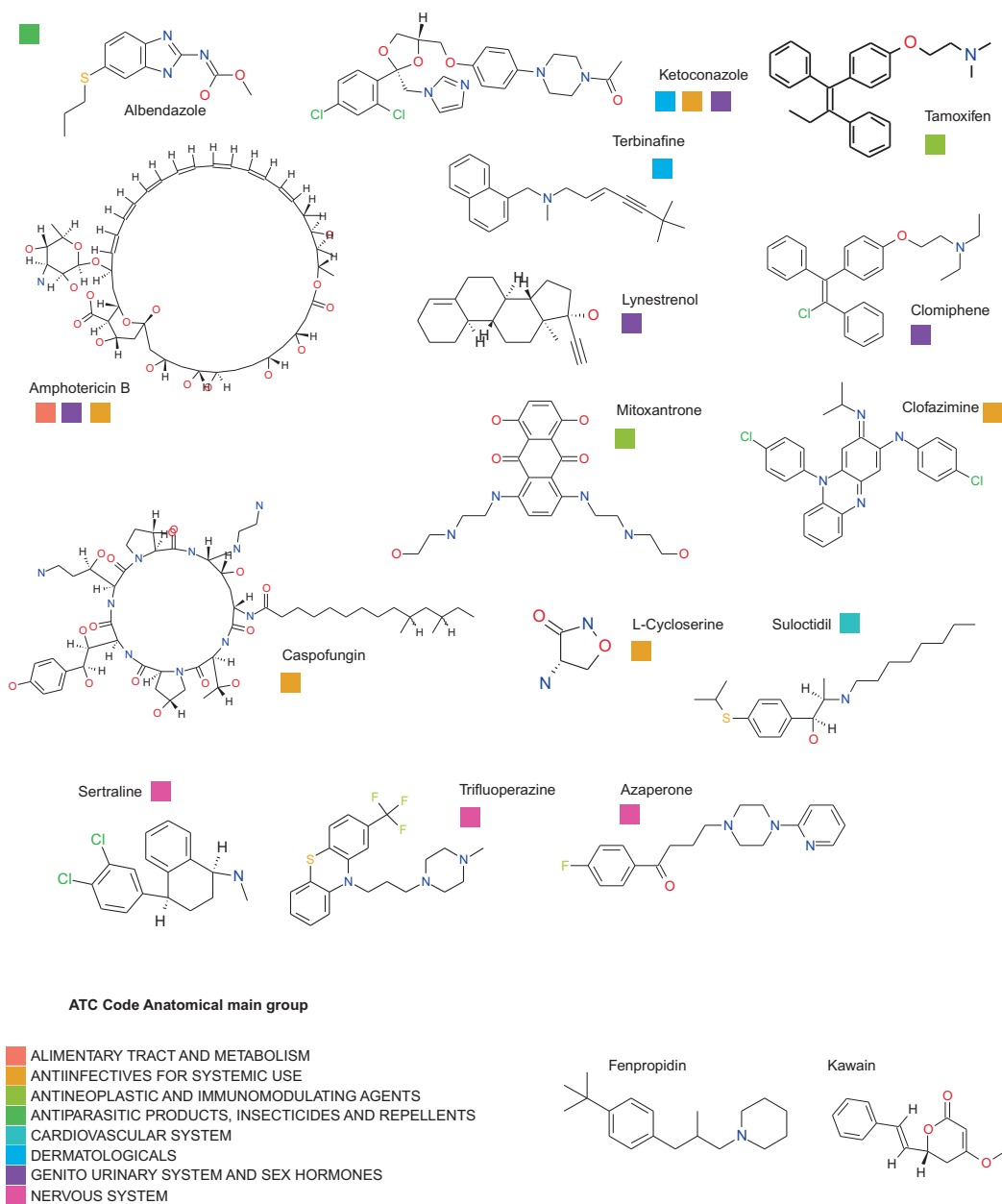


Figure 3.8: Chemical structures and application classification of 17 compounds selected for synergy confirmation experiments. Approved drugs are shown with their therapeutic application class. Structures were drawn from SDF files provided by Prestwick using Symyx Draw, now Accelrys Draw ([accelrys.com/resource-center/downloads/freeware](http://accelrys.com/resource-center/downloads/freeware)).

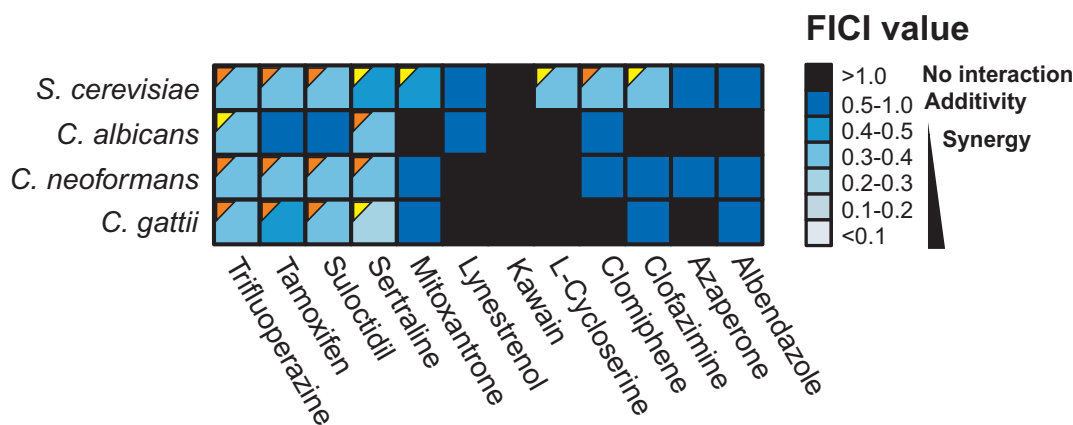


Figure 3.9: Heatmap of drug interactions with fluconazole in each species. Dark blue indicates additive effects (FICI of 0.5 to 1); lighter shades of blue represents synergy (FICI <0.5). Orange triangles indicate fungicidal drug combinations; yellow triangles indicate fungistatic drug combinations.

### Characterization of drug interactions

Figure 3.9 shows the FICI values for the 12 hit compounds. All compounds, except for kawain, exhibited drug interactions with fluconazole in at least one of the strains tested. In the case of albendazole, azaperone and lynestrenol, these interactions are merely additive. The remaining eight compounds had rather diverse activity profiles across the different species. Only sertraline and trifluoperazine interacted synergistically with fluconazole in all four fungal strains, whereas suloctidil, tamoxifen and terbinafine interact in three of the four species. Clofazimine, clomiphene, L-cycloserine and mitoxantrone A exerted synergistic effects exclusively in *S. cerevisiae*. Neither of the other three pathogens were uniquely susceptible to any of the molecules.

### Assessment of the high-throughput screen performance

Overall, most drug interactions from the high-throughput screen could be confirmed as synergistic interactions with fluconazole, except for albendazole, azaperone and kawain in *S. cerevisiae*, and azaperone, L-cycloserine and lynestrenol in *C. albicans* (Figure 3.10). Our quantification of drug interactions revealed five additional synergies that were not statistically significant in the screen. Trifluoperazine also exhibits synergy in *C. albicans*, tamoxifen is synergistic with

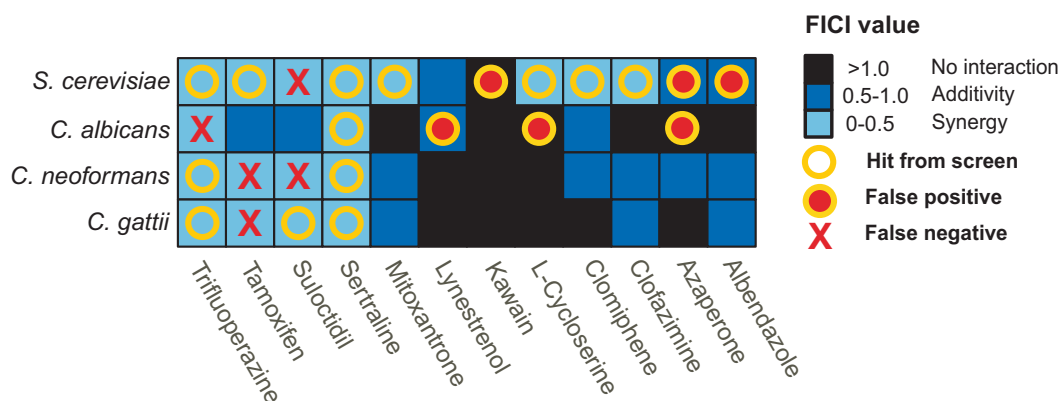


Figure 3.10: Assessment of high throughput screen performance. Heatmap represents additive (dark blue) and synergistic (light blue) drug interactions with fluconazole as shown in Figure 3.9. The symbols indicate agreement between confirmatory experiments and high throughput data.

fluconazole against *C. gattii* and *C. neoformans* and suloctidil exerts synergy in *C. neoformans* and *S. cerevisiae*. The sensitivity and specificity of the primary high throughput screen were determined based on the detailed analysis of these 12 compounds. Sensitivity of the screen indicates how many drug interactions are correctly identified by the screen. Specificity of the screen gives an indication of how certain we can be that a hit in the screen really represents a true drug interaction. Table 3.1 summarises the results from the high throughput screen and the confirmatory assays. Using this contingency table, the specificity was calculated as follows:

$$\text{Specificity} = 1 - \alpha = \frac{TN}{TN + FP} = \frac{24}{24 + 6} = 0.80$$

HTPS \ Confirmation	Confirmation		HTPS total
	Synergy	No interaction	
Hit compounds	True Positives 13	False Positives 6	19
No interaction	False Negatives 5	True Negatives 24	29
Confirmation total	18	30	48

Table 3.1: Contingency table for data from primary high-throughput screen and results of confirmatory assays. The 48 interactions of the subset of 12 compounds in all four species are considered.

This means that 80% of all non-interacting drug pairs were correctly classified as such based on high-throughput screen data. Consequently, the false positive rate  $\alpha$  is 0.2. The sensitivity was obtained according to this formula:

$$\text{Sensitivity} = 1 - \beta = \frac{TP}{TP + FN} = \frac{13}{13 + 5} = 0.72$$

This indicates that 72% of all synergistic interactions were correctly identified in the high-throughput screen. The corresponding false negative rate  $\beta$  is 0.28. Overall, the screen proved to be a powerful tool to identify synergistic drug interactions.

### **Fungicidal potential of synergistic drug combinations**

Fluconazole is a fungistatic drug because it inhibits fungal growth but does not kill the pathogens. Drugs with fungicidal properties are desirable therapies since they are less likely to promote the development of drug resistance. Synergistic drug combinations were therefore tested for their fungicidal potential (Figure 3.9).

The results were species-specific for sertraline and trifluoperazine. In contrast, all synergistic combinations with suloctidil and tamoxifen showed fungicidal effects. In total, five compounds were fungicidal in combination with fluconazole. Further, there is species specificity in the fungicidal potential of synergistic drug combinations.

### **Interactions of known antifungals with fluconazole**

The five known antifungals that were included in this analysis, exhibited very individual profiles. Like the hit compounds from the screen, the observed interactions were species specific in terms of drug interactions as well as fungicidal potential (Figure 3.11).

The cell wall-targeting drug caspofungin is only synergistic with fluconazole against *C. albicans*, but this interaction is the strongest of all drug combinations investigated and has fungicidal potential. Additive interactions with fluconazole were seen against the two *Cryptococcus* species. The synergistic effect in *C. albicans* makes sense since caspofungin is used to treat *Aspergillus* and *Candida*

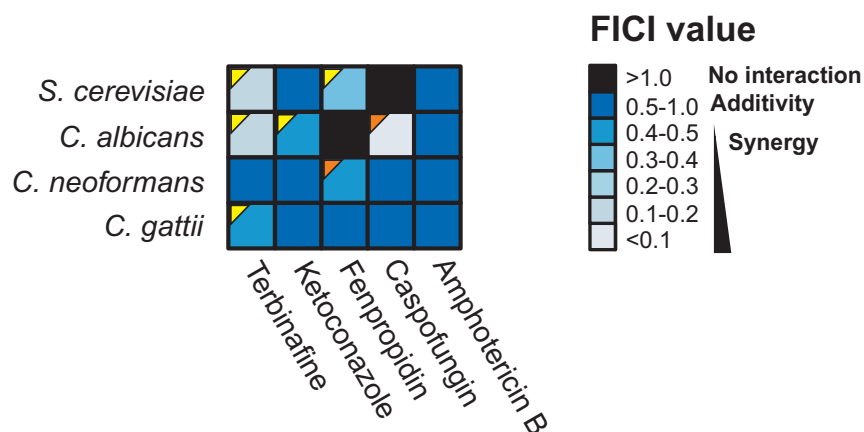


Figure 3.11: Heatmap of interactions between known antifungals and fluconazole. Dark blue indicates additive effects (FICI of 0.5 to 1); lighter shades of blue represents synergy (FICI <0.5). Orange triangles indicate fungicidal drug combinations; yellow triangles indicate fungistatic drug combinations.

infections and synergy with fluconazole against seven out of 50 clinical isolates of *Candida glabrata* has been reported in Kiraz *et al.* (2010).

The Erg1 inhibitor terbinafine exhibits synergy with fluconazole against three of the fungal pathogens, but none of these interactions are fungicidal. In *C. neoformans* the interaction is merely additive. Terbinafine and fluconazole both inhibit ergosterol biosynthesis, but act on different steps of the pathway. Lehár *et al.* (2007) investigated interactions between various drugs that target the ergosterol pathway in *Candida glabrata* and found that the terbinafine/fluconazole combination is highly synergistic. This synergy was also confirmed in clinical isolates of *C. albicans* by Barchiesi *et al.* (1997 and 1998). The observed synergistic interactions between fenpropidin and fluconazole against *S. cerevisiae* and *C. neoformans* are probably also based on the fact that these two drugs inhibit ergosterol biosynthesis at different steps. It is intriguing that one interaction is fungicidal and the other one is not.

Just like fluconazole, ketoconazole is an inhibitor of Erg11. Therefore, additive interactions would be expected between these two drugs. This is indeed observed in all species tested except for *C. albicans* where the combination is synergistic. This is somewhat surprising, but might be due to the fact that the triazole fluconazole and the imidazole ketoconazole are structurally different and do not have identical effects on the cell.

Amphotericin B was not synergistic in any of the fungal pathogens, but instead showed additive interaction with fluconazole in all species. This is in accordance with results from Barchiesi *et al.* (2000) who observed additive interactions between these two drugs in 15 clinical isolates of *Cryptococcus neoformans* as well as a mouse model of systemic cryptococcosis.

### 3.2.3 Interrogation of the mode of action of drug synergies by genome-wide screens in *S. cerevisiae*

Six compounds were selected for further studies into the molecular basis of their synergy with fluconazole. This set included all four compounds that were fungicidal in combination with fluconazole in *S. cerevisiae* - clomiphene, suloctidil, tamoxifen and trifluoperazine - as well as L-cycloserine which exhibits synergy in *S. cerevisiae* only and sertraline which shows synergy in all four species (Figure 3.12). For these six compounds, sensitivity profiles for the  $\sim 1000$  essential genes were generated using the heterozygous deletion pool (Giaever *et al.* 1999). In addition, the set of  $\sim 5000$  haploid deletion strains of non-essential genes was also screened for drug sensitivity. Both methods have been successfully used to identify essential drug-targets (Lum *et al.*, 2004) as well as biological pathways associated with drug action (Parsons *et al.*, 2004).

#### Haplo-insufficiency screens

Compound action was investigated with haplo-insufficiency screens, where 1000 deletion strains that are heterozygous for essential genes were tested for drug sensitivity to identify potential drug targets (Giaever *et al.*, 1999). The results of the screens for fluconazole, clomiphene, sertraline, L-cycloserine, tamoxifen and trifluoperazine are shown in Figures 3.13. An appropriate level of growth inhibition of the deletion pool could not be achieved with suloctidil. It was nevertheless included in the experiments to confirm chemical-genetic interactions of the other compounds.

As expected, deletion of one copy of the lanosterol  $14\alpha$ -demethylase gene *ERG11* conferred sensitivity to fluconazole (Figures 3.13). Deletion of one copy

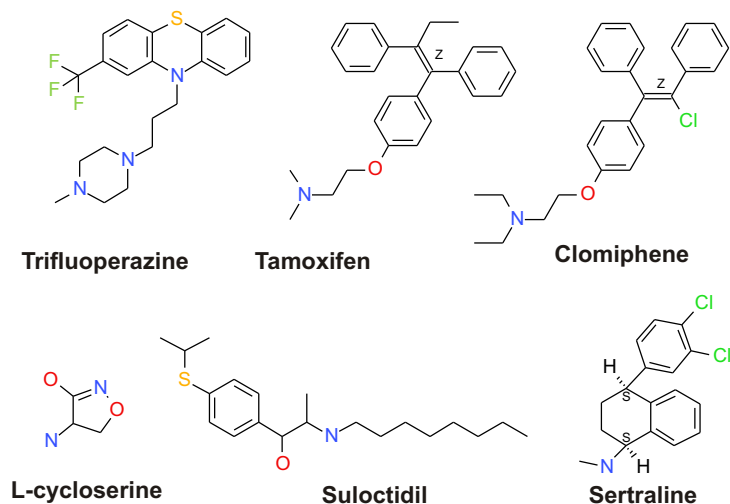


Figure 3.12: Chemical structures of the six drugs chosen for detailed mode of action studies. Structures were drawn from SDF files provided by Prestwick using Symyx Draw, now Accelrys Draw ([accelrys.com/resource-center/downloads/freeware](http://accelrys.com/resource-center/downloads/freeware)).

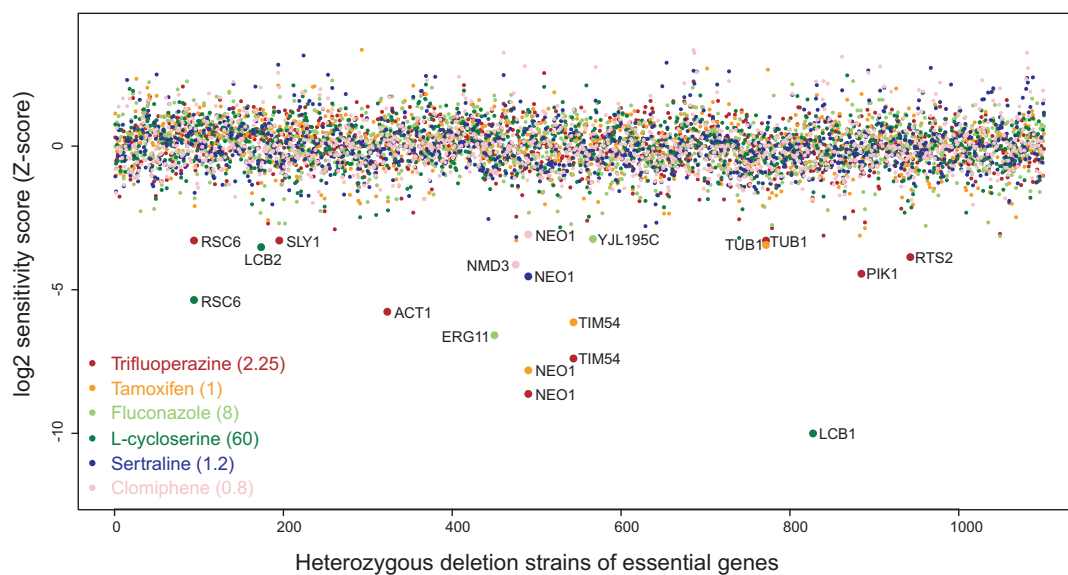


Figure 3.13: Sensitivity of heterozygous essential deletion strains to six different drugs. Genes along the x-axis are sorted by their ORF name. Negative Z-scores indicate hypersensitivity of a deletion strain in the presence of a drug. Values in parentheses indicate drug concentration in μg/mL.

of either *LCB1* and *LCB2*, which encode subunits of the enzyme serine palmitoyltransferase that catalyzes the committed step of sphingolipid biosynthesis, caused sensitivity to L-cycloserine. L-cycloserine is known to inhibit sphingolipid biosynthesis and it has been shown that in yeast membrane extracts, high concentrations of L-cycloserine (1 mM) partially inhibit serine palmitoyltransferase (Pinto *et al.*, 1992).

The four remaining compounds clomiphene, sertraline, trifluoperazine and tamoxifen conferred sensitivity to cells heterozygous in the *NEO1* gene, which encodes an essential aminophospholipid translocase required for vacuolar biogenesis and membrane trafficking. It has recently been shown that deletion of the ortholog of *NEO1* in *C. neoformans* (*APT1*) results in hypersensitivity to fluconazole and amphotericin B, as well as attenuated virulence (Hu and Kronstad, 2010). In addition, loss of one copy of *TIM54*, a translocase of the inner mitochondrial membrane, conferred sensitivity to tamoxifen and trifluoperazine in the high throughput screen.

Growth assays that were conducted to validate the results from the haplo-insufficiency screens confirmed the drug gene interactions observed in the screens. Further, the specificity of these interactions was affirmed by these experiments. Figure 3.14 shows that fluconazole sensitises *ERG11/erg11Δ*. *LCB1/lcb1Δ* and *LCB2/lcb2Δ* were sensitive to L-cycloserine and *NEO1/neo1Δ* is highly sensitive to clomiphene, sertraline, tamoxifen and trifluoperazine as well as suloctidil. The growth curves have also been quantified and the data for the strains shown here is included in Figure 3.18B. For the quantification, OD measurements were taken at the time point of control well saturation and log ratios of drug treated deletion strains versus the untreated strains were calculated. *TIM54* was also tested as well as *TIM18* and *TIM22*, which function in the TIM22 complex with *TIM54* (Figure 3.18B). The chemical-genetic interactions of *TIM54* with tamoxifen and trifluoperazine were confirmed. Additional interactions with clomiphene and sertraline were identified. Testing a range of drug concentrations in the growth curve assays, also revealed chemical-genetic interactions for *TIM18* and *TIM22*, that were not recovered at the single drug concentrations used to generate the chemical-genetic profiles.



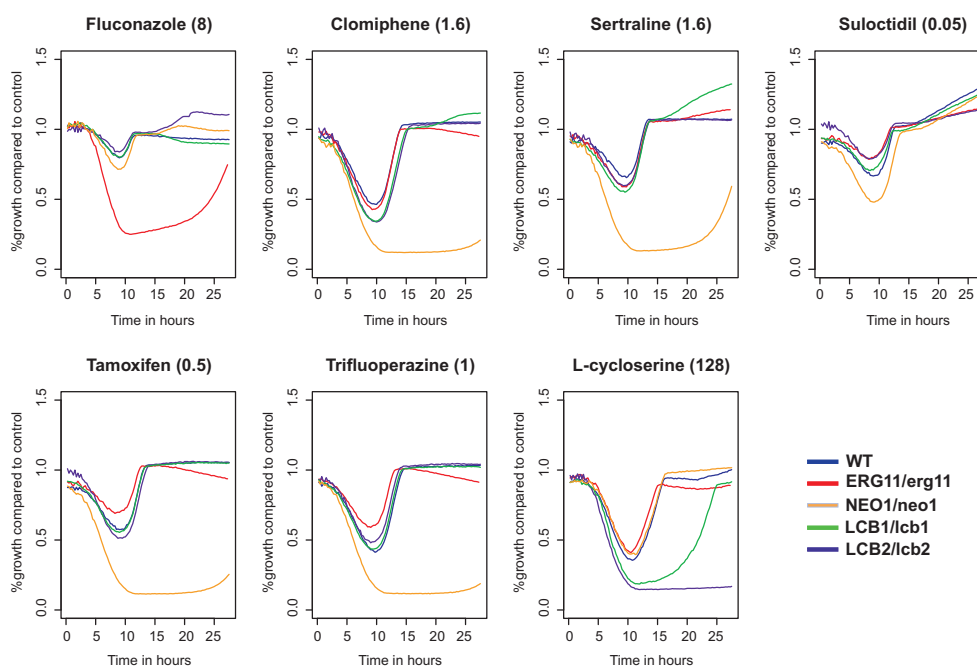


Figure 3.14: Confirmation of hits from haplo-insufficiency screen. Based on barcode array data for the heterozygous essential genes, *ERG11/erg11* $\Delta$ , *NEO1/neo1* $\Delta$ , *LCB1/lcb1* $\Delta$  and *LCB2/lcb2* $\Delta$  were selected for individual growth curve assays in the presence of the indicated drugs. Percentage growth of the different deletion strains and WT compared to control wells (strains treated with solvent control) is plotted for each drug. Values in parentheses indicate drug concentration in  $\mu\text{g}/\text{mL}$ .

### Chemical-genetic profiles of fluconazole and synergistic drug combinations

Chemical-genetic profiles obtained by screening the haploid deletion pool against compounds/compound combinations, point to target pathways and reveal genes that buffer against drug toxicity. In addition, compounds with similar chemical-genetic interaction profiles may comprise similar bioactivities (Hillenmeyer *et al.*, 2008). The haploid deletion pool was then subjected to the synergistic compounds individually and in combination with fluconazole (Figure 3.15). The heatmap displays, from left to right, chemical-genetic interactions of fluconazole alone, synergiser/fluconazole combinations and the synergising drugs alone. The profiles of the drug combinations are very similar to the profiles of fluconazole at higher concentrations (6-8  $\mu\text{M}$ ). The big clusters in the left part of the heatmap correspond to mutants that are sensitive to fluconazole and drug combination treatment.

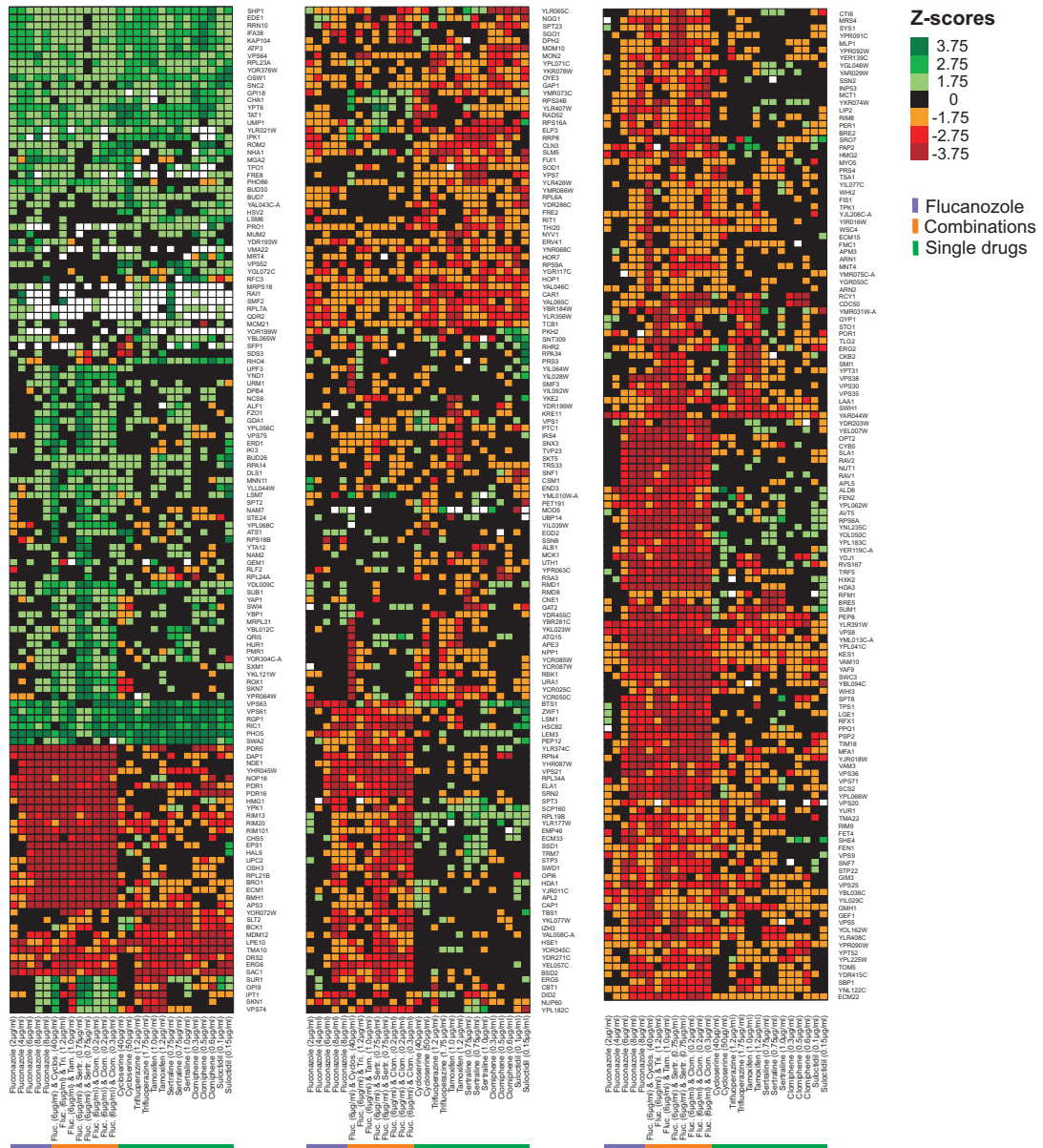


Figure 3.15: Heatmap representing all haploid chemical-genetic profiles generated for this study. The haploid deletion pool of 5000 non-essential deletion strains was screened for sensitivity to sertraline, clomiphene, tamoxifen, L-cycloserine, trifluoperazine and suloctidil alone and in combination with fluconazole. Screens are represented along the x-axis and deletion strains that were responsive in at least one of the screens are represented along the y-axis (about 400 strains). Screens and deletion strains were clustered hierarchically according to Pearson correlation between chemical-genetic profiles. Negative Z-scores (red) indicate sensitive deletion strains whereas positive Z-scores (green) represent resistant deletion strains. White squares indicate no signal for particular barcodes.

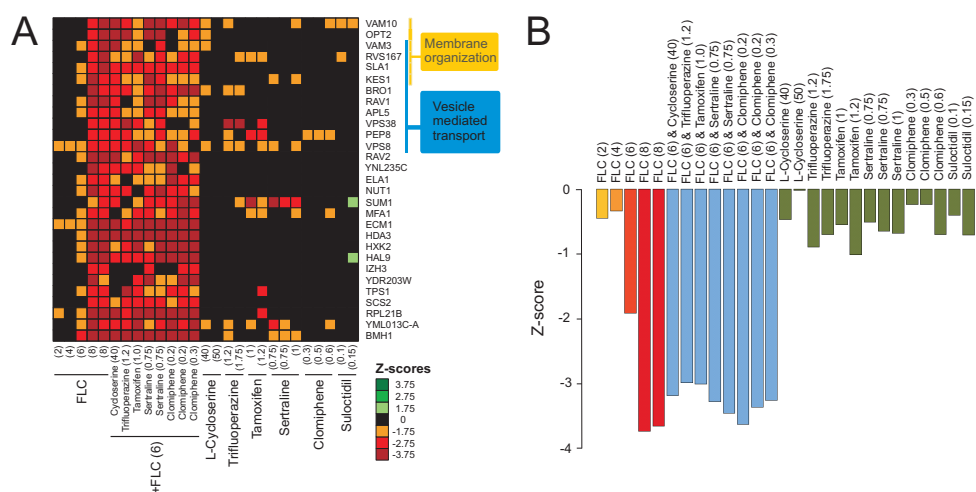


Figure 3.16: Haploid deletion strain sensitivity to different fluconazole concentrations and the synergistic drugs in the presence or absence of fluconazole. (A) Heatmap of Z-scores for fluconazole-specific deletion strains from all haploid chemical-genetic screens. GO annotations for genes involved in to vacuolar and vesicle mediated transport are indicated. (B) Average Z-score across all fluconazole-specific deletion strains for each screen. Different concentrations of fluconazole are represented by red bars; blue indicates fluconazole with synergistic drugs; green indicates synergistic drugs alone.

These fluconazole-responsive deletion strains were investigated in more detail.

Deletion strains sensitive to increasing concentrations of fluconazole alone were associated with vesicle mediated transport and membrane organisation (Figure 3.16A), as described in previous studies (Parsons *et al.*, 2006). For the drug combinations, a concentration of fluconazole ( $6 \mu\text{g}/\text{mL}$ ) that caused 20% growth inhibition compared to control treatment was used. At this concentration, the fluconazole-sensitive strains only have an average Z-score of around -2, whereas a concentration of  $8 \mu\text{g}/\text{mL}$  impairs growth of these deletion strains much more resulting in an average Z-score of -4 (Figure 3.16B). Importantly, the synergising drugs alone did not impair growth of fluconazole-sensitive deletion strains. However, they sensitised cells to lower doses of fluconazole when applied in combination (Figure 3.16A and B). P-values for the increased sensitivity of these deletion strains compared to the screen with  $6 \mu\text{g}/\text{mL}$  of fluconazole confirmed that the decrease in Z-score was significant for all synergisers (Table 3.2).



Screen	p-value	Difference
Fluconazole 2 $\mu$ g/mL	9.05E-08	1.98
Fluconazole 4 $\mu$ g/mL	3.25E-10	1.86
Fluconazole 6 $\mu$ g/mL	-	0.00
Fluconazole 8 $\mu$ g/mL	1.59E-17	-1.91
Fluconazole 8 $\mu$ g/mL	5.27E-14	-1.79
Fluc. 6 $\mu$ g/mL & Cyclos. 40 $\mu$ g/mL	5.85E-05	-1.00
Fluc. 7 $\mu$ g/mL & Tri. 1.2 $\mu$ g/mL	3.28E-05	-1.04
Fluc. 6 $\mu$ g/mL & Tam. 1 $\mu$ g/mL	2.39E-06	-1.09
Fluc. 6 $\mu$ g/mL & Sertr. 0.75 $\mu$ g/mL	1.36E-05	-1.22
Fluc. 6 $\mu$ g/mL & Sertr. 0.75 $\mu$ g/mL	1.71E-04	-1.12
Fluc. 6 $\mu$ g/mL & Clom. 0.2 $\mu$ g/mL	3.07E-08	-1.43
Fluc. 6 $\mu$ g/mL & Clom. 0.2 $\mu$ g/mL	3.53E-08	-1.58
Fluc. 6 $\mu$ g/mL & Clom. 0.3 $\mu$ g/mL	4.91E-07	-1.45
DMSO 1 (E)/ DMSO 2 (E)	4.46E-08	2.29
L-cycloserine 40 $\mu$ g/mL	9.21E-07	1.98
L-cycloserine 50 $\mu$ g/mL	7.07E-09	2.27
Trifluoperazine 1.75 $\mu$ g/mL	8.34E-05	1.78
Tamoxifen 1 $\mu$ g/mL	1.53E-05	1.75
Tamoxifen 1.2 $\mu$ g/mL	1.45E-04	1.51
Sertraline 0.75 $\mu$ g/mL	1.90E-05	1.59
Sertraline 1 $\mu$ g/mL	1.69E-05	1.63
Sertraline 0.75 $\mu$ g/mL	1.95E-06	1.77
Clomiphene 0.5 $\mu$ g/mL	2.27E-08	2.10
Clomiphene 0.6 $\mu$ g/mL	2.33E-06	1.84
Clomiphene 0.3 $\mu$ g/mL	9.38E-09	2.11
Suloctidil 0.15 $\mu$ g/mL	1.07E-07	2.31

Table 3.2: P-values for mean Z-scores of fluconazole-specific deletion strains in each of the chemical-genetic profiles as shown in Figure 3.16B.

### Chemical-genetic profiles of fluconazole synergisers

The chemical-genetic profiles of the six syncretic synergisers (Figure 3.15) were examined in detail to gain insight into the mode of action of their interaction with fluconazole. In Figure 3.17 the sensitivity of the 5000 deletion strains in the presence of each drug is shown. The plot shows that some deletion strains are sensitive or resistant to more than one of the synergisers.

The heatmap in Figure 3.18A focuses on these strains because they might help explain the observed synergies between the compounds and fluconazole. A list with the corresponding Z-scores can be found in Appendix Table S1. Clomiphene, sertraline, suloctidil, tamoxifen and trifluoperazine caused growth inhibition of

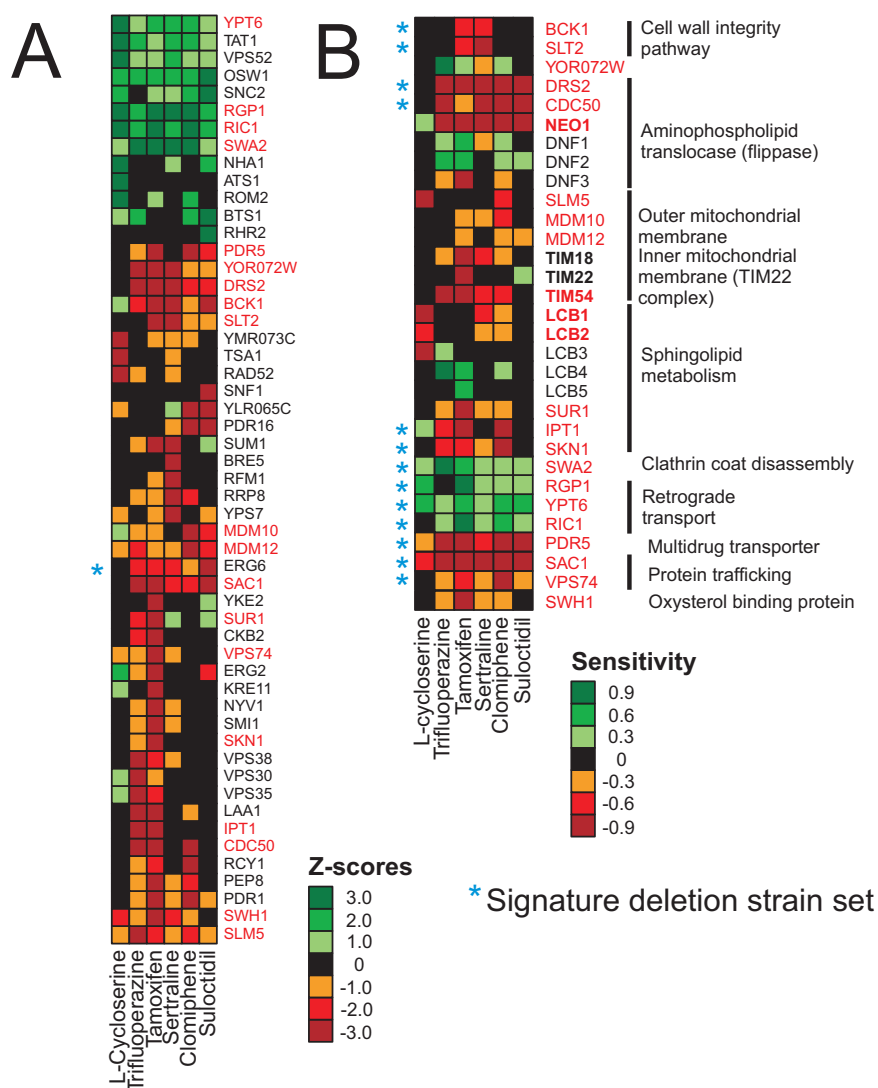


Figure 3.18: Haploid deletion strains sensitive to synergistic synergisers. (A) Deletion strain sensitivity to synergising drugs based on primary barcode screen data. From duplicate profiles for each compound, strains that have a Z-score more significant than  $\pm 3$  are shown. Gene names in red indicate deletion strains that were chosen for verification by individual growth assays. (B) Log-ratio scores were calculated from individual growth curve assays to confirm chemical-genetic interactions. For this, OD measurements were taken at the time point of control well saturation and log ratios of drug treated deletion strains versus the untreated strains were calculated. Gene names in bold indicate deletion strains that are heterozygous for essential genes. Negative Z-scores and log-ratios indicate sensitivity of a strain to a specific drug, whereas positive scores represent resistance. Blue asterisks indicate the 14 deletion strains that comprise the signature deletion strain set for the membrane active compounds.

a common set of deletion strains including genes that encode the non-essential post-Golgi associated aminophospholipid translocase (flippase) *DRS2* and its activating subunit Cdc50, the protein trafficking factors Sac1 and Vps74, the cell wall integrity MAPK kinase Slt2 and its upstream activating kinase Bck1, the ergosterol biosynthesis enzyme Erg6 and the mitochondrial outer membrane import factors Mdm10 and Mdm12. In addition, the deletion of genes involved in downstream steps of sphingolipid metabolism, including *IPT1*, *SKN1*, *SUR1*, *SWH1* and *YPK1* caused growth inhibition in the presence of these compounds. The majority of deletion mutants sensitive to clomiphene, sertraline, suloctidil, tamoxifen and trifluoperazine are involved in membrane processes and the cell wall integrity pathway.

Interestingly, strains disrupted for non-essential genes implicated in retrograde transport to the cis-Golgi network (*YPT6*, *RGP1*, *RIC1*, *VPS52*) and in uncoating of clathrin vesicles (*SWA2*) were resistant to all synergisers (Figure 3.18A), suggesting that limited vesicle trafficking may compensate for membrane perturbation. It is also possible that vesicle trafficking is required for drug import.

The chemical-genetic interactions described above were confirmed with quantitative growth curve assays (Figure 3.18B). With the exception of the dubious ORF *YOR072W*, the quantitative growth curves corroborated the barcode microarray results. Haploid deletion strains for *DNF1/2/3*, the other three flippases in *S. cerevisiae*, and *LCB3/4/5*, which function downstream of *LCB1/2*, were also tested because they are functionally related to essential genes that were identified as haplo-insufficient. The only chemical-genetic interaction observed for the *LCB3/4/5* genes was one between *LCB3* and L-cycloserine. Of the non-essential flippases, deletion of *DNF3* sensitised yeast to trifluoperazine, tamoxifen and clomiphene. The lack of chemical-genetic interactions for *DNF1/2* might be due to the localisation of the different flippases in the cell: Dnf1 and Dnf2 are found in the cell membrane whereas Neo1, Drs2 and Dnf3 localise to the Golgi membranes.

Since five of the drugs (clomiphene, sertraline, suloctidil, tamoxifen and trifluoperazine) shared a number of chemical-genetic interactions, these 14 deletion strains were defined as signature deletion strains in Figure 3.18.

## Summary

The results of these genome-wide chemical-genetic screens suggest two related modes of action for the synergistic interactions with fluconazole. Clomiphene, sertraline, suloctidil, tamoxifen and trifluoperazine appear to cause general perturbation of membrane, vesicle trafficking and lipid biosynthesis functions, whereas L-cycloserine interferes with an early step in sphingolipid biosynthesis, consistent with its previously established mechanism of action (Pinto *et al.*, 1992). To test the latter hypothesis, the effects of myriocin, another known inhibitor of the first step of the sphingolipid biosynthesis pathway was examined (Miyake *et al.*, 1995). It also potentiated the antifungal action of fluconazole (FICI = 0.625), thus confirming that the drug interaction between fluconazole and L-cycloserine is based on the inhibition of sphingolipid biosynthesis.

### 3.2.4 Cell biological effects of synergistic drug combinations

The effects of the syncretic synergisers alone and in combination with fluconazole on cell physiology were assessed. The distribution of different dyes in *S. cerevisiae* WT cells treated with compounds alone and in combination was visualised. The effect of sorbitol on yeast treated with the synergisers and fluconazole was also examined.

#### Microscopy images reveal effects on cell membrane

The effects of trifluoperazine, tamoxifen, sertraline, and L-cycloserine alone and in combination with fluconazole on *S. cerevisiae* cell physiology was evaluated. Different diagnostic fluorescent dyes that bind to various cellular structures were applied to investigate cell physiological changes in response to drug treatment. FM4-64, Calcofluor white and Mitotracker Green were used to visualise vacuolar membranes, the cell wall and bud scars, and mitochondria, respectively. Images shown are for cells treated with drugs for 1 hour. Staining patterns in response to 3 hour incubation with drugs looked similar.



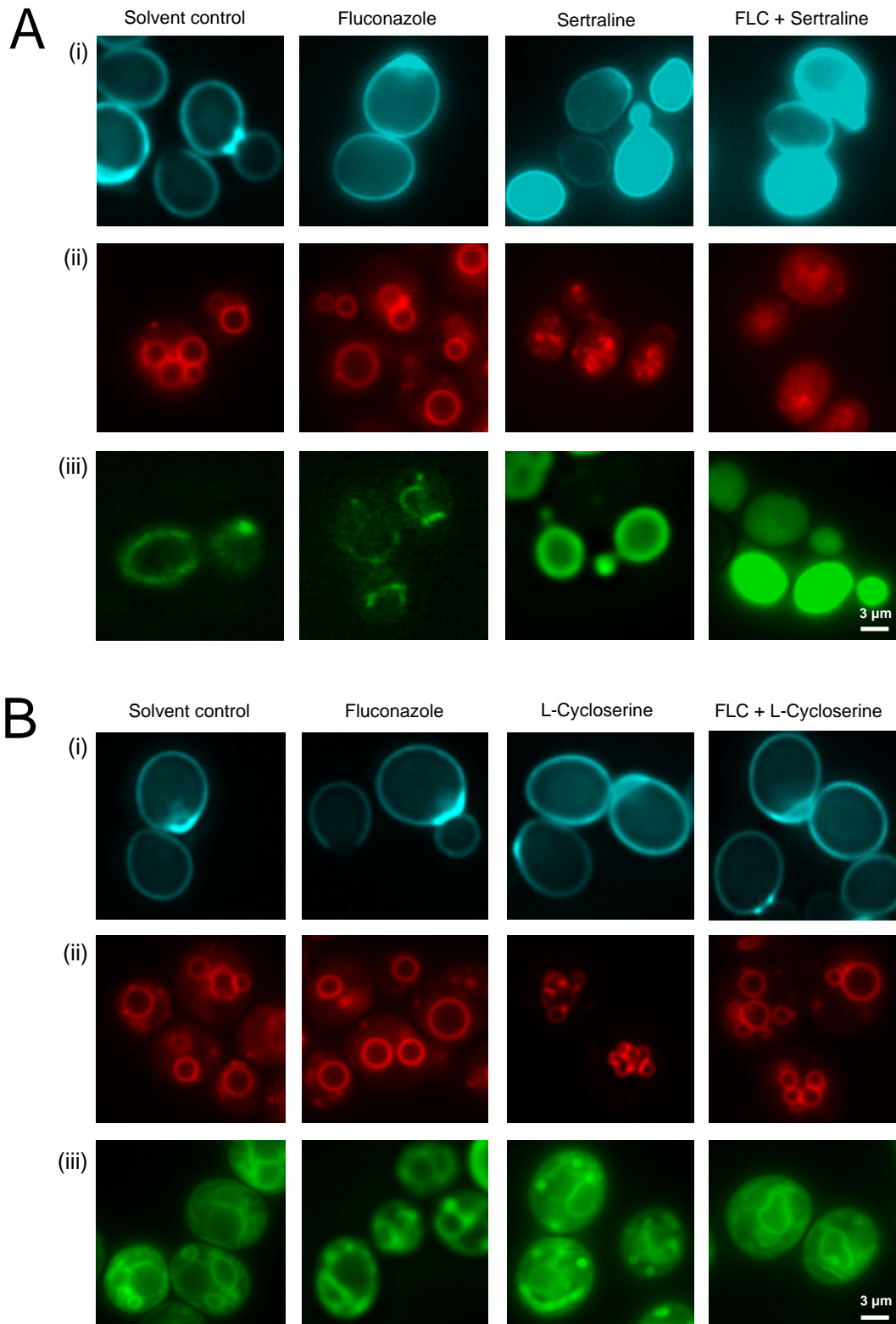


Figure 3.19: Images of wild type *S. cerevisiae* grown in the presence of the indicated drugs and stained with (i) Calcofluor White M2R, (ii) FM4-64 and (iii) Mitotracker Green FM, and imaged by fluorescence microscopy. (A) Sertraline (128  $\mu\text{g}/\text{mL}$ ) in the presence and absence of fluconazole (64  $\mu\text{g}/\text{mL}$ ). (B) L-cycloserine (128  $\mu\text{g}/\text{mL}$ ) in the presence and absence of fluconazole (128  $\mu\text{g}/\text{mL}$ ).

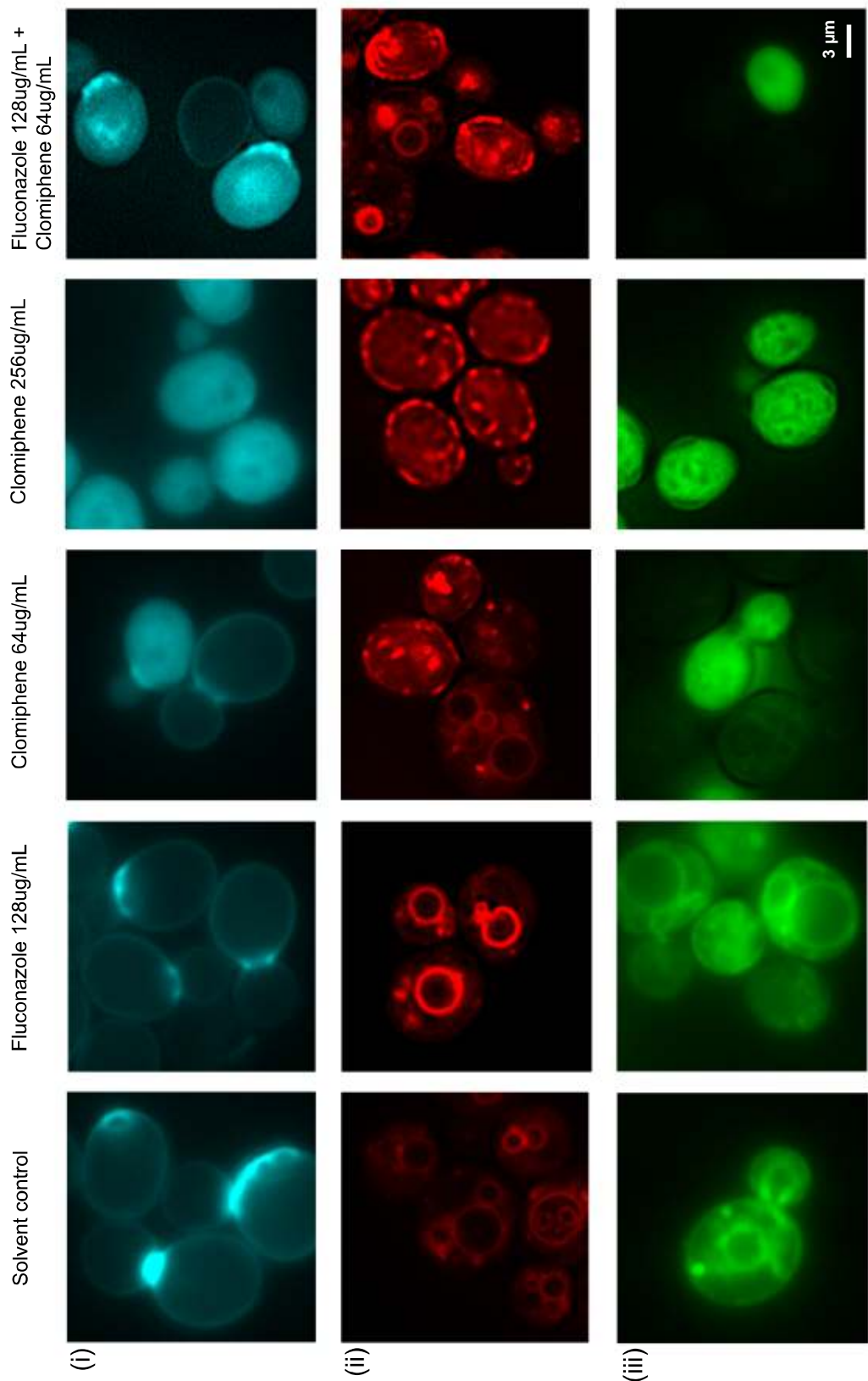


Figure 3.20: Images of wild type *S. cerevisiae* treated with either no drug, fluconazole (128  $\mu\text{g}/\text{mL}$ ), clomiphene (64  $\mu\text{g}/\text{mL}$  and 256  $\mu\text{g}/\text{mL}$ ), or a combination of fluconazole and clomiphene (at 128  $\mu\text{g}/\text{mL}$  and 64  $\mu\text{g}/\text{mL}$ , respectively). The fluorescent dyes used for staining were: (i) Calcofluor White M2R, (ii) FM4-64 and (iii) Mitotracker Green FM. Due to the high amount of dye in cells treated with clomiphene, the exposure time was greatly reduced in rows (i) and (iii) for samples treated with clomiphene. Exposure times for the images in row (iii) were as follows, from left to right: 2 seconds, 3 seconds, 35 milliseconds, 15 milliseconds and 15 milliseconds.

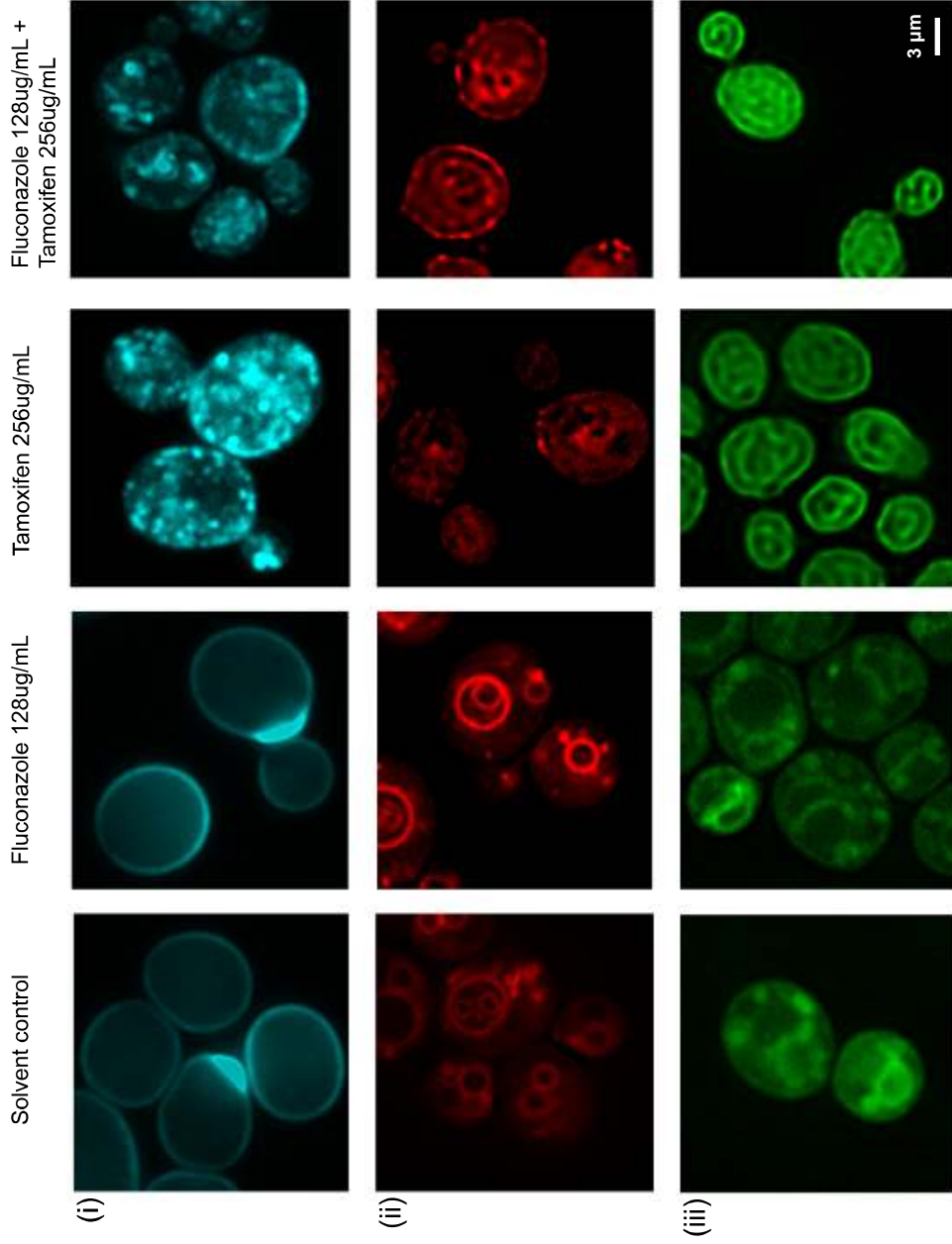


Figure 3.21: Images of wild type *S. cerevisiae* treated with either no drug, fluconazole (128  $\mu\text{g}/\text{mL}$ ), tamoxifen (256  $\mu\text{g}/\text{mL}$ ), or a combination of fluconazole and tamoxifen (at 128  $\mu\text{g}/\text{mL}$  and 256  $\mu\text{g}/\text{mL}$ , respectively). The fluorescent dyes used for staining were: (i) Calcofluor White M2R, (ii) FM4-64 and (iii) Mitotracker Green FM. The exposure time was greatly reduced for tamoxifen treated samples in rows (i) and (iii) to obtain images that are not overexposed. Exposure times for images in row (i) were as follows, from left to right: 2 seconds, 2 seconds, 100 milliseconds and 100 milliseconds. In row (iii) they were: 8 seconds, 4 seconds, 180 milliseconds and 180 milliseconds.

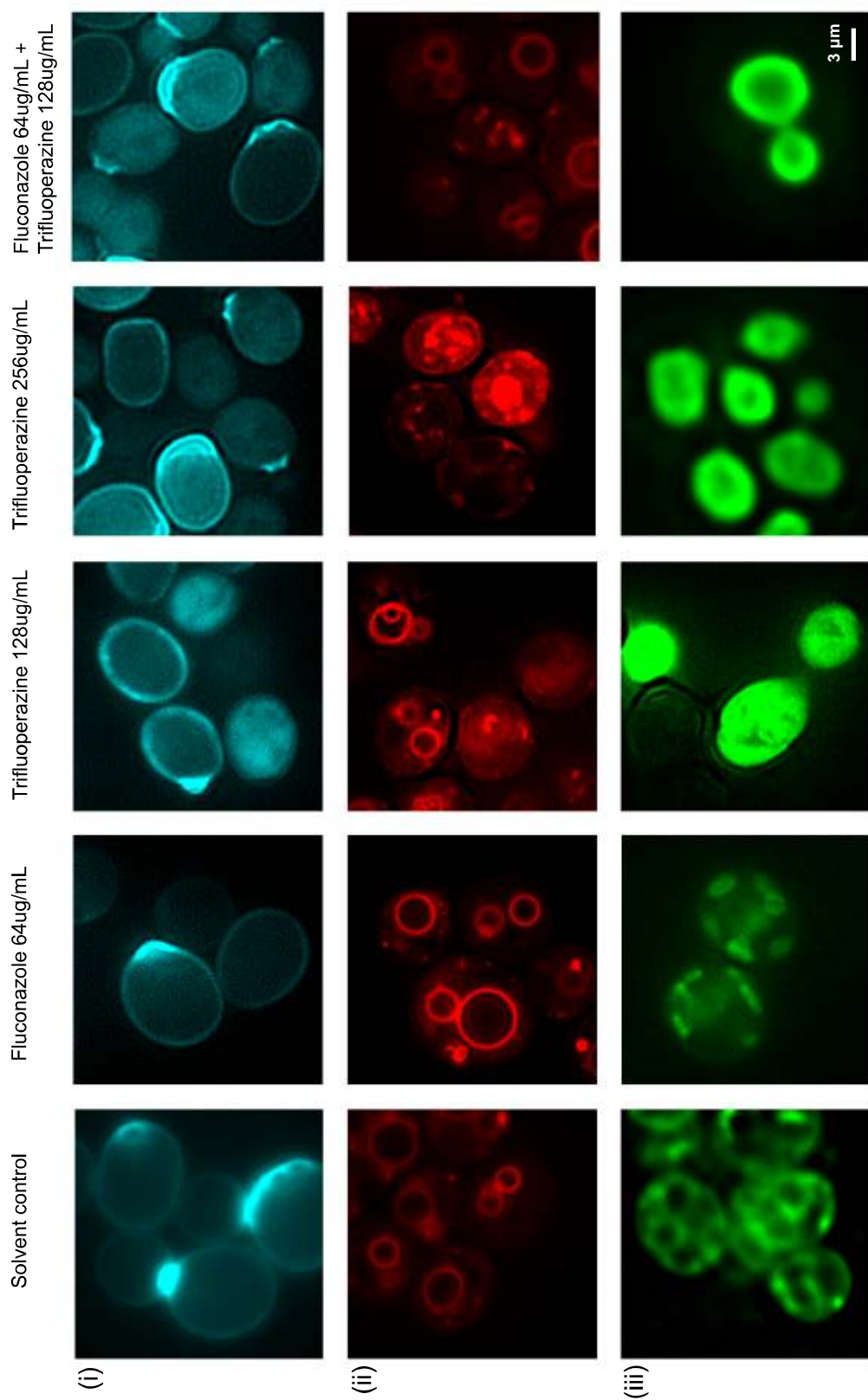


Figure 3.22: Images of wild type *S. cerevisiae* treated with either no drug, fluconazole (64  $\mu\text{g}/\text{mL}$ ), trifluoperazine (128  $\mu\text{g}/\text{mL}$  and 256  $\mu\text{g}/\text{mL}$ ), or a combination of fluconazole and trifluoperazine (at 64  $\mu\text{g}/\text{mL}$  and 128  $\mu\text{g}/\text{mL}$ , respectively). The fluorescent dyes used for staining were: (i) Calcofluor White M2R, (ii) FM4-64 and (iii) Mitotracker Green FM. The exposure time was greatly reduced for trifluoperazine treated samples in rows (i) and (iii) to obtain images that are not overexposed. Exposure times for images in row (iii) were as follows, from left to right: 2 seconds, 1 second, 100 milliseconds, 100 milliseconds and 100 milliseconds.

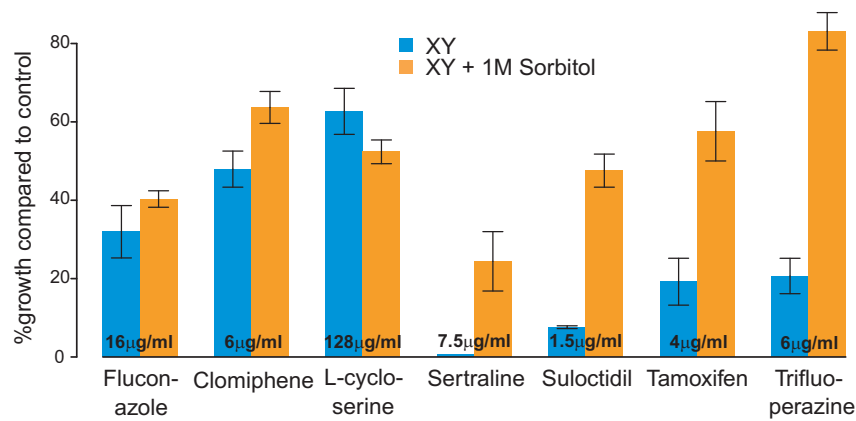


Figure 3.23: Growth of wild type *S. cerevisiae* treated with the synergisers or fluconazole in the presence and absence of 1 M sorbitol as a percentage of growth in control wells. The mean of four independent measurements is shown; error bars correspond to standard error.

For each of the reporter dyes, the staining pattern in response to fluconazole was similar to that generated with solvent controls (second column in Figures 3.19A, 3.19B, 3.20, 3.21, 3.22). In contrast, single drug treatment with trifluoperazine, tamoxifen, clomiphene and sertraline caused a drastic loss of dye localisation and strong intracellular accumulation (Figure 3.19A, 3.20, 3.21, 3.22). In particular, FM4-64 staining revealed the disruption of vacuolar structures. This suggests severe loss of cell membrane integrity. The same effects were observed when cells were treated with the synergistic drug combinations. The microscopy images confirm an effect on membrane integrity of trifluoperazine, tamoxifen, clomiphene and sertraline as suggested by the chemical-genetic interactions described in Section 3.2.3. Consistent with its different chemical-genetic profile, treatment with L-cycloserine alone or in combination with fluconazole had no obvious effects on the localisation of any of the dyes (Figure 3.19B).

### Sorbitol rescue assay

Osmotic stress caused by compromised membrane and/or cell wall structures can often be rescued with isotonic solutions such as NaCl or sorbitol that act as osmotic stabilisers. To test if the effect of the synergisers could be rescued by osmotic stabilisation, a *Saccharomyces cerevisiae* WT strain was grown in the presence of fluconazole, clomiphene, L-cycloserine, sertraline, suloctidil, tamox-

ifen and trifluoperazine with and without 1 M sorbitol added to the medium. Growth curves were obtained in 96-well plates. Addition of sorbitol was found to relieve the growth inhibitory effects of trifluoperazine, tamoxifen, clomiphene, sertraline, and suloctidil (Figure 3.23). This again supported the idea of a common membrane perturbation mechanism for these compounds. No such protective effects were observed in cells treated with fluconazole or L-cycloserine (Figure 3.23).

### **3.2.5 Integration of chemical-genetic interactions with genetic interaction networks**

The vast number of possible drug combinations is a major challenge in the discovery of synergistic drug pairs (Sharom *et al.*, 2004; Lehár *et al.*, 2008). As described in Section 1.3.5, different approaches have been developed to predict effective drug combinations computationally. Here, the chemical-genetic profiles described in 3.2.3 were examined for their predictive power by integrating them with genetic interaction data obtained from BIOGRID (Breitkreutz *et al.*, 2008; BIOGRID release 2.62). This global interaction network contains genetic interactions from both, low throughput and high throughput experiments.

#### **Genetic interactions to rationalise synergy**

Analogous to genetic interactions, chemical-genetic interactions are based on the idea of parallel pathways that converge onto an essential process in the cell. Chemical-genetic profiles of single drugs can be interpreted as a pathway response of the genes that are affected by drug treatment. The chemical genetic profiles of fluconazole and the synergising drugs were investigated to see if they represent such parallel pathways by analysing the genetic interaction space between the respective sets of sensitive deletion strains. The 50 most sensitive deletion strains to fluconazole were analysed in combination with the 50 most sensitive deletion strains for each of the synergising drugs. Many genetic interactions were found between the sets of sensitive deletion strains for all six syncretic drugs. This is especially true for the common set of deletion strains that are sensitive to the set

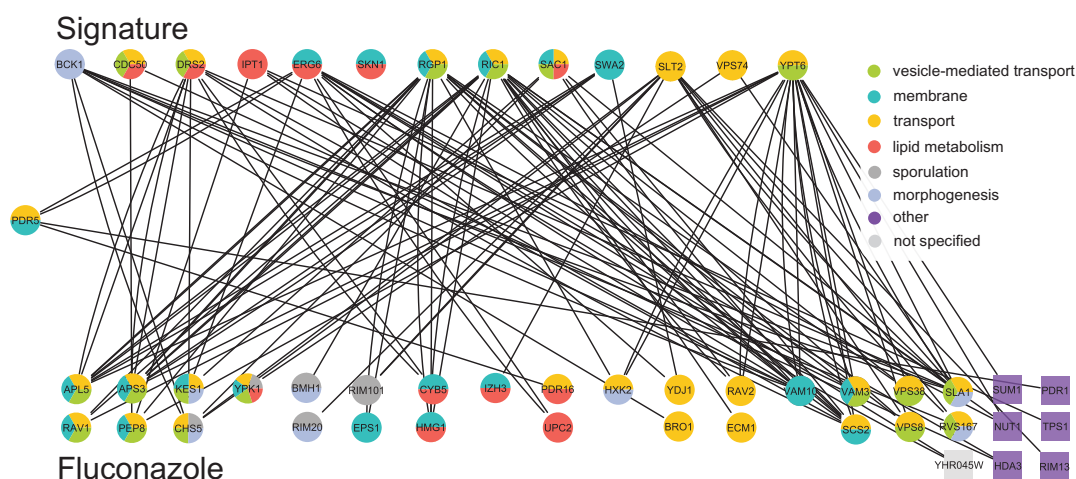


Figure 3.24: Integration of chemical-genetic and genetic networks. Bipartite graph representing known genetic interactions between the 50 deletion strains most sensitive to fluconazole treatment and the signature strains affected by the five membrane active compounds. *PDR5* was a member of both sets and is therefore positioned midway between the two sets. GO categories were visualised using Golorize (Garcia *et al.*, 2007).

of membrane active compounds that are referred to as 'signature' (Figure 3.24).

Two different tests were devised to determine the significance of this enrichment of genetic interactions. The first test was based on random sampling from a chemical genetic space (CGS) that was defined based on data from Hillenmeyer *et al.*, 2008. 1143 non-essential genes that are responsive to drug treatment when deleted comprised the CGS. The resulting background distributions for the number of genetic interactions between gene sets of fixed sizes randomly chosen from CGS are shown in Figure 3.25A. The black curve represents the background distribution for the syncretic drugs because 50 deletion stains were used for analysis of each drug. The background distribution for the signature deletion strains is shifted to the left since this set contains only 14 strains. Arrows indicate the actual number of genetic interactions for each drug. Calculation of p-values confirmed that there is a significant enrichment of interactions with tamoxifen, trifluoperazine, clomiphene, sertraline, suloctidil and the signature deletion strains sensitive to the membrane targeting compounds (p-values <0.05) whereas the p-value for L-cycloserine was not significant (Table 3.3).

A more conservative test was also applied to look at pathway separation (Kel-

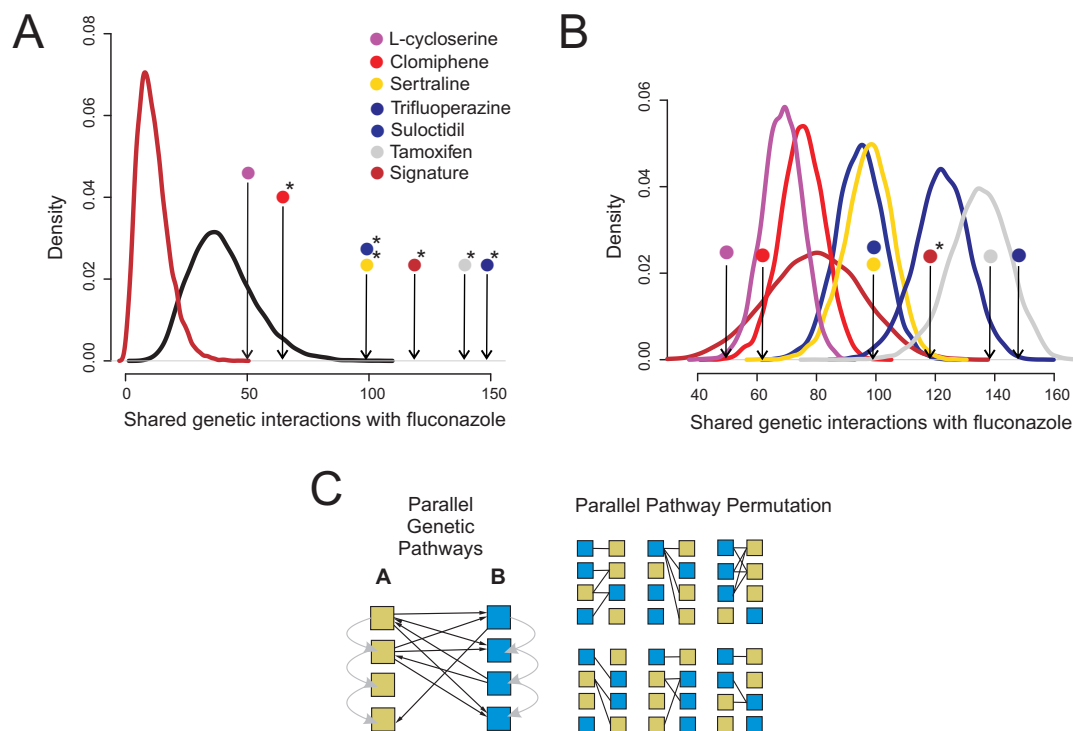


Figure 3.25: Rationalization of synergistic interactions. (A) Results of the chemical genetic space (CGS) simulations with the 50 most sensitive deletion strains for each synergiser as well as the signature strain set. The actual numbers of genetic interactions between gene sets are indicated by arrows. The black curve depicts the background distribution of genetic interactions between two random sets of 50 non-essential deletion strains chosen from 1143 strains that respond to a variety of drug treatments (Hillenmeyer *et al.*, 2008). The dark red curve corresponds to the same background distribution except that the size of the second sample set size matches the size of the signature deletion strain set. (B) Results of the parallel pathway permutation (PPP) simulations for each of the drugs as well as the signature strain set. Coloured curves represent background distributions for the different drugs. Arrows indicate the actual number of interactions and colour code is the same as in Figure 3.25A (C) Scheme of PPP simulations. \* in (A) and (B) indicate p-values  $<0.05$ .



Drug	CGS p-value	PPP p-value
L-cycloserine	0.0869	0.9283
Clomiphene	0.0468	0.9609
Sertraline	0.0001	0.4168
Tamoxifen	$< 10^{-7}$	0.327
Trifluoperazine	$< 10^{-7}$	0.001
Suloctidil	0.0006	0.2724
Signature strains	$< 10^{-7}$	0.0056

Table 3.3: P-values for the CGS and PPP simulations for profiles of L-cycloserine, clomiphene, sertraline, suloctidil, tamoxifen and trifluoperazine as well as for the signature deletion strains.

ley & Ideker, 2005). Parallel pathway permutation (PPP) was implemented, a simulation where the chemical genetic interactors of each of the synergistic drugs and fluconazole were pooled and randomly divided into two groups (Figure 3.25C). The background distributions and the actual values for each drug are shown in Figure 3.25B. Using this simulation, only the set of signature deletion strains and the top 50 most sensitive deletion strains for trifluoperazine showed significant enrichment (p-values  $< 0.05$ ; Table 3.3). It is thus possible to rationalise synergism based on the genetic interactions that link the chemogenomic profiles of compound pairs that exhibit synergy.

### Assessment of predictive power of signature deletion strain set

Following on from the results with the fluconazole synergisers, the predictive power of the signature deletion strain set (defined in Figure 3.18) was assessed. The chemical-genetic profiles of psychoactive drugs generated by (Ericson *et al.*, 2008) were analysed retrospectively. Of the 81 compounds that impaired yeast growth, 16 were represented in the Prestwick chemical library. The sensitivity of the signature strains in these chemical genetic profiles was examined (Figure 3.26). Seven of these compounds were predicted to synergise with fluconazole and indeed, all seven drugs showed activity in the screen. Four compounds have been classified as hits whereas the other three exhibited weak activity. These findings show, that synergistic drug combinations can be predicted based on chemical-

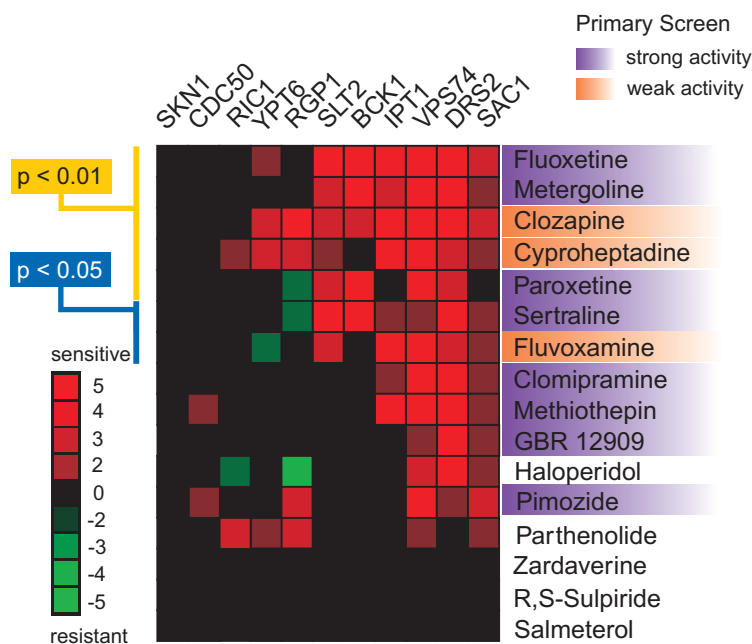


Figure 3.26: Chemical-genetic profiles of 11 signature deletion strains in response to 16 previously profiled psychiatric drugs (Ericson *et al.*, 2008) that are present in the Prestwick chemical library. P-values indicate significance of enrichment of signature strains. Compounds marked as active (purple) were clear hits in our screen (80% inhibition and/or 2 MADs away from diagonal) whereas weak activity refers to compounds that are 1 MAD away from the diagonal and show at least 20% growth inhibition.

genetic interaction profiles.

Analysis of the profiles of all 81 compounds from the Ericson *et al.*, 2008 dataset resulted in a list of 20 compounds that are predicted to interact with fluconazole (Figure 3.27). Seven of these drugs were also represented in Figure 3.26 since they are present in the Prestwick chemical library. This means that an additional 13 compounds were predicted based on the signature deletion strains meaning that the signature was actually found in various chemical-genetic profiles. Like sertraline, many of these drugs are inhibitors of dopamine (re-)uptake.

### 3.2.6 Further characterisation of drug synergies

Various additional experiments were conducted to further characterise the synergising drugs. First, potential drug interactions with other inhibitors of the ergosterol pathway were investigated. Drug interactions between synergisers were

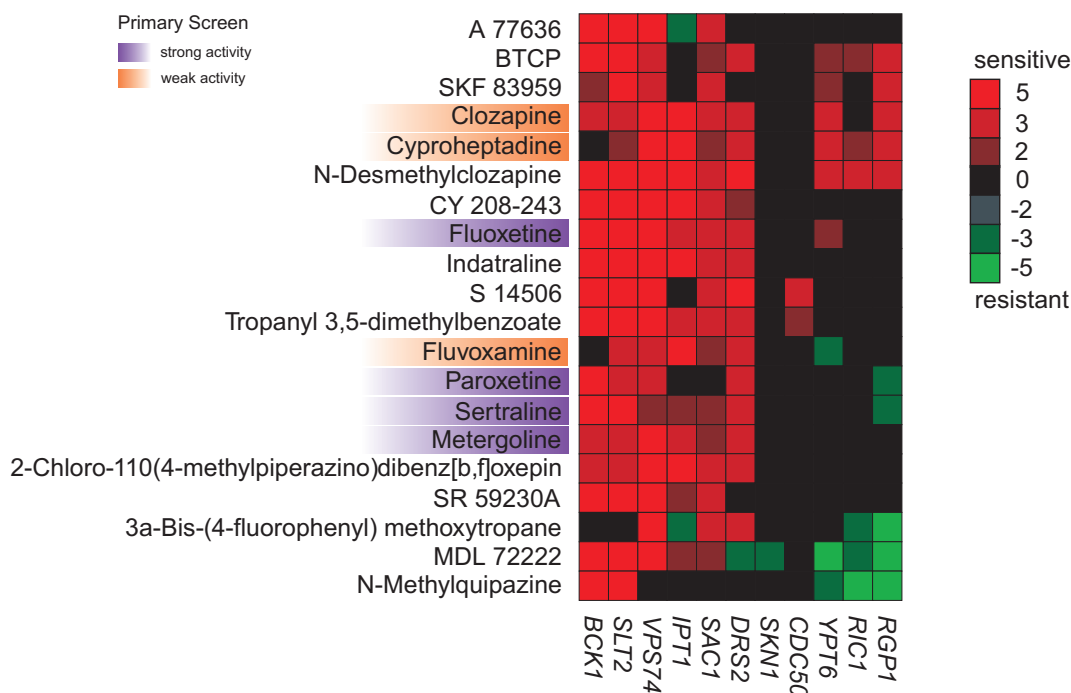


Figure 3.27: Top predictions for synergisers based on profiles of signature deletion strains. Chemical-genetic profiles of 11 signature deletion strains in response to all 81 profiled psychiatric drugs (Ericson *et al.*, 2008). Compounds marked as active (purple) were clear hits in our screen (80% inhibition and/or 2 MADs away from diagonal) whereas weak activity refers to compounds that are 1 MAD away from the diagonal and show at least 20% growth inhibition. Drugs with a p-value <0.05 for enrichment of signature strains are shown.

also assessed and the antifungal effects of 3-way combinations with fluconazole analysed. Finally, the combination of sertraline and fluconazole was tested in an *in vivo* model of *Cryptococcus* infection and the drug combination's efficacy was tested against clinical isolates of *Candida* strains.

### Fluconazole- and species-specificity of drug interactions

To investigate if the synergies are specific to fluconazole, two of the synergisers were tested in combination with other ergosterol biosynthesis inhibitors for drug interactions. Terbinafine, an inhibitor of the Erg1 squalene epoxidase, and ketoconazole, an imidazole inhibitor of ERG11 were used. To assess interactions in different fungal species, the psychoactive drugs trifluoperazine and sertraline were selected since they exhibited synergy with fluconazole against each of the fungal species tested in Section 3.2.2.

Strain	Terbinafine		Ketoconazole	
	Trifluoperazine	Sertraline	Trifluoperazine	Sertraline
<i>C. neoformans</i> (H99)	2	0.75	0.25	0.38
<i>C. albicans</i> (Caf2-1)	2	0.5	0.38	0.16
<i>S. cerevisiae</i> (BY4741)	0.38	0.52	0.38	0.31

Table 3.4: FICI values for combinations of sertraline and trifluoperazine with the ergosterol biosynthesis inhibitors terbinafine and ketoconazole in different species. Values smaller than 0.5 indicate synergy, values between 0.5 and 1 indicate additivity and values higher than 1 indicate no interaction.

The FICI values for the combinations in *Cryptococcus neoformans*, *Candida albicans* and *Saccharomyces cerevisiae* are summarised in Table 3.4. Ketoconazole was synergistic with both, trifluoperazine and sertraline, in all three fungal species. The results for terbinafine were less consistent. Synergy was observed with sertraline in *Candida* and *Saccharomyces* but not *Cryptococcus*. With trifluoperazine it only synergised in *Saccharomyces*. These findings suggest that even though mechanisms of synergy are conserved between different inhibitors of the same pathways, there are species-specific differences in response to different compounds. These are most likely due to differences in the genetic network structure between species (Kuo *et al.*, 2010).

### Higher order combination of synergisers

Drugs with identical mode of actions are not expected to show synergy, but instead should act in an additive manner. To further characterise the mode of action of the synergisers, pairwise combinations between the membrane active drugs sertraline, trifluoperazine, suloctidil and tamoxifen, as well as with the sphingolipid-selective synergiser L-cycloserine were examined in an *S. cerevisiae* WT strain (Table 3.5).

Despite their partially overlapping chemical-genetic profiles, synergistic interactions between tamoxifen and trifluoperazine (FICI = 0.5), sertraline and trifluoperazine (FICI = 0.4) and sertraline and tamoxifen (FICI = 0.5) were observed. These results suggest that in addition to the effects on membrane permeability, each compound likely elicits one or more other effects that contribute to their overall mechanism of action. The combination of these additional effects results

	<b>Sert (32)</b>	<b>Sert (64)</b>	<b>Tri</b>	<b>Tri +FLC</b>	<b>Tam</b>	<b>Tam +FLC</b>	<b>Suloc</b>	<b>Suloc +FLC</b>
Trifluoperazine	0.38	0.50						
Tamoxifen	0.50	0.63	0.50	0.75				
Suloctidil	1.25	1.50	2.00	0.56	1.00	0.75		
L-cycloserine	1.25	0.63	1.00	2.00	1.00	0.52	2.00	0.31

Table 3.5: Analysis of interactions between syncretic drugs and higher order combinations with fluconazole. L-Cycloserine, suloctidil (Suloc), tamoxifen (Tam) and trifluoperazine (Tri) were combined as indicated, in the presence or absence of 1/8 MIC fluconazole (4  $\mu\text{g}/\text{mL}$ ) and assayed for growth inhibition of the *S. cerevisiae* strain (BY4741). FICI values smaller than 0.5 indicate synergy, values between 0.5 and 1 indicate additivity and values higher than 1 indicate no interaction. Drug concentrations are indicated in  $\mu\text{g}/\text{mL}$ .

in further synergism. This means it should be possible to devise higher order combinations between synergisers that lead to even stronger growth inhibition in the presence of fluconazole. Thus, compound pairs were tested in the presence of fluconazole in three-way combinations (Table 3.5). In these assays, fungal growth was often potently inhibited. Specific sensitivity to the suloctidil/trifluoperazine, L-cycloserine/suloctidil and L-cycloserine/tamoxifen combinations was revealed by titration of fluconazole concentrations. The presence of just 1/8 MIC fluconazole showed strong effects (Table 3.5). L-cycloserine/suloctidil exhibited the most potent synergy with fluconazole with an FICI value of 0.3. These results demonstrate that the subtly different effects of the individual synergisers allow to incrementally build higher order synergistic combinations.

#### ***In vivo* assessment of anti-fungal synergy in an insect model of infection**

The efficacy of the synergistic drug combinations in an *in vivo* infection model of cryptococcal virulence, the caterpillar of the greater wax moth *Galleria mellonella* was also evaluated (Mylonakis *et al.*, 2005; Scully & Bidochka, 2006). The effect of treatment with single drugs and drug combinations on survival rates of caterpillars infected with *C. neoformans* was assessed because this virulent pathogen is prevalent in immune-compromised patients. Upon infection of *G. mellonella* with *C. neoformans*, the caterpillars were injected with drug(s) or DMSO the following day.

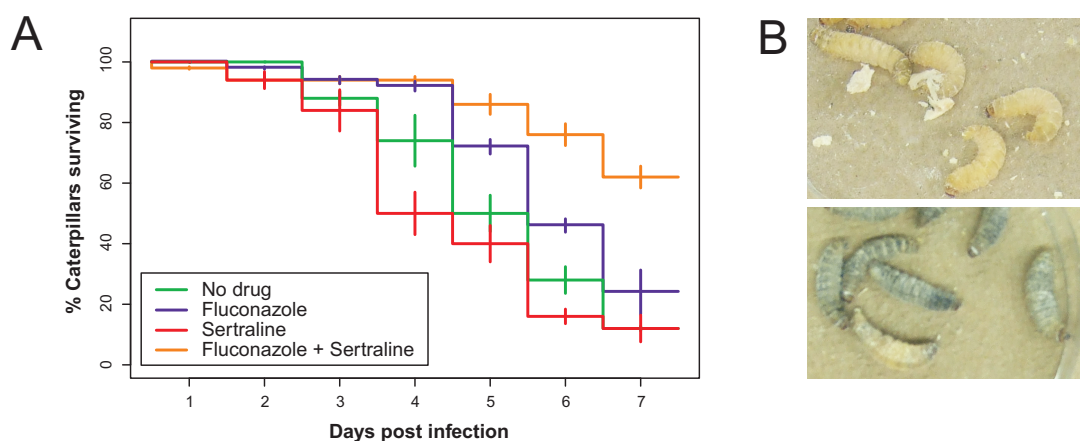


Figure 3.28: Synergistic activity of fluconazole with sertraline in an *in vivo* infection model. (A) *G. mellonella* caterpillars were injected with *C. neoformans* H99 ( $8 \times 10^3$  cfu) on day 0 and with drugs alone or in combination (26  $\mu$ g sertraline; 1  $\mu$ g fluconazole) on day 1 and incubated for one week at 37°C. Values plotted are the mean of three independent experiments. (B) Picture of uninfected *G. mellonella* caterpillars (top); melanisation of infected *G. mellonella* caterpillars (bottom). Emma Griffith provided the photos of *G. mellonella*.

Of the five synergising drugs suloctidil, sertraline, tamoxifen, trifluoperazine and fenpropidin, only sertraline showed a significant effect on worm survival rate in combination with fluconazole. Figure 3.28A shows the survival rates of worms treated with fluconazole, sertraline, both drugs in combination and with solvent control alone (DMSO). Without any drug treatment and in response to sertraline treatment, only about 10% of the worm population was alive after seven days. Application of fluconazole increased survival rates to 20%. Treatment with sertraline and fluconazole in combination, however, resulted in a significant increase of the survival rate to 60% which confirms the synergistic action between these two drugs *in vivo* (p-value < 0.02).

### Synergistic activity against fluconazole-resistant *Candida* isolates

Since the sertraline/fluconazole combination proved effective in an *in vivo* infection model, it was further tested against clinically resistant isolates of *Candida* species. The effect of the drug combination on the clinical isolates *C. albicans* 2007, *C. albicans* 2008 and *C. glabrata* as well as a resistant *C. parapsilosis* control strain was assessed with checkerboard assays.

The final OD readings of the growth assays are shown in Figure 3.29A for

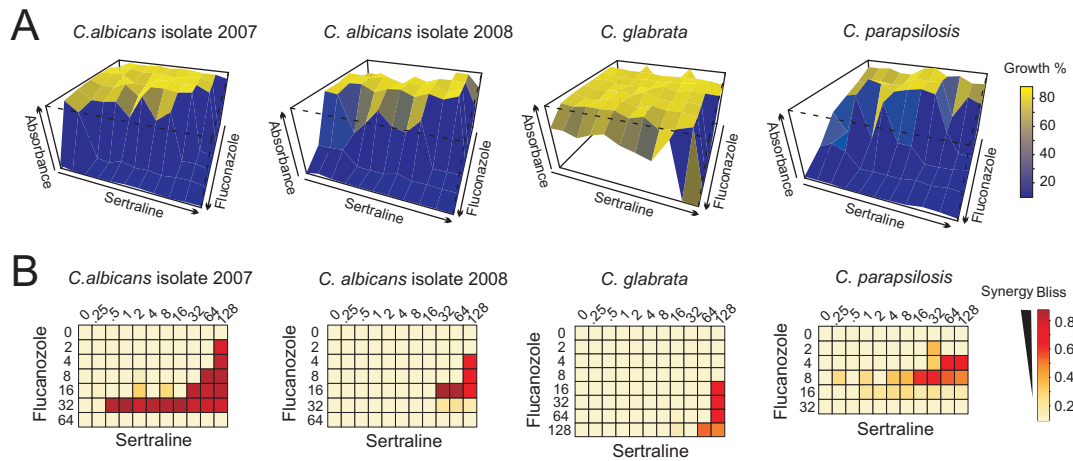


Figure 3.29: Synergistic activity of fluconazole with sertraline against clinical isolates of *Candida* strains. (A) Combination matrix assays against drug-resistant isolates of *C. albicans* 2007, *C. albicans* 2008, *C. glabrata* and *C. parapsilosis*. Optical density readings were plotted for the combinations of two-fold dilutions of each drug. (B) Analysis of Bliss synergy for the combination assays in panel A. Drug concentrations are in  $\mu\text{g/mL}$ . Jan Wildenhain generated the surfaces and heatmaps.

all four strains. Calculation of Bliss synergy scores for each of the matrices revealed that the sertraline/fluconazole combination has a synergistic effect in all four *Candida* strains because they all have Bliss scores greater than 0.5 (Figure 3.29B). Determination of the MIC of fluconazole in combination with sertraline shows that in the presence of sertraline, the susceptibility of the *Candida* strains to fluconazole increased by up to 32-fold (Table 3.6). MIC values of the fluconazole resistant strains ranged from 2-8  $\mu\text{g/mL}$  which is comparable to wild type (8  $\mu\text{g/mL}$ ) and the drug pump-deficient strains of *C. albicans* (2  $\mu\text{g/mL}$ ). The FICI values in Table 3.6 reveal that the combination of sertraline and fluconazole is synergistic in both *C. albicans* isolates as well as the *C. parapsilosis* reference strain. The FICI value for the *C. glabrata* isolate suggests that the drug combination has an additive effect only. This is inconsistent with the Bliss scores shown in Figure 3.29B and is most likely due to the fact that the MIC values of the single drugs that are used in the FICI calculation could not be determined in the *C. glabrata* isolate. These experiments show that the synergistic drug interactions in reference laboratory strains translate to drug-resistant pathogens derived from clinical environments.

Species	MIC <sub>FLC</sub>	MIC <sub>Sertr</sub>	Lowest MIC <sub>FLC+Sertr</sub>	FICI
<i>C. albicans</i> 2007	64	> 128	4	< 0.5
<i>C. albicans</i> 2008	64	> 128	2	< 0.5
<i>C. glabrata</i>	> 128	> 128	8	0.625*
<i>C. parapsilosis</i>	32	> 128	2	0.375

Table 3.6: MIC and FICI values for drug resistant *Candida* strains treated with combinations of fluconazole and sertraline. MIC values are given in  $\mu\text{g/mL}$ . \* indicates a FICI value based on two MICs that are  $> 128$  and is therefore probably unreliable.

### 3.2.7 Summary of Results

This project aims to extend the concept of chemical synthetic lethality from model organisms to clinically relevant fungal pathogens. The Prestwick Chemical library, which contains 1120 known drugs, was screened against *Candida albicans*, *Cryptococcus neoformans* and *Cryptococcus gattii*, as well as the genetically tractable budding yeast *Saccharomyces cerevisiae* to identify synergistic enhancers of the fungistatic drug fluconazole. Compounds, not previously known for their anti-fungal properties, showed potent growth inhibition in combination with fluconazole. These interactions were often genus- or species-specific and improved the action of fluconazole from fungistatic to fungicidal.

A subset of compounds was selected to investigate the mechanism of action of their interaction with fluconazole in more detail. Chemical-genetic profiles revealed two classes of compounds: one causes membrane perturbation and the other inhibits sphingolipid biosynthesis. Integration of the chemical-genetic profiles with genetic interaction data allowed for prediction of further synergistic drug combinations based on the mode of action studies. Strikingly, higher order combinations of fluconazole and synergisers, further increased antifungal activity. Synergistic combinations were shown to be active in the *in vivo* infection model of *G. mellonella* and efficacious against fluconazole-resistant fungal isolates. Overall, this approach successfully combines the 'drug combination' and the 'repurposing of known drugs' strategies to identify potential leads for new antifungal therapies.



## 3.3 Discussion

### 3.3.1 New antifungal chemical space revealed by systematic screens for syncretic drug combinations

In infectious disease control, the combination of known antifungal agents is an established therapeutic approach (Johnson & Perfect, 2010). The work presented in this chapter shows that the combination of a known antifungal with bioactive drugs that do not have antifungal potential on their own allows for the antifungal chemical space to easily be expanded. As described in this chapter, this also applies to off patent drugs that have previously been approved for other indications. Systematic screens against various pathogenic fungi in the presence of sub-therapeutic concentrations of the known antifungal fluconazole resulted in the identification of novel syncretic drug combinations. The 148 drugs identified as hits comprised a chemically diverse set of compounds covering a broad spectrum of human therapeutic areas. These drugs would probably not have been tested for their antifungal potential by infectious disease clinicians. (Section 1.3.4)

The fungicidal activity exhibited by many of the syncretic combinations, is a highly desirable feature for infectious disease control. The combination of fluconazole and sertraline (the antidepressant Zoloft<sup>®</sup>) was active against all species tested and showed fungicidal potential in two species. This combination was also successfully tested against clinical drug-resistant *Candida* isolates and in an *in vivo* insect model of *C. neoformans* infection. Fungal infections of the CNS are a particular clinical challenge because of the requirement for drugs to pass the blood-brain barrier. There is potential for the sertraline-fluconazole combination to be effective in the treatment of fungal meningitis because sertraline targets serotonin receptors in the CNS.

### 3.3.2 Molecular mechanisms of synergism

A subset of six fungicidal synergisers was subjected to genome-wide chemical genetic screens in the budding yeast *S. cerevisiae*. Two different mechanisms for synergy with fluconazole were revealed by these experiments. Five of the

compounds (trifluoperazine, tamoxifen, clomiphene, sertraline and suloctidil) exhibited genetic sensitivities and cell biological phenotypes that are typically associated with loss of membrane integrity. The membrane perturbation that these compounds cause may impair fluconazole export via drug efflux pumps, increase susceptibility of cells to the accumulation of toxic ergosterol pathway intermediates, and/or impair import of extracellular ergosterol (Kuo *et al.*, 2010). Notably, all five compounds are cationic amphiphilic drugs (CADs) that are known to intercalate preferentially into one side of the membrane lipid bilayer. This has previously been shown to cause membrane expansion and cell wall stress (Sheetz & Singer, 1974), consistent with the chemical-genetic interactions with *NEO1*, *DRS2*, *SLT2* and *BCK1* that were observed. Further, Rainey *et al.* (2010) found genetic resistance to the CAD sertraline to be conferred by perturbation of vesicular membrane biogenesis and/or trafficking. L-Cycloserine on the other hand, exhibited a different set of genetic interactions, mostly with genes involved in early steps of sphingolipid biosynthesis consistent with its known mode of action. A novel potentiation effect between myriocin, another known sphingolipid biosynthesis inhibitor, and fluconazole was correctly predicted based on this interaction profile. There is further evidence that the inhibition of sphingolipid biosynthesis is responsible for the fluconazole-potentiating effects seen with L-cycloserine and myriocin. Ergosterol and sphingolipids are both essential components of the fungal cell membrane. They are found in lipid rafts and are involved in the modulation of ABC transporter localisation and function (Klappe *et al.*, 2009). Van Leeuwen *et al.* (2008) showed that myriocin treatment in *S. cerevisiae* results in decrease of ergosterol levels in the cell membrane. The gene *IPT1* is involved in the last step of sphingolipid biosynthesis, synthesis of the most abundant sphingolipid mannose inositol phosphorylceramide and is regulated by Pdr1 and Pdr3, indicating that modulation of membrane composition is one component of the pleiotropic drug response (Hallstrom *et al.*, 2001).

New approaches to antifungal therapy might be developed based on our findings that CADs and inhibition of sphingolipid biosynthesis potentiate the action of fluconazole. In light of growing genetic and chemical-genetic interaction networks, mechanism- or pathway-based predictive approaches should become a

powerful tool in the discovery of synergistic drug combinations.

### 3.3.3 Species-specific synergistic effects

Hits from screens for fluconazole potentiation in the *S. cerevisiae* model system can generally be transposed to pathogenic fungi (Borisy *et al.*, 2003; Zhang *et al.*, 2007; Jansen *et al.*, 2009; Epp *et al.*, 2010). The primary screen data however suggests a considerable degree of species-specificity that by definition cannot be predicted from data generated with model organisms. While 63% (24/38) of hits against *S. cerevisiae* exhibited synergistic activity against one or more fungal pathogens in the primary screen, only 24% (24/101) of the all hits against the pathogenic species were identified in *S. cerevisiae*. This observation highlights the need to undertake primary screens in the pathogen of interest.

These genus- and species-specific syncretic interactions reflect differences in the genetic networks that govern cellular responses to different compounds (Perlstein *et al.*, 2007). Different pathogenic species diverged from a common ancestor over 100 million years ago and have since adapted to specific host environments. Drug susceptibility can also be affected by developmental system drift (True and Haag, 2001) as has been documented with nikkomycin Z. This drug has different effects on chitin synthase paralogs in *Candida* and *Saccharomyces* (Gaughran *et al.*, 1994; Sudoh *et al.*, 2000). The differences in transcriptional response to fluconazole treatment in *Saccharomyces*, *Candida* and *Kluyveromyces* also reflect the distinct mechanisms by which different species respond to the same perturbation (Kuo *et al.*, 2010). More generally, the evolutionary plasticity of genetic interaction networks might be reflected by these species-specific differences in the response to drug treatment (Kapitzky *et al.*, 2010). Species-selective drug combinations might enable development of antifungal therapies with increased efficacy and decreased host toxicity.

### 3.3.4 Devising higher order drug combinations

The structure of genetic networks predicts the existence of higher order drug combinations that exhibit greater potency and selectivity (Sharom *et al.*, 2004;

Ágoston *et al.*, 2005; Lehár *et al.*, 2007). In particular, compounds that target a number of genetically redundant parallel pathways may reveal n-way synergies. Consistent with this concept, the combination of a non-synergistic drug pair (sulactidil and L-cycloserine, a membrane active and sphingolipid inhibiting drug, respectively) with a low dose of fluconazole exhibited highly potent three-way synergism. Given the similarity of their chemical-genetic profiles, pairs of membrane active compounds unexpectedly showed synergistic interactions. This type of drug-drug interaction has been observed before in bacteria and yeast (Yeh *et al.*, 2006; Jansen *et al.*, 2009) and it suggests that each drug must have additional specific cellular targets that contribute to synergism. The chemical-genetic profiles of drugs are complex and reflect effects on primary and secondary targets in the cell, routes of drug metabolism and detoxification as well as genetic feedback between different network elements (Sharom *et al.*, 2004; Lehár *et al.*, 2008). Other interactions between fluconazole, Hsp90, reactive oxygen species, vesicle trafficking and calcium metabolism that have been documented, may play a role in these complex interactions (Cowen *et al.*, 2009; Xu *et al.*, 2009; Gamarra *et al.*, 2010; Epp *et al.*, 2010). Even though it has been suggested that drugs with similar chemical-genetic profiles are likely to interact synergistically (Jansen *et al.*, 2009), this is not very often the case (Yeh *et al.*, 2006). Even for drugs with well characterised mechanisms of action their genetic interaction profile can be very different from that of their presumptive target as seen for fluconazole, for example. Fluconazole shares many genetic interactions with *ERG11*, its known target, but more than half of the chemical-genetic interactors of fluconazole are not shared (Parsons *et al.*, 2004).

The concept of n-way synergies will become more important as combination therapies become more widely used. Given the complex action of small molecules in the cell, it will be a challenge to rationally predict n-way synergies. Our results however demonstrate, that it is not impossible to devise synergistic higher order drug combinations.

### 3.3.5 Therapeutic implications

Combinatorial anti-infective therapies have various benefits including lower efficient doses of individual drugs, lower rate of selection for drug resistant strains, enhanced antimicrobial activity and a decrease in host toxicity (Sharom *et al.*, 2004; Hopkins, 2008; Lehár *et al.*, 2008). This study and others (Zhang *et al.*, 2007; Jansen *et al.*, 2009; Epp *et al.*, 2010) have shown that syncretic drug combinations with increased antifungal potential can be readily identified in both model fungal species and pathogenic clinical isolates. While synergistic combinations have been shown to result in enhanced selectivity without adverse side effects (Lehár *et al.*, 2009) it is important to note that undesirable side effects may arise from these drug combinations as occurs with known contraindicated drugs, for example. In addition, the original therapeutic use of repurposed drugs can potentially lead to unwanted side effects.

Another important benefit may be improved activity in therapeutically recalcitrant tissues, such as the CNS. These combinatorial principles are also applicable to viral and bacterial pathogens as well as cancer and other genetic diseases (Borisy *et al.*, 2003; Fitzgerald *et al.*, 2006; Hopkins, 2008; Lehár *et al.*, 2009).

## CHAPTER 4

---

### Zebrafish and yeast

---

The work in Sections 4.2.1, 4.2.2, 4.2.3 has been published in:

- Hironori Ishizaki<sup>1</sup>, Michaela Spitzer<sup>1</sup>, Jan Wildenhain, Corina Anastasaki, Zhiqiang Zeng, Sonam Dolma, Michael Shaw, Erik Madsen, Jonathan Gitlin, Richard Marais, Mike Tyers and E. Elizabeth Patton: Combined zebrafish-yeast chemical-genetic screens reveal gene-copper-nutrition interactions that modulate melanocyte pigmentation. *Disease Models & Mechanisms*, 2010 Sep-Oct,3(9-10):639-51.

Permission to include a copy of the publication in this thesis has been obtained from The Company of Biologists. Images from the publication are reproduced with permission of the Company of Biologists.

Section 4.2.4 is part of the following paper that has been accepted for publication in *Nature Chemical Biology*:

- Hironori Ishizaki<sup>1</sup>, Linna Zhou<sup>1</sup>, Michaela Spitzer, Kerrie L. Taylor, Nicholas D. Temperley, Stephen L. Johnson, Paul Brear, Philippe Gautier, Amy Mitchell, Vikram Narayan, Terry K. Smith, Mike Tyers, Nicholas J. West-

---

<sup>1</sup>The first two authors are joint first authors and contributed equally to this work.

wood, and E. Elizabeth Patton: Off-target toxicity of 5-nitrofurans is mediated by ALDH2.

The work described in this chapter is the results of a collaboration with the Patton lab at the MRC Human Genetics Unit, Edinburgh. Dr. Hironori Ishizaki conducted the chemical screen in zebrafish and carried out many of the zebrafish experiments in collaboration with members of the lab. I designed and carried out experiments in *S. cerevisiae* to characterise 'interesting' compounds further.

## 4.1 Introduction

One of the advantages of chemical biology is that small molecules are likely to have the same mode of action in different species (see section introduction). This allows for interesting compounds identified in one species to be followed up in other model organisms. This chapter describes experiments I carried out in *S. cerevisiae* on compounds that were hits in a chemical high-throughput screen in zebrafish (*Danio rerio*) that was conducted in the lab of Liz Patton at the MRC Human Genetics Unit. The Patton lab studies melanocyte and melanoma biology. The introduction of this chapter is very specific to the collaborative zebrafish-yeast studies. The next two sections give background information about skin cancer (Section 4.1.1) and explain why zebrafish is a useful model to study melanocyte biology (Section 4.1.2). Sections 4.1.3 and 4.1.3 describe results from the chemical screen that was performed by the Patton lab in zebrafish to identify compounds that affect melanocyte development.

### 4.1.1 Skin cancer

The skin, consists of different cell types and skin cancers are classified by the types of cells involved. Basal cell carcinoma is the most common type of skin malignancy, followed by squamous cell carcinoma. They are both highly curable by local excision, radiotherapy and chemotherapy. Melanoma occurs in melanocytes, the pigment producing cells. It is far less common than the other two skin malignancies (~5%), but survival rates are very low, making melanoma the leading

cause of death from skin disease. Metastatic melanoma has a survival rate of less than one year. The primary cause of basal and squamous cell carcinoma is chronic accumulation of UV-induced skin damage. Melanoma, however, is thought to be promoted by multiple, intermittent severe burns, especially during early years of life. Pale skin pigmentation and hereditary factors are risk factors for melanoma, such that people with reduced skin melanin are highly susceptible to melanoma. Notably, in the Scottish population, many people have a polymorphism in an *Mc1r* gene that causes the production of red hair and freckling, which are also risk factors for melanoma.

The incidence of skin cancer has increased significantly over the last decades, especially in Western nations. This is presumably due to an increase in sunlight exposure caused by the reduction in the ozone layer as well as increased travel to warmer regions for holidays and social acceptance of tanned skin. In Scotland and northern England, melanoma incidence continues to increase in young women due to an increase in sun bed use. Malignant melanoma is ten times more common in Australasia than in Europe, but its frequency is increasing up to 7% per year in some parts of Europe. Scotland has the highest rise in incidence in the world. Annual incidence is 5-7 per 100,000 in Europe and the US, especially among Caucasians with fair skin and red hair.

Depending on the stage of the disease, treatment usually involves excision of the tumour together with a margin of skin. Malignant melanoma is highly resistant to radiotherapy and standard chemotherapy and is highly metastatic. The most commonly used drug is dacarbazine, an alkylating agent. Early promise of immunotherapy with interleukin-2, interferons and various vaccines was not followed by significant improvement of survival rates. The only exception is Ipilimumab, a recombinant human monoclonal antibody, that was approved by the FDA in March this year for immunotherapeutic treatment of unresectable or metastatic melanoma (Sondak *et al.*, 2011).

The rapid rise in skin cancer rates and the fact that it does not respond to well to available therapy options make melanoma a very challenging disease to treat. Studies of the development, proliferation, differentiation and migration of melanocytes might help answer the question why it is so difficult to treat and



might reveal starting points for new treatment options (Ko & Fisher, 2011).

#### **4.1.2 Zebrafish as a model to study melanocyte biology**

The zebrafish is an attractive model for the study of melanocytes as well as melanoma formation and progression for various reasons. As in other vertebrates, zebrafish body melanocytes are derived from the neural crest. Importantly, zebrafish embryos are easy to study because they develop outside the mother and are semi-transparent. This enables observation of melanocytes through all stages of development. Several studies have established melanoma models in the zebrafish. Patton *et al.* (2005) found that activating mutations in the BRAF gene, encoding a serine/threonine kinase involved in cell growth, led to development of nevi in fish and together with p53 pathway inactivation produces melanoma. Other genes that have been found to be involved in melanoma are conserved between mammals and zebrafish. These are melanocyte-specific genes like Mitf, Kit, endothelins and Snail/Slug as well as general genes like receptor tyrosine kinases, Ras family GTPases, BRAF, CDKN2A and the p53 pathway (reviewed in Ceol *et al.*, 2008 and Patton *et al.*, 2010).

#### **4.1.3 A chemical screen identified compounds that affect melanocytes and pigmentation in *D. rerio***

As described in section 1.3.3, zebrafish are very well suited for chemical screens (Taylor *et al.*, 2010). The Patton lab screened the 1280-member Library of Pharmacologically Active Compounds (LOPAC) and a chemical library of 1570 bioactive compounds (Spitzer *et al.*, in preparation) in zebrafish to identify compounds that cause developmental or melanocyte-specific phenotypes. The screen was conducted in 96-well format at a final compound concentration of 10  $\mu$ M with two zebrafish embryos per well. Nearly 200 compounds had an effect on melanocyte development and pigmentation. 45 of these compounds elicited a phenotype characteristic of copper depletion by causing hypopigmentation, an undulating notochord and an expanded hindbrain in the 2- to 3-day-old fish (Figure 4.1B). The group of copper metabolism compounds included known copper-

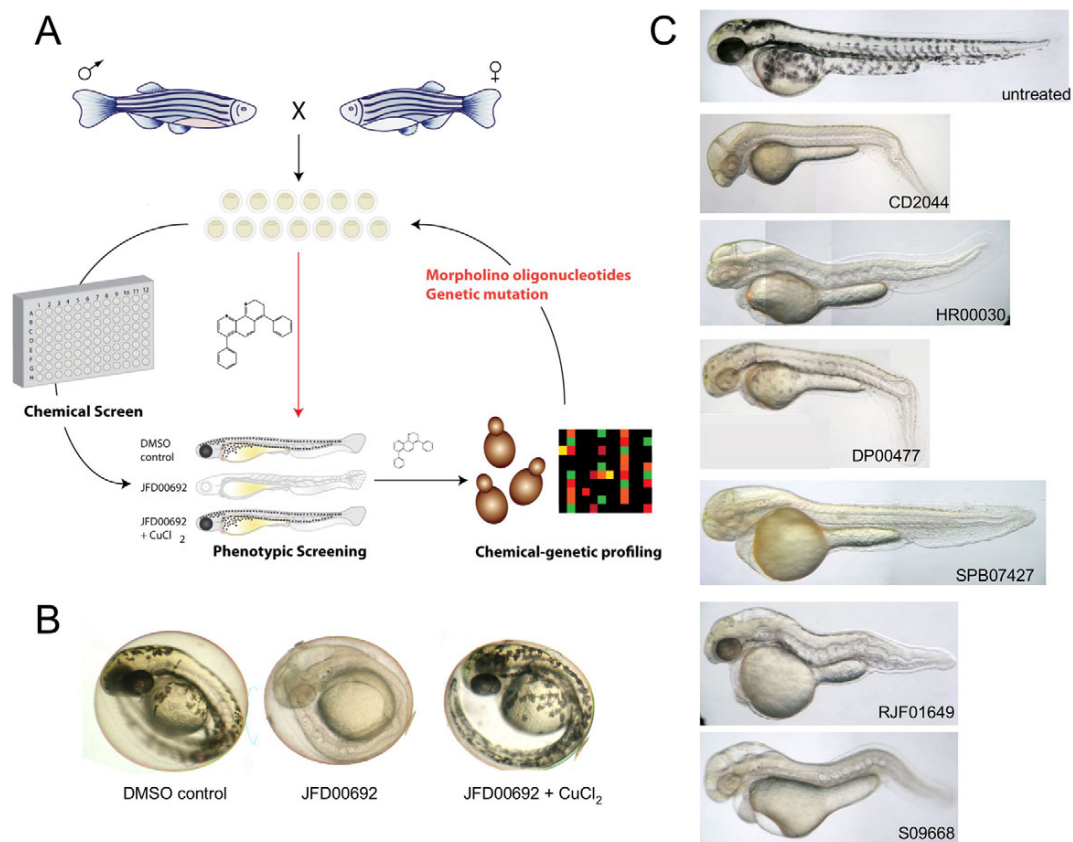


Figure 4.1: Phenotypic screen to identify compounds that affect melanocytes. (A) Overview of combined zebrafish and yeast approach. Phenotypic screens in zebrafish allow identification of compounds that target specific developmental and physiological pathways. Small molecules of interest are then subjected to genome-wide chemical-genetic screens in the budding yeast to identify potential target pathways based on genetics. Conserved genetic target pathways can then be directly tested in zebrafish using genetic mutant lines, blocking target gene expression with morpholino oligonucleotides or using small molecules known to act on the same cellular target. (B) Representative example of the copper-metabolism phenotype as caused by 10  $\mu\text{M}$  JFD00692. The characteristics of the copper-metabolism are clearly visible in the JFD00692 treated embryo: hypopigmentation, an undulating notochord and an expanded hindbrain (Mendelsohn *et al.*, 2006). Rescue was observed with addition of 5  $\mu\text{M}$  or 15  $\mu\text{M}$  exogenous copper. (C) Further examples of compounds that induce the copper-metabolism phenotype identified in the screen. This figure was taken from Ishizaki, Spitzer *et al.*, 2010.

binding molecules like 1-phenyl-3-(2-thiazolyl)-2-thiourea (PTT) (Mendelsohn *et al.*, 2006) as well as metal-binding thiourea derivates, thiosemicarbazones, pyridin-pyrimidinones and phenanthrolines (Table 4.1). Surprisingly, the widely used MEK inhibitor U0126 was identified as a copper-metabolism compound (Table 4.1). Further characterisation of all compounds listed in Table 4.1 revealed that the copper-metabolism phenotype could be rescued completely by the addition of 5  $\mu\text{M}$  exogenous copper for the majority of compounds. The effects of five of the compounds could only partially be rescued by addition of copper (15  $\mu\text{M}$ ) and for three compounds the addition of exogenous copper was lethal. Compounds that cause hypersensitivity to additional copper could be interfering with detoxification of excess copper ions in the cell. Copper levels are tightly regulated in the cell and controlled by copper chaperones and metallothionein levels (Rae *et al.*, 1999; Wegner *et al.*, 2011).

### **Identification of two compounds that selectively kill melanocytes in *Danio rerio***

The phenotypic screen in zebrafish also yielded a number of compounds that seemed to specifically affect melanocytes. Two of these compounds were RF 03928 and BTB 05727 (Figure 4.2A). Zebrafish embryos normally have black melanocytes in the eyes and patterning on the body. Treatment with each of the two compounds greatly reduced the number of melanocytes (first row in Figure 4.2B). Some compounds that are melanocyte-specific are pro-drugs that are activated by enzymes expressed in melanocytes. Tyrosinase is an enzyme that is expressed specifically in melanocytes and tyrosinase-dependent compounds have been of limited interest for melanoma treatment so far. Tyrosinase and other pigmentation enzymes are copper-dependent and addition of the copper-chelating PTU (4-hydroxy-2-mercapto-6-propylpyrimidine) prevents pigmentation of melanocytes. To test if RF 03928 and BTB 05727 required the activity of pigmentation enzymes for melanocyte specific activity, zebrafish embryos were treated with RF 03928 and BTB 05727 in combination with PTU. These experiments showed RF 03928 to be a tyrosinase-dependent drug since addition

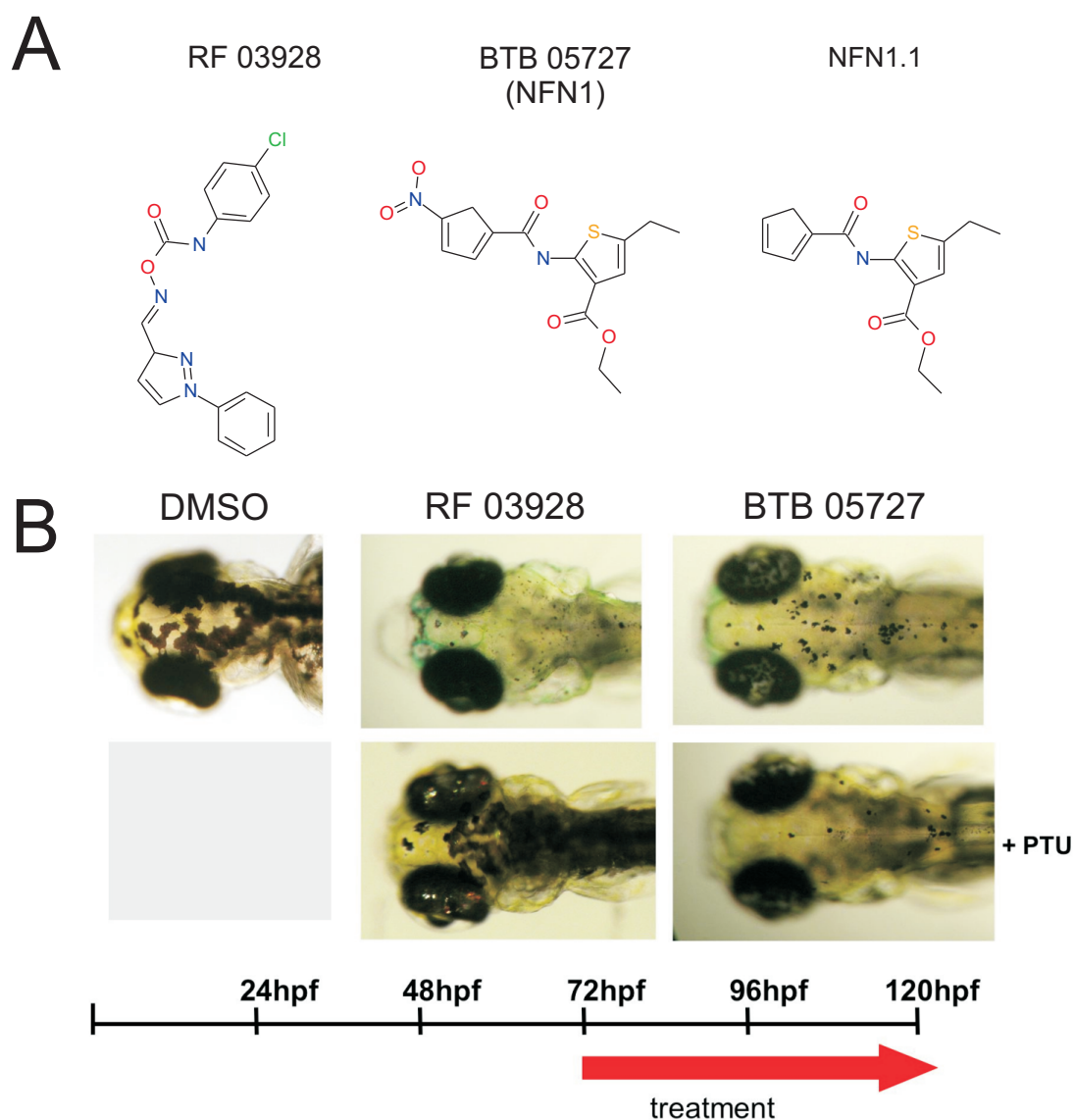


Figure 4.2: Compounds that are melanocytotoxic in zebrafish. (A) Structures of RF 03928, BTB 05727 (NFN1) and NFN1.1 (B) Examples of the effects of RF 03928 and BTB 05727 alone and in combination with the copper chelator PTU on zebrafish embryos. Three day old zebrafish embryos were treated with compound or DMSO for two days and images were taken at five days pf. Images in (B) were taken by Dr. Hironori Ishizaki in the Patton laboratory.

of PTU resulted in normal melanocyte development (second row in Figure 4.2B). In contrast, the effect of BTB 05727 on zebrafish melanocytes was not rescued by PTU, indicating that it is not a tyrosinase dependent drug.

In the first part of this chapter, I will present experiments that applied the genome-wide tools available in the model organism *S. cerevisiae* to investigate the mode of action of some of the compounds that caused melanocyte-specific

phenotypes in zebrafish. These experiments proved the budding yeast to be very useful to inform about pathways and proteins that are conserved in higher organisms. Sections 4.2.1, 4.2.2 and 4.2.3 focus on the compounds that affect copper metabolism. The two small molecules that specifically affect melanocyte viability were also studied in more detail (sections 4.2.4 and 4.2.5).

## 4.2 Results

### 4.2.1 Chemical-genetic profiles in *S. cerevisiae* reveal potential copper-metabolism pathways

To identify pathways affected by perturbation of copper metabolism, six of the copper metabolism compounds identified in the chemical screen in zebrafish (Section 4.1.3) as well as the known copper chelator neocuproine were subjected to genome-wide chemical-genetic screens in *S. cerevisiae*. The compounds selected represent the different structural groups and three of them cause hypersensitivity to exogenous copper (U0126, SEW01049 and SPB07427) while the other three can be rescued by copper (DP00477, JFD00692 and RJF01649).

This copper-metabolism subset (CM subset) contains neocuproine, U0126, DP00477, SEW01049, SPB07427, JFD00692 and RJF01649 (Table 4.1). Pools of 5000 haploid deletion strains in non-essential genes as well as the 1000 diploid deletion strains heterozygous for essential genes were screened against all seven drugs. Compounds were screened at concentrations that inhibited growth of the deletion pools by 20-30%. Pools were grown in the presence of drug or 0.4% DMSO for 20 generations. The response of the deletion strains to compound treatment at two different concentrations was assessed by spotted oligonucleotide microarrays (Cook *et al.*, 2008). Strains sensitive and resistant to the compounds were identified using quantile statistics as shown in Figure 4.3. The quantile statistics were similar for all experiments; only the two screens with JFD00692 displayed a different distribution of Z-scores.

Even though all drugs in the CM subset elicit a similar developmental phenotype in the zebrafish embryo, distinct and common pathways were identified with

Maybridge Code	Phenotype	Copper addition	Compound structure
Neocuproine	Copper metabolism	Rescue (5 $\mu$ M)	Phenanthroline
U0126	Copper metabolism	Lethal (5 $\mu$ M)	Sulfanylmethylidene-butanedinitrile
PTT	Copper metabolism	not determined	1-Phenyl-3-(2-thiazolyl)-2-thiourea
DP00477	Copper metabolism	Partial rescue (15 $\mu$ M)	Thiocarbamoyl-acetamide derivative
DP00750	Copper metabolism	Rescue (5 $\mu$ M)	Thiosemicarbazone
CD00707	Copper metabolism	Rescue (5 $\mu$ M)	Thio-urea
CD02745	Copper metabolism	Rescue (5 $\mu$ M)	Thiosemicarbazone
CD02044	Copper metabolism	Partial rescue (15 $\mu$ M)	Thiosemicarbazone
HR00030	Copper metabolism	Rescue (5 $\mu$ M)	Thio-urea derivate
FM00217	No pigmentation	Rescue (5 $\mu$ M)	Thiosemicarbazone
PD00357	No pigmentation	Rescue (5 $\mu$ M)	Thiosemicarbazone
RDR00803	Copper metabolism	Rescue (15 $\mu$ M)	Thiosemicarbazone
KM09752	Copper metabolism	Rescue (5 $\mu$ M)	Thio-urea derivate
RJC00588	Copper metabolism	Rescue (5 $\mu$ M)	Carbamic acid
RH01646	Copper metabolism	Rescue (5 $\mu$ M)	Thiosemicarbazone
RH01676	No pigmentation	Rescue (5 $\mu$ M)	Triazole-thiol
SEW02973	No pigmentation	Rescue (5 $\mu$ M)	Pyridin-pyrimidinone
SEW01049	Copper metabolism	Lethal (5 $\mu$ M)	Thiosemicarbazone
RJF01673	Wavy notochord	Rescue (5 $\mu$ M)	Pyridin-pyrimidinone
S02347	Copper metabolism	Partial rescue (15 $\mu$ M)	2,4-Diphenyl-2,3-dihydro-1,5-benzothiazepine
RJF01809	Copper metabolism	Rescue (5 $\mu$ M)	Pyridin-pyrimidinone
S02850	Copper metabolism	Rescue (5 $\mu$ M)	Carbamothioyl benzamide
SJC00393	Copper metabolism	Rescue (5 $\mu$ M)	Thiosemicarbazone
SPB02722	Copper metabolism	Partial rescue (15 $\mu$ M)	Benzoxazole derivate
SPB00258	Copper metabolism	Rescue (5 $\mu$ M)	Thiosemicarbazone
SPB05679	Copper metabolism	Rescue (5 $\mu$ M)	Pyridin-pyrimidinone
SPB07427	Copper metabolism	Lethal (5 $\mu$ M)	Thiadiazole derivate
SPB07119	No pigmentation	Rescue (15 $\mu$ M)	Thiosemicarbazone
SEW06186	Copper metabolism	Rescue (5 $\mu$ M)	Urea derivate (carboline-carboxamide)
SEW01792	No pigmentation	Rescue (15 $\mu$ M)	N-Hydroxy-benzamidine derivate
SPB01039	Copper metabolism	Rescue (5 $\mu$ M)	Triazole-thiol derivate
SPB07027	Copper metabolism	Rescue (5 $\mu$ M)	Thiosemicarbazone
SPB07028	Copper metabolism	Rescue (5 $\mu$ M)	Thiosemicarbazone
SPB00779	No pigmentation	Rescue (5 $\mu$ M)	Triazole-thiol
CD02543	Copper metabolism	Rescue (5 $\mu$ M)	Thiosemicarbazone
CD03007	Copper metabolism	Rescue (5 $\mu$ M)	Thiosemicarbazone
CD06646	Copper metabolism	Rescue (5 $\mu$ M)	Pyridin-pyrimidinone
DFP00275	Copper metabolism	Rescue (5 $\mu$ M)	Thio-urea derivate (carbamothioyl benzamide)
JFD00692	Copper metabolism	Rescue (5 $\mu$ M)	Phenanthroline (cisplatin analogues)
RF01893	Copper metabolism	Rescue (5 $\mu$ M)	N-Hydroxy-benzamidine derivate
RDR00093	No pigmentation	Rescue (5 $\mu$ M)	Thiourea derivate
RDR00691	Copper metabolism	Rescue (5 $\mu$ M)	Thiosemicarbazone
S04201	Copper metabolism	Rescue (5 $\mu$ M)	Thio-urea/Quinazolinone derivate
RJF01649	Copper metabolism	Rescue (5 $\mu$ M)	Pyridin-pyrimidinone
S09668	Copper metabolism	Partial rescue (15 $\mu$ M)	Thiourea derivate
S14458	Copper metabolism	Rescue (5 $\mu$ M)	Thiosemicarbazone

Table 4.1: Characterisation of small molecules that cause copper-metabolism phenotypes. The table was taken from Ishizaki, Spitzer *et al.*, 2010.

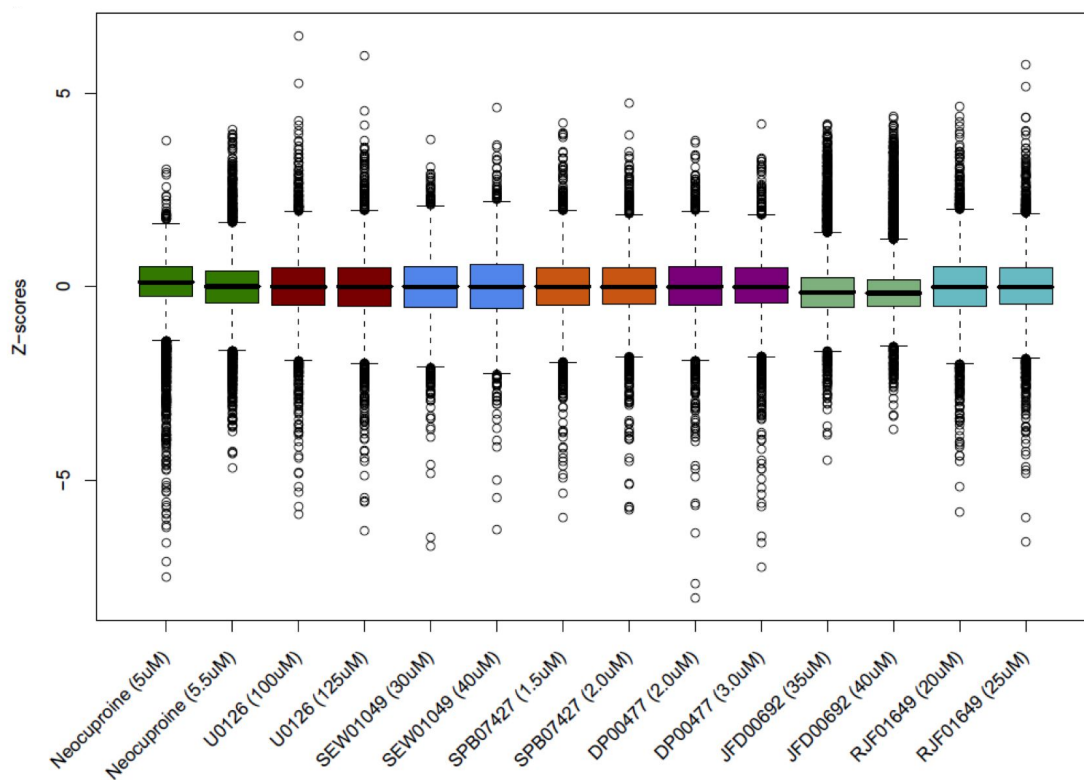


Figure 4.3: Boxplots of Z-scores for each of the microarrays visualise quantile statistics for all arrays. Boxplots visualise the distribution of Z-scores using quantiles: the box contains 50% of the data points (called interquartile range) and the black line represents the median. The hinges extend for 1.5 interquartile ranges from the box and data points that lie beyond this range are considered outliers.

the genome-wide chemical-genetic screens in yeast, reflecting differences in the molecular effects of each compound. The sensitivity of strains deleted for genes known to be involved in copper transport and homeostasis was examined in more detail (Figure 4.4A). Deletion strains defective in copper metabolism are rarely affected in chemical-genetic screens (Hillenmeyer *et al.*, 2008) probably because yeast is typically grown in rich medium that provides sufficient exogenous copper. Figure 4.4A reveals unique profiles of the strains defective in copper metabolism for each compound. Deletion strains that showed sensitivity include the copper transporter *Ctr1*, the copper-transporting ATPase *Ccc2*, the copper chaperones *Atx1* and *Atx2*, copper-dependent transcription factor *CUP2* and the copper-zinc superoxide dismutase *Sod1*. Copper is transported into cells by high-affinity transporters that require copper to be in the reduced  $\text{Cu(I)}$  state, which is dependent on the cupric and ferric reductases *Fre1* and *Fre2* (De Freitas *et al.*, 2003).

Iron and copper homeostasis are intimately linked in the budding yeast and in human disease (De Freitas *et al.*, 2003; van Bakel *et al.*, 2005; Madsen and Gitlin, 2007). Strains deleted for FRE1 and FRE2, the major cell surface reductases in *S. cerevisiae* were sensitive to copper starvation caused by different compounds. Finally, of the iron transporters Fet3 and Fet5, both copper-dependent enzymes, the *fet3* $\Delta$  strain also displayed sensitivity to some of the compounds. The chemical-genetic profiles of the CM subset thus reflected effects on copper homeostasis, as well as iron homeostasis (van Bakel *et al.*, 2005; Rustici *et al.*, 2007).

To link the action of the CM subset to cellular pathways, the effect of compound treatment on all genes of each GO categories was assessed. In Figure 4.4 groups of GO categories that are affected by each compound are visualised. Several biological processes were affected by several compounds. These shared processes, many of which can be linked to copper metabolism, included tubulin-complex assembly, the Swr1 histone-remodelling complex, vacuolar organisation and intracellular transport, mitochondrial translation initiation and peroxisome formation. For example, copper plays an important role in mitochondrial function, such as in cytochrome C oxidase activity (Madsen and Gitlin, 2007). The sensitivity of the Swr1 histone-exchange complex (Zilberman *et al.*, 2008) might reflect inappropriate levels of metallothionein (*CUP1-1* and *CUP1-2*) since expression of the copper metallothionein gene in *S. cerevisiae* is regulated by chromatin modification (Kuo *et al.*, 2005). Deletion of genes involved in the threonine biosynthesis pathway resulted in sensitivity to some of the CM subset compounds. Sensitivity of deletion strains in genes involved in the biosynthesis of amino acids has been observed before, also in response to high-copper concentrations. The threonine-biosynthesis pathway genes, however, were not among these known pleiotropic genes (Ericson *et al.*, 2008; Hillenmeyer *et al.*, 2008; Jo *et al.*, 2008). The findings in this study might highlight a novel relationship between copper metabolism and threonine biosynthesis in yeast. Alternatively, it is possible that the threonine pathway is required for detoxification of some of the CM subset compounds.

Strains deleted for proteins involved in tubulin binding and tubulin assembly displayed resistance to a few of the compounds. Microtubule assembly is complex



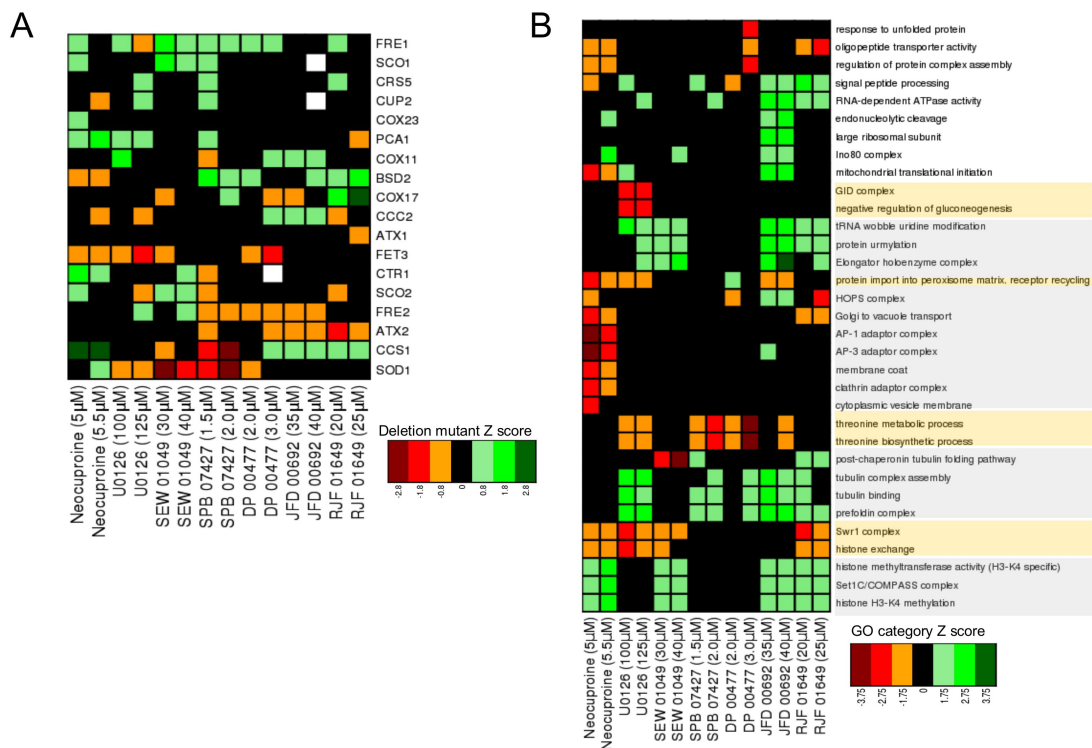


Figure 4.4: Chemical-genetic interactions of compounds that affect copper metabolism. (A) Response of deletion strains in copper-pathway genes to treatment with U0126, neocuproine or the copper metabolism compounds. Data from two screens at different drug concentrations is shown. Genes for proteins that contain copper as well as proteins involved in copper and/or iron transport and homeostasis were compiled from *Saccharomyces* Genome Database (SGD, <http://www.yeastgenome.org>). Colour scale indicates sensitivity (red) or resistance (green) of a deletion strain to a specific drug treatment; white indicates no data available in a given experiment. (B) Heatmap indicating GO categories that showed sensitivity (red) or resistance (green) in response to treatment with different compounds. Two concentrations were screened for each compound. Scores were calculated for each GO category that contained at least four genes by averaging the Z-scores of all deletion strains annotated in the category. Categories shown in the heatmap are the top 2% of affected GO categories. GO categories are grouped by overlap in their gene sets (see also Table 2).

and requires proper folding of  $\alpha$ - and  $\beta$ -tubulins and formation of heterodimers. Excess copper has been shown to cause microtubules to disassemble *in vitro* and in cell-based studies (Liliom *et al.*, 1999; Liliom *et al.*, 2000; Pribyl *et al.*, 2008; Liu *et al.*, 2009).

The peroxisome was identified as an organelle that is important when cells are treated with CM subset compounds. This dependency might arise because the cytosolic copper-zinc superoxide dismutase is targeted to peroxisomes by its interaction partner 'copper chaperone of SOD1' (CCS) in mammalian cells (Islinger *et al.*, 2009). In yeast, deletions in peroxisomal genes have been shown to sensitise cells to low-iron conditions which could be due to the fact that the requirement for peroxisomal  $\beta$ -oxidation is elevated when iron-dependent mitochondrial energy production is impaired (Jo *et al.*, 2009). Copper deficiency might cause a similar effect because copper is required for iron homeostasis and mitochondrial functions. Notably, high levels of copper and iron in tissues and blood are characteristics of human disorders of peroxisome biogenesis (Wanders & Waterham, 2005).

Copper concentrations and transport are highly regulated in the cell. Pathways involved in copper homeostasis include transport into the endoplasmic reticulum and through secretory and vacuolar pathways for delivery to copper-dependent enzymes as well as for excretion and detoxification of copper (Yuan *et al.*, 1997; González *et al.*, 2008; Jo *et al.*, 2008; Jo *et al.*, 2009). Deletion mutants in the AP1, the AP3 and the clathrin adaptor complexes, the HOPS complex and the Golgi-to-vacuole transport pathway were identified as sensitive in low-copper conditions (Figure 4.4). Disruption of these complexes has not been associated with sensitivity to low-copper conditions, but intracellular transport and vacuolar pathways have been shown to be sensitive to perturbations of iron homeostasis. For example, disruption of the AP3 adaptor complex in *apm3* $\Delta$  and *aps3* $\Delta$  strains causes sensitivity to low-copper and low-iron conditions (Jo *et al.*, 2009). These pathways might be required in low-copper conditions because copper is not able to reach essential copper-dependent proteins.

### 4.2.2 The MEK inhibitor U0126 elicits an unexpected copper-metabolism phenotype

The identification of U0126 as a compound that affects copper-metabolism in zebrafish is consistent with the phenotype described in a recent paper. Hawkins *et al.* (2008) who report that treatment with the MEK inhibitor produces zebrafish embryos without pigmentation, with a shorter tail and an undulated notochord. The authors explained this observation by suggesting a potential link between the MAPK-pathway and copper-dependent processes during notochord differentiation, although this speculative link has not been investigated further. The following experiments in zebrafish and yeast were devised to distinguish if the copper-metabolism phenotype caused by U0126 is due to its inhibition of MEK or if U0126 has additional targets in the cell that affect copper homeostasis, independent of its action on the MAPK pathway.

First of all, the phenotype induced by U0126 in the developing zebrafish was compared to that caused by the selective MEK inhibitor PD0325901 and the known copper chelator neocuproine. Figure 4.5A shows that treatment with U0126 and neocuproine caused the typical copper depletion phenotype. The 2-day-old fish exhibited hypopigmentation, an undulating notochord and an expanded hindbrain. Embryos treated with PD0325901 prevented development of posterior features but had no effect on pigmentation.

Even though the RAS-RAF-MEK-ERK signalling pathway is important in melanoma development in zebrafish, mice and humans, neither PD0325901 nor CI-1040 (another highly selective MEK inhibitor) affected melanocyte pigmentation in zebrafish (Figure 4.5A and data not shown). This observation suggests that U0126 has a previously undetected additional target in copper metabolism since selective inhibition of the MAPK-pathway does not affect pigmentation of zebrafish melanocytes.

U0126 also prevents blood development in zebrafish embryos as indicated by o-dianisidine staining (Figure 4.5B) and causes an undulating notochord (Figure 4.5A). A colour-change assay revealed that U0126, just like neocuproine, directly binds copper in aqueous solution whereas CI-1040 does not seem to interact with

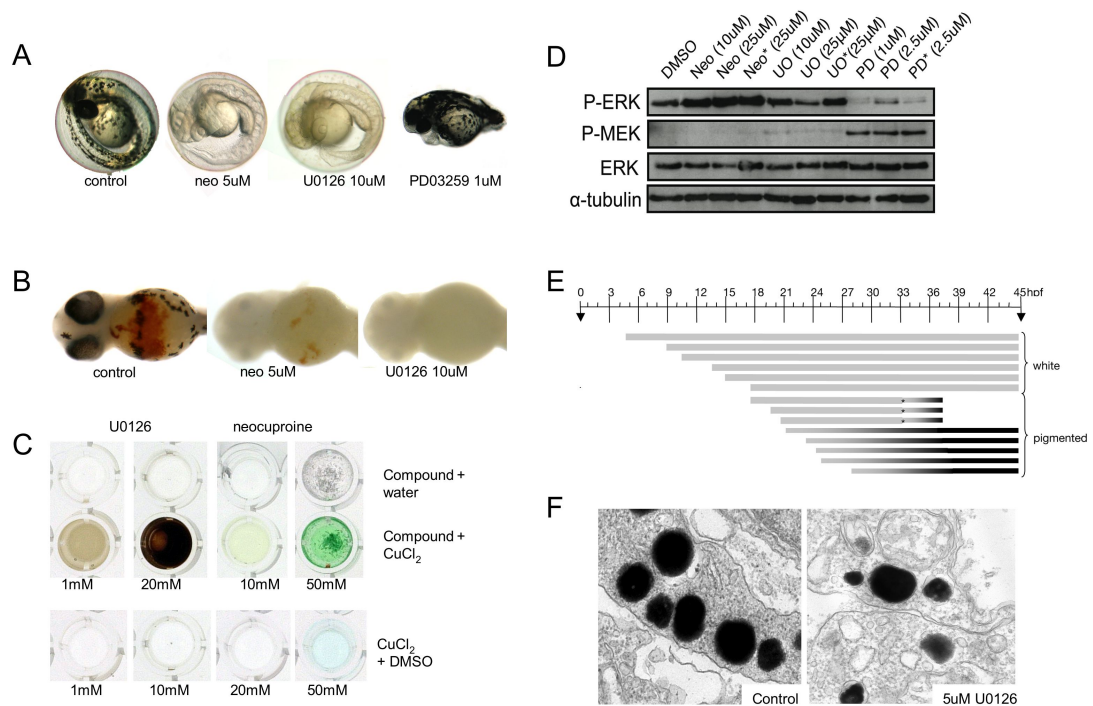


Figure 4.5: Phenotype caused by U0126 treatment in the developing zebrafish embryo. (A) Comparison of phenotypes elicited by treatment with the copper chelator neocuproine (neo), U0126 and the selective MEK inhibitor PD03259. (B) Neocuproine and U0126 treated embryos as well as control embryos were stained with *o*-dianisidine (red) to visualise red blood cells. (C) U0126 and neocuproine were added to aqueous copper chloride solution. A significant change in colour of the solution indicates that a compound form complexes with copper. (D) Phospho-ERK and phospho-MEK levels were assessed in lysates of 12-hpf zebrafish embryos that were treated with neocuproine (Neo), PD0325901 (PD) and U0126 (U0) as well as DMSO (solvent control). (E) Schematic that visualises the relationship between timing and outcome of U0126 treatment. Each barline represents a U0126 treatment (starting at different times post fertilisation). The colour of each barline corresponds to the level of pigmentation of the zebrafish melanocytes. Asterisks indicate time point when unpigmented 33 hpf zebrafish embryos were shifted to fresh embryo medium. (F) Electron microscopy of 2-day-old control and U0126-treated (5  $\mu$ M) zebrafish embryos. Dark organelles are pigmented melanosomes. This figure was taken from Ishizaki, Spitzer *et al.*, 2010.

copper (Figure 4.5C).

Figure 4.5D shows the effects of neocuproine (Neo), U0126 (U0) and PD0325901 (PD) on phospho-ERK and phospho-MEK levels. Probing lysates from compound-treated zebrafish embryos with an anti-phospho-ERK antibody revealed that U0126 and PD0325901 both inhibit MEK activity as seen by decreased phospho-ERK and increased phospho-MEK levels. These effects were much stronger with PD0325901 treatment, confirming its higher potency. Neocuproine had no obvious effects on reducing the phospho-ERK or phospho-MEK levels in zebrafish.

Mapping the timing of U0126 action during development revealed more details about the U0126-induced pigmentation phenotype (Figure 4.5E). Zebrafish melanocytes develop from the neural crest and start making pigment at about 28 hpf. Treatment with 10  $\mu$ M U0126 before 21 hpf prevented normal melanocyte pigmentation whereas addition of compound after 21 hpf did not affect pigmentation. The effect of U0126 in unpigmented zebrafish was easily reversible by placing the embryos into fresh medium without compound. Electron microscopy showed that melanocytes of embryos treated with 5  $\mu$ M U0126 have fewer and less-dense melanosomes (Figure 4.5F; Ishizaki, Spitzer *et al.*, 2010).

Yeast deletion pools were subjected to U0126, CI-1040 and neocuproine treatment for the generation of genome-wide chemical-genetic profiles to characterise potential target pathways for U0126. Analysis of the overlap between these profiles revealed that 13 deletion strains exhibited sensitivity to both U0126 and neocuproine, and that 12 deletion strains showed sensitivity to U0126 and CI-1040 (Figure 4.6A). In contrast, the chemical-genetic profiles of CI-1040 and neocuproine share only one sensitive deletion strain, the *pep10 $\Delta$*  strain, and only the *yaf9 $\Delta$*  strain was sensitive to treatment with each of the three compounds. Therefore, even though the profile of U0126 partially overlaps with those of CI-1040 and neocuproine, CI-1040 and neocuproine have different activities. These profiles fully corroborate the shared molecular phenotype of U0126 and CI-1040 (inhibition of ERK phosphorylation in zebrafish lysates) as well as the shared developmental and chemical phenotype of U0126 and neocuproine.

Comparison of GO biological processes affected by all three compounds revealed a complex network of shared and distinct processes. The genes affected

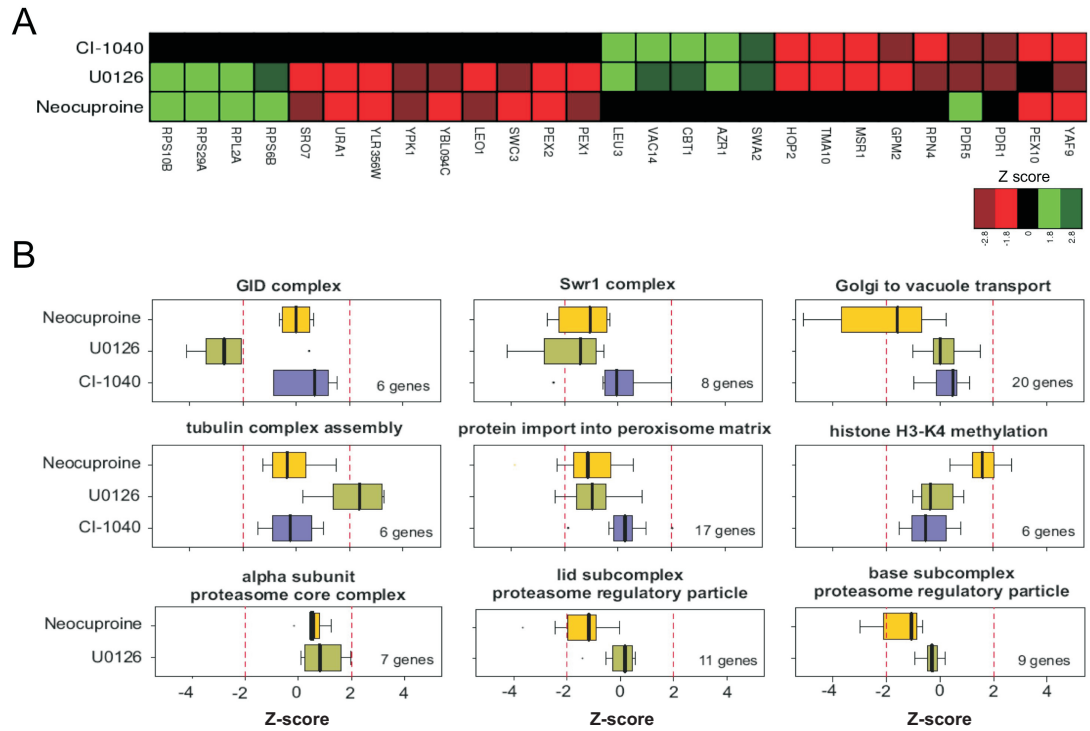


Figure 4.6: Novel target pathways for U0126, a MEK inhibitor. (A) Heat map shows *S. cerevisiae* deletion strains that are sensitive (red) or resistant (green) in response to treatment with U0126, neocuproine and CI-1040. (B) Z-scores of deletion strains annotated with GO categories that are affected by treatment with neocuproine (yellow), U0126 (green) and CI-1040 (purple) are represented as boxplots. Only GO categories with data for more than four genes were analysed.

GO category	Genes
Histone H3-K4 methylation	BRE2, SDC1, SHG1, SPP1, SWD1, SWD3
Protein import into peroxisome matrix	DJP1, PEX1, PEX2, PEX4, PEX5, PEX6, PEX7, PEX10, PEX12, PEX13, PEX14, PEX15, PEX17, PEX18, PEX21, PEX22, PEX25
Tubulin-complex assembly	GIM3, GIM4, GIM5, PAC10, RBL2, YKE2
Golgi-to-vacuole transport	APL2, APL4, APL5, APL6, APM1, APM2, APM3, APS1, APS3, GGA1, GGA2, PEP7, PEP12, TLG2, VAM3, VAM7, VPS52, VPS53, VTH1, YPT7
Swr1 complex	ARP6, SWC3, SWC5, SWC7, SWR1, VPS71, VPS72, YAF9
GID complex	FYV10, GID7, GID8, RMD5, VID24, VID30
alpha-subunit proteasome core complex	PRE10, PRE5, PRE6, PRE8, PRE9, PUP2, SCL1
Lid subcomplex (proteasome regulatory particle)	RPN3, RPN5, RPN6, RPN7, RPN8, RPN9, RPN10, RPN11, RPN12, RPN13, SEM1
Base subcomplex (proteasome regulatory particle)	RPT1, RPT2, RPT3, RPT4, RPT5, RPT6, RPN1, RPN10, RPN12

Table 4.2: Genes in the GO categories shown in Figure 4.6B. The table was taken from Ishizaki, Spitzer *et al.*, 2010.

by compound treatment in each of the GO categories are listed in Table 4.2. As already seen in Figure 4.4B, the peroxisome and the Swr1 histone-exchange complexes are required for resistance to both U0126 and neocuproine (Figure 4.6B). Intracellular transport and the proteasome 19S regulatory particle were required for growth only in the presence of neocuproine whereas disruption of histone H3-K4 methylation rendered cells resistant to the drug. Disruption of tubulin-binding processes led to U0126-resistance, an effect that was not seen with neocuproine or CI-1040. Most of the CM subset compounds, however, caused the same response and which indicates that U0126 affects microtubule-associated processes by perturbing copper homeostasis.

Intriguingly, the GID ubiquitin ligase complex was required for growth in the presence of U0126. The GID complex is an E3 ubiquitin ligase that targets fructose 1,6-bisphosphatase (FBPase), a key enzyme in gluconeogenesis, for proteasomal degradation (Santt *et al.*, 2008). Deletion of the GID complex caused slight sensitivity with all compounds in the CM subset except for neocuproine, but the effect was strongest in the presence of U0126. The GID complex might therefore either represent a new copper-dependent target or U0126 might have yet another function in addition to MEK inhibition and effects on copper-homeostasis.

### **4.2.3 Knockdown of trafficking proteins identified in yeast screens sensitises zebrafish to copper-dependent hypopigmentation**

Intracellular transport pathways are essential for all cells, but have an important role in melanosome biogenesis. The copper transporter ATP7A as well as pigmentation enzymes are selectively transported from the trans-Golgi network to maturing melanosomes. Two genes, that when deleted sensitised yeast to perturbations in copper-homeostasis caused by CM compound treatment, were selected to test whether they might inform about relevant copper pathways in zebrafish melanocytes. Two such genes with orthologs in zebrafish were the yeast genes APS1 and APS3 encoding components of the AP1 and AP3 transport complexes, respectively. A splicesite Morpholino antisense Oligonucleotide (MO)

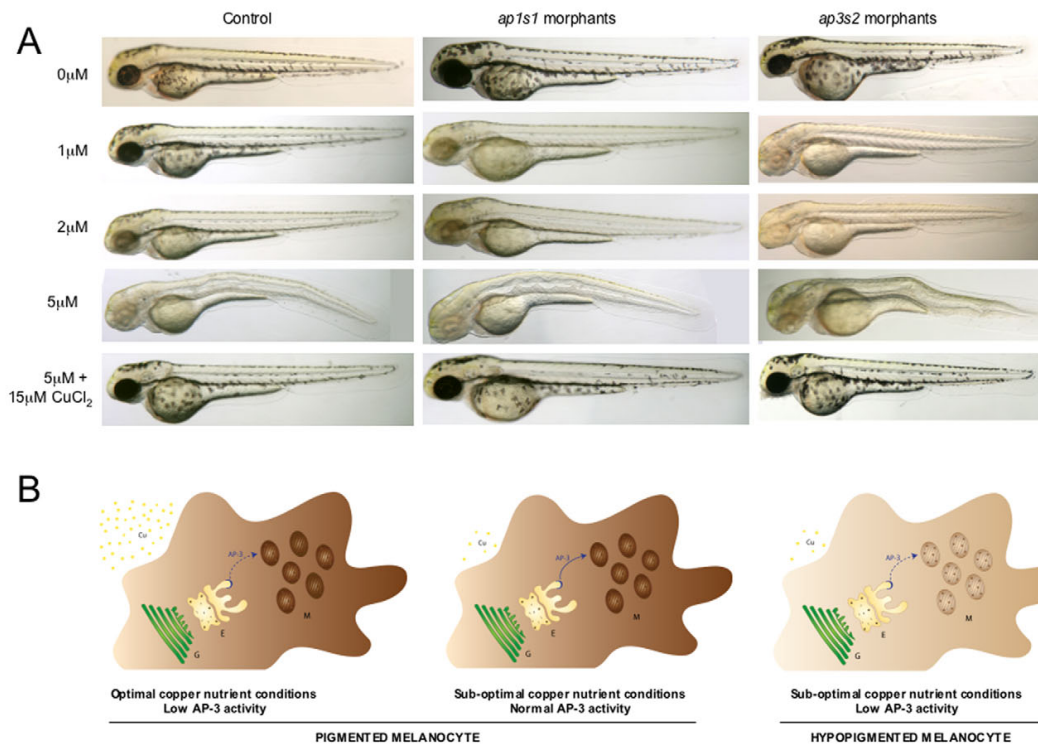


Figure 4.7: Identification of gene-nutrient interactions in melanocyte pigmentation. (A) Representative zebrafish embryos that were injected with morpholino oligonucleotides (1-3 pg) directed against *ap1s1* and *ap3s2* as well as control embryos were treated with increasing concentrations of neocuproine (0, 1, 2 and 5  $\mu$ M, rows 1-4). In the last row, the effect of neocuproine treatment is rescued by the addition of 15  $\mu$ M copper chloride. Experiments were repeated more than three times for each morpholine with  $n > 20$  for each treatment. (B) Schematic of gene-copper interactions in the zebrafish melanocyte. Effect of copper conditions and AP-3 activity on melanocyte pigmentation is visualised. Cu, copper; E, endosomal bodies; G, trans-Golgi network; M, melanosomes. This figure was taken from Ishizaki, Spitzer *et al.*, 2010.

designed against *ap3s2* (*ap3s2*-MO1) and a translation-blocking MO designed against *ap1s1* (*ap1s2*-MO1) (Montpetit *et al.*, 2008) were injected separately into single-celled zebrafish embryos and development was monitored. With low MO concentrations (1-3 pg), the *ap1s1* and *ap3s2* morphants underwent normal development until at least two days pf (Figure 4.7A, top row). Without the addition of neocuproine, neither the controls nor the morphants displayed any of the characteristics of developmental copper deficiency which include reduced pigmentation, a buckling notochord or an expanded hindbrain. Partial reduction of *ap1s1* or *ap3s2* function did not affect development of the zebrafish embryo in optimal



nutrient conditions. To mimic low copper conditions, 4-6 hpf morphants were treated with a range of neocuproine concentrations (1  $\mu\text{M}$ , 2  $\mu\text{M}$  and 5  $\mu\text{M}$ ) and zebrafish embryo development was observed over two days. At low neocuproine concentrations, the control embryos exhibited only a mild (at 1  $\mu\text{M}$ ) to moderate (at 2  $\mu\text{M}$ ) reduction in melanocyte pigmentation ( $n > 100$ ) whereas many ap3s2 and ap1s1 morphants showed severe hypopigmentation ( $n = 37/71$  embryos and  $n = 13/39$ , respectively). Addition of a higher concentration of neocuproine (5  $\mu\text{M}$ ), caused both wild-type and morphant embryos to exhibit features of developmental copper-metabolism deficiency. This could be prevented with the addition of 15  $\mu\text{M}$  exogenous copper (Figure 4.7A). At least two of the intracellular transport pathways that were identified in the budding yeast showed physiological relevance in the developing vertebrate.

#### **4.2.4 Investigation of off-target effects of nitrofurans with zebrafish and yeast**

Of the melanocyte-specific drugs, BTB 05727 was investigated in more detail for two reasons. It is not a tyrosinase-dependent pro-drug (Figure 4.2B) and it contains a 5-NO<sub>2</sub> moiety. BTB 05727 has therefore been named NFN1. 5-nitrofurans are widely used to treat parasitic trypanosome infections. The unicellular parasite *Trypanosoma* causes diseases in Africa and in Central and South America. *Trypanosoma brucei* causes sleeping sickness in parts of sub-saharan Africa where 50,000-70,000 people are infected. In Central and South America, *Trypanosoma cruzi* causes Chagaz disease. It is a tropical parasitic disease and affects 8-11 million people. Both infections are fatal if they are not treated. Nifurtimox is a drug that is used against both diseases, but treatment is discontinued in 30% of patients due to severe side-effects. Nifurtimox is a nitrofuran pro-drug that is activated by parasitic nitroreductases. Recently it has been suggested that it is converted into an unsaturated open chain nitrile (Hall *et al.*, 2011). The fact that NFN1 is melanocytotoxic in zebrafish provides a highly visible assay to study the activity of 5-nitrofurans in animals, independent of trypanosome infection.

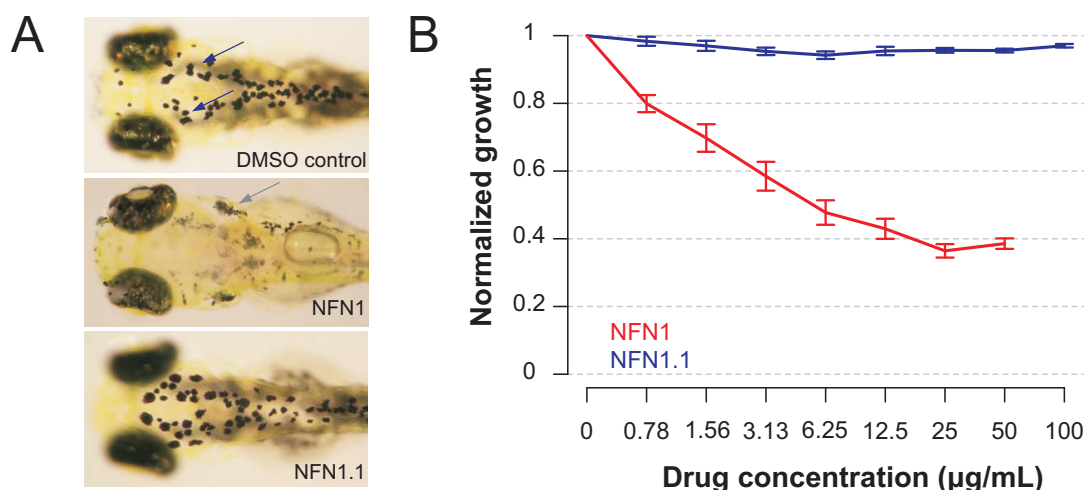


Figure 4.8: 5-NO<sub>2</sub> moiety is required for nitrofuran activity in zebrafish and yeast. (A) Effect of NFN1 and NFN1.1 on zebrafish melanocytes.(B) Yeast was grown in the presence of increasing concentrations of NFN1 (blue) and NFN1.1 (red). OD values were normalised against DMSO controls. The mean of two independent experiments with three replicates each was calculated; error bars represent standard deviation. Images in (A) were taken by the Patton lab.

### 5-Nitrofuran activity in zebrafish and yeast requires the 5-NO<sub>2</sub> moiety

5-nitrofurans are pro-drugs and for these drugs to be active against parasites, the 5-NO<sub>2</sub> moiety is essential for bioactivation by bacterial nitroreductases (Wilkinson *et al.*, 2008). *S. cerevisiae* has at least two nitroreductase-like proteins, but they share little similarity with the bacterial nitroreductases that activate 5-nitrofurans in *Trypanosoma*.

Removing the NO<sub>2</sub> moiety from NFN1 resulted in compound NFN1.1 (Figure 4.2A) which was used to investigate the role of the 5-NO<sub>2</sub> moiety in NFN1 bioactivity. Figure 4.8A shows that NFN1.1 did not have any effect on zebrafish melanocytes, confirming that nitrofuran activity in zebrafish is dependent on the 5-NO<sub>2</sub> moiety. In the budding yeast, treatment with NFN1 reduces yeast growth by 50% at 12.5 µM whereas NFN1.1 did not show any effect on growth, even at concentrations up to 100 µM (Figure 4.8B). This confirmed that the 5-NO<sub>2</sub> moiety is required for NFN1 bioactivation in zebrafish and budding yeast.

## **Aldh2 activity is required for NFN1 activity in zebrafish and yeast**

Affinity purifications were performed with zebrafish extracts (from three day pf embryos) to identify NFN1-interacting proteins (Ishizaki, Zhou *et al.*, submitted). A 56 kD protein was identified as aldehyde dehydrogenase 2 (Aldh2) and validated on a Western blot with anti-Aldh2 zebrafish antibodies (raised against Aldh2a and b forms). Purified human Aldh2 was also shown to bind to NFN1, indicating that the data obtained with the zebrafish model may also be applicable to humans (Zhou L, Westwood N, Patton E, unpublished data). Aldh2 fulfils several roles in the human body. After alcohol consumption it catabolises toxic aldehydes in the liver. It also catabolises toxic metabolites after heart ischemia and acts in dopamine metabolism.

Aldh2 inhibitors were used to test if Aldh2 activity is required for 5-nitrofurantoin toxicity in zebrafish and yeast. Zebrafish Aldh2 a and b are closely related to human Aldh2. Two chemically different Aldh2-inhibitors were used: daidzin and disulfiram. Both compounds did not affect melanocyte integrity on their own in three day pf embryos. Treatment of three day pf zebrafish with combinations of NFN1 with daidzin or disulfiram however, fully protected melanocytes from 5-nitrofurantoin activity (Figure 4.9A, Ishizaki, Zhou *et al.*, submitted).

*S. cerevisiae* has five aldehyde dehydrogenase genes (*ALD2-6*) (Navarro-Aviño *et al.*, 1999) and they all share 42-48% similarity with human *ALDH2*. Ald4 and Ald5 are mitochondrial aldehyde dehydrogenases and the other three are cytosolic isoforms. Ald6 is constitutively expressed whereas *ALD2* and *ALD3* are induced in response to various stresses and are repressed by glucose.

The two Aldh2-inhibitors were also tested in the budding yeast for interactions with NFN1. Figure 4.9B shows that daidzin alone had no effect on yeast growth at concentrations up to 50  $\mu$ M (blue). Treatment of yeast cultures with increasing concentrations of daidzin in the presence of 50 $\mu$ M NFN1 (black) showed that daidzin could completely rescue the effects of NFN1. The Aldh2-inhibitor disulfiram was also tested but rescue was not observed with this compound. Disulfiram is already toxic on its own and has an MIC of 16  $\mu$ M. Alleviating effects were not observed with this drug. This could be due to the fact that disulfiram has

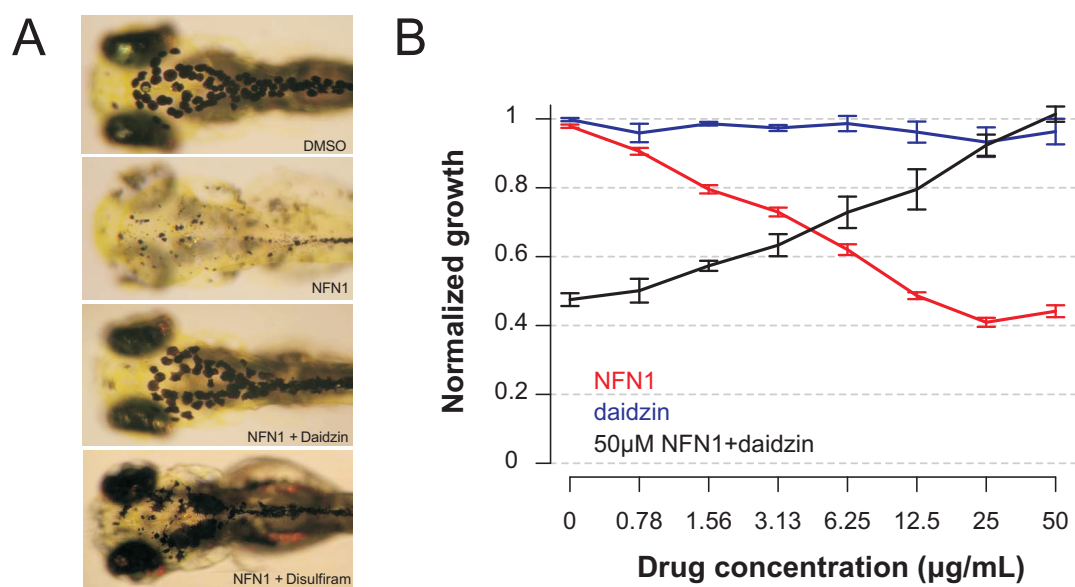


Figure 4.9: Rescue of 5-nitrofurantoin toxicity by Aldh2 inhibitors. (A) Examples of three day old zebrafish embryos that were treated with 10  $\mu$ M Aldh2 inhibitors (daidzin or disulfiram) for one hour and then treated with 5  $\mu$ M NFN1 in 0.1% DMSO or DMSO alone. Zebrafish embryos treated with NFN1 only are shown as well. (B) Drug interaction between daidzin and NFN1 in the budding yeast was assessed by combination matrix assays in 96-well plates. Yeast cultures were treated with increasing concentrations of NFN1 alone (red), increasing concentrations of daidzin alone (blue) or in the presence of 50  $\mu$ M NFN1 (black). The average of three independent experiments was calculated shown; error bars represent standard deviation. Images in (A) were taken by the Patton lab.

various effects in yeast that are not related to aldehyde dehydrogenase inhibition. Experiments in zebrafish have shown that disulfiram is a copper chelator (Ishizaki, Zhou *et al.*, submitted). Disulfiram has been shown to be a multidrug resistance modulator acting via P-glycoproteins (Loo & Clarke, 2000) as well as ATP-binding cassette transporters (Shukla *et al.*, 2004; Sauna *et al.*, 2004). This effect even has therapeutic relevance since disulfiram has been shown to have activity against clinical isolates of the fungal pathogens *Aspergillus* and *Candida*, some of which were drug resistant (Khan *et al.*, 2007). Recently, disulfiram has also been identified as an inhibitor of V-ATPase pumps (Johnson *et al.*, 2010).

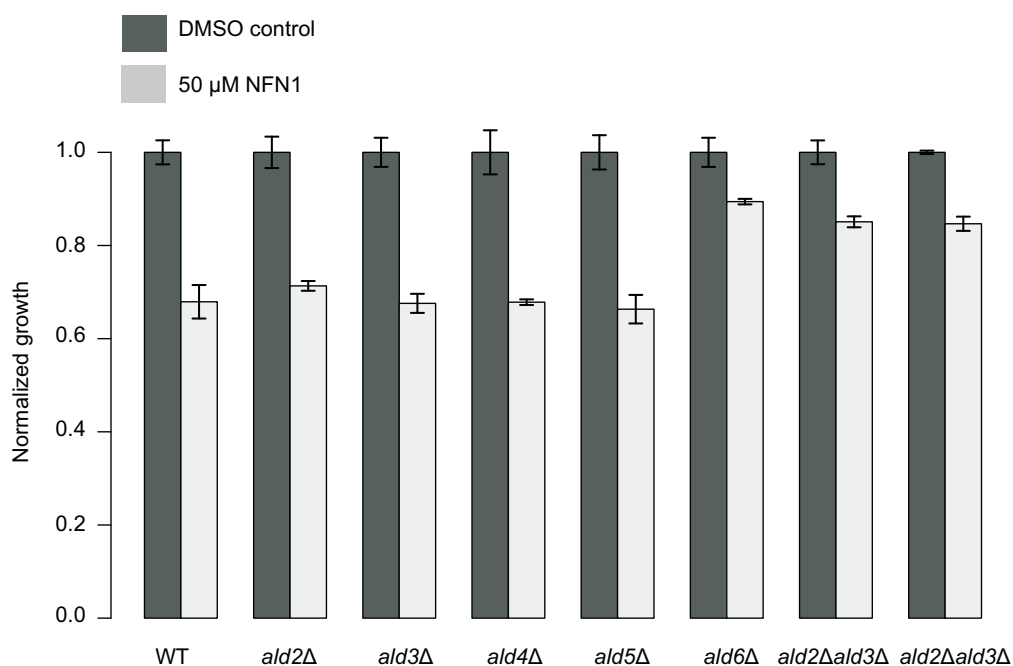


Figure 4.10: Effect of NFN1 on aldehyde dehydrogenase gene deletions in *S. cerevisiae*. The growth inhibitory effect of 50  $\mu$ M NFN1 was measured in wild type haploid yeast, single deletion strains for each of the five aldehyde dehydrogenase genes *ALD2-6* and two different isolates of the *ald2* $\Delta*ald3* $\Delta$  strain. Normalised growth at the time of saturation of the corresponding control culture (1% DMSO, dark grey) is compared to growth of the NFN1-treated cultures (light grey). The mean of three replicates is shown for each strain; error bars represent standard deviation.$

### Deletion of aldehyde dehydrogenase genes renders *S. cerevisiae* resistant to 5-nitrofurans

As described in detail in Section 1.2.5, mutations that confer resistance to a compound can directly point to drug targets or target pathways. This concept was the basis for the following experiments that were devised to confirm aldehyde dehydrogenase as the drug target of NFN1 in the budding yeast.

Figure 4.10 shows the effect of single deletions in each of the aldehyde dehydrogenase genes on NFN1 sensitivity. Growth of *ald2* $\Delta$ , *ald3* $\Delta$ , *ald4* $\Delta$ , *ald5* $\Delta$ , *ald6* $\Delta$  strains was inhibited by 30-40% upon treatment with 50  $\mu$ M NFN1. This level of growth inhibition was similar to the one observed for the wild type strain. The *ald6* $\Delta$  strain however showed only 15% growth inhibition in response to the

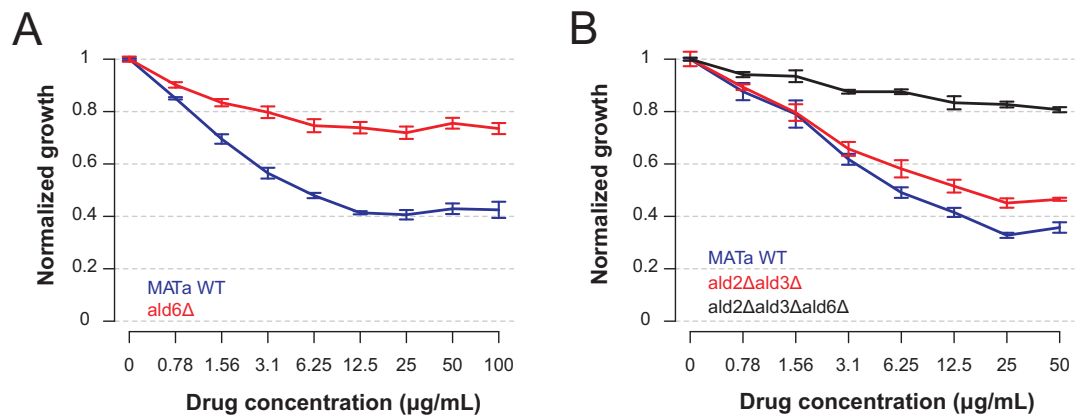


Figure 4.11: Rescue of 5-nitrofurantoin toxicity by aldehyde dehydrogenase deletions in *S. cerevisiae*. (A) *ALD6* deletion partially rescues the growth-inhibitory effect of NFN1 in yeast cultures. MATa wild type (blue) and the *ald6Δ* strain (red) were treated with increasing concentrations of NFN1 (up to 100 μM). Normalised growth is plotted. Data points represent the mean of four replicates; error bars represent standard error. (B) Deletion of the yeast genes *ALD2*, *ALD3* and *ALD6* has additive effects on rescue of NFN1 cytotoxicity in yeast. Dose response curves for WT budding yeast (blue), *ald2Δald3Δ* (red) and the *ald2Δald3Δald6Δ* (black) strains were generated. OD readings were normalised against DMSO controls. The average of three replicates is plotted; error bars represent standard error.

same dose of NFN1. *ald2Δald3Δ* double deletion mutants were also found to be less sensitive to 50 μM NFN1 (about 20% growth inhibition). To confirm the resistance of the *ald6Δ* and the *ald2Δald3Δ* strains, dose response curves were generated. Again, *ald6Δ* was found to confer resistance to NFN1 by decreasing the observed growth inhibition from 60% to just over 20% (Figure 4.11A). The *ald2Δald3Δ* strains alleviated growth inhibition by about 10% compared to wild type (Figure 4.11B). Finally, the triple deletion strain *ald2Δald3Δald6Δ* was constructed and was slightly more resistant than the *ald6Δ* strain. It showed less than 20% inhibition when growth of wild type yeast was inhibited by over 60%. These results indicate a strong genetic dependence on aldehyde dehydrogenase activity for 5-nitrofurantoin cytotoxicity in yeast.

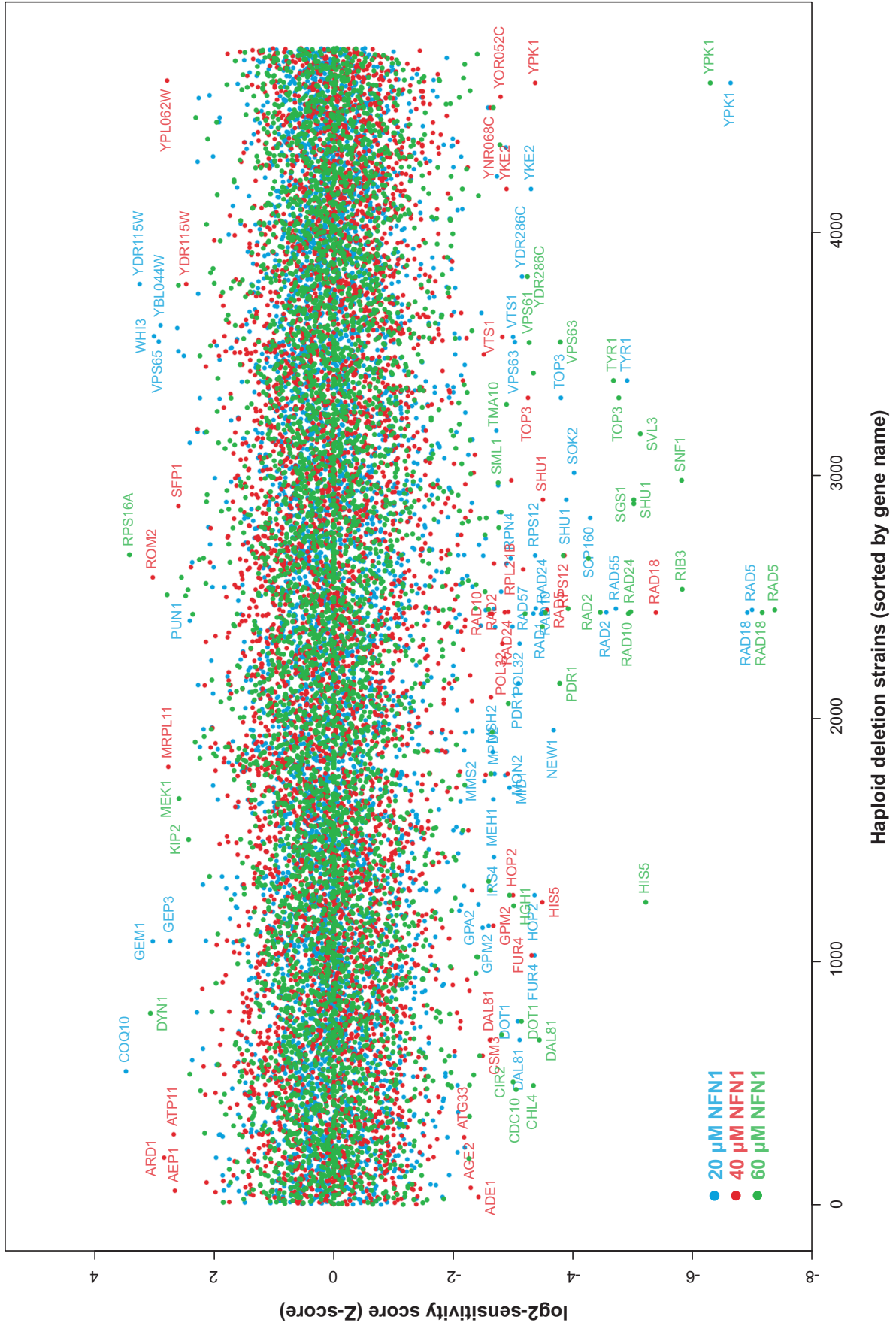


Figure 4.12: Sensitivity of haploid deletion strains to three different concentrations of NFN1.

#### 4.2.5 Mode of action of a compound that selectively kills melanocytes in *D. rerio*

Early work has shown that nifurtimox causes DNA damage in trypanosoma (Goi-jman *et al.*, 1985). The 5-nitrofurantoin nifurtimox has recently been shown to be converted to cytotoxic nitrile metabolites (Hall *et al.*, 2011). Work by Hironori Ishizaki revealed that NFN1 causes cell cycle arrest and DNA damage, increases levels of reactive oxygen species (ROS) and triggers apoptosis in melanocytes. To investigate the mode of action of NFN1 further, genome-wide chemical-genetic profiles were generated in the budding yeast *S. cerevisiae*. Three different concentrations of NFN1 were screened against the haploid deletion pool to identify deletion strains sensitive to NFN1 treatment. Figure 4.12 shows the Z-scores of the log<sub>2</sub> ratios of all haploid deletion strains in the presence of 20, 40 and 60  $\mu$ M of NFN1. A group of the deletion strains that were sensitive to NFN1 treatment were the *RAD* genes that are sensitive to radiation and involved in DNA damage repair. The most sensitive deletion strain in two of the screens were *RAD5* and *RAD18*. *RAD5* is a DNA helicase and it is thought that it promotes replication fork regression during post-replication repair by template switching. It is a RING finger containing ubiquitin ligase that stimulates the synthesis of free and PCNA-bound polyubiquitin chains by Ubc13p-Mms2p. *RAD18* is an E3 ubiquitin ligase that forms a heterodimer with Rad6p to mono-ubiquitinate PCNA-K164. The heterodimer binds single-stranded DNA and has single-stranded DNA dependent ATPase activity. *RAD18* is required for post-replication repair.

Analysis of the most sensitive deletion strains reveals that many of the genes that overlap between the screens at different concentrations are involved in DNA damage. In fact, of the 23 deletion strains that are sensitive in all three drug screens, 13 function in DNA damage repair (Figure 4.13).

The hits from the NFN1 chemical-genetic profiles were further characterised using GO annotations. For each GO category, the average Z-score across all genes that are associated with the GO category was calculated. GO categories with an average Z-score of  $\pm 2$  or more significant in at least one of the three screens are shown in Figure 4.14. The sensitive GO categories represent different



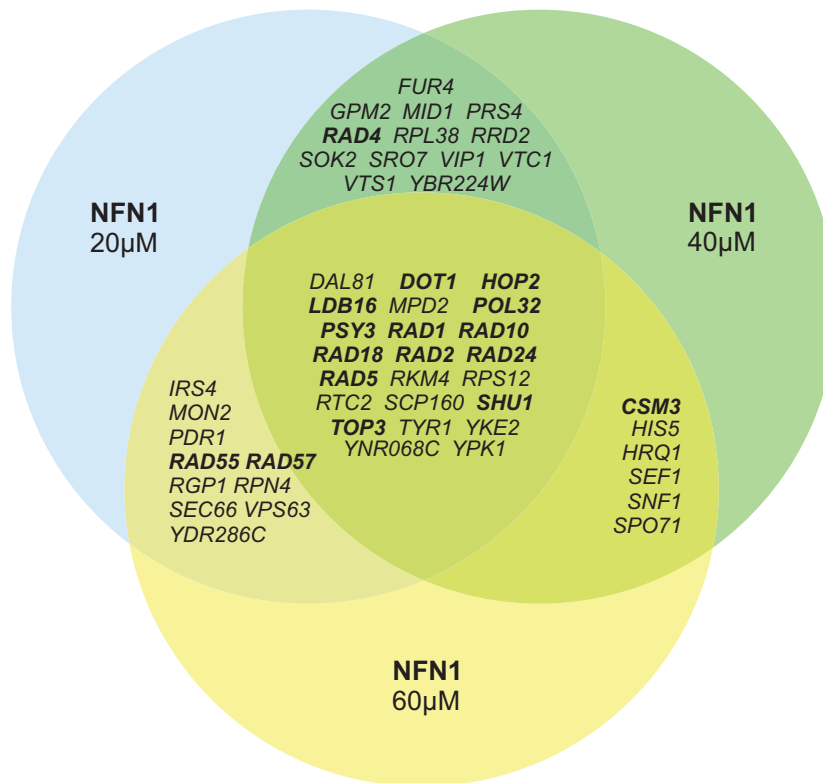


Figure 4.13: Haploid deletion strains sensitive to NFN1 treatment. The haploid deletion pool was screened against three different concentrations of NFN1: 20, 40 and 60  $\mu\text{M}$ . Deletion strains with a Z-score smaller than -2 in at least two of the screens are shown. The total numbers of sensitive deletion strains in the 20, 40 and 60  $\mu\text{M}$  screens were 100, 65 and 94, respectively.

DNA damage repair pathways like single and double strand break repair as well as repair via recombination and nucleotide excision. However, just based on this data it is not possible to determine if NFN1 causes a specific type of DNA damage. There were no GO categories with positive average Z-scores greater than 2.

The sensitivity of 14 deletion strains to NFN1 was assessed by spot dilution assays (Figure 4.15). The following genes caused increased sensitivity to NFN1 when deleted: *RAD5*, *RAD54*, *RAD55*, *RAD57* and *TOP3*. A subset of eight deletion strains, containing strains deleted for the five genes that caused sensitivity in the spot dilution assay, was selected for confirmation of the gene-drug interaction (Figure 4.16) in liquid cultures. All five strains identified as sensitive before also showed sensitivity in this assay. *rad5* $\Delta$  was the most sensitive deletion strain from the barcode arrays and also showed the strongest response in both

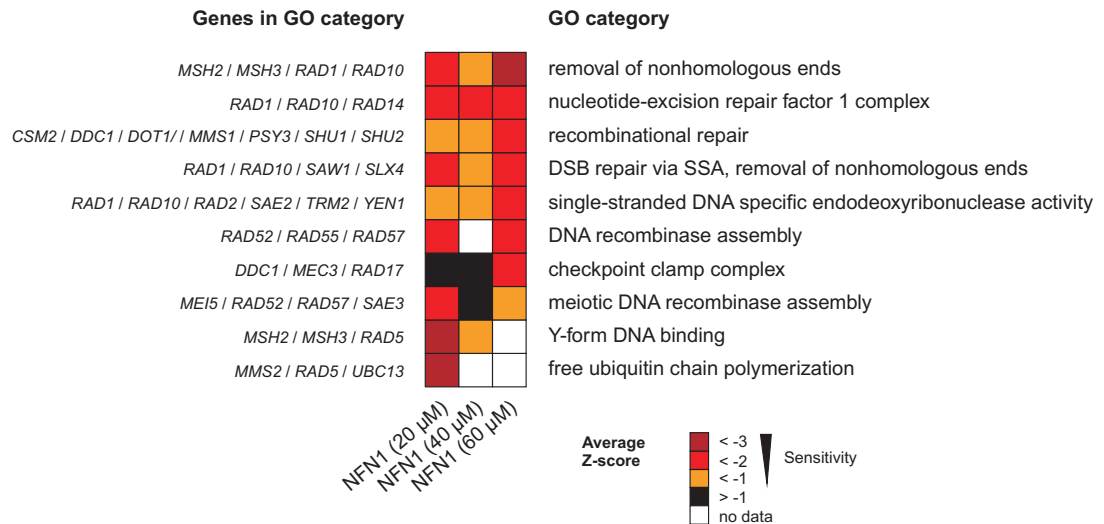


Figure 4.14: GO categories of deletion mutants affected by *NFN1* treatment. For each of the three *NFN1* chemical-genetic screens, average Z-scores were calculated for each GO category. The most significantly affected GO categories are shown (Z-score < -2; there were no categories with a Z-score > 2). Heatmap represents log<sub>2</sub> sensitivity Z-score. Genes annotated with each GO category are listed on the left hand side of the heatmap. DSB - double-strand break; SSA - single-strand annealing.

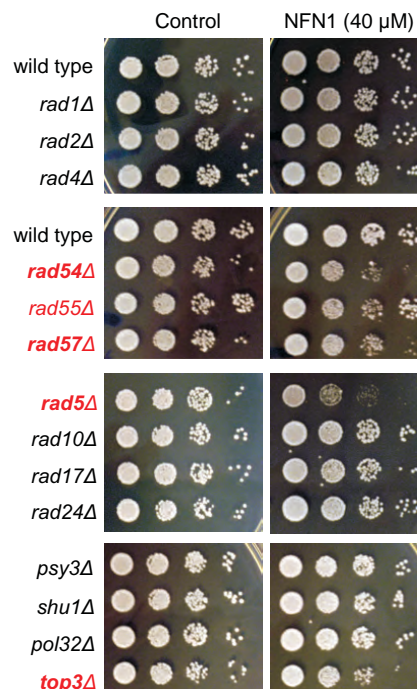


Figure 4.15: Spot dilution assay of *S. cerevisiae* strains deleted for genes involved in DNA damage repair pathways. Yeast strain dilutions were spotted onto XY plates as well as XY plates containing 40  $\mu$ M *NFN1*.

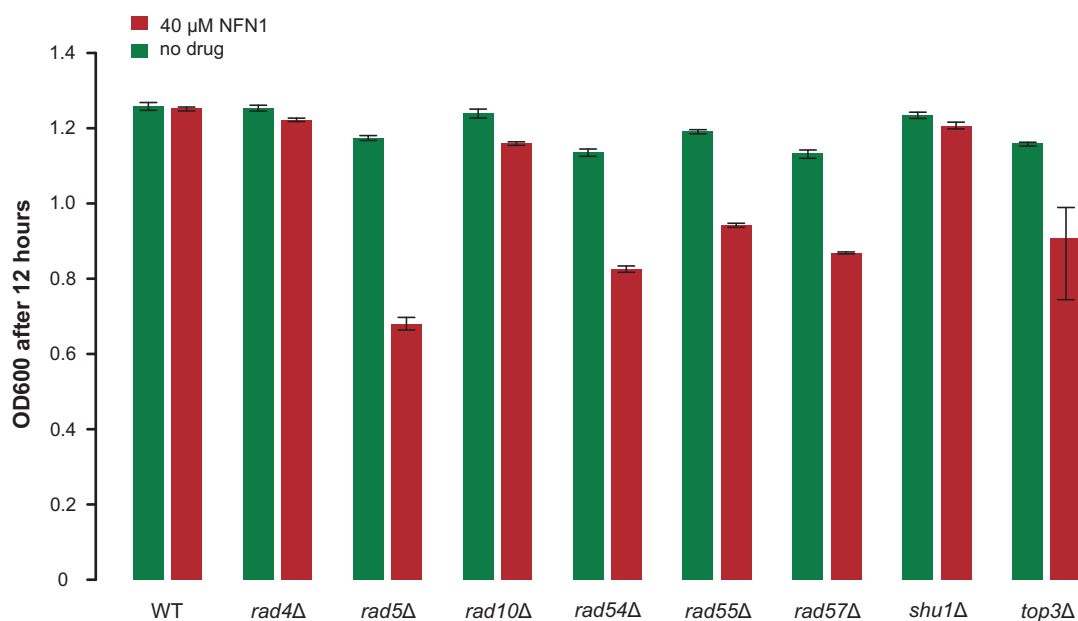


Figure 4.16: Confirmation of a subset of drug-gene interactions for NFN1. (A) Spot dilution assay of 14 deletion strains on plates with and without NFN1. (B) A set of eight deletion strains was tested for their sensitivity to NFN1. OD600 values after 12 hours are shown. The mean of triplicate measurements are shown; error bars represent standard deviation.

assays. *rad4Δ*, *rad10Δ* and *shu1Δ* did not have a significant effect on NFN1 susceptibility in either assay.

Among the 75 compounds that were profiled in Parsons *et al.* (2006) are four drugs that are known to cause DNA damage. These compounds are cisplatin, hydroxyurea, methanesulfonic acid methyl ester (MMS) and mitomycin C. Cisplatin is a chemotherapeutic agent that is used against different types cancers. It cross-links to DNA leading to apoptosis of affected cells.. Hydroxyurea is used against a variety of diseases including sickle-cell disease and AIDS. It is thought to scavenge tyrosyl free radicals and therefore inhibits ribonucleotide reductase which leads to DNA damage. MMS is an alkylating agent and is considered a carcinogen. It is used to treat cancer. Mitomycin C is a natural product that is used as a chemotherapeutic agent. It is a potent DNA crosslinker. Comparison of the chemical-genetic profiles of these compounds from the Parsons *et al.* (2006) dataset with the NFN1 profile (60 μM) revealed that quite a few of the deletion strains most sensitive to NFN1 are also sensitive to each of these four drugs (Figure 4.17). The majority of these shared sensitive deletion strains are involved in

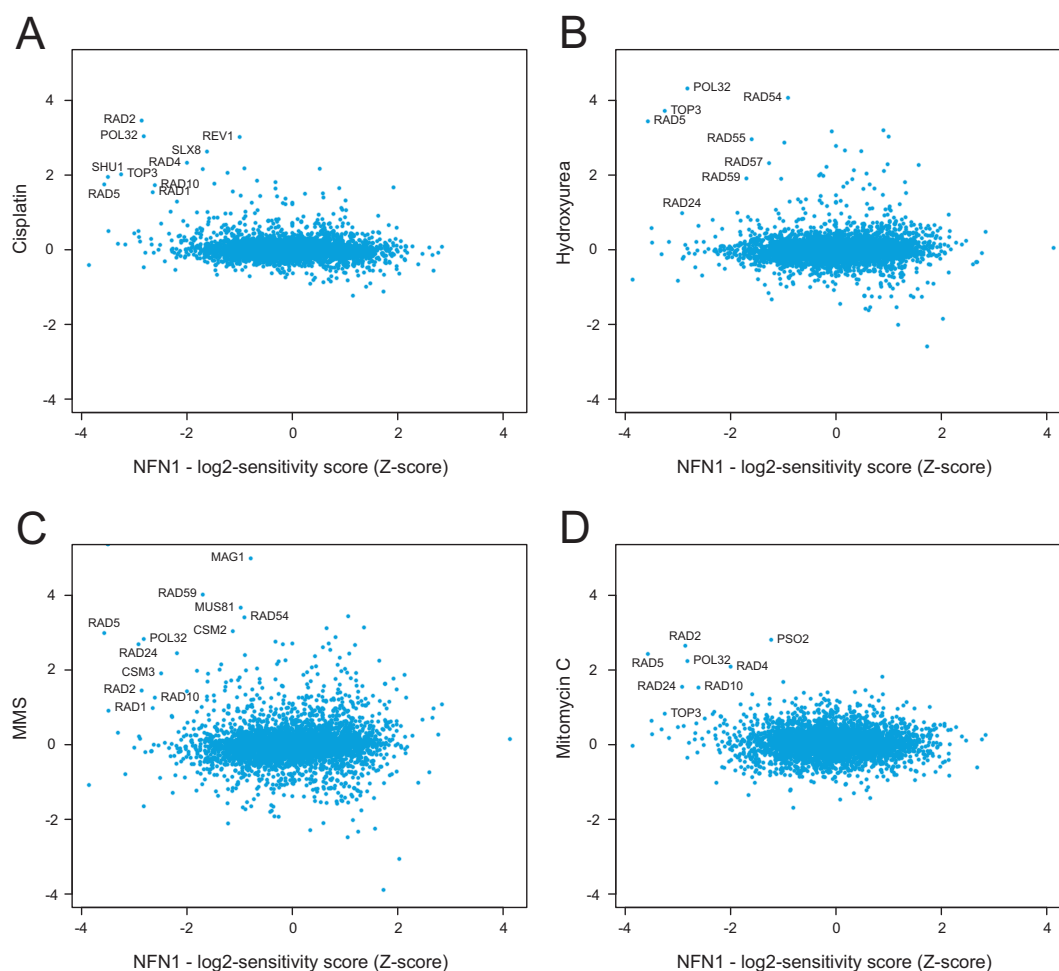


Figure 4.17: Comparison of chemical-genetic profile of NFN1 with that of DNA damaging drugs. The chemical-genetic profile of NFN1 was compared with those of (A) cisplatin, (B) hydroxyurea, (C) MMS and (D) mitomycin C from Parsons *et al.*, 2006. Note that for scores along the y-axis, positive scores indicate sensitivity of a deletion strain.

DNA damage repair. These results strengthen the argument that NFN1 causes DNA damage in the budding yeast *S. cerevisiae*.

## 4.2.6 Summary of Results

Using chemical-genetic screens in *S. cerevisiae* it was shown that compounds affecting melanocyte pigmentation do so by interfering with copper metabolism. Defects in intracellular AP1 and AP3 trafficking pathways were shown to cause sensitivity to low copper conditions in zebrafish embryos. Surprisingly, the MAP-kinase inhibitor U0126 was found to affect copper metabolism. Further, a ni-

trofuran compound was found to specifically promote melanocyte cell death in zebrafish. This enabled the study of off-target effects of nitrofurans that are used to treat trypanosome infections. Nifurtimox is a nitrofuran prodrug that is activated by pathogen-specific nitroreductases. With yeast and zebrafish it was shown that nitrofurans are also bioactivated by host-specific aldehyde dehydrogenases suggesting that a combination therapy with an aldehyde dehydrogenase inhibitor might reduce side effects associated with nifurtimox.

## 4.3 Discussion

### Combination of zebrafish and yeast screens revealed gene-environment interactions

Pathways involved in uptake, trafficking and excretion of transition metals are well conserved between yeast, zebrafish and human (Thiele & Gitlin, 2008; for copper: Rees & Thiele, 2004). This allows for human diseases related to allelic variants in genes involved in copper metabolism to be characterised in model organisms. Compounds that were identified as copper chelators in phenotypic screens in zebrafish as well as the known copper chelator neocuproine, were subjected to genome-wide chemical-genetic screens in the budding yeast. These screens revealed overlap in target pathways of these small molecules. Intracellular transport pathways were affected in particular and these pathways are essential for transport of copper to copper-enzymes, for recycling of ATP7a, a copper transporter, and for detoxification in high copper conditions (Jo *et al.*, 2008). In melanocytes, the activation of copper-dependent pigmentation enzymes, like tyrosinase, is restricted to melanosomes by transport of ATP7A to these specialised organelles (Setty *et al.*, 2008). The transport of tyrosinase into melanosomes is mediated by components of the AP1 and AP3 complexes whereas BLOC-1 is required for selective ATP7A-transport. Rare alleles of the AP3 and the AP1s1 genes have been linked to diseases. The combination of zebrafish and yeast data suggest that reduced levels of functional AP1 and AP3 do not affect pigmentation in optimal nutritional conditions but have dramatic effects of pigmentation

in low-copper conditions (Figure 4.7B). The budding yeast was therefore successfully used to identify at least two intracellular transport pathways that are physiologically relevant in the developing vertebrate.

### **Unbiased screens detected unexpected drug target(s) for U0126**

Characterisation of the *in vivo* mode of action of a compound is the most important and most challenging question in chemical biology. Phenotypic screens and genome-scale genetic analysis in model organisms have been successfully used to identify target pathways for known and new compounds. There has been some success in predicting new molecular targets for known drugs computationally (Keiser *et al.*, 2009). Cellbased, biochemical and *in silico* methods are usually applied to identify molecular targets, but these approaches are quite limited because they look for specific effects. In addition, a molecular target in specific experimental conditions does not fully reflect the complex action of a compound within the developing animal. Indeed, unbiased screens in zebrafish and budding yeast revealed unexpected copper-dependent effects of the MEK inhibitor U0126 in this study.

### **Integration of data from different model organisms to investigate off-target effects of nitrofurans**

The beauty of chemical biology is that it is generally possible to investigate the effect of small molecules in different model organisms or assays. Identification of the nitrofurans compound NFN1 as melanocyte-specific in a zebrafish phenotypic screen provided a model for the study of off-target effects of nitrofurans independent of trypanosome infections. Nitrofurans are pro-drugs that are converted to unsaturated open chain nitriles by parasitic nitroreductases (Hall *et al.*, 2011). These drugs are widely used even though many patients suffer severe drug-induced side-effects. Experiments in zebrafish extracts revealed ALDH2 to be bound by NFN1. Purified human ALDH2 was also shown to bind to NFN1 (Ishizaki, Zhou *et al.*, submitted). Further experiments in zebrafish and yeast showed that the 5-NO<sub>2</sub> moiety is indeed required for bioactivity

of NFN1 in these two organisms. Small molecule inhibitors of aldehyde dehydrogenase prevented the effects of NFN1 yeast and zebrafish, indicating that NFN1 bioactivation depends on ALDH2 activity. This was also confirmed genetically in the budding yeast where deletion of *ALD2*, *ALD3* and *ALD6* had additive effects on NFN1 rescue. These results from experiments in zebrafish, yeast and human supported the hypothesis that nitrofurans can also be activated by aldehyde dehydrogenase 2 which may cause the side-effects observed in many patients. Experiments in zebrafish (Ishizaki, unpublished data) and yeast indicate that nitrofurans cause DNA damage in these organisms which is the mode of action of nifurtimox against *Trypanosoma* (Goijman *et al.*, 1985).

### **Drug combinations as new therapeutic strategy to treat trypanosome infections**

The knowledge that ALDH2 activates nitrofurans in host cells, led to the hypothesis that inhibition of these enzymes, that are not present in the genomes of *Trypanosoma brucei* and *Trypanosoma cruzi*, could prevent host toxicity. Experiments in trypanosome showed that a combination of nifurtimox and an Aldh2-inhibitor does not affect the trypanocidal potential of nifurtimox (Ishizaki, Zhou *et al.*, submitted). The observation that Aldh2 inhibitors prevent 5-nitrofurans activity specifically in animals, suggested that combination treatment of 5-nitrofurans compounds together with Aldh2-inhibitors could prevent toxic off-target effects in the host while still effectively treating *Trypanosoma* infections.

---

### Summary and Concluding Remarks

---

#### 5.1 Summary

Functional genomic approaches in the budding yeast *Saccharomyces cerevisiae* revealed that membrane-perturbing compounds as well as inhibitors of sphingolipid biosynthesis synergise with fluconazole in fungal strains. Experiments in zebrafish and yeast revealed a gene-copper-nutrition interaction. A combined zebrafish-yeast approach also resulted in a combination treatment for *Trypanosoma* infections with reduced side effects.

#### 5.2 Concluding Remarks

I think that drug discovery, especially for neglected diseases, will greatly benefit from the approaches applied in the context of this thesis. Known drugs are a valuable resource and there is already a variety of applications and screening approaches. Drug combination screens using a well chosen known drug as an “anchor drug” seem to be a fruitful approach to discover effective drug combinations against different diseases. The idea of the vast combinatorial chemical space is daunting, especially when more than two compounds are combined. Progress



in systems biology will be necessary to guide drug discovery because biological systems are much more complex than we are currently able to handle. Organism-based screening will probably soon be applied to across-species profiling of small molecule collections. The effects of drugs in different species will inform about the compounds as well as the species.

---

## Bibliography

---

- Abruzzi, K., Denome, S., Olsen, J. R., Assenholt, J., Haaning, L. L., Jensen, T. H., and Rosbash, M. A novel plasmid-based microarray screen identifies suppressors of *rrp6Delta* in *Saccharomyces cerevisiae*. *Mol Cell Biol*, 27(3): 1044–55 (2007).
- Ágoston, V., Csermely, P., and Pongor, S. Multiple weak hits confuse complex systems: a transcriptional regulatory network as an example. *Phys Rev E Stat Nonlin Soft Matter Phys*, 71(5 Pt 1): 051909 (2005).
- Ashburn, T. T. and Thor, K. B. Drug repositioning: identifying and developing new uses for existing drugs. *Nat Rev Drug Discov*, 3(8): 673–83 (2004).
- Askree, S. H., Yehuda, T., Smolikov, S., Gurevich, R., Hawk, J., Coker, C., Krauskopf, A., Kupiec, M., and McEachern, M. J. A genome-wide screen for *Saccharomyces cerevisiae* deletion mutants that affect telomere length. *Proc Natl Acad Sci USA*, 101(23): 8658–63 (2004).
- Balgi, A. D., Fonseca, B. D., Donohue, E., Tsang, T. C. F., Lajoie, P., Proud, C. G., Nabi, I. R., and Roberge, M. Screen for chemical modulators of autophagy reveals novel therapeutic inhibitors of mTORC1 signaling. *PLoS ONE*, 4(9): e7124 (2009).
- Barchiesi, F., Francesco, L. F. D., and Scalise, G. In vitro activities of terbinafine in combination with fluconazole and itraconazole against isolates of *Candida albicans* with reduced susceptibility to azoles. *Antimicrob Agents Chemother*, 41(8): 1812–4 (1997).
- Barchiesi, F., Francesco, L. F. D., Compagnucci, P., Arzeni, D., Giacometti, A., and Scalise, G. In-vitro interaction of terbinafine with amphotericin B, fluconazole and itraconazole against clinical isolates of *Candida albicans*. *J Antimicrob Chemother*, 41(1): 59–65 (1998).
- Barchiesi, F., Schimizzi, A. M., Caselli, F., Novelli, A., Fallani, S., Giannini, D., Arzeni, D., Cesare, S. D., Francesco, L. F. D., Fortuna, M., Giacometti, A.,

- Carle, F., Mazzei, T., and Scalise, G. Interactions between triazoles and amphotericin B against *Cryptococcus neoformans*. *Antimicrob Agents Chemother*, 44(9): 2435–41 (2000).
- Bauer, J. A., Ye, F., Marshall, C. B., Lehmann, B. D., Pendleton, C. S., Shyr, Y., Arteaga, C. L., and Pietenpol, J. A. RNA interference (RNAi) screening approach identifies agents that enhance paclitaxel activity in breast cancer cells. *Breast Cancer Res*, 12(3): R41 (2010).
- Berenbaum, M. C. Direct search methods in the optimisation of cancer chemotherapy regimens. *Br J Cancer*, 61(1): 101–9 (1990).
- Berenbaum, M. C., Yu, V. L., and Felegie, T. P. Synergy with double and triple antibiotic combinations compared. *J Antimicrob Chemother*, 12(6): 555–63 (1983).
- Birmingham, A., Selfors, L. M., Forster, T., Wrobel, D., Kennedy, C. J., Shanks, E., Santoyo-Lopez, J., Dunican, D. J., Long, A., Kelleher, D., Smith, Q., Beijersbergen, R. L., Ghazal, P., and Shamu, C. E. Statistical methods for analysis of high-throughput RNA interference screens. *Nat Methods*, 6(8): 569–75 (2009).
- Birrell, G. W., Giaever, G., Chu, A. M., Davis, R. W., and Brown, J. M. A genome-wide screen in *Saccharomyces cerevisiae* for genes affecting UV radiation sensitivity. *Proc Natl Acad Sci USA*, 98(22): 12608–13 (2001).
- Bliss, C. I. The toxicity of poisons applied jointly. *Ann Appl Biol*, 26: 585–615 (1939).
- Boguski, M. S., Mandl, K. D., and Sukhatme, V. P. Drug discovery. Repurposing with a difference. *Science*, 324(5933): 1394–5 (2009).
- Bonangelino, C. J., Chavez, E. M., and Bonifacino, J. S. Genomic screen for vacuolar protein sorting genes in *Saccharomyces cerevisiae*. *Mol Biol Cell*, 13(7): 2486–501 (2002).
- Borisy, A. A., Elliott, P. J., Hurst, N. W., Lee, M. S., Lehár, J., Price, E. R., Serbedzija, G., Zimmermann, G. R., Foley, M. A., Stockwell, B. R., and Keith, C. T. Systematic discovery of multicomponent therapeutics. *Proc Natl Acad Sci USA*, 100(13): 7977–82 (2003).
- Breitkreutz, B.-J., Stark, C., Reguly, T., Boucher, L., Breitkreutz, A., Livstone, M., Oughtred, R., Lackner, D. H., Bähler, J., Wood, V., Dolinski, K., and Tyers, M. The BioGRID Interaction Database: 2008 update. *Nucleic acids research*, 36(Database issue): D637–40 (2008).
- Butcher, R. and Schreiber, S. Using genome-wide transcriptional profiling to elucidate small-molecule mechanism. *Curr Opin Chem Biol*, 9(1): 25–30 (2005).
- Butcher, R. A. and Schreiber, S. L. Identification of Ald6p as the target of a class of small-molecule suppressors of FK506 and their use in network dissection. *Proc Natl Acad Sci USA*, 101(21): 7868–73 (2004).

- Butcher, R. A., Bhullar, B. S., Perlstein, E. O., Marsischky, G., LaBaer, J., and Schreiber, S. L. Microarray-based method for monitoring yeast overexpression strains reveals small-molecule targets in TOR pathway. *Nat Chem Biol*, 2(2): 103–109 (2006). ISSN 1552-4450.
- Cannon, R. D., Lamping, E., Holmes, A. R., Niimi, K., Baret, P. V., Keniya, M. V., Tanabe, K., Niimi, M., Goffeau, A., and Monk, B. C. Efflux-mediated antifungal drug resistance. *Clin Microbiol Rev*, 22(2): 291–321, Table of Contents (2009).
- Ceol, C. J., Houvras, Y., White, R. M., and Zon, L. I. Melanoma biology and the promise of zebrafish. *Zebrafish*, 5(4): 247–55 (2008).
- Chan, D. A. and Giaccia, A. J. Harnessing synthetic lethal interactions in anti-cancer drug discovery. *Nat Rev Drug Discov*, 10(5): 351–64 (2011).
- Chassoux, G. Molsidomine and lipid metabolism. *J Cardiovasc Pharmacol*, 14 Suppl 11: S137–8 (1989).
- Cheadle, C., Cho-Chung, Y. S., Becker, K. G., and Vawter, M. P. Application of z-score transformation to Affymetrix data. *Appl Bioinformatics*, 2(4): 209–17 (2003).
- Chong, C. R. and Chabner, B. A. Mysterious metformin. *Oncologist*, 14(12): 1178–81 (2009).
- Chong, C. R. and Sullivan, D. J. New uses for old drugs. *Nature*, 448(7154): 645–6 (2007).
- Chong, C. R., Chen, X., Shi, L., Liu, J. O., and Sullivan, D. J. A clinical drug library screen identifies astemizole as an antimalarial agent. *Nature Chemical Biology*, 2(8): 415–6 (2006).
- Chung, N., Zhang, X. D., Kreamer, A., Locco, L., Kuan, P.-F., Bartz, S., Linsley, P. S., Ferrer, M., and Strulovici, B. Median absolute deviation to improve hit selection for genome-scale RNAi screens. *J Biomol Screen*, 13(2): 149–58 (2008).
- Clark, T. A. and Hajjeh, R. A. Recent trends in the epidemiology of invasive mycoses. *Curr Opin Infect Dis*, 15(6): 569–74 (2002).
- Clatworthy, A. E., Pierson, E., and Hung, D. T. Targeting virulence: a new paradigm for antimicrobial therapy. *Nature Chemical Biology*, 3(9): 541–8 (2007).
- Cook, M. A., Chan, C.-K., Jorgensen, P., Ketela, T., So, D., Tyers, M., and Ho, C.-Y. Systematic validation and atomic force microscopy of non-covalent short oligonucleotide barcode microarrays. *PLoS ONE*, 3(2): e1546 (2008).
- Costanzo, M., Baryshnikova, A., Bellay, J., Kim, Y., Spear, E. D., Sevier, C. S., Ding, H., Koh, J. L. Y., Toufighi, K., Mostafavi, S., Prinz, J., Onge, R. P. S., VanderSluis, B., Makhnevych, T., Vizeacoumar, F. J., Alizadeh, S., Bahr, S.,

- Brost, R. L., Chen, Y., Cokol, M., Deshpande, R., Li, Z., Lin, Z.-Y., Liang, W., Marback, M., Paw, J., Luis, B.-J. S., Shuteriqi, E., Tong, A. H. Y., van Dyk, N., Wallace, I. M., Whitney, J. A., Weirauch, M. T., Zhong, G., Zhu, H., Houry, W. A., Brudno, M., Ragibizadeh, S., Papp, B., Pál, C., Roth, F. P., Giaefer, G., Nislow, C., Troyanskaya, O. G., Bussey, H., Bader, G. D., Gingras, A.-C., Morris, Q. D., Kim, P. M., Kaiser, C. A., Myers, C. L., Andrews, B. J., and Boone, C. The genetic landscape of a cell. *Science*, 327(5964): 425–31 (2010).
- Cowen, L. E., Singh, S. D., Köhler, J. R., Collins, C., Zaas, A. K., Schell, W. A., Aziz, H., Mylonakis, E., Perfect, J. R., Whitesell, L., and Lindquist, S. Harnessing Hsp90 function as a powerful, broadly effective therapeutic strategy for fungal infectious disease. *Proc Natl Acad Sci USA*, 106(8): 2818–23 (2009).
- Csermely, P. Strong links are important, but weak links stabilize them. *Trends Biochem Sci*, 29(7): 331–4 (2004).
- Csermely, P., Ágoston, V., and Pongor, S. The efficiency of multi-target drugs: the network approach might help drug design. *Trends Pharmacol Sci*, 26(4): 178–82 (2005).
- D’Amato, R. J., Loughnan, M. S., Flynn, E., and Folkman, J. Thalidomide is an inhibitor of angiogenesis. *Proc Natl Acad Sci USA*, 91(9): 4082–5 (1994).
- Das, A., Durrant, D., Mitchell, C., Mayton, E., Hoke, N. N., Salloum, F. N., Park, M. A., Qureshi, I., Lee, R., Dent, P., and Kukreja, R. C. Sildenafil increases chemotherapeutic efficacy of doxorubicin in prostate cancer and ameliorates cardiac dysfunction. *Proc Natl Acad Sci USA*, 107(42): 18202–7 (2010).
- Davis, J. M., Clay, H., Lewis, J. L., Ghori, N., Herbomel, P., and Ramakrishnan, L. Real-time visualization of mycobacterium-macrophage interactions leading to initiation of granuloma formation in zebrafish embryos. *Immunity*, 17(6): 693–702 (2002).
- de Freitas, J., Wintz, H., Kim, J. H., Poynton, H., Fox, T., and Vulpe, C. Yeast, a model organism for iron and copper metabolism studies. *Biometals*, 16(1): 185–97 (2003).
- Drews, J. Drug discovery: a historical perspective. *Science*, 287(5460): 1960–4 (2000).
- Driever, W., Solnica-Krezel, L., Schier, A. F., Neuhauss, S. C., Malicki, J., Stemple, D. L., Stainier, D. Y., Zwartkruis, F., Abdelilah, S., Rangini, Z., Belak, J., and Boggs, C. A genetic screen for mutations affecting embryogenesis in zebrafish. *Development*, 123: 37–46 (1996).
- Dudley, J. T., Deshpande, T., and Butte, A. J. Exploiting drug-disease relationships for computational drug repositioning. *Brief Bioinformatics*, 12(4): 303–11 (2011).

- Ejim, L., Farha, M., Falconer, S. B., Wildenhain, J., Coombes, B. K., Tyers, M., Brown, E. D., and Wright, G. D. Combinations of antibiotics and nonantibiotic drugs enhance antimicrobial efficacy. *Nature Chemical Biology* (2011).
- Ekins, S., Williams, A. J., Krasowski, M. D., and Freundlich, J. S. In silico repositioning of approved drugs for rare and neglected diseases. *Drug Discov Today* (2011).
- Eliopoulos, G. M. and Moellering, R. C. Antimicrobial combinations. In Baltimore, L. V., editor, *Antibiotics in laboratory medicine*, pages 432–492. The Williams & Wilkins Co (1991).
- Epp, E., Vanier, G., Harcus, D., Lee, A. Y., Jansen, G., Hallett, M., Sheppard, D. C., Thomas, D. Y., Munro, C. A., Mullick, A., and Whiteway, M. Reverse genetics in *Candida albicans* predicts ARF cycling is essential for drug resistance and virulence. *PLoS Pathog*, 6(2) (2010).
- Ericson, E., Gebbia, M., Heisler, L. E., Wildenhain, J., Tyers, M., Giaever, G., and Nislow, C. Off-target effects of psychoactive drugs revealed by genome-wide assays in yeast. *PLoS Genet*, 4(8) (2008).
- Falconer, S. B., Czarny, T. L., and Brown, E. D. Antibiotics as probes of biological complexity. *Nature Chemical Biology*, pages 415–423 (2011).
- Farha, M. A. and Brown, E. D. Chemical probes of *Escherichia coli* uncovered through chemical-chemical interaction profiling with compounds of known biological activity. *Chemistry & Biology*, 17(8): 852–62 (2010).
- Farr, M. and Bacon, P. A. How and when should combination therapy be used? The role of an anchor drug. *Br J Rheumatol*, 34 Suppl 2: 100–3 (1995).
- Fischbach, M. A. and Walsh, C. T. Antibiotics for emerging pathogens. *Science*, 325(5944): 1089–93 (2009).
- Fitzgerald, J. B., Schoeberl, B., Nielsen, U. B., and Sorger, P. K. Systems biology and combination therapy in the quest for clinical efficacy. *Nat Chem Biol*, 2(9): 458–466 (2006).
- Fleming, A. On the antibacterial action of cultures of a penicillium, with special reference to their use in the isolation of *B. influenzae*. 1929. *The British Journal of Experimental Pathology*, 10(8): 226–236 (1929).
- Fried, H. M. and Warner, J. R. Molecular cloning and analysis of yeast gene for cycloheximide resistance and ribosomal protein L29. *Nucleic Acids Res*, 10(10): 3133–48 (1982).
- Gamarra, S., Rocha, E. M. F., Zhang, Y.-Q., Park, S., Rao, R., and Perlin, D. S. Mechanism of the synergistic effect of amiodarone and fluconazole in *Candida albicans*. *Antimicrobial Agents and Chemotherapy*, 54(5): 1753–61 (2010).

- Garcia, O., Saveanu, C., Cline, M., Fromont-Racine, M., Jacquier, A., Schwikowski, B., and Aittokallio, T. GOLORize: a Cytoscape plug-in for network visualization with Gene Ontology-based layout and coloring. *Bioinformatics*, 23(3): 394–6 (2007).
- Gaughran, J. P., Lai, M. H., Kirsch, D. R., and Silverman, S. J. Nikkomycin Z is a specific inhibitor of *Saccharomyces cerevisiae* chitin synthase isozyme Chs3 in vitro and in vivo. *Journal of Bacteriology*, 176(18): 5857–60 (1994).
- Giacomotto, J. and Ségalat, L. High-throughput screening and small animal models, where are we? *Br J Pharmacol*, 160(2): 204–16 (2010).
- Giaever, G., Shoemaker, D. D., Jones, T. W., Liang, H., Winzeler, E. A., Astromoff, A., and Davis, R. W. Genomic profiling of drug sensitivities via induced haploinsufficiency. *Nat Genet*, 21(3): 278–83 (1999).
- Giaever, G., Chu, A. M., Ni, L., Connelly, C., Riles, L., Véronneau, S., Dow, S., Lucau-Danila, A., Anderson, K., André, B., Arkin, A. P., Astromoff, A., El-Bakkoury, M., Bangham, R., Benito, R., Brachat, S., Campanaro, S., Curtiss, M., Davis, K., Deutschbauer, A., Entian, K.-D., Flaherty, P., Foury, F., Garfinkel, D. J., Gerstein, M., Gotte, D., Güldener, U., Hegemann, J. H., Hempel, S., Herman, Z., Jaramillo, D. F., Kelly, D. E., Kelly, S. L., Kötter, P., LaBonte, D., Lamb, D. C., Lan, N., Liang, H., Liao, H., Liu, L., Luo, C., Lussier, M., Mao, R., Menard, P., Ooi, S. L., Revuelta, J. L., Roberts, C. J., Rose, M., Ross-Macdonald, P., Scherens, B., Schimmack, G., Shafer, B., Shoemaker, D. D., Sookhai-Mahadeo, S., Storms, R. K., Strathern, J. N., Valle, G., Voet, M., Volckaert, G., yun Wang, C., Ward, T. R., Wilhelmy, J., Winzeler, E. A., Yang, Y., Yen, G., Youngman, E., Yu, K., Bussey, H., Boeke, J. D., Snyder, M., Philippsen, P., Davis, R. W., and Johnston, M. Functional profiling of the *Saccharomyces cerevisiae* genome. *Nature*, 418(6896): 387–91 (2002).
- Giaever, G., Flaherty, P., Kumm, J., Proctor, M., Nislow, C., Jaramillo, D. F., Chu, A. M., Jordan, M. I., Arkin, A. P., and Davis, R. W. Chemogenomic profiling: identifying the functional interactions of small molecules in yeast. *Proc Natl Acad Sci USA*, 101(3): 793–8 (2004).
- Gloeckner, C., Garner, A. L., Mersha, F., Oksov, Y., Tricoche, N., Eubanks, L. M., Lustigman, S., Kaufmann, G. F., and Janda, K. D. Repositioning of an existing drug for the neglected tropical disease Onchocerciasis. *Proceedings of the National Academy of Sciences*, 107(8): 3424 (2010).
- Goffeau, A., Barrell, B. G., Bussey, H., Davis, R. W., Dujon, B., Feldmann, H., Galibert, F., Hoheisel, J. D., Jacq, C., Johnston, M., Louis, E. J., Mewes, H. W., Murakami, Y., Philippsen, P., Tettelin, H., and Oliver, S. G. Life with 6000 genes. *Science*, 274(5287): 546, 563–7 (1996).
- Goijsman, S. G., Frasch, A. C., and Stoppani, A. O. Damage of *Trypanosoma cruzi* deoxyribonucleic acid by nitroheterocyclic drugs. *Biochem Pharmacol*, 34(9): 1457–61 (1985).

- González, M., Reyes-Jara, A., Suazo, M., Jo, W. J., and Vulpe, C. Expression of copper-related genes in response to copper load. *Am J Clin Nutr*, 88(3): 830S–4S (2008).
- Greco, W. R., Bravo, G., and Parsons, J. C. The search for synergy: a critical review from a response surface perspective. *Pharmacol Rev*, 47(2): 331–85 (1995).
- Groll, A. H., Lucca, A. J. D., and Walsh, T. J. Emerging targets for the development of novel antifungal therapeutics. *Trends Microbiol*, 6(3): 117–24 (1998).
- Gross, G. J. Evidence for Pleiotropic Effects of Phosphodiesterase-5 (PDE5) Inhibitors: Emerging Concepts in Cancer and Cardiovascular Medicine. *Circulation research*, 108(9): 1040–1041 (2011).
- Gullo, A. Invasive fungal infections: the challenge continues. *Drugs*, 69 Suppl 1: 65–73 (2009).
- Gyertvai, A., Emri, T., Takács, K., Dergez, T., Fekete, A., Pesti, M., Pócsi, I., and Lenkey, B. Lovastatin possesses a fungistatic effect against *Candida albicans*, but does not trigger apoptosis in this opportunistic human pathogen. *FEMS Yeast Research*, 6(8): 1140–8 (2006).
- Haffter, P., Granato, M., Brand, M., Mullins, M. C., Hammerschmidt, M., Kane, D. A., Odenthal, J., van Eeden, F. J., Jiang, Y. J., Heisenberg, C. P., Kelsh, R. N., Furutani-Seiki, M., Vogelsang, E., Beuchle, D., Schach, U., Fabian, C., and Nüsslein-Volhard, C. The identification of genes with unique and essential functions in the development of the zebrafish, *Danio rerio*. *Development*, 123: 1–36 (1996).
- Haggarty, S. J., Mayer, T. U., Miyamoto, D. T., Fathi, R., King, R. W., Mitchison, T. J., and Schreiber, S. L. Dissecting cellular processes using small molecules: identification of colchicine-like, taxol-like and other small molecules that perturb mitosis. *Chem Biol*, 7(4): 275–86 (2000).
- Hall, B. S., Bot, C., and Wilkinson, S. R. Nifurtimox activation by trypanosomal type I nitroreductases generates cytotoxic nitrile metabolites. *Journal of Biological Chemistry*, 286(15): 13088 (2011).
- Hallstrom, T. C., Lambert, L., Schorling, S., Balzi, E., Goffeau, A., and Moye-Rowley, W. S. Coordinate control of sphingolipid biosynthesis and multidrug resistance in *Saccharomyces cerevisiae*. *J Biol Chem*, 276(26): 23674–80 (2001).
- Hartwell, L. H., Szankasi, P., Roberts, C. J., Murray, A. W., and Friend, S. H. Integrating genetic approaches into the discovery of anticancer drugs. *Science*, 278(5340): 1064–8 (1997).
- Hauptman, P. J. and Kelly, R. A. Digitalis. *Circulation*, 99(9): 1265–70 (1999).



- Hawkins, T. A., Cavodeassi, F., Erdélyi, F., Szabó, G., and Lele, Z. The small molecule Mek1/2 inhibitor U0126 disrupts the chordamesoderm to notochord transition in zebrafish. *BMC Dev Biol*, 8: 42 (2008).
- Hillenmeyer, M. E., Fung, E., Wildenhain, J., Pierce, S. E., Hoon, S., Lee, W., Proctor, M., Onge, R. P. S., Tyers, M., Koller, D., Altman, R. B., Davis, R. W., Nislow, C., and Giaever, G. The chemical genomic portrait of yeast: uncovering a phenotype for all genes. *Science*, 320(5874): 362–5 (2008).
- Hirsch, H. A., Iliopoulos, D., Tschlis, P. N., and Struhl, K. Metformin selectively targets cancer stem cells, and acts together with chemotherapy to block tumor growth and prolong remission. *Cancer Res*, 69(19): 7507–11 (2009).
- Ho, C. H., Magtanong, L., Barker, S. L., Gresham, D., Nishimura, S., Natarajan, P., Koh, J. L. Y., Porter, J., Gray, C. A., Andersen, R. J., Giaever, G., Nislow, C., Andrews, B., Botstein, D., Graham, T. R., Yoshida, M., and Boone, C. A molecular barcoded yeast ORF library enables mode-of-action analysis of bioactive compounds. *Nat Biotechnol*, 27(4): 369–77 (2009).
- Honore, S., Kamath, K., Braguer, D., Horwitz, S. B., Wilson, L., Briand, C., and Jordan, M. A. Synergistic suppression of microtubule dynamics by discodermolide and paclitaxel in non-small cell lung carcinoma cells. *Cancer Res*, 64(14): 4957–64 (2004).
- Hoon, S., Smith, A. M., Wallace, I. M., Suresh, S., Miranda, M., Fung, E., Proctor, M., Shokat, K. M., Zhang, C., Davis, R. W., Giaever, G., Onge, R. P. S., StOnge, R. P., and Nislow, C. An integrated platform of genomic assays reveals small-molecule bioactivities. *Nat Chem Biol*, 4(8): 498–506 (2008).
- Hopkins, A. L. Network pharmacology: the next paradigm in drug discovery. *Nature Chemical Biology*, 4(11): 682–90 (2008).
- Hopkins, A. L. and Groom, C. R. The druggable genome. *Nat Rev Drug Discov*, 1(9): 727–30 (2002).
- Howard, B., Thompson, P. E., and Manallack, D. T. Active site similarity between human and Plasmodium falciparum phosphodiesterases: considerations for antimalarial drug design. *J Comput Aided Mol Des* (2011).
- Hu, G. and Kronstad, J. W. A putative P-type ATPase, Apt1, is involved in stress tolerance and virulence in Cryptococcus neoformans. *Eukaryotic Cell*, 9(1): 74–83 (2010).
- Huang, R., Southall, N., Wang, Y., Yasgar, A., Shinn, P., Jadhav, A., Nguyen, D. T., and Austin, C. P. The NCGC pharmaceutical collection: A comprehensive resource of clinically approved drugs enabling repurposing and chemical genomics. *Science Translational Medicine*, 3(80): 80ps16 (2011).
- Hughes, T. R., Marton, M. J., Jones, A. R., Roberts, C. J., Stoughton, R., Armour, C. D., Bennett, H. A., Coffey, E., Dai, H., He, Y. D., Kidd, M. J., King, A. M., Meyer, M. R., Slade, D., Lum, P. Y., Stepaniants, S. B., Shoemaker,

- D. D., Gachotte, D., Chakraborty, K., Simon, J., Bard, M., and Friend, S. H. Functional discovery via a compendium of expression profiles. *Cell*, 102(1): 109–26 (2000).
- Iadevaia, S., Lu, Y., Morales, F. C., Mills, G. B., and Ram, P. T. Identification of optimal drug combinations targeting cellular networks: integrating phosphoproteomics and computational network analysis. *Cancer Res*, 70(17): 6704–14 (2010).
- Ignarro, L. J., Bush, P. A., Buga, G. M., Wood, K. S., Fukuto, J. M., and Rajfer, J. Nitric oxide and cyclic GMP formation upon electrical field stimulation cause relaxation of corpus cavernosum smooth muscle. *Biochem Biophys Res Commun*, 170(2): 843–50 (1990).
- Ishizaki, H., Spitzer, M., Wildenhain, J., Anastasaki, C., Zeng, Z., Dolma, S., Shaw, M., Madsen, E., Gitlin, J., Marais, R., Tyers, M., and Patton, E. E. Combined zebrafish-yeast chemical-genetic screens reveal gene-copper-nutrition interactions that modulate melanocyte pigmentation. *Dis Model Mech*, 3(9-10): 639–51 (2010).
- Islinger, M., Li, K. W., Seitz, J., Völkl, A., and Lüers, G. H. Hitchhiking of Cu/Zn superoxide dismutase to peroxisomes—evidence for a natural piggyback import mechanism in mammals. *Traffic*, 10(11): 1711–21 (2009).
- Jansen, G., Lee, A. Y., Epp, E., Fredette, A., Surprenant, J., Harcus, D., Scott, M., Tan, E., Nishimura, T., Whiteway, M., Hallett, M., and Thomas, D. Y. Chemogenomic profiling predicts antifungal synergies. *Mol Syst Biol*, 5: 338 (2009).
- Jeong, H., Tombor, B., Albert, R., Oltvai, Z. N., and Barabási, A. L. The large-scale organization of metabolic networks. *Nature*, 407(6804): 651–4 (2000).
- Jia, J., Zhu, F., Ma, X., Cao, Z., Cao, Z. W., Li, Y., Li, Y. X., and Chen, Y. Z. Mechanisms of drug combinations: interaction and network perspectives. *Nat Rev Drug Discov*, 8(2): 111–28 (2009).
- Jo, W. J., Loguinov, A., Chang, M., Wintz, H., Nislow, C., Arkin, A. P., Giaever, G., and Vulpe, C. D. Identification of genes involved in the toxic response of *Saccharomyces cerevisiae* against iron and copper overload by parallel analysis of deletion mutants. *Toxicol Sci*, 101(1): 140–51 (2008).
- Jo, W. J., Kim, J. H., Oh, E., Jaramillo, D., Holman, P., Loguinov, A. V., Arkin, A. P., Nislow, C., Giaever, G., and Vulpe, C. D. Novel insights into iron metabolism by integrating deletome and transcriptome analysis in an iron deficiency model of the yeast *Saccharomyces cerevisiae*. *BMC Genomics*, 10: 130 (2009).
- Johnson, M. D. and Perfect, J. R. Combination antifungal therapy: what can and should we expect? *Bone Marrow Transplant*, 40(4): 297–306 (2007).

- Johnson, M. D. and Perfect, J. R. Use of Antifungal Combination Therapy: Agents, Order, and Timing. *Curr Fungal Infect Rep*, 4(2): 87–95 (2010).
- Johnson, R. M., Allen, C., Melman, S. D., Waller, A., Young, S. M., Sklar, L. A., and Parra, K. J. Identification of inhibitors of vacuolar proton-translocating ATPase pumps in yeast by high-throughput screening flow cytometry. *Anal Biochem*, 398(2): 203–11 (2010).
- Jorgensen, P., Nelson, B., Robinson, M. D., Chen, Y., Andrews, B., Tyers, M., and Boone, C. High-resolution genetic mapping with ordered arrays of *Saccharomyces cerevisiae* deletion mutants. *Genetics*, 162(3): 1091–9 (2002).
- Kapitzky, L., Beltrao, P., Berens, T. J., Gassner, N., Zhou, C., W&Uuml;ster, A., Wu, J., Babu, M. M., Elledge, S. J., Toczyski, D., Lokey, R. S., and Krogan, N. J. Cross-species chemogenomic profiling reveals evolutionarily conserved drug mode of action. *Mol Syst Biol*, 6: 1–13 (2010).
- Kaplan, J. C. and Junien, C. Genomics and medicine: an anticipation. From Boolean Mendelian genetics to multifactorial molecular medicine. *C R Acad Sci III, Sci Vie*, 323(12): 1167–74 (2000).
- Keiser, M. J., Setola, V., Irwin, J. J., Laggner, C., Abbas, A. I., Hufeisen, S. J., Jensen, N. H., Kuijter, M. B., Matos, R. C., Tran, T. B., Whaley, R., Glennon, R. A., Hert, J., Thomas, K. L. H., Edwards, D. D., Shoichet, B. K., and Roth, B. L. Predicting new molecular targets for known drugs. *Nature*, 462(7270): 175–81 (2009).
- Keith, C. T., Borisy, A. A., and Stockwell, B. R. Multicomponent therapeutics for networked systems. *Nat Rev Drug Discov*, 4(1): 71–8 (2005).
- Kelley, R. and Ideker, T. Systematic interpretation of genetic interactions using protein networks. *Nat Biotechnol*, 23(5): 561–6 (2005).
- Khan, S., Singhal, S., Mathur, T., Upadhyay, D. J., and Rattan, A. Antifungal potential of disulfiram. *Nippon Ishinkin Gakkai Zasshi*, 48(3): 109–13 (2007).
- Kim, J. W. and Dang, C. V. Cancer’s molecular sweet tooth and the Warburg effect. *Cancer Res*, 66(18): 8927–30 (2006).
- Kitamura, A., Someya, K., Hata, M., Nakajima, R., and Takemura, M. Discovery of a small-molecule inhibitor of beta-1,6-glucan synthesis. *Antimicrob Agents Chemother*, 53(2): 670–7 (2009).
- Kitano, H. A robustness-based approach to systems-oriented drug design. *Nat Rev Drug Discov*, 6(3): 202–10 (2007).
- Klappe, K., Hummel, I., Hoekstra, D., and Kok, J. W. Lipid dependence of ABC transporter localization and function. *Chem Phys Lipids*, 161(2): 57–64 (2009).
- Ko, J. M. and Fisher, D. E. A new era: melanoma genetics and therapeutics. *J Pathol*, 223(2): 241–50 (2011).

- Kokel, D., Bryan, J., Laggner, C., White, R., Cheung, C. Y. J., Mateus, R., Healey, D., Kim, S., Werdich, A. A., Haggarty, S. J., Macrae, C. A., Shoichet, B., and Peterson, R. T. Rapid behavior-based identification of neuroactive small molecules in the zebrafish. *Nature Chemical Biology*, 6(3): 231–237 (2010).
- Koo, S.-H., Flechner, L., Qi, L., Zhang, X., Screatton, R. A., Jeffries, S., Hedrick, S., Xu, W., Boussouar, F., Brindle, P., Takemori, H., and Montminy, M. The CREB coactivator TORC2 is a key regulator of fasting glucose metabolism. *Nature*, 437(7062): 1109–11 (2005).
- Kozka, I. J. and Holman, G. D. Metformin blocks downregulation of cell surface GLUT4 caused by chronic insulin treatment of rat adipocytes. *Diabetes*, 42(8): 1159–65 (1993).
- Kroiss, J., Kaltenpoth, M., Schneider, B., Schwinger, M.-G., Hertweck, C., Madula, R. K., Strohm, E., and Svatos, A. Symbiotic Streptomyces provide antibiotic combination prophylaxis for wasp offspring. *Nat Chem Biol*, 6(4): 261–3 (2010).
- Kublin, J. G., Cortese, J. F., and Njunju, E. M. Reemergence of chloroquine-sensitive Plasmodium falciparum malaria after cessation of chloroquine use in Malawi. *Journal of Infectious Diseases*, 187(12): 1870 (2003).
- Kuo, D., Tan, K., Zinman, G., Ravasi, T., Bar-Joseph, Z., and Ideker, T. Evolutionary divergence in the fungal response to fluconazole revealed by soft clustering. *Genome Biol*, 11(7): R77 (2010).
- Kuo, H.-C., Moore, J. D., and Krebs, J. E. Histone H2A and Spt10 cooperate to regulate induction and autoregulation of the CUP1 metallothionein. *J Biol Chem*, 280(1): 104–11 (2005).
- Kwok, T. C. Y., Ricker, N., Fraser, R., Chan, A. W., Burns, A., Stanley, E. F., McCourt, P., Cutler, S. R., and Roy, P. J. A small-molecule screen in *C. elegans* yields a new calcium channel antagonist. *Nature*, 441(7089): 91–5 (2006).
- Lamb, J., Crawford, E. D., Peck, D., Modell, J. W., Blat, I. C., Wrobel, M. J., Lerner, J., Brunet, J.-P., Subramanian, A., Ross, K. N., Reich, M., Hieronymus, H., Wei, G., Armstrong, S. A., Haggarty, S. J., Clemons, P. A., Wei, R., Carr, S. A., Lander, E. S., and Golub, T. R. The Connectivity Map: using gene-expression signatures to connect small molecules, genes, and disease. *Science*, 313(5795): 1929–35 (2006).
- Langheinrich, U. Zebrafish: a new model on the pharmaceutical catwalk. *Bioessays*, 25(9): 904–12 (2003).
- Laufer, M. K., Thesing, P. C., Eddington, N. D., Masonga, R., Dzinjalama, F. K., Takala, S. L., Taylor, T. E., and Plowe, C. V. Return of chloroquine antimalarial efficacy in Malawi. *N Engl J Med*, 355(19): 1959–66 (2006).

- Launhardt, H., Hinnen, A., and Munder, T. Drug-induced phenotypes provide a tool for the functional analysis of yeast genes. *Yeast*, 14(10): 935–42 (1998).
- Lee, M. S., Johansen, L., Zhang, Y., Wilson, A., Keegan, M., Avery, W., Elliott, P., Borisy, A. A., and Keith, C. T. The novel combination of chlorpromazine and pentamidine exerts synergistic antiproliferative effects through dual mitotic action. *Cancer Res*, 67(23): 11359–67 (2007).
- Lehár, J., Zimmermann, G. R., Krueger, A. S., Molnar, R. A., Ledell, J. T., Heilbut, A. M., Short, G. F., Giusti, L. C., Nolan, G. P., Magid, O. A., Lee, M. S., Borisy, A. A., Stockwell, B. R., and Keith, C. T. Chemical combination effects predict connectivity in biological systems. *Mol Syst Biol*, 3: 80 (2007).
- Lehár, J., Stockwell, B. R., Giaever, G., and Nislow, C. Combination chemical genetics. *Nature Chemical Biology*, 4(11): 674–81 (2008).
- Lehár, J., Krueger, A. S., Avery, W., Heilbut, A. M., Johansen, L. M., Price, E. R., Rickles, R. J., Short, G. F., Staunton, J. E., Jin, X., Lee, M. S., Zimmermann, G. R., and Borisy, A. A. Synergistic drug combinations tend to improve therapeutically relevant selectivity. *Nat Biotechnol*, 27(7): 659–66 (2009).
- Li, H., Black, P. N., Chokshi, A., Sandoval-Alvarez, A., Vatsyayan, R., Sealls, W., and DiRusso, C. C. High-throughput screening for fatty acid uptake inhibitors in humanized yeast identifies atypical antipsychotic drugs that cause dyslipidemias. *J Lipid Res*, 49(1): 230–44 (2008).
- Liliom, K., Wágner, G., Kovács, J., Comin, B., Cascante, M., Orosz, F., and Ovádi, J. Combined enhancement of microtubule assembly and glucose metabolism in neuronal systems in vitro: decreased sensitivity to copper toxicity. *Biochem Biophys Res Commun*, 264(2): 605–10 (1999).
- Liliom, K., Wágner, G., Pácz, A., Cascante, M., Kovács, J., and Ovádi, J. Organization-dependent effects of toxic bivalent ions microtubule assembly and glycolysis. *Eur J Biochem*, 267(15): 4731–9 (2000).
- Liu, D., Xue, P., Meng, Q., Zou, J., Gu, J., and Jiang, W. Pb/Cu effects on the organization of microtubule cytoskeleton in interphase and mitotic cells of *Allium sativum* L. *Plant Cell Rep*, 28(4): 695–702 (2009).
- Loewe, S. Die quantitativen Probleme der Pharmakologie. *Ergebnisse der Physiologie*, 27: 47–187 (1928).
- Loewe, S. The problem of synergism and antagonism of combined drugs. *Arzneimittelforschung*, 3(6): 285–90 (1953).
- Loktionov, A. Common gene polymorphisms and nutrition: emerging links with pathogenesis of multifactorial chronic diseases (review). *J Nutr Biochem*, 14(8): 426–51 (2003).
- Loo, T. W. and Clarke, D. M. Blockage of drug resistance in vitro by disulfiram, a drug used to treat alcoholism. *J Natl Cancer Inst*, 92(11): 898–902 (2000).

- Luesch, H., Wu, T. Y. H., Ren, P., Gray, N. S., Schultz, P. G., and Supek, F. A genome-wide overexpression screen in yeast for small-molecule target identification. *Chemistry & Biology*, 12(1): 55–63 (2005).
- Lum, P. Y., Armour, C. D., Stepaniants, S. B., Cavet, G., Wolf, M. K., Butler, J. S., Hinshaw, J. C., Garnier, P., Prestwich, G. D., Leonardson, A., Garrett-Engele, P., Rush, C. M., Bard, M., Schimmack, G., Phillips, J. W., Roberts, C. J., and Shoemaker, D. D. Discovering modes of action for therapeutic compounds using a genome-wide screen of yeast heterozygotes. *Cell*, 116(1): 121–37 (2004).
- Lundholt, B. K., Scudder, K. M., and Pagliaro, L. A simple technique for reducing edge effect in cell-based assays. *J Biomol Screen*, 8(5): 566–70 (2003).
- Macrae, C. A. and Peterson, R. T. Zebrafish-based small molecule discovery. *Chemistry & Biology*, 10(10): 901–8 (2003).
- Madsen, E. and Gitlin, J. D. Copper and iron disorders of the brain. *Annu Rev Neurosci*, 30: 317–37 (2007).
- Malo, N., Hanley, J. A., Cerquozzi, S., Pelletier, J., and Nadon, R. Statistical practice in high-throughput screening data analysis. *Nat Biotechnol*, 24(2): 167–75 (2006).
- Mammi, C., Pastore, D., Lombardo, M. F., Ferrelli, F., Caprio, M., Consoli, C., Tesauro, M., Gatta, L., Fini, M., Federici, M., Sbraccia, P., Donadel, G., Bellia, A., Rosano, G. M., Fabbri, A., and Lauro, D. Sildenafil reduces insulin-resistance in human endothelial cells. *PLoS ONE*, 6(1): e14542 (2011).
- Marie, C. and White, T. C. Genetic Basis of Antifungal Drug Resistance. *Curr Fungal Infect Rep*, 3(3): 163–169 (2009).
- Marston, A. L., Tham, W.-H., Shah, H., and Amon, A. A genome-wide screen identifies genes required for centromeric cohesion. *Science*, 303(5662): 1367–70 (2004).
- Mayer, T. U., Kapoor, T. M., Haggarty, S. J., King, R. W., Schreiber, S. L., and Mitchison, T. J. Small molecule inhibitor of mitotic spindle bipolarity identified in a phenotype-based screen. *Science*, 286(5441): 971–4 (1999).
- Mendelsohn, B. A., Yin, C., Johnson, S. L., Wilm, T. P., Solnica-Krezel, L., and Gitlin, J. D. Atp7a determines a hierarchy of copper metabolism essential for notochord development. *Cell Metab*, 4(2): 155–62 (2006).
- Milan, D. J., Peterson, T. A., Ruskin, J. N., Peterson, R. T., and Macrae, C. A. Drugs that induce repolarization abnormalities cause bradycardia in zebrafish. *Circulation*, 107(10): 1355–8 (2003).
- Miyake, Y., Kozutsumi, Y., Nakamura, S., Fujita, T., and Kawasaki, T. Serine palmitoyltransferase is the primary target of a sphingosine-like immunosuppressant, ISP-1/myriocin. *Biochem Biophys Res Commun*, 211(2): 396–403 (1995).

- Montpetit, A., Côté, S., Brustein, E., Drouin, C. A., Lapointe, L., Boudreau, M., Meloche, C., Drouin, R., Hudson, T. J., Drapeau, P., and Cossette, P. Disruption of AP1S1, causing a novel neurocutaneous syndrome, perturbs development of the skin and spinal cord. *PLoS Genet*, 4(12): e1000296 (2008).
- Morales, A., Gingell, C., Collins, M., Wicker, P. A., and Osterloh, I. H. Clinical safety of oral sildenafil citrate (VIAGRA) in the treatment of erectile dysfunction. *Int J Impot Res*, 10(2): 69–73 (1998).
- Morrison, K. L. and Weiss, G. A. The origins of chemical biology. *Nature Chemical Biology*, 2(1): 3–6 (2006).
- Mukhopadhyay, A. and Peterson, R. T. Fishing for new antimicrobials. *Curr Opin Chem Biol*, 10(4): 327–33 (2006).
- Murphey, R. D., Stern, H. M., Straub, C. T., and Zon, L. I. A chemical genetic screen for cell cycle inhibitors in zebrafish embryos. *Chemical biology & drug design*, 68(4): 213–9 (2006).
- Mylonakis, E., Moreno, R., Khoury, J. B. E., Idnurm, A., Heitman, J., Calderwood, S. B., Ausubel, F. M., and Diener, A. *Galleria mellonella* as a model system to study *Cryptococcus neoformans* pathogenesis. *Infect Immun*, 73(7): 3842–50 (2005).
- Navarro-Aviño, J. P., Prasad, R., Miralles, V. J., Benito, R. M., and Serrano, R. A proposal for nomenclature of aldehyde dehydrogenases in *Saccharomyces cerevisiae* and characterization of the stressinducible *ald2* and *ald3* genes. *Yeast*, 15(10A): 829–842 (1999).
- Nelander, S., Wang, W., Nilsson, B., She, Q.-B., Pratilas, C., Rosen, N., Genemark, P., and Sander, C. Models from experiments: combinatorial drug perturbations of cancer cells. *Mol Syst Biol*, 4: 1–11 (2008).
- Ni, L. and Snyder, M. A genomic study of the bipolar bud site selection pattern in *Saccharomyces cerevisiae*. *Mol Biol Cell*, 12(7): 2147–70 (2001).
- Nyilasi, I., Kocsubé, S., Krizsán, K., Galgóczy, L., Pesti, M., Papp, T., and Vágvölgyi, C. In vitro synergistic interactions of the effects of various statins and azoles against some clinically important fungi. *FEMS Microbiol Lett*, 307(2): 175–84 (2010).
- Ockaili, R., Salloum, F., Hawkins, J., and Kukreja, R. C. Sildenafil (Viagra) induces powerful cardioprotective effect via opening of mitochondrial K(ATP) channels in rabbits. *Am J Physiol Heart Circ Physiol*, 283(3): H1263–9 (2002).
- Odds, F. C. Synergy, antagonism, and what the checkerboard puts between them. *J Antimicrob Chemother*, 52(1): 1 (2003).
- Ohnuki, S., Oka, S., Nogami, S., and Ohya, Y. High-Content, Image-Based Screening for Drug Targets in Yeast. *PLoS ONE*, 5(4): e10177 (2010).

- Overington, J. P., Al-Lazikani, B., and Hopkins, A. L. How many drug targets are there? *Nat Rev Drug Discov*, 5(12): 993–6 (2006).
- Owen, M. R., Doran, E., and Halestrap, A. P. Evidence that metformin exerts its anti-diabetic effects through inhibition of complex 1 of the mitochondrial respiratory chain. *Biochem J*, 348 Pt 3: 607–14 (2000).
- Parsons, A. B., Brost, R. L., Ding, H., Li, Z., Zhang, C., Sheikh, B., Brown, G. W., Kane, P. M., Hughes, T. R., and Boone, C. Integration of chemical-genetic and genetic interaction data links bioactive compounds to cellular target pathways. *Nat Biotechnol*, 22(1): 62–9 (2004).
- Parsons, A. B., Lopez, A., Givoni, I. E., Williams, D. E., Gray, C. A., Porter, J., Chua, G., Sopko, R., Brost, R. L., Ho, C.-H., Wang, J., Ketela, T., Brenner, C., Brill, J. A., Fernandez, G. E., Lorenz, T. C., Payne, G. S., Ishihara, S., Ohya, Y., Andrews, B., Hughes, T. R., Frey, B. J., Graham, T. R., Andersen, R. J., and Boone, C. Exploring the mode-of-action of bioactive compounds by chemical-genetic profiling in yeast. *Cell*, 126(3): 611–25 (2006).
- Patton, E. E. and Zon, L. I. The art and design of genetic screens: zebrafish. *Nat Rev Genet*, 2(12): 956–66 (2001).
- Patton, E. E., Widlund, H. R., Kutok, J. L., Kopani, K. R., Amatruda, J. F., Murphey, R. D., Berghmans, S., Mayhall, E. A., Traver, D., Fletcher, C. D. M., Aster, J. C., Granter, S. R., Look, A. T., Lee, C., Fisher, D. E., and Zon, L. I. BRAF mutations are sufficient to promote nevi formation and cooperate with p53 in the genesis of melanoma. *Curr Biol*, 15(3): 249–54 (2005).
- Patton, E. E., Mitchell, D. L., and Nairn, R. S. Genetic and environmental melanoma models in fish. *Pigment Cell Melanoma Res*, 23(3): 314–37 (2010).
- Peal, D. S., Peterson, R. T., and Milan, D. Small Molecule Screening in Zebrafish. *J. of Cardiovasc. Trans. Res.*, 3(5): 454–460 (2010).
- Perlman, Z. E., Slack, M. D., Feng, Y., Mitchison, T. J., Wu, L. F., and Altschuler, S. J. Multidimensional drug profiling by automated microscopy. *Science*, 306(5699): 1194–8 (2004).
- Perlstein, E. O., Ruderfer, D. M., Roberts, D. C., Schreiber, S. L., and Kruglyak, L. Genetic basis of individual differences in the response to small-molecule drugs in yeast. *Nat Genet*, 39(4): 496–502 (2007).
- Peterson, R. T., Link, B. A., Dowling, J. E., and Schreiber, S. L. Small molecule developmental screens reveal the logic and timing of vertebrate development. *Proc Natl Acad Sci USA*, 97(24): 12965–9 (2000).
- Peterson, R. T., Shaw, S. Y., Peterson, T. A., Milan, D. J., Zhong, T. P., Schreiber, S. L., Macrae, C. A., and Fishman, M. C. Chemical suppression of a genetic mutation in a zebrafish model of aortic coarctation. *Nat Biotechnol*, 22(5): 595–9 (2004).



- Pfaller, M. A. and Diekema, D. J. Epidemiology of invasive candidiasis: a persistent public health problem. *Clin Microbiol Rev*, 20(1): 133–63 (2007).
- Pincus, T., Yazici, Y., Sokka, T., D, D. A., and Smolen, J. S. Methotrexate as the "anchor drug" for the treatment of early rheumatoid arthritis. *Clin Exp Rheumatol*, 21(5 Suppl 31): S179–85 (2003).
- Pinto, W. J., Wells, G. W., and Lester, R. L. Characterization of enzymatic synthesis of sphingolipid long-chain bases in *Saccharomyces cerevisiae*: mutant strains exhibiting long-chain-base auxotrophy are deficient in serine palmitoyl-transferase activity. *J Bacteriol*, 174(8): 2575–81 (1992).
- Pirker, R. Two- versus three-drug combinations in the chemotherapy of advanced non-small-cell lung cancer. *Lung Cancer*, 38 Suppl 3: S53–5 (2002).
- Pluta, K., Morak-Młodawska, B., and Jeleń, M. Recent progress in biological activities of synthesized phenothiazines. *Eur J Med Chem*, 46(8): 3179–89 (2011).
- Pribyl, P., Cepák, V., and Zachleder, V. Cytoskeletal alterations in interphase cells of the green alga *Spirogyra decimina* in response to heavy metals exposure: II. The effect of aluminium, nickel and copper. *Toxicol In Vitro*, 22(5): 1160–8 (2008).
- Quackenbush, J. Microarray data normalization and transformation. *Nat Genet*, 32 Suppl: 496–501 (2002).
- Rae, T. D., Schmidt, P. J., Pufahl, R. A., Culotta, V. C., and O’Halloran, T. V. Undetectable intracellular free copper: the requirement of a copper chaperone for superoxide dismutase. *Science*, 284(5415): 805–8 (1999).
- Rainey, M. M., Korostyshevsky, D., Lee, S., and Perlstein, E. O. The Antidepressant Sertraline Targets Intracellular Vesiculogenic Membranes in Yeast. *Genetics*, 185(4): 1221–1233 (2010).
- Ramón-García, S., Ng, C., Anderson, H., Chao, J. D., Zheng, X., Pfeifer, T., Av-Gay, Y., Roberge, M., and Thompson, C. J. Synergistic drug combinations for tuberculosis therapy identified by a novel high-throughput screen. *Antimicrob Agents Chemother*, 55(8): 3861–9 (2011).
- Rauha, J. P., Remes, S., Heinonen, M., Hopia, A., Kähkönen, M., Kujala, T., Pihlaja, K., Vuorela, H., and Vuorela, P. Antimicrobial effects of Finnish plant extracts containing flavonoids and other phenolic compounds. *Int J Food Microbiol*, 56(1): 3–12 (2000).
- Rees, E. M. and Thiele, D. J. From aging to virulence: forging connections through the study of copper homeostasis in eukaryotic microorganisms. *Curr Opin Microbiol*, 7(2): 175–84 (2004).
- Reich, D. E. and Lander, E. S. On the allelic spectrum of human disease. *Trends Genet*, 17(9): 502–10 (2001).

- Revankar, S. G., Fu, J., Rinaldi, M. G., Kelly, S. L., Kelly, D. E., Lamb, D. C., Keller, S. M., and Wickes, B. L. Cloning and characterization of the lanosterol 14 $\alpha$ -demethylase (ERG11) gene in *Cryptococcus neoformans*. *Biochem Biophys Res Commun*, 324(2): 719–28 (2004).
- Rine, J., Hansen, W., Hardeman, E., and Davis, R. W. Targeted selection of recombinant clones through gene dosage effects. *Proc Natl Acad Sci USA*, 80(22): 6750–4 (1983).
- Rothstein, J. D., Patel, S., Regan, M. R., Haenggeli, C., Huang, Y. H., Bergles, D. E., Jin, L., Hoberg, M. D., Vidensky, S., Chung, D. S., Toan, S. V., Bruijn, L. I., Su, Z.-Z., Gupta, P., and Fisher, P. B. Beta-lactam antibiotics offer neuroprotection by increasing glutamate transporter expression. *Nature*, 433(7021): 73–7 (2005).
- Rustici, G., van Bakel, H., Lackner, D. H., Holstege, F. C., Wijmenga, C., Bähler, J., and Brazma, A. Global transcriptional responses of fission and budding yeast to changes in copper and iron levels: a comparative study. *Genome Biol*, 8(5): R73 (2007).
- Sahra, I. B., Marchand-Brustel, Y. L., Tanti, J.-F., and Bost, F. Metformin in cancer therapy: a new perspective for an old antidiabetic drug? *Mol Cancer Ther*, 9(5): 1092–9 (2010).
- Sams-Dodd, F. Target-based drug discovery: is something wrong? *Drug Discov Today*, 10(2): 139–47 (2005).
- Santt, O., Pfirrmann, T., Braun, B., Juretschke, J., Kimmig, P., Scheel, H., Hofmann, K., Thumm, M., and Wolf, D. H. The yeast GID complex, a novel ubiquitin ligase (E3) involved in the regulation of carbohydrate metabolism. *Mol Biol Cell*, 19(8): 3323–33 (2008).
- Sardana, D., Zhu, C., Zhang, M., Gudivada, R. C., Yang, L., and Jegga, A. G. Drug repositioning for orphan diseases. *Brief Bioinformatics*, 12(4): 346–56 (2011).
- Sauna, Z. E., Peng, X.-H., Nandigama, K., Tekle, S., and Ambudkar, S. V. The molecular basis of the action of disulfiram as a modulator of the multidrug resistance-linked ATP binding cassette transporters MDR1 (ABCB1) and MRP1 (ABCC1). *Molecular Pharmacology*, 65(3): 675–84 (2004).
- Scully, L. R. and Bidochka, M. J. Developing insect models for the study of current and emerging human pathogens. *FEMS Microbiol Lett*, 263(1): 1–9 (2006).
- Setty, S. R. G., Tenza, D., Sviderskaya, E. V., Bennett, D. C., Raposo, G., and Marks, M. S. Cell-specific ATP7A transport sustains copper-dependent tyrosinase activity in melanosomes. *Nature*, 454(7208): 1142–6 (2008).

- Seyhan, A. A., Varadarajan, U., Choe, S., Liu, Y., McGraw, J., Woods, M., Murray, S., Eckert, A., Liu, W., and Ryan, T. E. A genome-wide RNAi screen identifies novel targets of neratinib sensitivity leading to neratinib and paclitaxel combination drug treatments. *Mol. BioSyst.* (2011).
- Sharom, J. R., Bellows, D. S., and Tyers, M. From large networks to small molecules. *Curr Opin Chem Biol*, 8(1): 81–90 (2004).
- Sheetz, M. P. and Singer, S. J. Biological membranes as bilayer couples. A molecular mechanism of drug-erythrocyte interactions. *Proc Natl Acad Sci USA*, 71(11): 4457–61 (1974).
- Shi, Z., Tiwari, A. K., Patel, A. S., Fu, L.-W., and Chen, Z.-S. Roles of sildenafil in enhancing drug sensitivity in cancer. *Cancer Res*, 71(11): 3735–8 (2011).
- Shoemaker, D. D., Lashkari, D. A., Morris, D., Mittmann, M., and Davis, R. W. Quantitative phenotypic analysis of yeast deletion mutants using a highly parallel molecular bar-coding strategy. *Nat Genet*, 14(4): 450–6 (1996).
- Shuhendler, A. J., O'Brien, P. J., Rauth, A. M., and Wu, X. Y. On the synergistic effect of doxorubicin and mitomycin C against breast cancer cells. *Drug Metabol Drug Interact*, 22(4): 201–33 (2007).
- Shukla, S., Sauna, Z. E., Prasad, R., and Ambudkar, S. V. Disulfiram is a potent modulator of multidrug transporter Cdr1p of *Candida albicans*. *Biochem Biophys Res Commun*, 322(2): 520–5 (2004).
- Singh, S. D., Robbins, N., Zaas, A. K., Schell, W. A., Perfect, J. R., and Cowen, L. E. Hsp90 governs echinocandin resistance in the pathogenic yeast *Candida albicans* via calcineurin. *PLoS Pathog*, 5(7): e1000532 (2009).
- Sondak, V., Smalley, K., Kudchadkar, R., Gripon, S., and Kirkpatrick, P. Ipilimumab. *Nat Rev Drug Discov* (2011).
- Spitzer, M., Griffiths, E., Blakely, K. M., Wildenhain, J., Ejim, L., Rossi, L., Pascale, G. D., Curak, J., Brown, E., Tyers, M., and Wright, G. D. Cross-species discovery of syncretic drug combinations that potentiate the antifungal fluconazole. *Mol Syst Biol*, 7: 499 (2011).
- Stermitz, F. R., Lorenz, P., Tawara, J. N., Zenewicz, L. A., and Lewis, K. Synergy in a medicinal plant: antimicrobial action of berberine potentiated by 5'-methoxyhydrnocarpin, a multidrug pump inhibitor. *Proc Natl Acad Sci USA*, 97(4): 1433–7 (2000).
- Stilwell, G. E., Saraswati, S., Littleton, J. T., and Chouinard, S. W. Development of a *Drosophila* seizure model for in vivo high-throughput drug screening. *Eur J Neurosci*, 24(8): 2211–22 (2006).
- Streisinger, G., Walker, C., Dower, N., Knauber, D., and Singer, F. Production of clones of homozygous diploid zebra fish (*Brachydanio rerio*). *Nature*, 291 (5813): 293–6 (1981).

- Sudoh, M., Yamazaki, T., Masubuchi, K., Taniguchi, M., Shimma, N., Arisawa, M., and Yamada-Okabe, H. Identification of a novel inhibitor specific to the fungal chitin synthase. Inhibition of chitin synthase 1 arrests the cell growth, but inhibition of chitin synthase 1 and 2 is lethal in the pathogenic fungus *Candida albicans*. *J Biol Chem*, 275(42): 32901–5 (2000).
- Takimoto, E., Champion, H. C., Li, M., Belardi, D., Ren, S., Rodriguez, E. R., Bedja, D., Gabrielson, K. L., Wang, Y., and Kass, D. A. Chronic inhibition of cyclic GMP phosphodiesterase 5A prevents and reverses cardiac hypertrophy. *Nat Med*, 11(2): 214–22 (2005).
- Tatonetti, N. P., Denny, J. C., Murphy, S. N., Fernald, G. H., Krishnan, G., Castro, V., Yue, P., Tsau, P. S., Kohane, I., Roden, D. M., and Altman, R. B. Detecting drug interactions from adverse-event reports: interaction between paroxetine and pravastatin increases blood glucose levels. *Clin Pharmacol Ther*, 90(1): 133–42 (2011).
- Taylor, K. L., Grant, N. J., Temperley, N. D., and Patton, E. E. Small molecule screening in zebrafish: an in vivo approach to identifying new chemical tools and drug leads. *Cell Commun Signal*, 8: 11 (2010).
- Thiele, D. J. and Gitlin, J. D. Assembling the pieces. *Nature Chemical Biology*, 4(3): 145–7 (2008).
- Tong, A. H., Evangelista, M., Parsons, A. B., Xu, H., Bader, G. D., Pagé, N., Robinson, M., Raghizadeh, S., Hogue, C. W., Bussey, H., Andrews, B., Tyers, M., and Boone, C. Systematic genetic analysis with ordered arrays of yeast deletion mutants. *Science*, 294(5550): 2364–8 (2001).
- Tong, A. H. Y., Lesage, G., Bader, G. D., Ding, H., Xu, H., Xin, X., Young, J., Berriz, G. F., Brost, R. L., Chang, M., Chen, Y., Cheng, X., Chua, G., Friesen, H., Goldberg, D. S., Haynes, J., Humphries, C., He, G., Hussein, S., Ke, L., Krogan, N., Li, Z., Levinson, J. N., Lu, H., Ménard, P., Munyana, C., Parsons, A. B., Ryan, O., Tonikian, R., Roberts, T., Sdicu, A.-M., Shapiro, J., Sheikh, B., Suter, B., Wong, S. L., Zhang, L. V., Zhu, H., Burd, C. G., Munro, S., Sander, C., Rine, J., Greenblatt, J., Peter, M., Bretscher, A., Bell, G., Roth, F. P., Brown, G. W., Andrews, B., Bussey, H., and Boone, C. Global mapping of the yeast genetic interaction network. *Science*, 303(5659): 808–13 (2004).
- True, J. R. and Haag, E. S. Developmental system drift and flexibility in evolutionary trajectories. *Evol Dev*, 3(2): 109–19 (2001).
- Tucker, C. L. and Fields, S. Quantitative genome-wide analysis of yeast deletion strain sensitivities to oxidative and chemical stress. *Comp Funct Genomics*, 5(3): 216–24 (2004).
- Vahlensieck, H. F., Pridzun, L., Reichenbach, H., and Hinnen, A. Identification of the yeast ACC1 gene product (acetyl-CoA carboxylase) as the target of the polyketide fungicide soraphen A. *Curr Genet*, 25(2): 95–100 (1994).

- van Bakel, H., Strengman, E., Wijmenga, C., and Holstege, F. C. P. Gene expression profiling and phenotype analyses of *S. cerevisiae* in response to changing copper reveals six genes with new roles in copper and iron metabolism. *Physiol Genomics*, 22(3): 356–67 (2005).
- van der Sar, A. M., Musters, R. J. P., van Eeden, F. J. M., Appelmelk, B. J., Vandenbroucke-Grauls, C. M. J. E., and Bitter, W. Zebrafish embryos as a model host for the real time analysis of *Salmonella typhimurium* infections. *Cell Microbiol*, 5(9): 601–11 (2003).
- van Leeuwen, M. R., Smant, W., de Boer, W., and Dijksterhuis, J. Filipin is a reliable in situ marker of ergosterol in the plasma membrane of germinating conidia (spores) of *Penicillium discolor* and stains intensively at the site of germ tube formation. *J Microbiol Methods*, 74(2-3): 64–73 (2008).
- Wanders, R. J. A. and Waterham, H. R. Peroxisomal disorders I: biochemistry and genetics of peroxisome biogenesis disorders. *Clin Genet*, 67(2): 107–33 (2005).
- Watts, D. J. and Strogatz, S. H. Collective dynamics of 'small-world' networks. *Nature*, 393(6684): 440–2 (1998).
- Wegner, S. V., Sun, F., Hernandez, N., and He, C. The tightly regulated copper window in yeast. *Chem Commun (Camb)*, 47(9): 2571–3 (2011).
- Wilkinson, S. R., Taylor, M. C., Horn, D., Kelly, J. M., and Cheeseman, I. A mechanism for cross-resistance to nifurtimox and benznidazole in trypanosomes. *Proc Natl Acad Sci USA*, 105(13): 5022–7 (2008).
- Winzeler, E. A., Shoemaker, D. D., Astromoff, A., Liang, H., Anderson, K., Andre, B., Bangham, R., Benito, R., Boeke, J. D., Bussey, H., Chu, A. M., Connelly, C., Davis, K., Dietrich, F., Dow, S. W., Bakkoury, M. E., Foury, F., Friend, S. H., Gentalen, E., Giaever, G., Hegemann, J. H., Jones, T., Laub, M., Liao, H., Liebundguth, N., Lockhart, D. J., Lucau-Danila, A., Lussier, M., M'Rabet, N., Menard, P., Mittmann, M., Pai, C., Rebischung, C., Revuelta, J. L., Riles, L., Roberts, C. J., Ross-Macdonald, P., Scherens, B., Snyder, M., Sookhai-Mahadeo, S., Storms, R. K., Véronneau, S., Voet, M., Volckaert, G., Ward, T. R., Wysocki, R., Yen, G. S., Yu, K., Zimmermann, K., Philippsen, P., Johnston, M., and Davis, R. W. Functional characterization of the *S. cerevisiae* genome by gene deletion and parallel analysis. *Science*, 285(5429): 901–6 (1999).
- Xu, Y., Wang, Y., Yan, L., Liang, R.-M., Dai, B.-D., Tang, R.-J., Gao, P.-H., and Jiang, Y.-Y. Proteomic analysis reveals a synergistic mechanism of fluconazole and berberine against fluconazole-resistant *Candida albicans*: endogenous ROS augmentation. *J. Proteome Res.*, 8(11): 5296–304 (2009).
- Yan, Z., Berbenetz, N. M., Giaever, G., and Nislow, C. Precise Gene-Dose Alleles for Chemical Genetics. *Genetics*, 182(2): 623–626 (2009).

- Yeh, P., Tschumi, A. I., and Kishony, R. Functional classification of drugs by properties of their pairwise interactions. *Nat Genet*, 38(4): 489–94 (2006).
- Young, D. W., Bender, A., Hoyt, J., McWhinnie, E., Chirn, G.-W., Tao, C. Y., Tallarico, J. A., Labow, M., Jenkins, J. L., Mitchison, T. J., and Feng, Y. Integrating high-content screening and ligand-target prediction to identify mechanism of action. *Nat Chem Biol*, 4(1): 59–68 (2008).
- Young, J., Park, Y., Lee, Y.-U., Kim, H., Shim, Y.-H., Ahn, J.-H., and Lim, Y. Antimicrobial effects of flavone analogues and their structure-activity relationships. *J Microbiol Biotechnol*, 17(3): 530–3 (2007).
- Yuan, D. S., Dancis, A., and Klausner, R. D. Restriction of copper export in *Saccharomyces cerevisiae* to a late Golgi or post-Golgi compartment in the secretory pathway. *J Biol Chem*, 272(41): 25787–93 (1997).
- Zakikhani, M., Dowling, R., Fantus, I. G., Sonenberg, N., and Pollak, M. Metformin is an AMP kinase-dependent growth inhibitor for breast cancer cells. *Cancer Res*, 66(21): 10269–73 (2006).
- Zhai, B., Zhou, H., Yang, L., Zhang, J., Jung, K., Giam, C. Z., Xiang, X., and Lin, X. Polymyxin B, in combination with fluconazole, exerts a potent fungicidal effect. *Journal of Antimicrobial Chemotherapy*, 65(5): 931–938 (2010).
- Zhang, L., Yan, K., Zhang, Y., Huang, R., Bian, J., Zheng, C., Sun, H., Chen, Z., Sun, N., An, R., Min, F., Zhao, W., Zhuo, Y., You, J., Song, Y., Yu, Z., Liu, Z., Yang, K., Gao, H., Dai, H., Zhang, X., Wang, J., Fu, C., Pei, G., Liu, J., Zhang, S., Goodfellow, M., Jiang, Y., Kuai, J., Zhou, G., and Chen, X. High-throughput synergy screening identifies microbial metabolites as combination agents for the treatment of fungal infections. *Proc Natl Acad Sci USA*, 104(11): 4606–11 (2007).
- Zhou, G., Myers, R., Li, Y., Chen, Y., Shen, X., Fenyk-Melody, J., Wu, M., Ventre, J., Doebber, T., Fujii, N., Musi, N., Hirshman, M. F., Goodyear, L. J., and Moller, D. E. Role of AMP-activated protein kinase in mechanism of metformin action. *J Clin Invest*, 108(8): 1167–74 (2001).
- Zhuang, Y. and Miskimins, W. K. Cell cycle arrest in Metformin treated breast cancer cells involves activation of AMPK, downregulation of cyclin D1, and requires p27Kip1 or p21Cip1. *J Mol Signal*, 3: 18 (2008).
- Zilberman, D., Coleman-Derr, D., Ballinger, T., and Henikoff, S. Histone H2A.Z and DNA methylation are mutually antagonistic chromatin marks. *Nature*, 456(7218): 125–9 (2008).
- Zinner, R. G., Barrett, B. L., Popova, E., Damien, P., Volgin, A. Y., Gelovani, J. G., Lotan, R., Tran, H. T., Pisano, C., Mills, G. B., Mao, L., Hong, W. K., Lippman, S. M., and Miller, J. H. Algorithmic guided screening of drug combinations of arbitrary size for activity against cancer cells. *Mol Cancer Ther*, 8(3): 521–32 (2009).

Zon, L. I. and Peterson, R. T. In vivo drug discovery in the zebrafish. *Nat Rev Drug Discov*, 4(1): 35–44 (2005).

# Appendices



---

## Development and implementation of methods for the analysis of chemogenomic profiles of small molecules

---

Genome-wide chemical-genetic profiles can provide a lot of information. This section will give a short overview of different methods that can be used to analyse these profiles. The methods were developed and implemented while I worked with various data sets and they will eventually be implemented as an analysis pipeline. The Gene Ontology (GO) contains a lot of information about protein function and is widely used to analyse genome-wide data sets. I used the GO annotations of proteins and I will therefore briefly introduce it in Section A.1. Sections A2 to A11 give an overview of analysis methods that I have applied to various data sets.

### **A.1 Gene Ontology**

The GO Consortium is a bioinformatics initiative that aims to develop a dynamic, yet controlled vocabulary to describe the role of genes and proteins across different

<b>Species</b>	<b>Databases/Organisations</b>
Yeast	<i>Saccharomyces</i> Genome Database, SGD; <i>S. pombe</i> via GeneDB
Bacteria	EcoliWiki
Slime mold	dictyBase
Flies	Berkeley <i>Drosophila</i> Genome Project; FlyBase
Mice	Mouse Genome Informatics, MGI
Plants	Maize Genetics and Genomics Database, MaizeGDB; The <i>Arabidopsis</i> Information Resource, TAIR; Gramene, a comparative mapping resource for grains
Rats	Rat Genome Database RGD
Worms	WormBase
Zebrafish	The Zebrafish Information Network, ZFIN
Humans	British Heart Foundation, Cardiovascular GO Annotation Initiative

Table A.1: List of species databases that are members of the GO consortium (from [www.geneontology.org](http://www.geneontology.org)).

species (Ashburner *et al.*, 2000; [www.geneontology.org](http://www.geneontology.org)). The consortium is made up of the model organism and protein databases as well as the biological research community and has the aim to develop, maintain and actively use GO. The GO consortium was founded 10 years ago by the three model organism databases for mouse, yeast and fly. Today, a wide range organisations are GO consortium members, including species-specific databases for microbial, plant and animal genomes (Table A.1). Several databases (UniProtKB-Gene Ontology Annotation, GeneDB, Reactome) as well as the Institute of Genome Sciences at the University of Maryland and the J Craig Venter Institute are also members of the consortium.

To capture different aspects of protein function three independent ontologies have been developed: biological process, molecular function and cellular component. These ontologies describe the context of action, elemental activities and subcellular location(s) of gene products, respectively. Normally, annotations in any of these three ontologies are based on the scientific literature. In 2008, SGD started using results from functional genomic and proteomic experiments to in-

Biological processes	17,069
Molecular functions	8,637
Cellular components	2,432
Annotation datasets	52
Speices with annotation	197,439
Annotated gene products	
Total	44.5 Mio
Electronic (IEA)	43.7 Mio
Manual	890,094

Table A.2: Status of Gene Ontology as of September 4, 2009 (adapted from The Gene Ontology Consortium, 2010).

fer GO annotations based on high-throughput data (Hong *et al.*, 2008, Christie *et al.*, 2009). Another source of GO annotation are computationally predicted annotations for UniProt proteins based on sequence similarity. The evidence code 'Inferred from Electronic Annotation' is associated with all computationally derived GO annotations.

One of the key motivations behind GO is that GO annotations in one species can be transferred to other species, enabling a fast initial functional annotation of newly sequenced genomes. The results of this concept can be seen in Table A.2: only 52 species are actively curated, but there are nearly 200,000 species with GO annotations. It is also important to note that less than one million manual annotations give rise to over 44 million annotations in total. The GO Reference Genome Project is committed to the comprehensive annotation of the 12 GO Reference Genomes: human, *Arabidopsis thaliana*, *Caenorhabditis elegans*, *Danio rerio*, *Dictyostelium discoideum*, *Drosophila melanogaster*, *Escherichia coli*, *Gallus gallus*, *Mus musculus*, *Rattus norvegicus*, *Saccharomyces cerevisiae*, and *Schizosaccharomyces pombe* (The Reference Genome Group of the Gene Ontology Consortium, 2009).

As of 2009, about 5000 protein-coding genes of the budding yeast were annotated with information from the biological process and molecular function on-

tologies.

There are also cut-down versions of GO that are called GO Slims. They give a broad overview of the terms, but I did not find GO SLIM useful in the context of chemical-genetic profiles.

### A.1.1 GO annotation data files

The Saccharomyces Genome Database ([www.yeastgenome.org](http://www.yeastgenome.org)) is one of the model organism databases that contribute to GO. Annotation files for the budding yeast can be downloaded from [http://downloads.yeastgenome.org/literature\\_curation](http://downloads.yeastgenome.org/literature_curation).

I used the following data files for my GO analyses:

- `gene_association.tab` (version from April 23, 2011) - all GO annotations for *S. cerevisiae* genes
- `go_slim_mapping.tab` (version from April 23, 2011) - maps all yeast gene products to GO SLIM terms
- `go_terms` (version from April 23, 2011) - contains the definitions of all GO terms
- `SGD_features` (from [http://downloads.yeastgenome.org/chromosomal\\_feature](http://downloads.yeastgenome.org/chromosomal_feature), version from April 23, 2011) - contains all chromosomal features in SGD. These include all ORFs and RNAs (snRNAs, tRNAs, ncRNAs, rRNAs, snoRNAs), but also annotations for chromosome features like centromeres and telomeres.

## A.2 Optimisation of chemical-genetic screens

Chemical-genetic screens are competitive growth assays during which pools of deletion strains are grown in the presence of a compound. Compound is added to cultures with a starting OD of 0.025 and growth inhibition is assessed after 12 hours. To identify deletion strains that are sensitive or resistant to compound treatment, the compound should be added at a concentration that inhibits growth at a moderate level. The optimal level of growth inhibition to observe compound-specific hypersensitivity phenotypes varies between compounds.

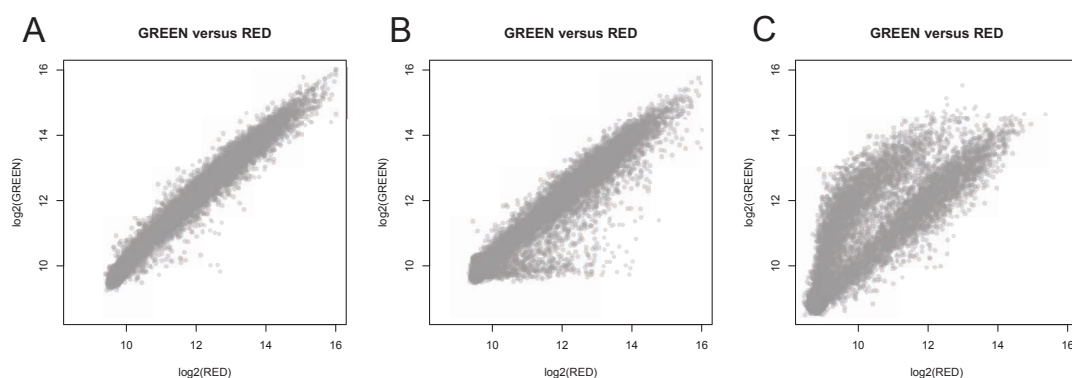


Figure A.1: Scatter plots of green versus red intensities of barcode array data. (A) Profile with specific hits. (B) Profile with many sensitive deletion strains. (C) Barcode array where one of the labelling PCRs did not work properly.

Generally, 20-30% growth inhibition compared to solvent control results in good profiles where most deletion strains are not differentially affected by compound treatment. Therefore, most data points fall along the diagonal, as is the case in Figure A.1A. Some compounds give very informative profiles with only 5% growth inhibition. However, there are compounds that affect growth of many deletion strains even at very low levels of growth inhibition. Neocuproine is a compound that affects growth of many deletion strains even at concentrations that only cause 8% growth inhibition (Figure A.1B). Neocuproine is a very strong copper chelator which probably explains the observed effect.

To identify the optimal concentration range for a compound, a 2 fold dilution series from 1  $\mu\text{M}$  to 128  $\mu\text{M}$  is set up for each new compound and growth inhibition assessed at 12 hours. Typically, cell pellets are frozen down for concentrations that show 5-40% growth inhibition. Chemical-genetic profiles are then generated with samples that showed 20-30% growth inhibition. Depending on the profiles, lower or higher concentrations are also tested.

I observed that levels of growth inhibition can be very different between cultures grown in glass tube and cultures grown in a plate reader in 96-well plates, even if the cultures in the plate reader are aliquots taken from the glass tube cultures. There were several instances where a culture would grow with little

inhibition in the plate reader, but there was no growth at all in the glass tube. This could be due to the compound interacting with the polystyrene plates or precipitation of the compounds because the shaking of the plates is different from rotating the glass tubes on a wheel. It is therefore advisable to determine levels of growth inhibition directly on the cultures in glass tubes that will be used for the chemical-genetic screens.

### A.3 Quality control

Quality control is an important step to assess quality and reliability of the chemical-genetic profiles. A simple scatter plot of red versus green intensities from the microarray gives a first impression of the data. Three examples are given in Figure A.1. These plots give an idea about how many deletion strains are affected by compound treatment (Figure A.1A & B). They can also reveal problems that occurred during the barcode microarray experiment. The plot in Figure A.1C for example shows that the red signal is very low for about half the data points. This probably means that the Cy5-labelling PCR for one of the barcode tags (UP or DOWN) did not work properly. This microarray will have to be repeated.

To identify deletion mutants affected by compound treatment, two different samples (drug treated and control) are hybridised competitively to the barcode arrays. To ensure that the resulting fold changes are reliable, the red and green data points should have similar intensity distributions. In the second column of Figure A.2 the intensities of the red and the green channel are summarised in a histogram. The first peak corresponds to empty and control spots, the second peak, that is lower and wider than the first one, contains the barcodes of deletion strains that are present in the pool. In Figure A.2A, the distributions of red and green are very similar. A problem that occurred in Toronto as well as in Edinburgh was oxidation of the Cy5 dye, probably caused by ozone in the air.

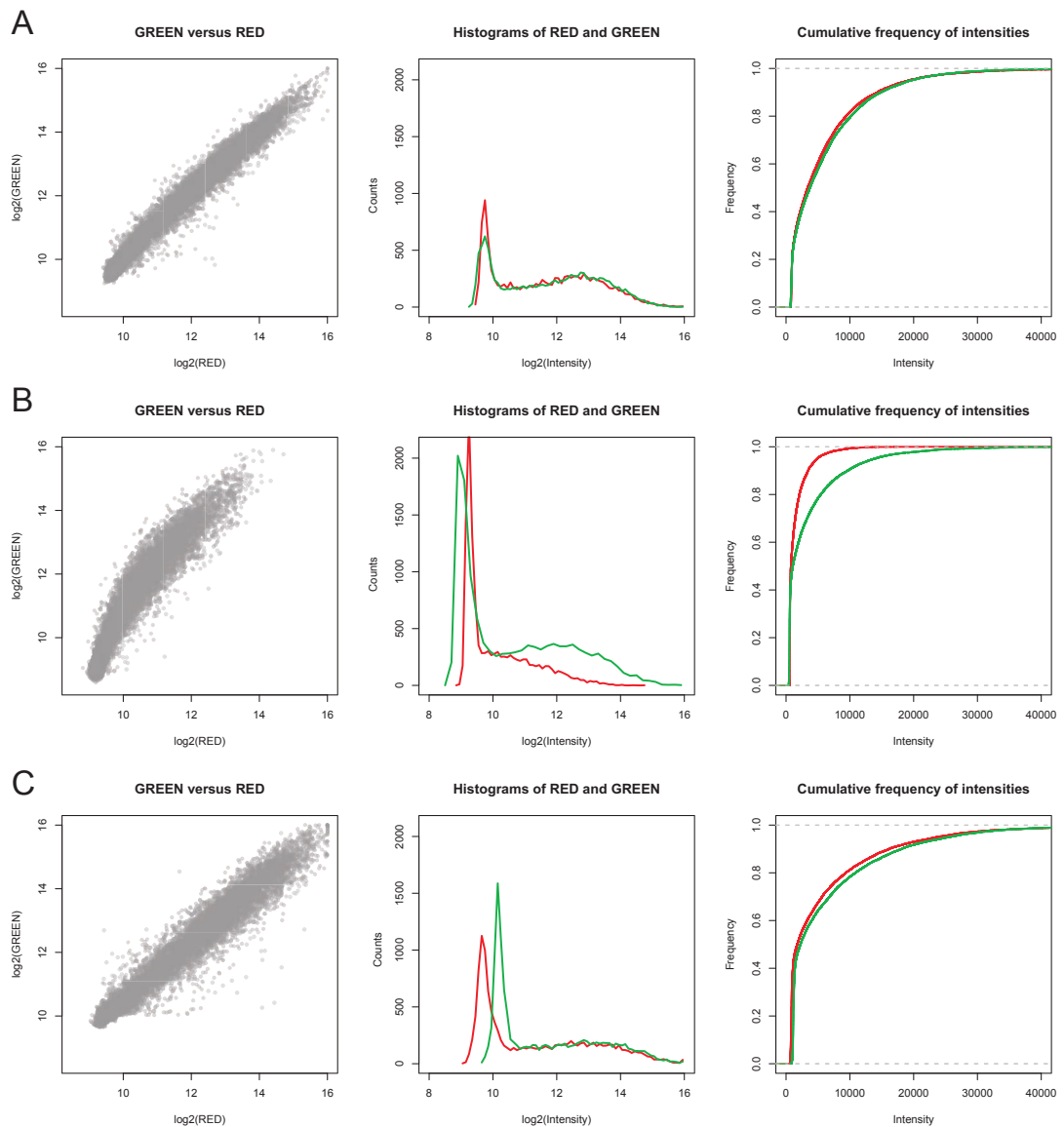


Figure A.2: Quality control plots for barcode microarrays. (A) Barcode array with similar red and green intensities. (B) Barcode array where the Cy5 dye (red) has low intensity due to oxidation caused by ozone. (C) Barcode microarray treated with stabilising solution from Agilent. In (A), (B) and (C) the first panel is a scatter plot of green vs red intensities, the second panel shows frequency histograms for red and green intensities and in the third panel the cumulative frequencies are plotted for red and green intensities.

This was usually only a problem during the summer months. In the histogram in Figure A.2B, the oxidation of the red dye can clearly be seen. The red channel has been scanned with higher laser power as indicated by the shift of the first peak to the right, but the second peak is nevertheless clearly below the green one. The problem was eventually solved by treating the barcode microarrays with stabilising solution from Agilent which protects the Cy5 dye from oxidation. The array in Figure A.2C has been treated with this solution and in the histogram the second peak has similar shapes for the green and red channel. The shift to the right of the green first peak indicates that the solution increases the background noise in the green channel. All these effects can also be visualised with cumulative frequencies of the intensities (Figure A.2A-C, last column).

## A.4 Data analysis procedure to calculate Z-scores

First, low quality spots are identified and excluded from further analysis. An intensity cut-off is determined based on the data from the control spots that are present in each block of the barcode microarray. For each microarray, a cut-off is chosen such that 95% of all empty spots are classified as such. Application of this cut-off to all spots on the microarray usually means that for about 4200 deletion strains at least one barcode has a good signal. Each barcode is present in replicate on the barcode microarray. If the two replicates have very different intensities, then these barcodes are excluded from further analysis.

Next, the red and green intensities of the two replicates are averaged for all barcodes that were found to have high quality data.  $\log_2$  fold changes are calculated (drug treatment/solvent-only control) for UP and DOWN tags separately. Z-scores are calculated from the fold changes as follows:  $Z = (x - \mu)/\sigma$  where  $\mu$  is the mean  $\log_2$  fold change for the whole array and  $\sigma$  the standard deviation. For each strain, the two Z-scores for UP and DOWN barcode tags are averaged to obtain the final Z-score.



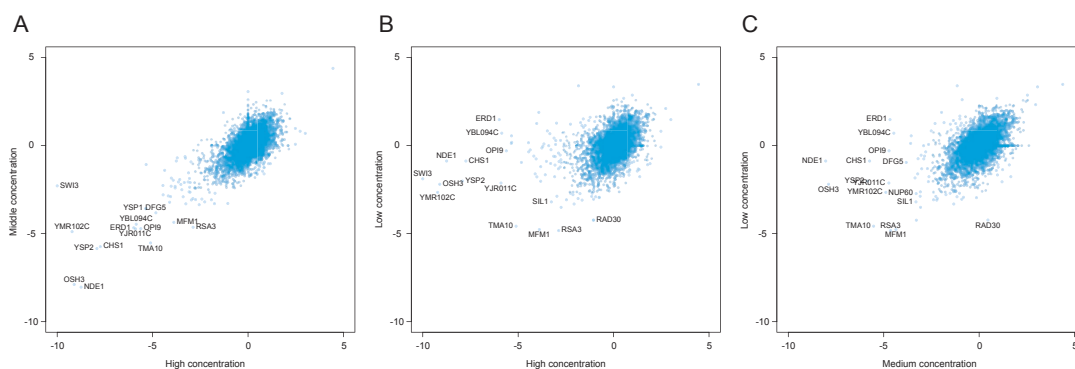


Figure A.3: Correlation between profiles of one compound screened at different concentrations. The concentrations plotted are (A) medium versus high, (B) low versus high and (C) low versus medium.

## A.5 Correlation between chemical-genetic screens

It can be very informative to plot the Z-scores of chemical-genetic profiles of the same compound screened at different concentrations against each other. Figure A.3 shows correlation plots between three different concentrations of the same compound. The screens done with high and medium concentrations share many strong hits (Figure A.3A) whereas the low concentration screen does not share these hits (Figure A.3B & C).

For larger datasets it can be very informative to cluster all screens based on the correlation between the chemical-genetic profiles. Replicate screens and screens conducted with different concentrations of the same drug should cluster together. The clusters can also inform about mode of action of the compounds because compounds with similar profiles have similar effects on the deletion pool. In Figure A.4 the correlation coefficients for a set of 60 chemical-genetic profiles are represented as a heatmap. The compound profiles were clustered using complete linkage to find clusters based on the correlation coefficients. Most replicates of different compounds clustered together.

Large data sets are normally generated in batches. It is advisable to check if the clusters obtained are in any way biased towards these batches. If that is the case, data can for example be discretised by defining resistant and sensitive

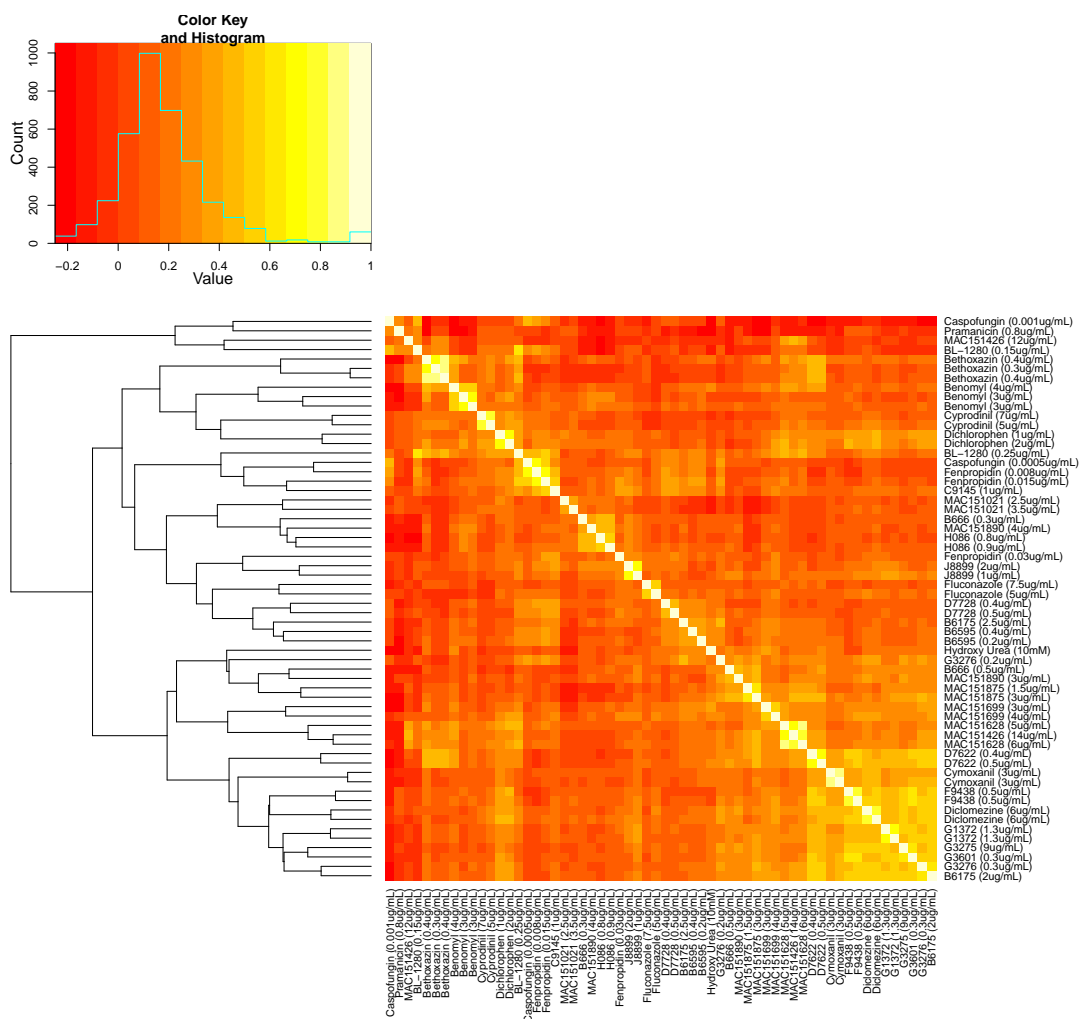


Figure A.4: Correlation coefficients for 60 profiles for 30 different compounds. As indicated in the colour key, white indicates high correlation coefficients and red indicates low correlation coefficients. The tree on the left hand side shows how similar the profiles are.

deletion strains and only working with these.

## A.6 Overview plots

For single screens, the chemical-genetic profiles can be visualised by plotting the Z-scores of all deletion strains. Sorting the strains by gene name can already reveal trends if they are present because the gene names contain some functional information. For example, ribosomal protein gene names all start with *RP* or genes for proteins involved in vacuolar protein sorting start with *VPS*. Strong

hits in the profile are also visible in these plots. This is especially interesting for the set of heterozygous deletion mutants in essential genes because single strong hits might represent the drug target as seen with *ERG11* in the fluconazole screen and *LCB1/2* for L-cycloserine in Figure 3.13. A good example for haploid deletion pools can be seen in Figure 4.12. The *RAD* genes are an obvious group of genes that are sensitive to different concentrations of NFN1.

For larger data sets it is useful to generate a heatmap with the most sensitive/resistant deletion strains to get an overview of the strongest hits for each screen as well as deletion strains that are affected in more than one screen. Figure 3.18A, for example, shows the most affected deletion strains for 6 different compounds.

## A.7 Testing for GO enrichment

The standard analysis of high-throughput screens that yield genome-wide data, is the test for enrichment of specific GO categories among the set of genes that are defined as hits. There are different methods to define hits from a screen. Three different methods are shown in Figure A.5. Each method will result in a different number of hits and the various sets of genes might show differences in their GO enrichment. In addition, the selection of a subset of the thousands of genes is a serious limitation because the majority of the data points is excluded from further analysis. I therefore developed and implemented a method that makes use of all data generated by determining average Z-scores for each GO category and for protein complexes. The next two sections will describe these methods and give examples.

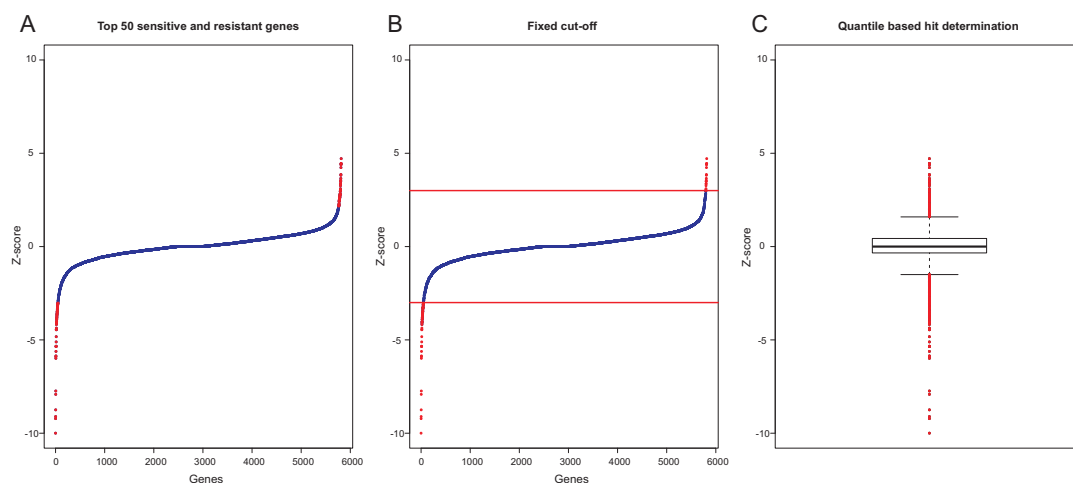


Figure A.5: Different methods to determine deletion strains sensitive or resistant to drug treatment. (A) Using the top hits from both ends of the distribution of scores. (B) Application of a predefined cut-off to identify hits. (C) Quantile-based selection of hits.

## A.8 Z-scores for GO categories

Calculation of average Z-scores for each GO category is a much more comprehensive analysis of chemical-genetic profiles because the data for all genes that are annotated with GO categories is used. This method has been used to analyse the chemical-genetic profiles of the copper-metabolism compounds (Figure 4.4B) and for the screens with different concentrations of NFN1 (Figure 4.14). A larger data set of 60 screens for 30 different compounds is shown in Figure A.6. Screens conducted with the same compound at different concentrations generally have very similar scores across the GO categories. The heatmap reveals that some GO categories are sensitive or resistant in response to many compounds, like 'tryptophane biosynthesis' at the bottom of the heat map. There are also many GO categories that only have strong Z-scores in a few profiles, indicating specific effects of compounds. Since there are many GO categories in Figure A.6, it might be worth clustering the GO categories based on the genes that they have in common.



## **A.9 Evaluation of chemogenomic data on the level of protein complexes**

Similar to the analysis described above, information about protein complexes can be used to analyse chemical-genetic profiles. The CYC2008 set of protein complexes (Pu *et al.*, 2008) provides a comprehensive catalogue of heteromeric protein complexes. 408 protein complexes have been manually curated and are supported by small-scale experiments in the literature. Figure A.7 shows the scores for the protein complexes in the same 60 profiles that were analysed for GO categories in Figure A.6. Similar to the GO category analysis, there are some protein complexes that have significant scores in response to several drugs and some protein complexes are only affected by specific compounds.

## **A.10 Physical and genetic interactions to interpret chemical-genetic interactions**

Different data sets are frequently integrated to interrogate the mode of action of small molecules. For example, Parsons *et al.* (2004) showed that it is possible to cluster the chemical-genetic profiles with genetic interaction profiles to identify target pathways for chemical compounds. Hoon *et al.* (2008) combined results from three different experimental approaches to investigate the mode of action of 188 novel synthetic compounds. I have tried to integrate genetic and physical interaction data with chemical-genetic profiles. For example, the chemical genetic profile of benomyl does not point to microtubule-related protein complexes or GO categories. However, analysis of genetic interactions among the most sensitive deletion mutants reveals a highly connected cluster of 9 genes most of which are involved in microtubule-related processes (Figure A.8A). The deletion strains most sensitive to a different compound exhibit many genetic interactions that



seem to point to different pathways (Figure A.8B). In addition, integration of physical interactions reveals three or four potential protein complexes (Figure A.8C) that have also been identified by calculation of average Z-scores for protein complexes.

## A.11 Follow-up experiments

Confirmation of the most interesting hits from genome-wide chemical-genetic profiles improves confidence about these hits and also gives an estimate for the quality of the screens. It is also a good idea to assess specific chemical-genetic interactions if a deletion strain does not behave as expected. The chemical-genetic screens do not directly assess each strain, but rely on microarray read-outs to quantify abundance of strains. It is possible that deletion strains drop out of the pool or that mutations occur in the barcode or the primer regions which will result in low or no signal for the affected strain.

Follow-up experiments that were conducted in the context of this thesis include sorbitol rescue and microscopy to assess physiological changes in yeast cells in response to compound treatment. Different dyes can be used to look at various cellular structures. Brenda Andrews' lab in Toronto, Canada is working on a set of yeast strains will enable analysis of sub-cellular morphology in response to compounds. 'The marker project' aims to assemble a set strains with GFP-tagged proteins to allow visualisation of these organelles. This set of strains would provide a rapid means to assess the effect of compounds on cellular physiology.

Depending on the chemical-genetic profiles, various assays can be conducted to confirm hypotheses about the effect of small molecules.



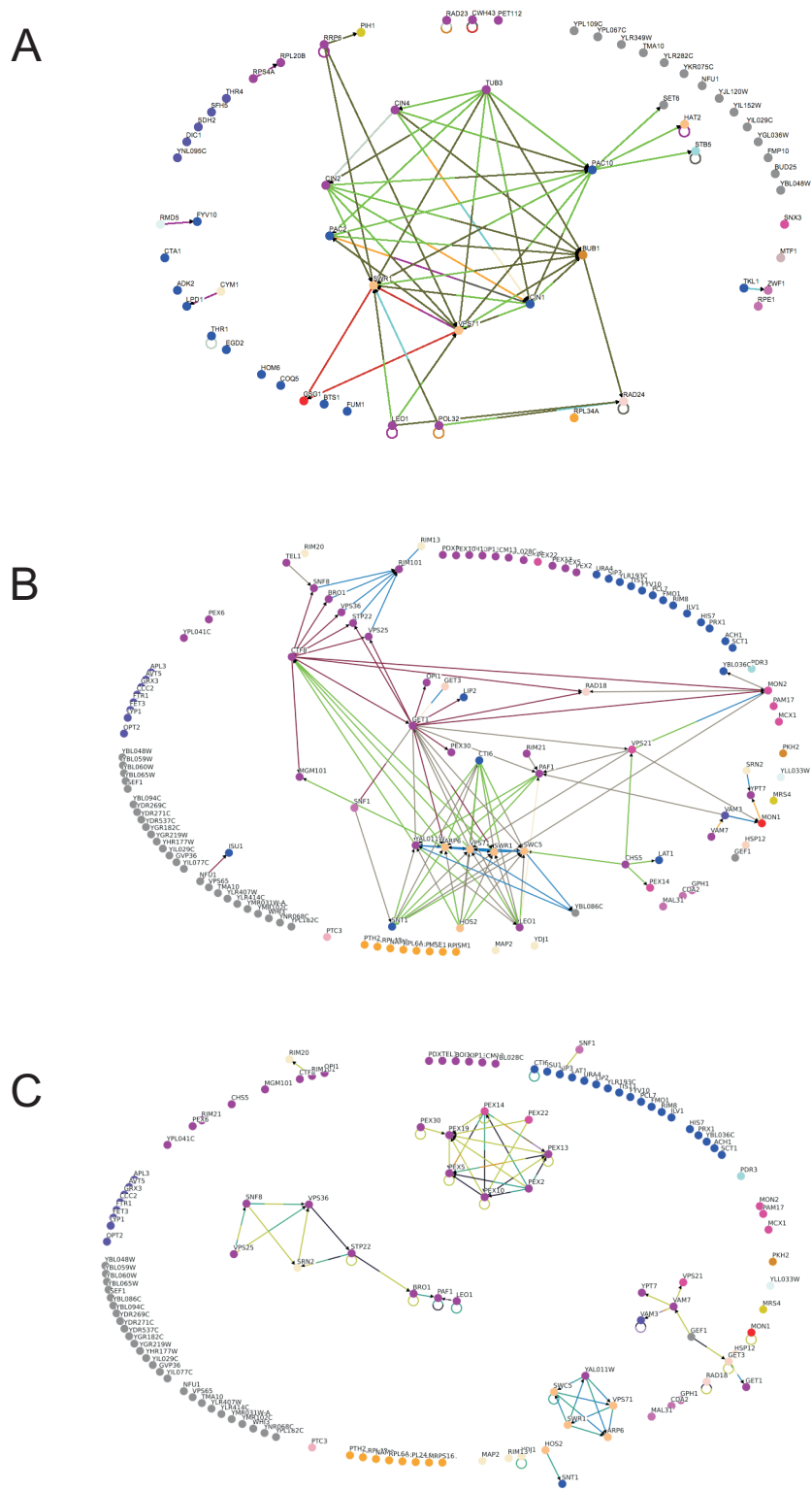


Figure A.8: Integration of chemical-genetic profiles and genetic and physical interaction data. Network images were generated with Osprey. (A) Genetic interactions among deletions trains sensitive to benomyl. (B) Genetic interactions among deletion mutants from a chemical-genetic profile. (C) Physical interactions among deletion mutants from (B).

## A.12 Concluding remarks

This appendix gives an overview of different data analysis approaches that can be applied to chemical-genetic profiles. Many approaches are available to analyse genome-wide data and I have here described the ones that I have used for the analysis of data presented in this thesis. Some of the described methods are already available as online tools on our lab website. My goal is to implement a comprehensive analysis pipeline and make it available as an R package and a web interface. I am hoping to extend the integration of different data sources with the chemical-genetic profiles considerably.

## References

- Ashburner, M., Ball, C. A., Blake, J. A., Botstein, D., Butler, H., Cherry, J. M., Davis, A. P., Dolinski, K., Dwight, S. S., Eppig, J. T., Harris, M. A., Hill, D. P., Issel-Tarver, L., Kasarskis, A., Lewis, S., Matese, J. C., Richardson, J. E., Ringwald, M., Rubin, G. M., and Sherlock, G. Gene ontology: tool for the unification of biology. The Gene Ontology Consortium. *Nat Genet*, 25(1): 25-9 (2000).
- Christie, K. R., Hong, E. L., and Cherry, J. M. Functional annotations for the *Saccharomyces cerevisiae* genome: the knowns and the known unknowns. *Trends Microbiol*, 17(7): 286-94 (2009).
- Hong, E. L., Balakrishnan, R., Dong, Q., Christie, K. R., Park, J., Binkley, G., Costanzo, M. C., Dwight, S. S., Engel, S. R., Fisk, D. G., Hirschman, J. E., Hitz, B. C., Krieger, C. J., Livstone, M. S., Miyasato, S. R., Nash, R. S., Oughtred, R., Skrzypek, M. S., Weng, S., Wong, E. D., Zhu, K. K., Dolinski, K., Botstein, D., and Cherry, J. M. Gene Ontology annotations at SGD: new data sources and annotation methods. *Nucleic Acids Research*, 36(Database issue): D577-81 (2008).
- Hoon, S., Smith, A. M., Wallace, I. M., Suresh, S., Miranda, M., Fung, E., Proctor, M., Shokat, K. M., Zhang, C., Davis, R. W., Giaever, G., Onge, R. P. S., St Onge, R. P., and Nislow, C. An integrated platform of genomic assays reveals small-molecule bioactivities. *Nat Chem Biol*, 4(8): 498-506 (2008).
- Reference Genome Group of the Gene Ontology Consortium. The Gene Ontology's Reference Genome Project: a unified framework for functional annotation across species. *PLoS Comput Biol*, 5(7): e1000431 (2009).

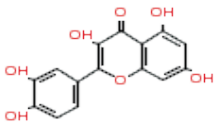
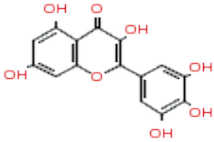
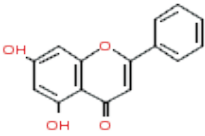
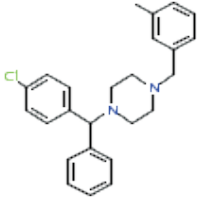
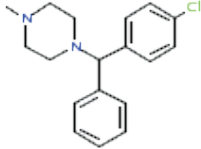
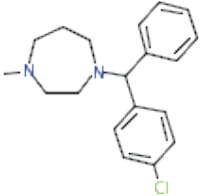
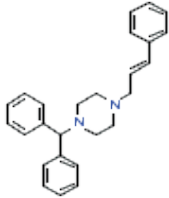
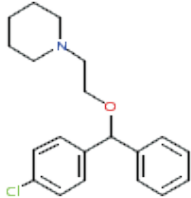
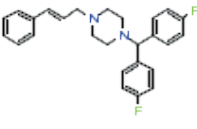
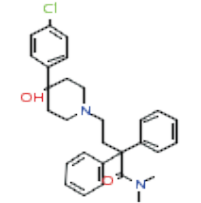
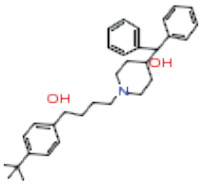
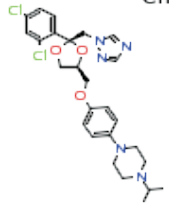
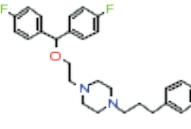
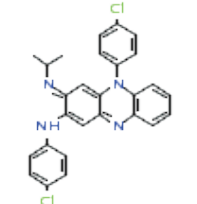
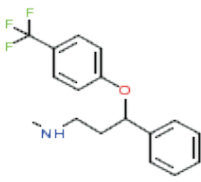
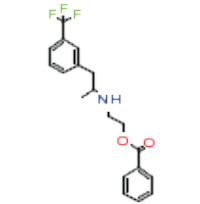
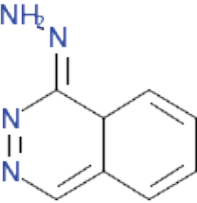
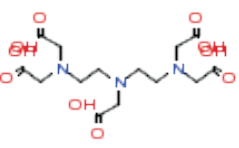
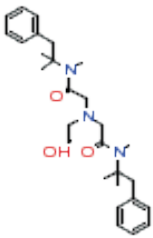
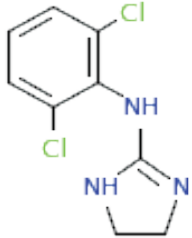
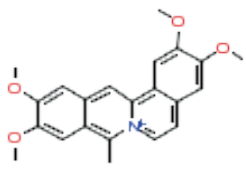
- Parsons, A. B., Brost, R. L., Ding, H., Li, Z., Zhang, C., Sheikh, B., Brown, G. W., Kane, P. M., Hughes, T. R., and Boone, C. Integration of chemical-genetic and genetic interaction data links bioactive compounds to cellular target pathways. *Nat Biotechnol*, 22(1): 62-9 (2004).
- Pu, S., Wong, J., Turner, B., Cho, E., and Wodak, S. J. Up-to-date catalogues of yeast protein complexes. *Nucleic Acids Research*, 37(3): 825-831 (2009).

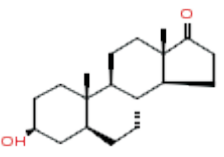
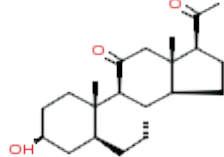
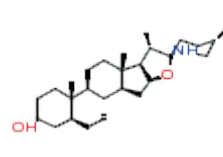
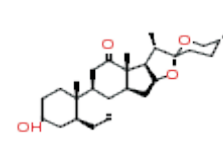
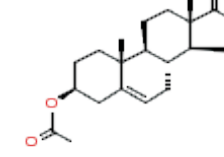
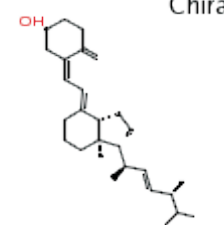
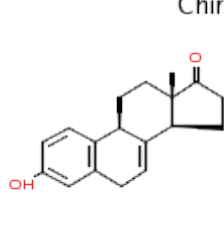
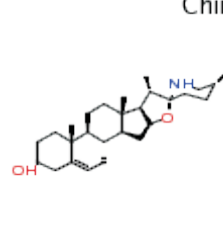
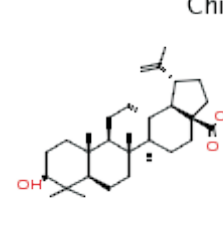
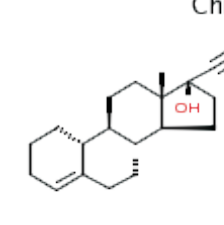
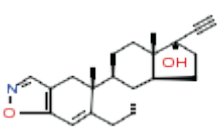
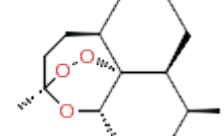
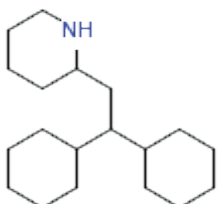
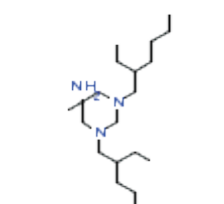
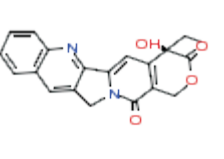
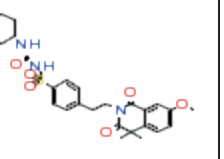
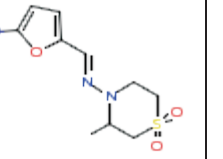
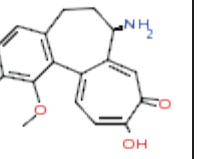
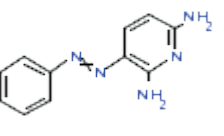
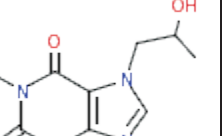
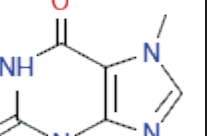
## APPENDIX B

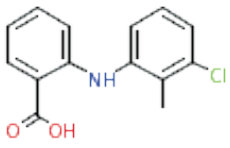
---

### Structural clusters of 148 hit compounds

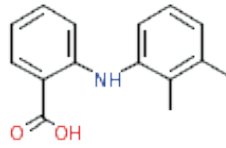
---

Cluster: 1				
				
Quercetin dihydrate	Myricetin	Chrysin		
Cluster: 2				
				
Meclozine dihydrochloride	(1-[(4-Chlorophenyl)phenylmethyl]-4-methylpiperazine)	Homochlorcyclizine dihydrochloride	Cinnarizine	Cloperastine hydrochloride
			 Chiral	
Flunarizine dihydrochloride	Loperamide hydrochloride	Terfenadine	Terconazole	GBR 12909 dihydrochloride
				
Clofazimine	Fluoxetine hydrochloride	Benfluorex hydrochloride		
Cluster: 3				
				
Hydralazine hydrochloride				
Cluster: 4	Cluster: 5	Cluster: 6		
				
Pentetic acid	Oxethazaine	Clonidine hydrochloride	Coralyne chloride hydrate	

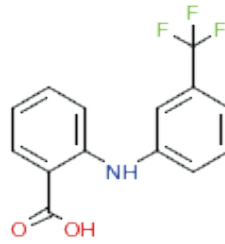
Cluster: 7				
Chiral  Epiandrosterone	Chiral  Alfaxalone	Chiral  Tomatidine	Chiral  Hecogenin	Chiral  Dehydroisoandrosterone 3-acetate
Chiral  Calciferol	Chiral  Equilin	Chiral  Solasodine	Chiral  Betulinic acid	Chiral  Lynestrenol
Chiral  Danazol	Chiral  Artemisinin			
Cluster: 8		Cluster: 9		
 Perhexiline maleate		 Hexetidine		
Cluster: 10				
Chiral  Camptothecin (S,+)	 Gliquidone	 Nifurtimox	Chiral  Trimethylcolchicinic acid	
Cluster: 11		Cluster: 12		
 Phenazopyridine hydrochloride		 Proxiphylline	 Theobromine	

**Cluster: 13**

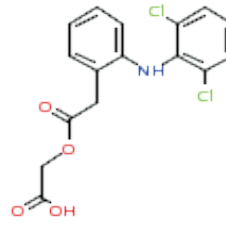
Tolfenamic acid



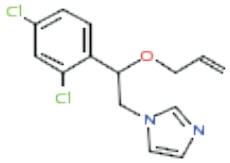
Mefenamic acid



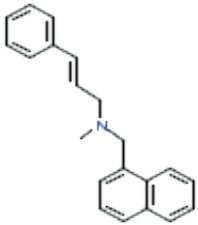
Flufenamic acid



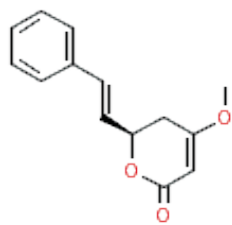
Aceclofenac

**Cluster: 14**

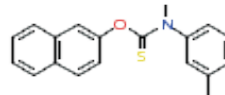
Enilconazole

**Cluster: 15**

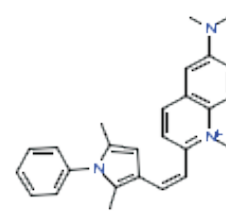
Naftifine hydrochloride



Kawain

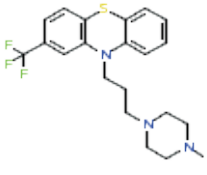
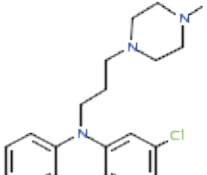
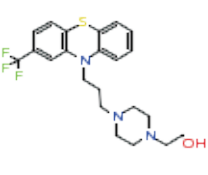
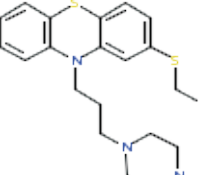
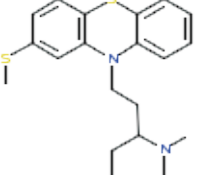
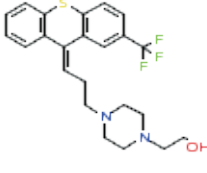
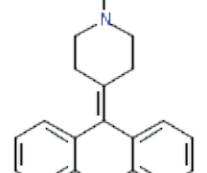
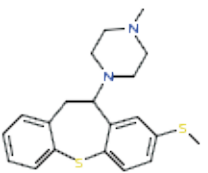
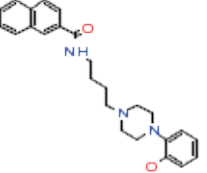
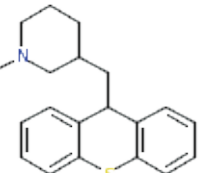
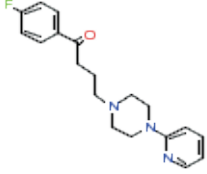
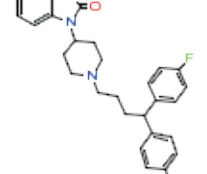
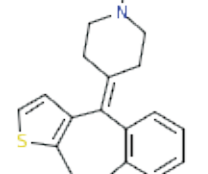


Tolnaftate

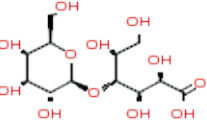


Pyrvinium pamoate

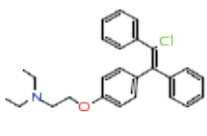
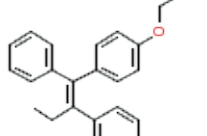
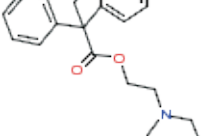
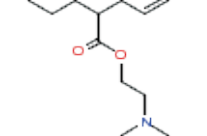
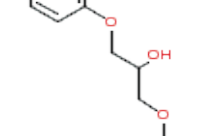
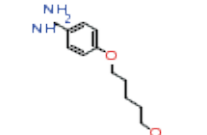
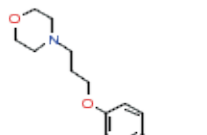
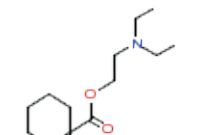
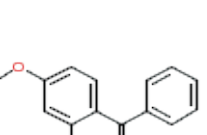
**Cluster: 16**

				
Trifluoperazine dihydrochloride	Prochlorperazine dimaleate	Fluphenazine dihydrochloride	Thiethylperazine malate	Thioridazine hydrochloride
				
Flupentixol dihydrochloride cis-(Z)	Pimethixene maleate	Methiothepin maleate	DO 897/99	Metixene hydrochloride
				
Azaperone	Pimozide	Pizotifen maleate		

**Cluster: 17**

Chiral 				
Lactobionic acid				

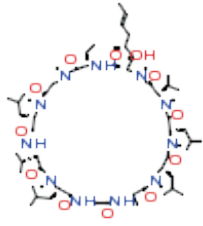
**Cluster: 18**

				
Clomiphene citrate (Z,E)	Tamoxifen citrate	Proadifen hydrochloride	Drofenine hydrochloride	Chlorphensin carbamate
				
Pentamidine isethionate	Pramoxine hydrochloride	Dicyclimine hydrochloride	Oxybenzone	



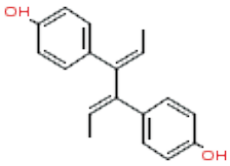
**Cluster: 19**

Chiral

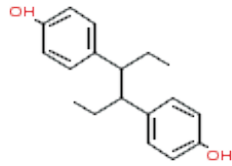


Cyclosporin A

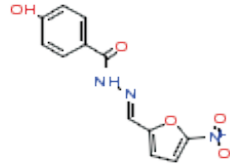
**Cluster: 20**



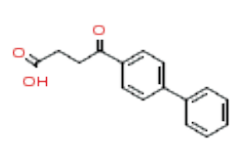
Dienestrol



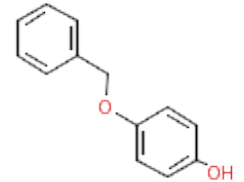
Hexestrol



Nifuroxazide

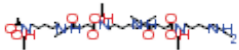


Fenbufen



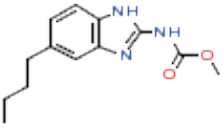
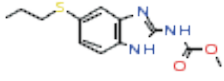
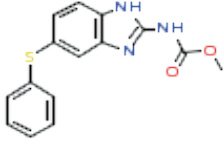
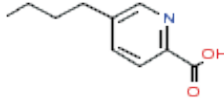
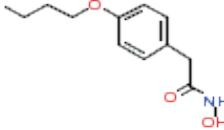
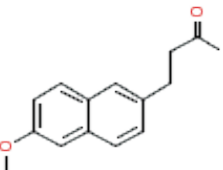
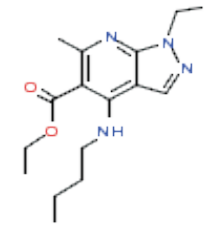
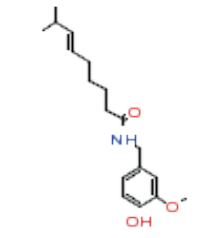
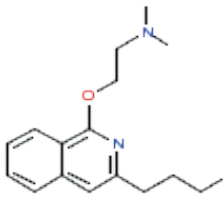
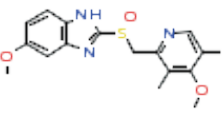
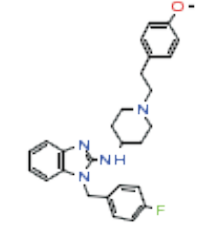
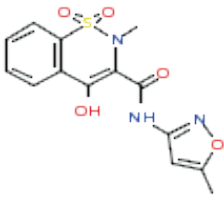
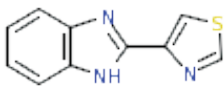
Monobenzene

**Cluster: 21**

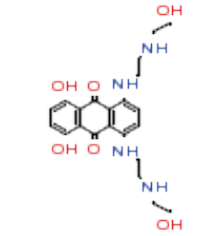
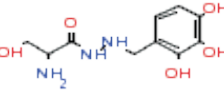
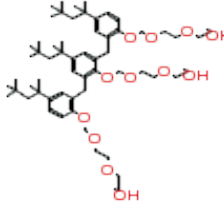


Deferoxamine mesylate

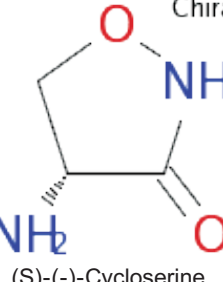
**Cluster: 22**

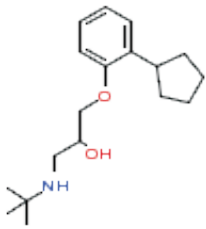
				
Parbendazole	Albendazole	Fenbendazole	Fusaric acid	Bufexamac
				
Nabumetone	Tracazolate hydrochloride	Capsaicin	Dimethisoquin hydrochloride	Omeprazole
				
Astemizole	Isoxicam	Tiabendazole		

**Cluster: 23**

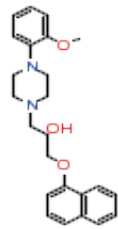
			
Mitoxantrone dihydrochloride	Benserazide hydrochloride	Tyloxapol	

**Cluster: 24**

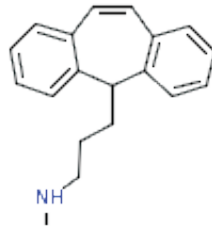
 Chiral (S)-(-)-Cycloserine	
--	--

**Cluster: 25**

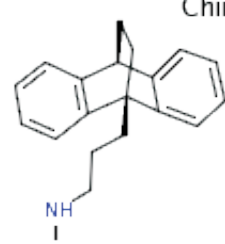
Penbutolol sulfate



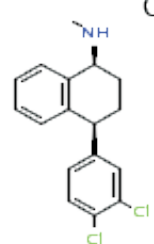
Naftopidil dihydrochloride



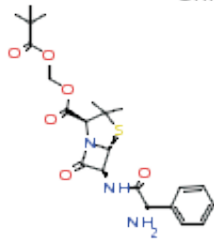
Protriptyline hydrochloride



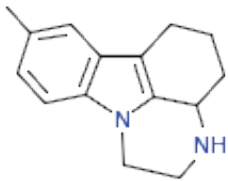
Maprotiline hydrochloride



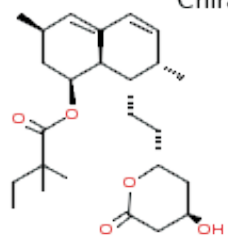
Sertraline



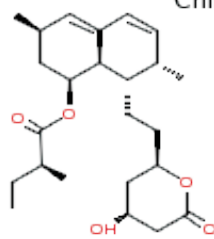
Pivampicillin

**Cluster: 26**

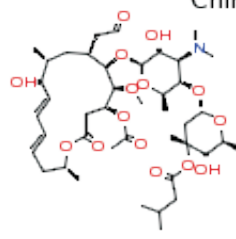
Pirlindole mesylate

**Cluster: 27**

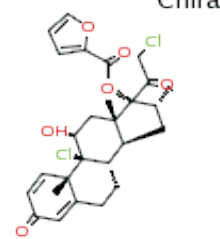
Simvastatin



Lovastatin

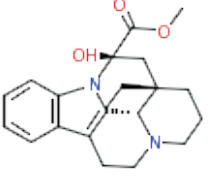
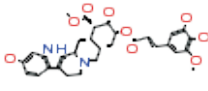
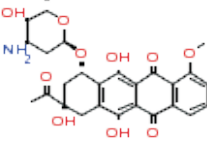
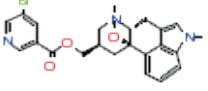
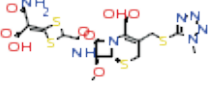
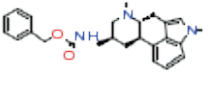
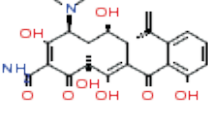
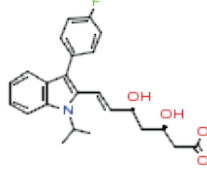
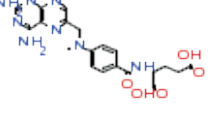
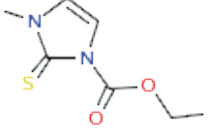
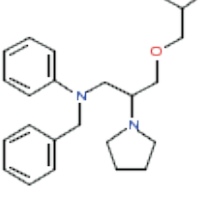
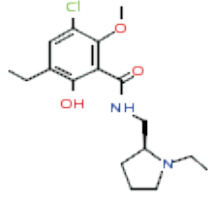
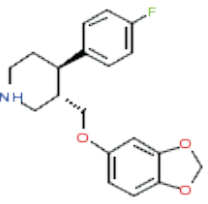


Josamycin

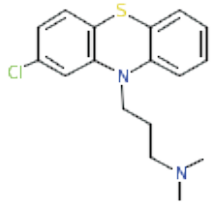


Mometasone furoate

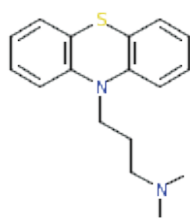
**Cluster: 28**

<p>Chiral</p>  <p>Epivincamine</p>	<p>Chiral</p>  <p>Rescinnamin</p>	<p>Chiral</p>  <p>Daunorubicin hydrochloride</p>	<p>Chiral</p>  <p>Nicergoline</p>	<p>Chiral</p>  <p>Cefotetan</p>
<p>Chiral</p>  <p>Metergoline</p>	<p>Chiral</p>  <p>Methacycline hydrochloride</p>	<p>Chiral</p>  <p>Fluvastatin sodium salt</p>	<p>Chiral</p>  <p>Amethopterin (R,S)</p>	<p>Chiral</p>  <p>Carbimazole</p>
<p>Chiral</p>  <p>Bepidil hydrochloride</p>	<p>Chiral</p>  <p>S(-)-Eticlopride hydrochloride</p>			
<p><b>Cluster: 29</b></p>				
<p>Chiral</p>  <p>Paroxetine Hydrochloride</p>				

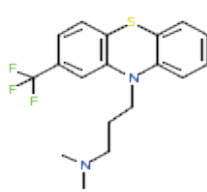
**Cluster: 30**



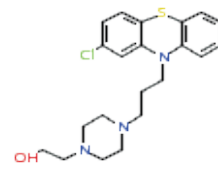
Chlorpromazine hydrochloride



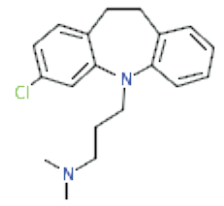
Promazine hydrochloride



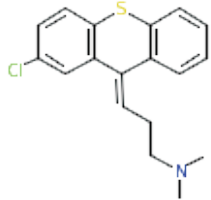
Triflupromazine hydrochloride



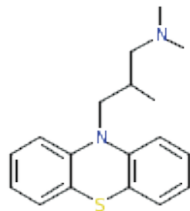
Perphenazine



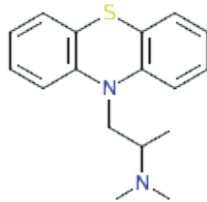
Clomipramine hydrochloride



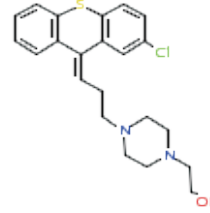
Chlorprothixene hydrochloride



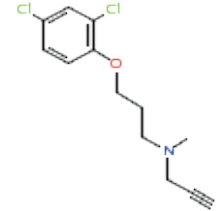
Trimeprazine tartrate



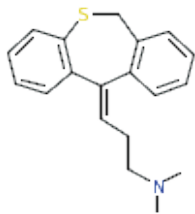
Promethazine hydrochloride



Zuclopenthixol hydrochloride

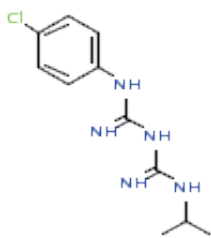


Clorgyline hydrochloride



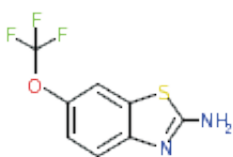
Dosulepin hydrochloride

**Cluster: 31**

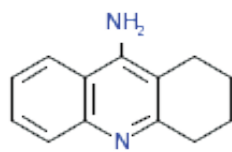


Proguanil hydrochloride

**Cluster: 32**

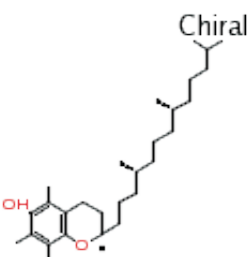


Riluzole hydrochloride

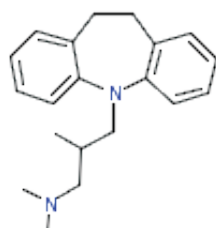


Tacrine hydrochloride hydrate

**Cluster: 33**

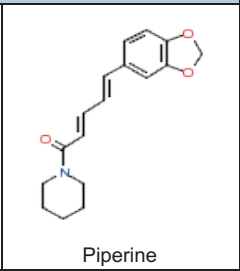
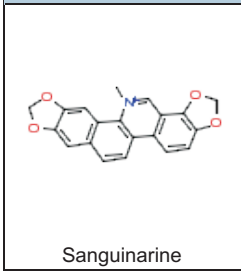


Tocopherol (R,S)

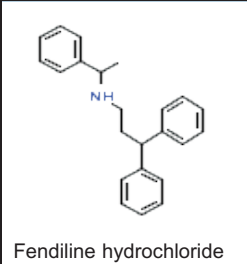
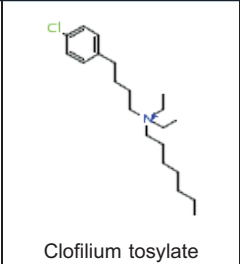
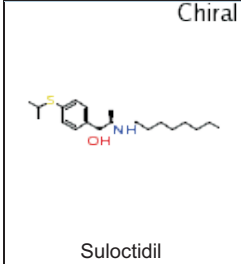


Trimipramine maleate salt

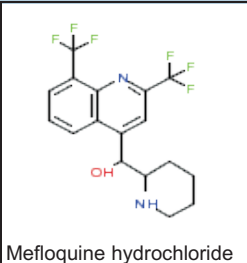
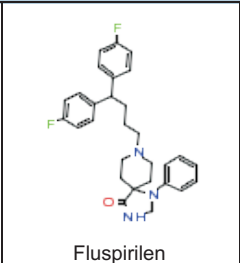
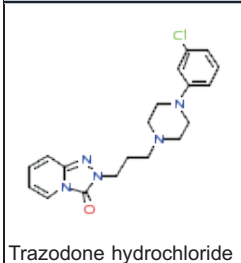
**Cluster: 34**



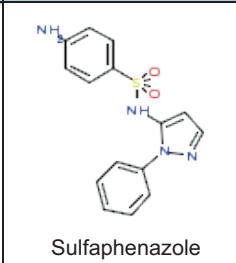
**Cluster: 35**



**Cluster: 36**



**Cluster: 37**



# Combined zebrafish–yeast chemical–genetic screens reveal gene–copper–nutrition interactions that modulate melanocyte pigmentation

Hironori Ishizaki<sup>1,\*</sup>, Michaela Spitzer<sup>2,\*</sup>, Jan Wildenhain<sup>2</sup>, Corina Anastasaki<sup>1</sup>, Zhiqiang Zeng<sup>1</sup>, Sonam Dolma<sup>3,‡</sup>, Michael Shaw<sup>4</sup>, Erik Madsen<sup>5</sup>, Jonathan Gitlin<sup>5</sup>, Richard Marais<sup>6</sup>, Mike Tyers<sup>2,3</sup> and E. Elizabeth Patton<sup>1,§</sup>

## SUMMARY

Hypopigmentation is a feature of copper deficiency in humans, as caused by mutation of the copper ( $\text{Cu}^{2+}$ ) transporter ATP7A in Menkes disease, or an inability to absorb copper after gastric surgery. However, many causes of copper deficiency are unknown, and genetic polymorphisms might underlie sensitivity to suboptimal environmental copper conditions. Here, we combined phenotypic screens in zebrafish for compounds that affect copper metabolism with yeast chemical–genetic profiles to identify pathways that are sensitive to copper depletion. Yeast chemical–genetic interactions revealed that defects in intracellular trafficking pathways cause sensitivity to low-copper conditions; partial knockdown of the analogous Ap3s1 and Ap1s1 trafficking components in zebrafish sensitized developing melanocytes to hypopigmentation in low-copper environmental conditions. Because trafficking pathways are essential for copper loading into cuproproteins, our results suggest that hypomorphic alleles of trafficking components might underlie sensitivity to reduced-copper nutrient conditions. In addition, we used zebrafish–yeast screening to identify a novel target pathway in copper metabolism for the small-molecule MEK kinase inhibitor U0126. The zebrafish–yeast screening method combines the power of zebrafish as a disease model with facile genome-scale identification of chemical–genetic interactions in yeast to enable the discovery and dissection of complex multigenic interactions in disease–gene networks.

## INTRODUCTION

Melanins are pigment granules that provide the color for human hair, skin and eyes, and serve to protect surrounding cells from the DNA-damaging effects of ultraviolet (UV) light. Melanins are synthesized and stored in the melanosomes, specialized lysosome-related organelles of the melanocytes that are transferred to surrounding skin or hair cells or concentrated within the retinal pigmented epithelium (Rapoport and Marks, 2007). The restriction of melanosome biogenesis to melanocytes results from the cell-specific expression and production of pigment enzymes coupled with their trafficking through the Golgi and early endosomal pathways to the maturing melanosomal organelles. For example, the melanocyte regulator *Mitf* promotes expression of the rate-limiting enzyme tyrosinase, which is directed through the Golgi and then to the endosome-to-melanosome pathway by the AP1 and AP3 adaptor complexes. Once at the melanosome, tyrosinase

promotes melanin synthesis and deposition along the Pmel fibrillar matrix (Chin et al., 2006; Raposo and Marks, 2007).

Copper ( $\text{Cu}^{2+}$ ) is essential for melanin production, and consequently hypopigmentation is a feature of copper deficiency. Genetic mutations of the copper transporters ATP7A or ATP7B lead to Menkes disease or Wilson's disease, respectively; these childhood syndromes cause acute clinical symptoms in the bone, skin, hair, blood and nervous system (Madsen and Gitlin, 2008). The transporters ATP7A and ATP7B reside in the trans-Golgi network and shuttle copper from the cytoplasm to copper-dependent enzymes in the Golgi. Environmental conditions can also lead to copper deficiency. For example, lambs born to ewes feeding on copper-deficient grass share many clinical features with children diagnosed with Menkes disease; this observation established copper-metabolism deficiencies as an underlying cause of the pathology of Menkes disease (Danks et al., 1972). Copper deficiency can also occur in patients undergoing gastric surgery or after excessive consumption of zinc or iron, all of which can inhibit absorption of copper through the intestine (Kumar, 2006). However, as the causes of many cases of copper deficiency remain unknown (Madsen and Gitlin, 2007b), a more systematic approach to understanding copper-metabolism deficiency in humans is required, including the development of robust cell and animal models (Thiele and Gitlin, 2008).

Melanocytes have a cell-type-specific requirement for copper in pigmentation because tyrosinase is a copper-dependent enzyme, and its activity is dependent on ATP7A (Petris et al., 2000). Transport of ATP7A into melanosomes spatially restricts melanin synthesis to melanocytes; this process is dependent on the biogenesis of the lysosome-related organelle complex (BLOC)-1, which is required for exit of endosomal cargo (Setty et al., 2008).

<sup>1</sup>Institute of Genetics and Molecular Medicine, MRC Human Genetics Unit and The University of Edinburgh, Western General Hospital, Crewe Road, Edinburgh, EH4 2XU, UK

<sup>2</sup>Wellcome Trust Centre for Cell Biology, University of Edinburgh, Michael Swann Building, King's Buildings, Mayfield Road, Edinburgh, EH9 3JR, UK

<sup>3</sup>Center for Systems Biology, Samuel Lunenfeld Research Institute, 600 University Avenue, Toronto, Ontario, M5G 1X5, Canada

<sup>4</sup>Sir William Dunn School of Pathology, University of Oxford, South Parks Road, Oxford, OX1 3RE, UK

<sup>5</sup>Department of Pediatrics, Vanderbilt University School of Medicine, Nashville, TN 37232, USA

<sup>6</sup>The Institute of Cancer Research, Signal Transduction Team, Section of Cell and Molecular Biology, 237 Fulham Road, London, SW3 6JB, UK

\*These authors contributed equally to this work

<sup>‡</sup>Present address: The Hospital for Sick Children, Developmental Stem Cell Biology, TMDT Building, 13-601G, 101 College Street, Toronto, Ontario, M5G 1L7, Canada

<sup>§</sup>Author for correspondence (e.patton@hgu.mrc.ac.uk)

Excess exogenous copper can restore pigmentation to BLOC-1-deficient melanocytes in vitro (Setty et al., 2008). Components of BLOC-1 are mutated in Hermansky-Pudlak syndrome (HPS), a disorder characterized by defects in lysosome-related organelles, particularly melanosomes and platelet-dense granules (Wei, 2006). Aberrant transport of ATP7A might be responsible for the HPS pathology of melanocytes from BLOC-1-deficient individuals (Setty et al., 2008). In zebrafish, mutation of *atp7a* or treatment with the copper-chelator neocuproine causes a phenotype with features of Menkes disease, including hypopigmentation, neurological disorders, and loss of lysyl oxidase cuproenzyme activity in the developing notochord (Mendelsohn et al., 2006). In zebrafish, hypomorphic alleles of *atp7a* and the vacuolar ATPase (*v-ATPase*) cause hypopigmentation at low copper concentrations, demonstrating that genetic mutations can result in copper-deficiency symptoms in suboptimal nutrient conditions (Madsen and Gitlin, 2008).

We have developed a coupled zebrafish phenotypic and yeast chemical-genetic screening approach to identify novel genetic pathways that underlie copper-nutrient sensitivity in the developing vertebrate melanocyte (Fig. 1A). Phenotypic chemical screens in zebrafish enable the identification of novel biological pathways by virtue of chemically induced phenotypes (Zon and Peterson, 2005). Such zebrafish screens are typically carried out by treating developing embryos with libraries of small molecules to identify compounds that elicit a specific phenotype. The small size and transparency of the embryo, which can be arrayed in 96-well plates, coupled with tractable genetic tools for target validation and disease modelling make the zebrafish a highly effective system for phenotype-driven small-molecule screens. However, despite its tractability, identification of the target pathways in zebrafish is usually arduous (Peterson, 2008). Chemical-genetic approaches in the budding yeast *Saccharomyces cerevisiae* can provide rich functional information on the mechanism of action of compounds

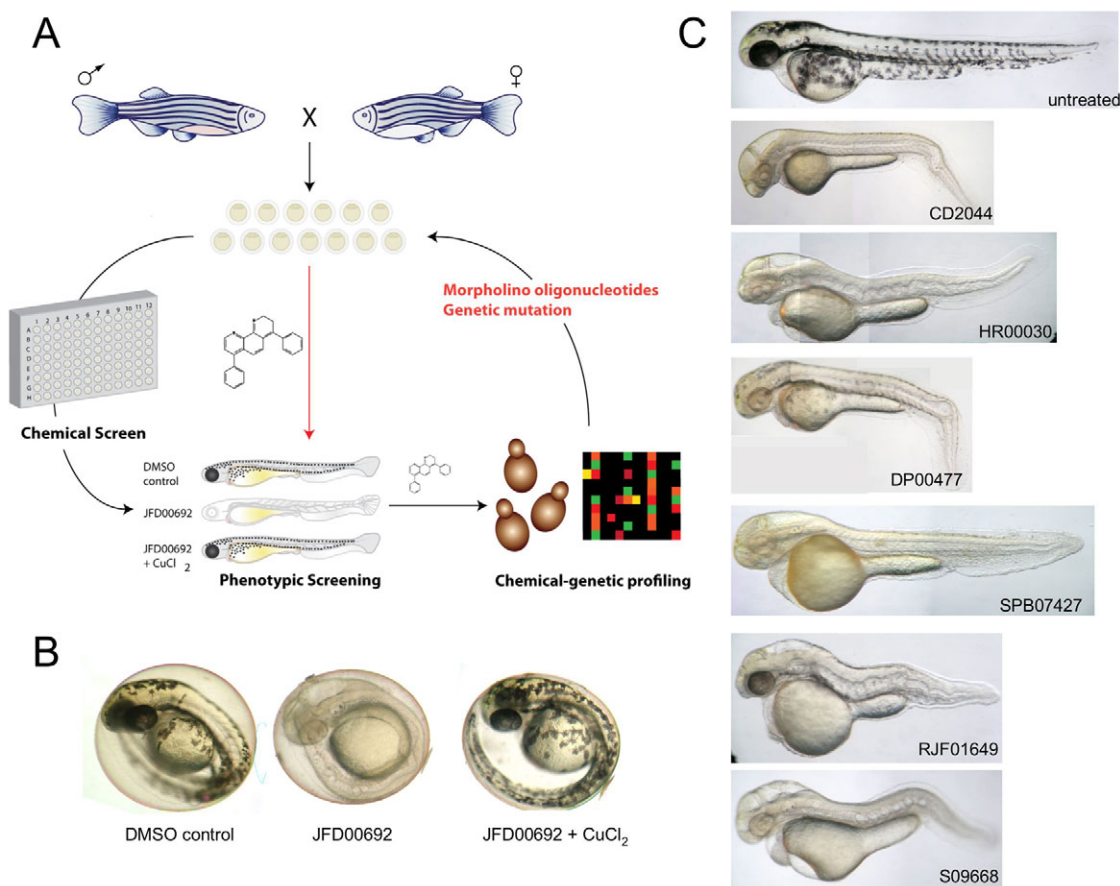


**Fig. 1. A combined zebrafish and yeast approach to probe chemical-genetic interactions in melanocyte pigmentation.** (A) Overview of work flow. Phenotypic screening in zebrafish informs as to the developmental and physiological target pathway. Small molecules that promote similar phenotypes in zebrafish are then tested in genome-wide chemical-genetic screens in yeast to reveal potential target genetic pathways. Conserved target pathways are then directly re-tested for chemical-genetic interactions in the zebrafish system using genetic mutant lines, morpholino oligonucleotides or small molecules known to impinge on the same target. (B) Phenotypic screening of a >1500-compound yeast-bioactive library (S.D., J.W., M. Spitzer and M.T., unpublished data) and the Sigma LOPAC library for altered pigmentation in zebrafish embryos revealed a copper-metabolism phenotype characterized by hypopigmentation, an expanded hindbrain and an undulating notochord (Mendelsohn et al., 2006). Representative phenotype caused by 10  $\mu$ M JFD00692 was rescued by treatment with exogenous copper chloride (5  $\mu$ M or 15  $\mu$ M) during development. (C) Examples of the copper-metabolism phenotype induced by some of the compounds identified in the screen.



(Boone et al., 2007; Hillenmeyer et al., 2008). Mutations that render yeast sensitive to a particular compound – that is, chemical-genetic interactions – often establish links to the cellular target pathways (Hartwell et al., 1997; Parsons et al., 2004; Parsons et al., 2006). The yeast genome-wide gene-deletion collection, in which each of the ~6000 genes has been individually replaced with a deletion cassette marked with unique sequence identifiers (barcodes) that can be quantified in parallel by microarray hybridization, is a powerful resource for chemical genetics (Winzeler et al., 1999; Giaever et al., 2002). Chemical-genetic profiling, whereby growth of the pooled deletion collection is scored for hypersensitivity to a compound, enables the identification of target and off-target pathways. This approach has been used to interrogate the mechanism of action of both novel and clinically approved drugs, including chemotherapeutics and neuroleptics (Lum et al., 2004; Parsons et al., 2004; Parsons et al., 2006; Ericson et al., 2008; Hillenmeyer et al., 2008). Compounds with similar chemical-genetic profiles can be grouped to reveal similar modes of action and similar targets (Parsons et al., 2006; Hillenmeyer et al., 2008). Often the gene networks that confer sensitivity or resistance to a given compound are conserved from yeast to mammalian cells (Ericson et al., 2008; Yu et al., 2008).

We identified a novel panel of compounds that affect pathways of copper metabolism and pigmentation in zebrafish and then interrogated the mode of action of several of these compounds. Based on the identification of target genes in yeast encoding intracellular transport proteins, we show that reduced expression of the orthologous target genes, *ap1s1* and *ap3s2*, in zebrafish cause hypopigmentation specifically under conditions of copper limitation. We also demonstrate that the commonly used MEK inhibitor U0126 affects copper metabolism in zebrafish, and use chemical-genetic profiles in yeast to show that U0126 has at least two target pathways in vivo. This combined zebrafish-yeast chemical-genetic approach should be applicable to the study of many other processes associated with disease and development.

## RESULTS

### A chemical screen identifies small molecules that elicit a copper-deficiency phenotype in zebrafish

Using phenotypic screening in zebrafish, we identified a panel of 45 small molecules that caused a phenotype characteristic of copper depletion (Fig. 1; Table 1). We screened the 1280-member Library of Pharmacologically Active Compounds (LOPAC) and a collection of 1576 bioactive compounds (S.D., J.W., M. Spitzer and M.T., unpublished data) for effects on zebrafish pigmentation. Two embryos at 4 hours post-fertilization (hpf) were placed in each well of a 96-well plate and treated with 10  $\mu$ M of compound and observed at multiple time points over 48 hours for a copper-metabolism phenotype as exemplified by the *atp7a*-mutant zebrafish or treatment with neocuproine. These phenotypic manifestations include hypopigmentation, an expanded hindbrain and an undulating notochord in a 2- to 3-day-old fish (Fig. 1B). Active compounds included known copper-binding molecules, such as 1-phenyl-3-(2-thiazolyl)-2-thiourea (PTT) (Mendelsohn et al., 2006), as well as the metal-binding thiosemicarbazones, thiourea derivatives, phenanthrolines and pyridin-pyrimidinones (Fig. 1B). Unexpectedly, the commonly used MEK inhibitor U0126 was also identified as causing a phenotype consistent with defective copper

metabolism (Table 1); this phenotypic effect of U0126 has been recently described elsewhere (Hawkins et al., 2008).

Further phenotypic characterization showed the copper-metabolism phenotype caused by many of the small molecules could be prevented with the addition of exogenous copper, indicating that the characteristic zebrafish Menkes phenotypes in pigmentation, notochord, blood and hindbrain development are dependent upon the loss of environmental copper availability (Fig. 1B; Table 1). Interestingly, three compounds caused hypersensitivity to exogenous copper addition (Table 1; supplementary material Fig. S1). One possibility is that these three compounds interfere with detoxification of excess copper ions in the cell; elevated copper levels are highly toxic, and intracellular levels are finely balanced by copper chaperones and metallothionein levels (Rae et al., 1999).

### Genome-wide genetic-sensitivity profiles reveal potential copper-metabolism pathways

We then used yeast chemical-genetic profiles to identify gene deletions that resulted in sensitivity to a selected subset of compounds that affected copper metabolism in our zebrafish screen: this copper-metabolism subset (CM subset) comprised the compounds neocuproine, U0126, DP00477, SEW01049, SPB07427, JFD00692 and RJF01649. Evolutionarily conserved genetic pathways that are sensitive to copper nutrition in yeast could then be directly tested in the zebrafish vertebrate system (Fig. 1A). We screened pools of ~5000 haploid yeast deletion mutants and ~1000 heterozygous diploid mutants for growth after treatment with the CM subset. Compound concentrations were titrated such that overall growth of the yeast pool was diminished by 20-30% (Parsons et al., 2006). Aliquots of the deletion pools were grown for 20 generations in the presence of the different compounds as specified in supplementary material Table S1 or in the presence of 0.4% DMSO (control samples). Genomic DNA was isolated from each pool, the barcodes were amplified with fluorescently labeled primers, and the PCR products were hybridized to spotted oligonucleotide microarrays (Cook et al., 2008). Scatter plots demonstrated that for most chemical-genetic screens, the majority of deletion mutants were not affected by treatment with compound (supplementary material Fig. S2). Boxplots and quantile statistics of *z*-scores for each microarray allowed identification of sensitive and resistant mutants (see Methods).

Although all the chemicals in the CM subset produced a similar developmental *atp7a*-mutant phenotype in zebrafish, we found both distinct and common genetic pathways in yeast to be sensitive or resistant to individual compounds in the CM subset, reflecting the unique action of each chemical (Fig. 2). First, we examined the sensitivity of deletions in genes known to be involved in copper uptake and metabolism. Deletion strains defective in copper metabolism are in fact rarely affected by chemical treatments in large-scale surveys (Hillenmeyer et al., 2008), probably because yeast cultures in these studies are typically grown in rich medium that contains adequate amounts of available copper. We found the fitness profiles of strains deleted for known copper-uptake and -metabolism genes to be unique to each compound (Fig. 2A). Deletion of genes such as the copper transporter *CTR1*, the copper chaperones *ATX1* and *ATX2*, the copper-transporting ATPase *CCC2*, the copper-zinc superoxide dismutase *SOD1* and the copper-dependent transcription factor *CUP2* all caused sensitivity to

Table 1. Small molecules and copper-metabolism phenotypes

Molecule <sup>a</sup>	Maybridge Code	Phenotype <sup>b</sup>	Copper addition <sup>c</sup>	Compound structure
<b>Neocuproine</b>	–	<b>Copper metabolism</b>	<b>Rescue (5 μM)</b>	Phenanthroline
<b>U0126</b>	–	<b>Copper metabolism</b>	<b>Lethal (5 μM)</b>	Sulfanylmethylidene-butanedinitrile
PTT	–	Copper metabolism	not determined	1-Phenyl-3-(2-thiazolyl)-2-thiourea
<b>BIO2A11</b>	<b>DP00477</b>	<b>Copper metabolism</b>	<b>Partial rescue (15 μM)</b>	<b>Thiocarbamoyl-acetamide derivative</b>
BIO2B11	DP00750	Copper metabolism	Rescue (5 μM)	Thiosemicarbazone
BIO2F3	CD00707	Copper metabolism	Rescue (5 μM)	Thio-urea
BIO2G5	CD02745	Copper metabolism	Rescue (5 μM)	Thiosemicarbazone
BIO2H4	CD02044	Copper metabolism	Partial rescue (15 μM)	Thiosemicarbazone
BIO3C5	HR 00030	Copper metabolism	Rescue (5 μM)	Thio-urea derivate
BIO3E2	FM00217	No pigmentation	Rescue (5 μM)	Thiosemicarbazone
BIO5C9	PD00357	No pigmentation	Rescue (5 μM)	Thiosemicarbazone
BIO5F10	RDR 00803	Copper metabolism	Rescue (15 μM)	Thiosemicarbazone
BIO5H4	KM 09752	Copper metabolism	Rescue (5 μM)	Thio-urea derivate
BIO6C9	RJC 00588	Copper metabolism	Rescue (5 μM)	Carbamic acid
BIO6D7	RH 01646	Copper metabolism	Rescue (5 μM)	Thiosemicarbazone
BIO6F7	RH 01676	No pigmentation	Rescue (5 μM)	Triazole-thiol
BIO7C11	SEW 02973	No pigmentation	Rescue (5 μM)	Pyridin-pyrimidinone
<b>BIO7C9</b>	<b>SEW 01049</b>	<b>Copper metabolism</b>	<b>Lethal (5 μM)</b>	<b>Thiosemicarbazone</b>
BIO7D2	RJF01673	Wavy notochord	Rescue (5 μM)	Pyridin-pyrimidinone
BIO7D3	S 02347	Copper metabolism	Partial rescue (15 μM)	2,4-Diphenyl-2,3-dihydro-1,5-benzothiazepine
BIO7F2	RJF 01809	Copper metabolism	Rescue (5 μM)	Pyridin-pyrimidinone
BIO7G3	S 02850	Copper metabolism	Rescue (5 μM)	Carbamothioyl benzamide
BIO8A7	SJC 00393	Copper metabolism	Rescue (5 μM)	Thiosemicarbazone
BIO8C11	SPB 02722	Copper metabolism	Partial rescue (15 μM)	Benzoxazole derivate
BIO8F8	SPB 00258	Copper metabolism	Rescue (5 μM)	Thiosemicarbazone
BIO9C3	SPB 05679	Copper metabolism	Rescue (5 μM)	Pyridin-pyrimidinone
<b>BIO9D5</b>	<b>SPB 07427</b>	<b>Copper metabolism</b>	<b>Lethal (5 μM)</b>	<b>Thiadiazole derivate</b>
BIO9F4	SPB 07119	No pigmentation	Rescue (15 μM)	Thiosemicarbazone
CYTO10B10	SEW 06186	Copper metabolism	Rescue (5 μM)	Urea derivate (carboline-carboxamide)
CYTO10F4	SEW 01792	No pigmentation	Rescue (15 μM)	N-Hydroxy-benzamidine derivate
CYTO11A5	SPB 01039	Copper metabolism	Rescue (5 μM)	Triazole-thiol derivate
CYTO11B10	SPB 07027	Copper metabolism	Rescue (5 μM)	Thiosemicarbazone
CYTO11C10	SPB 07028	Copper metabolism	Rescue (5 μM)	Thiosemicarbazone
CYTO11D4	SPB 00779	No pigmentation	Rescue (5 μM)	Triazole-thiol
CYTO2A9	CD 02543	Copper metabolism	Rescue (5 μM)	Thiosemicarbazone
CYTO2E9	CD 03007	Copper metabolism	Rescue (5 μM)	Thiosemicarbazone
CYTO3A2	CD 06646	Copper metabolism	Rescue (5 μM)	Pyridin-pyrimidinone
CYTO3A6	DFP 00275	Copper metabolism	Rescue (5 μM)	Thio-urea derivate (carbamothioyl benzamide)
<b>CYTO4A11</b>	<b>JFD 00692</b>	<b>Copper metabolism</b>	<b>Rescue (5 μM)</b>	<b>Phenanthroline (cisplatin analogues)</b>
CYTO7C6	RF01893	Copper metabolism	Rescue (5 μM)	N-Hydroxy-benzamidine derivate
CYTO7D2	RDR00093	No pigmentation	Rescue (5 μM)	Thiourea derivate
CYTO7F2	RDR00691	Copper metabolism	Rescue (5 μM)	Thiosemicarbazone
CYTO8C11	S04201	Copper metabolism	Rescue (5 μM)	Thio-urea/Quinazolinone derivate
<b>CYTO8C5</b>	<b>RJF01649</b>	<b>Copper metabolism</b>	<b>Rescue (5 μM)</b>	<b>Pyridin-pyrimidinone</b>
CYTO9C5	S09668	Copper metabolism	Partial rescue (15 μM)	Thiourea derivatives
CYTO9D11	S14458	Copper metabolism	Rescue (5 μM)	Thiosemicarbazone

<sup>a</sup>Compounds used in yeast genetic profiling are indicated in a bold font. U0126 and PTT were found in the Sigma LOPAC screening library.

<sup>b</sup>Copper-metabolism phenotype is defined as having hypopigmentation, a wavy notochord and expanded hindbrain, as described for the copper-transport *atp7a*-mutant zebrafish (Mendelsohn et al., 2006) and shown in Fig. 1.

<sup>c</sup>Addition of copper chloride (5 μM or 15 μM) with the compound either rescued the copper-metabolism phenotype or caused lethality.

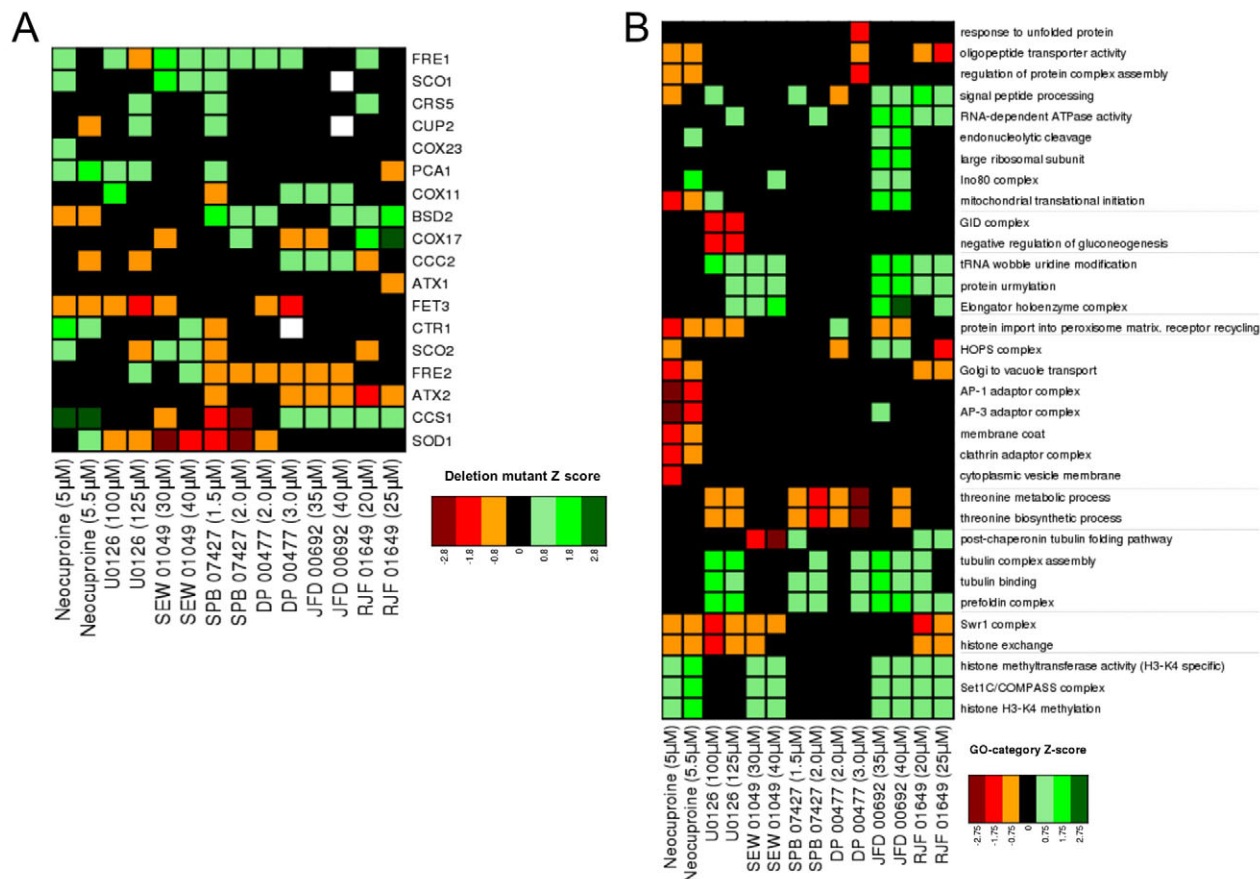


**Fig. 2. Yeast chemical-genetic profiles of small molecules that affect copper metabolism.** (A) Copper-pathway mutant strains that were specifically sensitive or resistant to U0126, neocuproine or the CM subset compounds. At least two concentrations for each compound were used for analysis. Genes with copper-dependent functions were compiled from Saccharomyces Genome Database (SGD, <http://www.yeastgenome.org>); this list includes copper-containing proteins and known factors in copper and/or iron transport and homeostasis. Color scale indicates degrees of sensitivity (red) or resistance (green); white indicates no data available in a given experiment. (B) Yeast chemical-genetic profiles reveal shared and distinct modes of action for CM subset compounds. A heatmap of GO biological process categories that correlated with sensitivity (red) or resistance (green) to different compounds is shown. Two different concentrations of each compound were screened. Scores for each GO category that contained at least four genes were calculated as the average z-score of all mutants in the category. GO categories contained in the heatmap represent the top 2% of affected categories. GO categories with overlapping gene sets are clustered (see also Table 2).

chemically induced copper deficiency. Copper transport into the cell by high-affinity transporters requires copper to be in the reduced Cu(I) state, which is dependent on the ferric and cupric (ferric/cupric) reductases Fre1 and Fre2 (De Freitas et al., 2003). In yeast, and in human disease, copper and iron homeostasis are intimately linked (De Freitas et al., 2003; van Bakel et al., 2005; Madsen and Gitlin, 2007a). We observed that both *fre1Δ* and *fre2Δ* strains were highly sensitive to copper starvation caused by different compounds. Finally, the iron transporters Fet3 and Fet5 are known copper-dependent enzymes, and we found that a *fet3Δ* strain was also highly sensitive to copper depletion. The effects of the CM subset on specific gene-deletion strains thus reflected action of compounds on copper homeostasis, as well as iron homeostasis (van Bakel et al., 2005; Rustici et al., 2007).

To understand the biological processes affected by the CM subset, we next assessed the Gene Ontology (GO) biological processes affected by each compound (Fig. 2B; Table 2; supplementary material Fig. S3; see Methods). Although each chemical caused a unique fingerprint of genetic sensitivity, several

core pathways were shared by the different compounds. These shared processes included mitochondrial translation initiation, the Swr1 histone-remodeling complex, tubulin-complex assembly, vacuolar organization and intracellular transport, and peroxisome formation. Many of these pathways are linked to copper homeostasis. For example, copper plays a vital role in mitochondrial function, such as in cytochrome *c* oxidase activity (Madsen and Gitlin, 2007b). Expression of the copper metallothionein gene in yeast is regulated by chromatin modification (Kuo et al., 2005), such that sensitivity of the Swr1 histone-exchange complex (Zilberman et al., 2008) to low-copper conditions might reflect inappropriate control of metallothionein (Kuo et al., 2005). Interestingly, loss of genes involved in threonine biosynthesis resulted in sensitivity to some CM subset compounds. Depletion of genes involved in the biosynthesis of certain amino acids causes sensitivity to multiple treatment conditions, including high-copper concentrations (Ericson et al., 2008; Hillenmeyer et al., 2008; Jo et al., 2008). However, genes involved in the threonine-biosynthesis pathway are not among

**Table 2. Genes within Gene Ontology (GO) category biological processes in Fig. 2**

GO category	Genes
Histone H3-K4 methylation	<i>BRE2, SDC1, SHG1, SPP1, SWD1, SWD3</i>
Protein import into peroxisome matrix	<i>DJP1, PEX10, PEX12, PEX18, PEX2, PEX21, PEX25, PEX13, PEX14, PEX17, PEX5, PEX7, PEX1, PEX15, PEX22, PEX4, PEX6</i>
Tubulin-complex assembly	<i>GIM3, GIM4, GIM5, PAC10, RBL2, YKE2</i>
Golgi-to-vacuole transport	<i>APL2, APL4, APL5, APL6, APM1, APM2, APM3, APS1, APS3, GGA1, GGA2, PEP12, PEP7, TLG2, VAM3, VAM7, VPS52 VPS53, VTH1, YPT7</i>
Swr1 complex	<i>ARP6, SWC3, SWC5, SWC7, SWR1, VPS71, VPS72, YAF9</i>
GID complex	<i>FYV10, GID7, GID8, RMD5, VID24, VID30</i>
$\alpha$ -subunit complex (proteasome core complex)	<i>PRE10, PRE5, PRE6, PRE8, PRE9, PUP2, SCL1</i>
Lid subcomplex (proteasome regulatory particle)	<i>RPN3, RPN5, RPN6, RPN7, RPN8, RPN9, RPN10, RPN11, RPN12, RPN13, SEM1</i>
Base subcomplex (proteasome regulatory particle)	<i>RPT1, RPT2, RPT3, RPT4, RPT5, RPT6, RPN1, RPN10, RPN12</i>

this known set of pleiotropic genes (Ericson et al., 2008; Hillenmeyer et al., 2008), suggesting a previously unknown relationship between threonine biosynthesis and copper metabolism in yeast.

The identification of strains defective in tubulin binding and assembly (Geissler et al., 1998) as resistant to copper starvation revealed an unexpected link between tubulin and copper homeostasis. Tubulins require post-translation folding, assembly into heterodimers, and then assembly into microtubules. In vitro and cell-based studies have shown that microtubules disassemble in excess copper (Liliom et al., 1999; Liliom et al., 2000; Nawaz et al., 2005; Pribyl et al., 2008; Liu et al., 2009). Copper might bind the sulfhydryl groups of microtubules and thereby block microtubule assembly and/or induce disassembly (Wallin et al., 1977). The GIM (genes involved in microtubule biogenesis) proteins are highly conserved and form a complex that promotes the formation of functional tubulins (Geissler et al., 1998). The *gimΔ* strains all have a slow-growth phenotype in rich medium, such that the resistance of *gimΔ* strains to copper limitation might reflect reduced activity of a copper-dependent process that normally inhibits tubulin biogenesis. This effect seems to be specific to the *gimΔ* strains because all other strains with a slow-growth phenotype did not suppress growth defects caused by copper depletion.

Copper transport is highly regulated in the cell and involves transport into the endoplasmic reticulum, as well as through secretory and vacuolar pathways for delivery to copper-dependent enzymes, copper excretion and copper detoxification (Yuan et al., 1997; Howell et al., 2006; Gonzalez et al., 2008; Jo et al., 2008; Jo et al., 2009). GO biological process category enrichment for cell growth in low-copper conditions revealed the importance of the AP1 adaptor complex, the AP3 adaptor complex, the HOPS complex, the clathrin adaptor complex and the Golgi-to-vacuole transport pathway. AP1, AP3 and HOPS complex subunits are highly conserved and mutated in some human genetic disorders (Dell'Angelica, 2009). Although disruption of the AP1, AP3 and HOPS complexes has not previously been shown to cause sensitivity to low-copper conditions, intracellular transport and vacuolar pathways share some overlap with sensitivity to iron homeostasis. For example, disruption of the AP3 adaptor complex in *aps3Δ* and *apm3Δ* strains causes sensitivity to both low-iron and low-copper conditions (Jo et al., 2009) (supplementary material Fig. S3). The

requirement for these pathways in the presence of low levels of copper might reflect the inability of copper to reach essential copper-dependent proteins, including the activity of copper-dependent proteins in iron homeostasis, such as Fet3.

Finally, yeast gene-deletion profiles uncovered an important role for the peroxisome in coping with copper depletion. We speculate this dependency arises because the copper-zinc SOD is a constituent enzyme of the peroxisome matrix, which is essential for its dismutase and peroxidase function (Titorenko and Mullen, 2006; Islinger et al., 2009). Deletions in other peroxisomal genes have also recently been shown to sensitize to low-iron conditions, possibly because of an elevated requirement for peroxisomal  $\beta$ -oxidation in energy production when iron-dependent mitochondrial energy production is impaired (Jo et al., 2009). A similar effect might occur upon copper deficiency because copper is also essential for mitochondrial functions and iron homeostasis. Notably, human disorders of peroxisome biogenesis such as Zellweger syndrome are characterized in part by high levels of copper and iron in blood and tissues (Wanders and Waterham, 2005).

### The MEK inhibitor U0126 elicits an unexpected copper-metabolism phenotype

The identification of U0126 in our zebrafish phenotypic screen is consistent with a recently suggested role for this MEK inhibitor in copper metabolism (Hawkins et al., 2008). Although U0126 partially phenocopies the *atp7a*-mutant zebrafish, the speculative link between MEK signaling and copper pathways has not been investigated (Hawkins et al., 2008). We thus set out to determine whether the copper-metabolism phenotype induced by U0126 in zebrafish development and in yeast chemical-genetic profiles was directly due to inhibition of MEK activity or whether U0126 might have an additional target in copper homeostasis independent of its activity as a MEK inhibitor.

We compared the U0126-induced phenotype with those induced by the selective MEK inhibitor PD0325901 and the known copper chelator neocuproine (Fig. 3A). In vitro kinase-inhibition profiles suggest that the MEK inhibitors CI-1040 and PD0325901 are the most highly selective inhibitors of MEK activity, as compared with U0126 and other commercially available compounds (Davies et al., 2000; Sebolt-Leopold, 2008). Despite

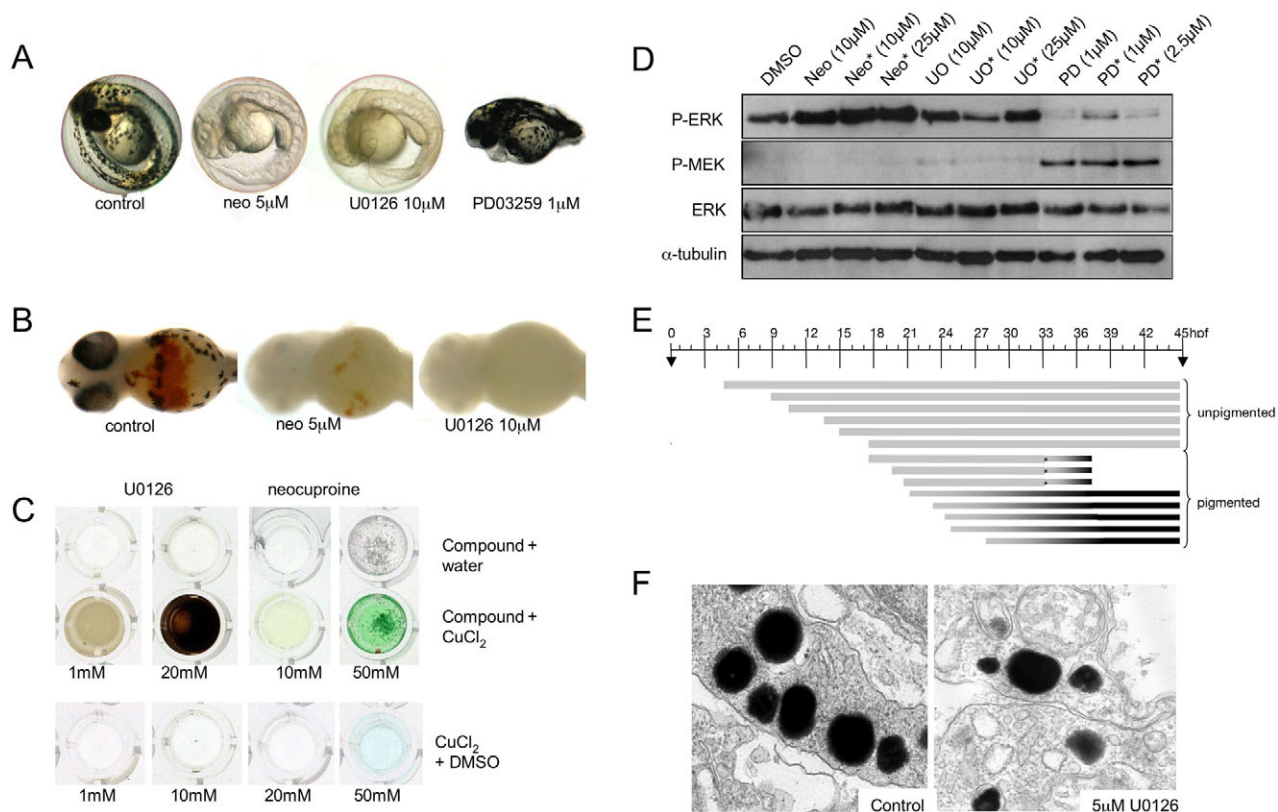


**Fig. 3. Phenotype elicited by U0126 treatment in zebrafish embryos.** (A) U0126 phenocopy of neocuproine (neo) in 2-day-old zebrafish embryos. As a control, the more selective MEK inhibitor PD0325901 did not affect pigmentation but instead prevented development of posterior features. (B) U0126 caused blood loss as detected by o-dianisidine (red) staining. (C) U0126 and neocuproine complex with copper, as indicated by color change upon addition to aqueous copper chloride solution. (D) Inhibition of MEK activity in vivo. Lysates from 12-hpf zebrafish embryos were assessed for phospho-ERK and phospho-MEK levels after treatment with PD0325901 (PD) and U0126 (UO). Note inhibitor treatment is known to increase phospho-MEK (Pratils et al., 2009). A short (2-hour) treatment (asterisk) with PD0325901 also reduced phospho-ERK levels in zebrafish embryos, demonstrating the elevated potency of PD0325901. (E) U0126 (10  $\mu$ M) treatments prevent pigmentation when administered before 21 hpf. When administered at 21 hpf or later, the embryos develop pigment at about 28 hpf, similar to untreated zebrafish embryos. U0126 treatments are each represented by a barline, and the color of the barline represents the color of the zebrafish melanocytes. The effects on pigmentation are reversible, and pigmentation can rapidly recover from U0126 treatment. For example, U0126-treated unpigmented 33 hpf zebrafish embryos recover pigmentation 4 hours after shifting to fresh embryo medium (asterisk). These phenotypes are consistent with a role for U0126 in blocking the copper-dependent pigmentation enzyme, tyrosinase (Rawls and Johnson, 2000). (F) Electron microscopy of 2-day-old untreated and U0126-treated (5  $\mu$ M) zebrafish embryos reveals smaller and less densely pigmented melanosomes in the latter.

the fact that the RAS-RAF-MEK-ERK signaling pathway plays an important role in melanoma development in humans, mice and zebrafish, we found that neither CI-1040 nor PD0325901 affects melanocyte pigmentation in zebrafish development (Fig. 3A) (see also Grzmil et al., 2007; Anastasaki et al., 2009). This result suggests that selective inhibition of MEK activity does not affect pigmentation in zebrafish melanocytes, and that the similarity between the U0126-induced phenotype and the *atp7a*-mutant phenotype most likely reflects a previously undetected additional target pathway for U0126 in copper homeostasis. Like neocuproine, U0126 also causes a loss of blood development in the embryo and an undulating notochord (Fig. 3A,B). In support of the hypothesis that U0126 can directly affect copper metabolism, we found that U0126, but not CI-1040, avidly binds copper in aqueous solution (Fig. 3C; supplementary material Fig. S4). Thus, despite its frequent use as a specific inhibitor of MEK kinase activity, our analysis based on pigment formation in zebrafish has identified a novel action for U0126 in vivo.

Western blotting of extracts from treated zebrafish embryos with an anti-phospho-ERK antibody confirmed that PD0325901 and U0126 both effectively inhibit MEK activity during development, whereas neocuproine had no obvious inhibitory effect on phospho-ERK levels in zebrafish (Fig. 3D) or in human cells (supplementary material Fig. S7). PD0325901 was a substantially more potent inhibitor than U0126 as a 2-hour treatment was sufficient to strongly inhibit ERK activity (Fig. 3D). To study the U0126-induced pigmentation phenotype in more detail, we mapped the timing of action of U0126 on developing melanocytes (Fig. 3E). In zebrafish development, melanocytes develop from the neural crest and become pigmented at about 28 hpf. Treatment with U0126 after 21 hpf did not affect normal melanocyte pigmentation, whereas treatment before 21 hpf prevented pigmentation; this effect was not a permanent developmental defect as melanocyte pigmentation rapidly recovered after U0126 wash-out (Fig. 3E). By electron microscopy, we also found evidence of fewer and less-dense melanosomes in melanocytes of embryos treated with 5  $\mu$ M of

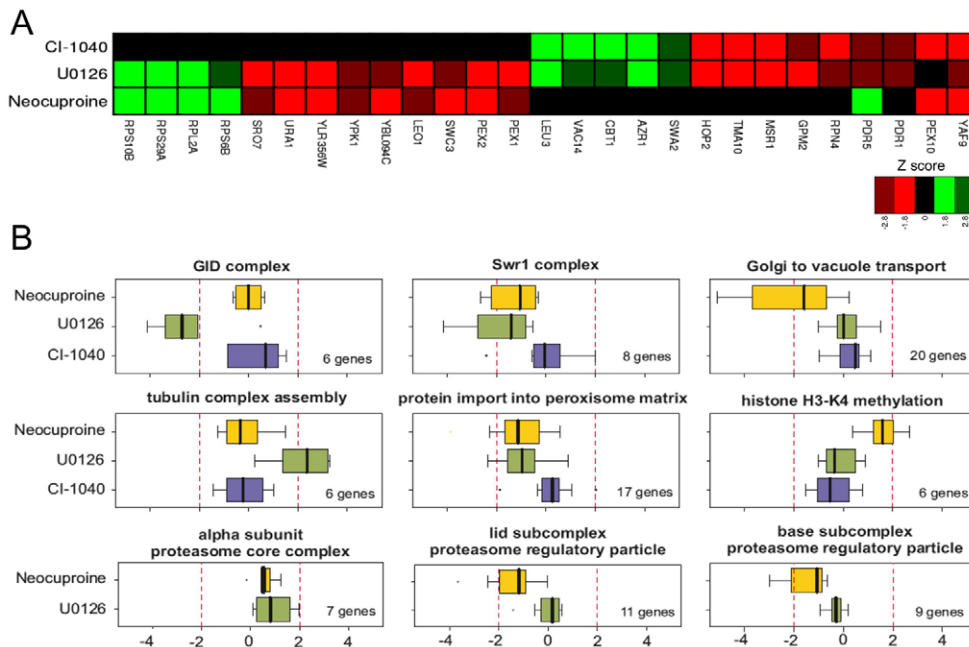


**Fig. 4. Novel target pathways for the MEK inhibitor U0126.** (A) Heat map of deletion strains that are sensitive (red) or resistant (green) to U0126, neocuproine and CI-1040. U0126 shares a chemical profile with neocuproine and with CI-1040, whereas neocuproine and CI-1040 do not share a common profile. (B) Neocuproine (yellow), U0126 (green) and CI-1040 (blue) treatment affect common and distinct biological processes. GO categories were examined for each of the deletion mutants that were affected by each compound (see Table 2). The genes in a specific GO category were compared with the number of strains actually affected by each compound and the *P* values determined. Only GO categories with more than four genes were examined and only *P* values <0.05 were considered.

U0126 (Fig. 3F). The timing of action of U0126 on melanocyte pigmentation is consistent with the known kinetics of appearance of the rate-limiting copper-dependent enzyme tyrosinase in development (Hultman and Johnson, 2010).

We compared the genome-wide chemical-genetic profiles of U0126, CI-1040 and neocuproine to determine the potential target pathways of U0126. These profiles revealed that 13 deletion strains were sensitive to both U0126 and neocuproine, and that 12 deletion strains exhibited shared sensitivities to U0126 and CI-1040 (Fig. 4A). By contrast, only the *pep10Δ* strain was sensitive to both CI-1040 and neocuproine, and only the *yaf9* strain was sensitive to all three compounds. Therefore, although U0126 has a partially overlapping chemical-genetic fingerprint with CI-1040 and neocuproine, CI-1040 and neocuproine have overtly different activities. These profiles are fully consistent with the shared molecular phenotype between U0126 and CI-1040 of inhibition of ERK phosphorylation in zebrafish lysates (Fig. 3D), and the shared developmental and chemical phenotype between U0126 and neocuproine (Fig. 3A).

Comparison of GO biological processes (Table 2) affected by the different inhibitors revealed both shared and distinct processes. Disruption of the peroxisome and the Swr1 histone-exchange complexes caused sensitivity to both U0126 and neocuproine (Fig. 4B). Impaired intracellular transport and the function of the proteasome 19S regulatory particle compromised growth only in the presence of neocuproine. Loss of the GID ubiquitin ligase complex reduced growth in the presence of U0126, whereas disruption of tubulin-binding processes actually led to resistance in the presence of U0126 (Fig. 4B). A comparison of GO processes affected by the CM subset compounds and CI-1040 allowed us to determine whether the U0126 target pathways were due to copper-dependent pathways, MEK pathways or additional target pathways. Whereas CI-1040 and neocuproine had no effect on tubulin binding and tubulin-complex assembly, treatment with SPB07427,

DP00477, JFD00692 and RJF01649 caused resistance of strains defective in tubulin binding and tubulin-complex assembly. Given the shared zebrafish and yeast phenotypes between U0126 and these compounds, it seems that U0126 acts on tubulin-associated processes via alterations in copper metabolism. Notably, in contrast to the shared chemical profiles between U0126, neocuproine and CI-1040, mutations in all six components of the GID complex resulted in high sensitivity to U0126 (Fig. 3B, Fig. 4B). The GID complex is an E3 ubiquitin ligase that targets a key enzyme in gluconeogenesis, fructose 1,6-bisphosphatase (FBPase), for proteasomal degradation (Santt et al., 2008). With the exception of neocuproine, the GID complex also showed sensitivity to CM subset compounds, albeit most strongly with U0126 (Fig. 2; supplementary material Fig. S3). The GID complex might thus represent a new target of copper metabolism in yeast. Collectively, these data reveal new copper-dependent target pathways for U0126, which have remained cryptic despite the extensive use of U0126 in biochemical and cell biological assays in many different signaling contexts.

#### Knockdown of trafficking components sensitizes zebrafish to copper-dependent hypopigmentation

Intracellular transport pathways, although essential for all cells, have a specific role in melanosome biogenesis. Pigmentation enzymes and the copper transporter ATP7A are selectively transported from the trans-Golgi network to the maturing melanosomes (Raposo and Marks, 2007; Setty et al., 2008). To test whether the genes that affect copper sensitivity in yeast might inform about relevant copper pathways in melanocytes, we selected two genes that had orthologs in zebrafish for knockdown by morpholino oligonucleotides (MOs) in the developing embryo. For this purpose we designed MOs against genes that encode a component of the AP1 transport complex (*APS1* in yeast, *ap1s1* in zebrafish) and a component of the AP3 transport complex (*APS3* in yeast, *ap3s2* in zebrafish)

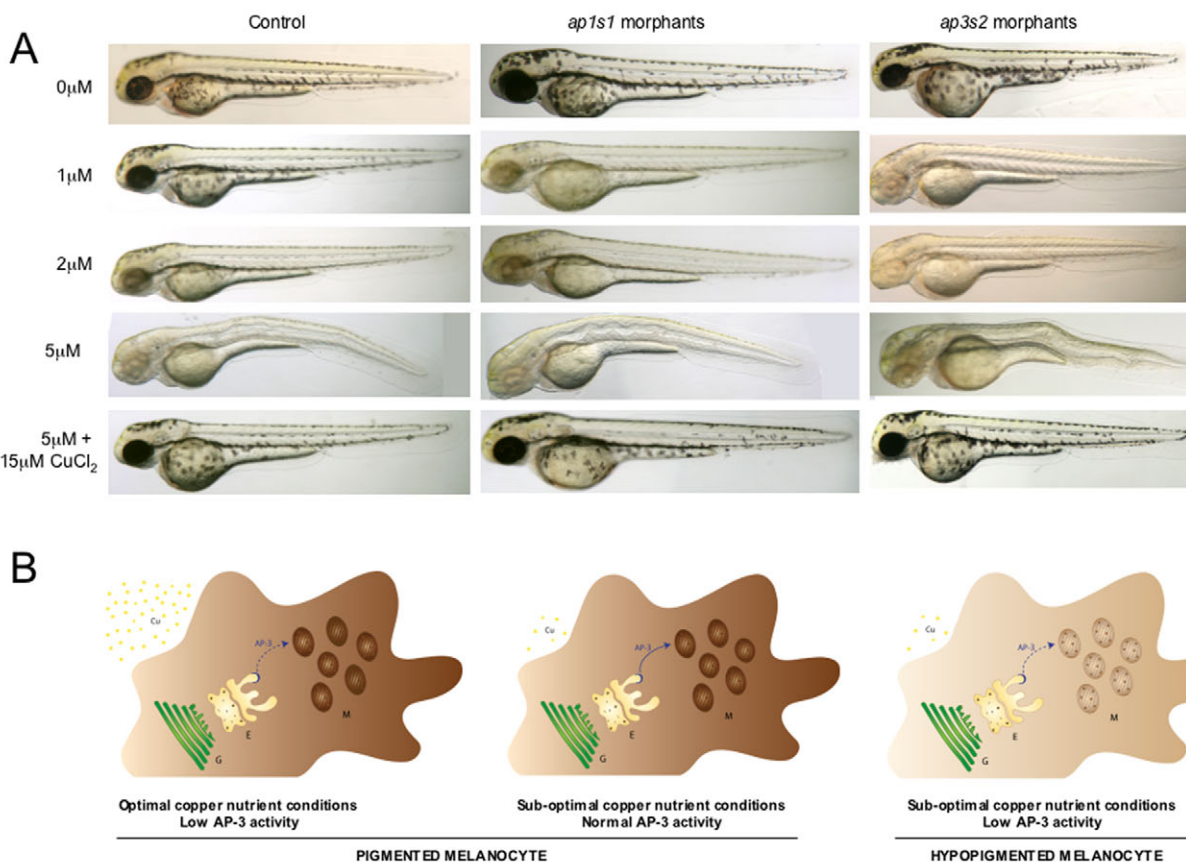


**Fig. 5. Identification of two new gene-nutrient interactions in melanocyte pigmentation.** Morpholino oligonucleotides (1-3 pg) directed against *ap1s1* and *ap3s2* result in morphants with normal development and pigmentation. Higher concentrations of *ap1s1*-MO have been reported to cause pigmentation phenotypes (Montpetit et al., 2008). Treatment with 5 μM neocuproine caused a copper-deficiency phenotype in all animals that could be rescued with the addition of 15 μM copper chloride. At a concentration of 1.0 μM neocuproine, copper limitation caused a loss of pigmentation in the *ap3s2* morphants compared with control-treated embryos, and a severe loss of pigmentation at 2 μM neocuproine, compared with mild (1 μM) to moderate (2 μM) loss of pigmentation in control animals. A milder pigmentation phenotype was also visible in the *ap1s1* morphants treated with 1 μM neocuproine. Experiments were repeated multiple times (more than three times for each morpholino;  $n > 20$  per treatment), and similar results could be obtained with an additional splice-site MO designed to target each gene (see Methods). (B) Simplified schematic of gene-copper interactions in a zebrafish melanocyte. Partial reduction of AP3 complex activity (such as in the *ap3s2* morphant; represented by a dotted line) retains sufficient AP3 activity for melanosome pigmentation in optimal-copper nutrient conditions, and the melanocyte is darkly pigmented. Likewise, melanocytes with normal AP3 activity in suboptimal-copper nutrient conditions retain the ability to generate pigment. By contrast, in low-copper nutrient conditions, reduced AP3 function is no longer sufficient for promoting proper melanosome maturation, and the melanocytes are hypopigmented. Cu, copper; E, endosomal bodies; G, trans-Golgi network; M, melanosomes.

(supplementary material Fig. S5). We separately injected a splice-site MO designed against *ap3s2* (*ap3s2*-MO1) and a translation-blocking MO designed against *ap1s1* (*ap1s1*-MO1) (Montpetit et al., 2008) into single-celled zebrafish embryos and monitored development in low-neocuproine conditions. Splice-site MOs were verified by PCR analysis (supplementary material Fig. S6). At low MO concentrations (1-3 pg), the *ap1s1* and *ap3s2* morphants developed normally to at least 2 days pf (Fig. 5A). Next, we treated 4-6 hpf morphants with a range of neocuproine concentrations (1 μM, 2 μM and 5 μM) and followed the development of the treated animals over 2 days. Without neocuproine, neither the uninjected controls nor the morphant animals displayed any of the principal features of developmental copper deficiency, including reduced pigmentation, a buckling notochord or an expanded hindbrain (Fig. 5A). This result suggests that under optimal nutrition conditions, partial reduction of *ap1s1* or *ap3s2* function does not affect

development of the zebrafish embryo. At 5 μM neocuproine, developing wild-type and morphant embryos exhibited features of developmental copper-metabolism deficiency, which could be prevented with the addition of exogenous copper chloride at a concentration of 5 μM (Fig. 5A). At intermediate neocuproine concentrations (1 μM, 2 μM), we often observed severe hypopigmentation in the *ap3s2* morphants ( $n=37/71$  embryos), whereas control animals exhibited only a mild (at 1 μM) to moderate (at 2 μM) reduction in melanocyte pigmentation ( $n > 100$ ). The *ap1s1* morphants also displayed melanocyte pigmentation sensitivity at 1 μM neocuproine ( $n=13/39$ ) compared with the control-treated animals. A similar effect was seen using the splice-site MOs *ap3s2* (*ap3s2*-MO2) and *ap1s1* (*ap1s1*-MO2) (see Methods). Thus, at least two of the yeast intracellular transport pathways that affected sensitivity to the CM subset compounds proved to be physiologically relevant in the developing vertebrate.

## DISCUSSION

Identification of the allelic variants that underlie gene-nutrient interactions is important for understanding the genetic differences between individuals that contribute to disease susceptibility (Thiele and Gitlin, 2008). We used the zebrafish and yeast model systems to identify small molecules that affect copper metabolism, to uncover conserved cognate genetic pathways that sensitize to copper deficiency and to test physiological relevance of these pathways in zebrafish (Fig. 1A). The identification of the dual targets of the commonly used MEK inhibitor U0126 underscores the power of a combined zebrafish and yeast platform to elucidate multiple target pathways of small molecules *in vivo*.

The conservation of copper-metabolism pathways in yeast, zebrafish and humans suggests that our analysis of genetic sensitivities to copper limitation can provide insight into the molecular pathogenesis of hypocupremia. Comparison of the chemical profiles of the five copper chelators identified by phenotypic screening, as well as neocuproine and U0126, revealed a substantial overlap in target pathways, including intracellular transport pathways. Intracellular trafficking is crucial for transport of copper to copper-dependent enzymes, recycling of the copper transporter ATP7a, and also for copper detoxification in environments of high copper concentrations (Jo et al., 2008). In melanocytes, ATP7A itself is transported to maturing melanosomes in order to restrict the activation of copper-dependent pigmentation enzymes, such as tyrosinase, to this specialized structure (Setty et al., 2008). Tyrosinase, as well as other pigmentation enzymes, is selectively transported to the maturing melanosome by components of the AP1 and AP3 complex; another transporter, the BLOC-1 complex, is required for the selective transport of ATP7A (Wei, 2006; Raposo and Marks, 2007). Known but rare alleles of the AP3 gene give rise to the disorder HPS, and AP1s1 components are mutated in a neurocutaneous syndrome that is characterized by mental retardation, enteropathy, deafness, peripheral neuropathy, ichthyosis and keratoderma, termed MEDNIK. Our yeast and zebrafish data suggest that reduced but otherwise functional levels of AP1 and AP3 that have no effect on pigmentation in optimal nutritional conditions can cause dramatic effects on pigmentation under reduced-copper nutrition conditions (Fig. 5B). The combination of zebrafish and yeast screens might be particularly suited to detection of gene-environment interactions in vertebrates that are characterized by allelic variants of modest quantitative effect (Manolio et al., 2009).

Phenotypic and genome-scale genetic analysis in model organisms is an effective method for identifying new target pathways for known and novel compounds. A major question in chemical biology is how a chemically induced phenotype relates to the *in vivo* mechanism of compound action and how this knowledge can be exploited to predict off-target effects. Biochemical, *in silico* and cell-based methods are usually applied in an effort to identify molecular targets, but these approaches can often fail because of limitations in sensitivity and specificity. Predicted drug-target associations of 3665 US Food and Drug Administration (FDA)-approved drugs and other pharmaceutical agents correctly identified 23 new molecular targets for known drugs (Keiser et al., 2009). However, a molecular target under a specific experimental context does not always reflect the action of the compound within the complexity of the developing animal, as

illustrated by the unexpected copper-dependent effects of the MEK inhibitor U0126 in our study. Although not all processes or genes are conserved between yeast, zebrafish and human, we note that complex disease states often converge on highly conserved gene networks (Tan et al., 2009), suggesting that the zebrafish-yeast screening approach might be applicable to many other human genetic diseases. To our knowledge, our study is the first to explicitly couple phenotype-based screens in zebrafish to genome-wide chemical-genetic profiles in yeast in order to identify gene-environment interactions during animal development. This approach holds promise for interrogating networks of gene-environment interactions in other complex human genetic diseases.

## METHODS

### Zebrafish husbandry and phenotypic screening

Zebrafish were raised and maintained in compliance with the Animals (Scientific Procedures) Act 1986 of the UK. Embryos were acquired by pair breedings of wild-type AB, AB\* and TL zebrafish lines. For small-molecule screening, two 4-hpf zebrafish embryos were arrayed in 96-well plates, and 300  $\mu$ l of E3 embryo medium (Westerfield, 2000) with 10  $\mu$ M of compound in 1% DMSO was added. Compounds were from the LOPAC (1280) Small Scale International Version (Sigma-Aldrich) and a subselection of the Maybridge screening collection (Fisher Scientific International). Embryos were assessed and imaged for phenotypic changes at 28 hpf, 36 hpf, 48 hpf and 56 hpf. Small molecules that prevented pigmentation, and caused an expanded hindbrain and a wavy notochord, were classed as having a copper-metabolism phenotype. The classification was confirmed by treating developing embryos with freshly prepared compound in the presence or absence of excess copper chloride at concentrations of 5  $\mu$ M and 15  $\mu$ M. CI-1040 was kindly provided by Richard Marais (London, UK) and PD0325901 was obtained from Hilary McLauchlan (University of Dundee, UK). Embryos were treated with 10  $\mu$ M or 25  $\mu$ M neocuproine or U0126 and 1  $\mu$ M or 2.5  $\mu$ M PD0325901 at different developmental stages. To inhibit pathway activity during development, 4 hpf embryos were treated with compounds continuously until 12 hpf; acute effects were assessed using a pulse of compound from 10 hpf to 12 hpf.

### Western blotting

Embryos (12 hpf) were frozen at  $-80^{\circ}\text{C}$  after removal of the embryo buffer. Samples were lysed in RIPA buffer [2 M Tris pH 7.5, 5 M NaCl, 1% NP40, Na-deoxycholate, 10% SDS, 0.5 M NaF, 1 M  $\beta$ -glycosyl phosphate and protease-inhibitor cocktail tablet (Roche)]. Samples were normalized by protein as measured by Bradford assay, separated by SDS-PAGE, transferred to Hybond-C Extra nitrocellulose membrane (Amersham Biosciences), probed with rabbit [p44/42 MAPK (1:2000) and phospho-MEK1/2 (Ser217/221) (1:500) (Cell Signaling Technology)] or mouse [phospho-p44/42 MAPK (E10) (1:2000), alpha-tubulin B-5-1-2 (1:50,000) (Santa Cruz)] antibodies and detected with horseradish-peroxidase-conjugated secondary antibodies (Roche).

### Electron microscopy

Embryos were fixed with 2.5% glutaraldehyde, 2% paraformaldehyde in 100 mM cacodylate buffer (pH 7.2) with 2 mM  $\text{MgCl}_2$  and 0.1% picric acid. Following a wash with 200 mM



cacodylate buffer, samples were fixed with 1% osmium tetroxide in 100 mM cacodylate buffer (pH 7.0), washed with distilled water, stained en bloc with 0.5% aqueous uranyl acetate, and dehydrated with ethanol. Samples were embedded in Agar 100 resin and sections were cut, stained with lead citrate and viewed on a FEI Tecnai 12 transmission electron microscope.

### Yeast chemical-genetic profiles

The *MATa* haploid and the essential heterozygous yeast deletion sets were obtained from Research Genetics (Germany). Chemical-genetic profiles were generated essentially as described (Giaever et al., 2002). Briefly, for growth-inhibition screens, 5-ml pool cultures were seeded at an OD<sub>600</sub> of 0.025 and compound (or DMSO for control samples) was added after a 2-h pre-growth period. Compound concentrations were selected to inhibit pool growth by 20-30% compared with DMSO controls at 12 hours; cultures were diluted back to an OD<sub>600</sub> of 0.025 twice with addition of fresh compound to allow growth for a total of 20 generations. Each compound was screened at two different concentrations (supplementary material Table S1). The final concentration of DMSO was 0.4% for all screens. Genomic DNA was isolated for control and experimental pools, barcodes were amplified with fluorescently labeled primers, and PCR products were hybridized to in-house short-oligonucleotide microarrays (Cook et al., 2008). A GenePix 4200AL was used to scan the slides, and hybridization intensity for each spot was determined using GenePix Pro 6.0 software.

### Identification of sensitive and resistant mutant strains

The identification of sensitive and resistant strains in the chemical-genetic screens was performed using R and limma, an R package for the analysis of gene expression microarray data. Spots with low intensity and low quality were excluded from further analysis. Intensities of duplicate spots for each barcode on the array were averaged. *z*-scores for up and down barcode tags were calculated based on log<sub>2</sub> fold-change ratios (compound treated vs DMSO control):  $z = (x - \mu) / \sigma$  where  $\mu$  is the mean log<sub>2</sub>-fold change for all up or down barcodes on an array and  $\sigma$  is the standard deviation. The two barcode scores were averaged for each deletion strain to give the final *z*-score. Microarray raw data and *z*-scores for each mutant were stored in a custom MySQL database. Standard procedures for *z*-score and quantile-based statistics for microarray data were used to identify sensitive and resistant deletion strains (Quackenbush, 2002; Cheadle et al., 2003). The microarray data are available at ArrayExpress (accession number E-TABM-922).

### Assignment of GO biological process terms

Instead of relying on arbitrary cut-offs to define enriched sets of deletion strains that were most affected by treatment with the compounds, we calculated average *z*-scores for all GO biological process categories in each experiment for GO categories that contained data for at least four genes. Quartile-based statistics were used to identify significantly affected GO biological processes (Saccharomyces Genome Database, <http://www.yeastgenome.org>, release 02/07/2009).

### Morpholino oligonucleotides

The MOs were designed by GeneTools (USA) and prepared as a 1 mM stock solution in water. For Fig. 5A, 1-3 pg was injected into

## TRANSLATIONAL IMPACT

### Clinical issue

Genetic differences contribute to the variation among individuals in coping with environmental stresses, such as nutritional deficiency. Copper is an essential nutrient, and disorders of copper metabolism can lead to severe neuronal, muscular and pigmentation clinical symptoms. Genetic mutations in the copper transporter ATP7A lead to a copper-deficiency syndrome called Menkes disease, and copper deficiency can also develop after intestinal bypass surgery or an excess intake of iron. However, many causes of copper deficiency are unknown, and genetic factors might contribute to the sensitivity of some individuals to reduced nutritional availability of copper.

### Results

Many crucial enzymes require copper as a cofactor, and melanocytes have a specific requirement for copper in the maturation of pigmented melanosomes. Here, the authors use a zebrafish- and yeast-based approach to identify genetic pathways that modulate melanocyte pigmentation in conditions of copper nutritional deficiency. First, they carry out a chemical screen for small molecules that affect copper homeostasis in zebrafish on the basis of a hypopigmentation phenotype. Next, they use budding yeast to systematically map the genetic pathways that underlie sensitivity to the small molecules identified in the zebrafish-based chemical screen. They then demonstrate that two genes encoding intracellular transport proteins identified in the yeast genetic screen are physiologically relevant, as their zebrafish orthologs, *aps1s* and *aps2s*, are involved in sensitizing zebrafish melanocytes to hypopigmentation in conditions of mild copper deficiency. Notably, the authors also use the zebrafish-yeast approach to identify an off-target effect for a small molecule commonly used in cell-signaling studies, the MEK inhibitor U0126, which was previously not known to affect pathways of copper metabolism.

### Implications and future directions

The copper-gene interactions identified in this study illustrate the larger issue of how disease susceptibility can be underpinned by complex environment-gene interactions. This zebrafish-yeast approach will be applicable to the dissection of many complex disease-gene networks, particularly because such networks are enriched for highly conserved genes. This approach is also well suited for investigating gene-environment interactions, which are a challenge to assess given that modest genetic effects can be difficult to identify through classical quantitative methods. Importantly, the zebrafish-yeast approach provides a systematic means by which to elucidate the *in vivo* actions of small molecules in a vertebrate system, which is a challenge in chemical biology applications. Finally, the identification of copper-metabolism pathways in zebrafish is a starting point for exploring the role of analogous pathways in human diseases of copper deficiency.

doi:10.1242/dmm.006205

each one-cell stage embryo. MO sequences were designed to block splicing for a zebrafish ortholog of the yeast gene *APS3*, called *aps3s2* (Ensembl(Zv8): ENSDARG00000039882) (*aps3s2-MO1*: 5'-TGCAAAGCCTCTCCATCACCTTCC-3'). Confirmation of *aps3s2-MO1* activity was determined by PCR with primers AP3S2-F1 [5'-TCAACAACCATGGGAAACCC-3' (forward primer)] and AP3S2-R1 [5'-TGAAGTGCAGAAACGGCTCG-3' (reverse primer)]. Inclusion of intron 2 was determined by sequencing of the longer cDNA product. A translation-block MO for *aps1s1* (Ensembl(Zv8): ENSDARG00000056803), an ortholog of *APS1*, was directly purchased from GeneTools (*aps1s1-MO1*: 5'-ACAGA-AGCATAAAGCGCATCATTTC-3'), and has been previously verified by western blotting morphant embryo extracts with an antibody (Montpetit et al., 2008). Two additional splice-site MOs were designed and ordered from GeneTools: *aps3s2-MO2*

(5'-TGCAGTTACGTTACCTGTATAAGA-3') and *ap1s1-MO2* (5'-GACTAGCATACCTACGTAAACACAC-3') (Montpetit et al., 2008). Confirmation of *ap3s2-MO2* activity was determined by PCR with primers AP3S2-F2 [5'-TGCAGCAGCAGATCATCAGGG-3' (forward primer)] and AP3S2-R2 [5'-GACTGTCAGTAATGG-CAAGAGG-3' (reverse primer)]. Results were consistent with both MOs for each gene, with greater effects seen with increasing concentration of MO (5-10 pg). All MOs were labeled with a fluorescent tag and assessed for even MO distribution throughout the embryo. Changes in pigmentation were assessed by two or three individuals who scored the phenotypes blinded to the MO genotypes.

#### ACKNOWLEDGEMENTS

We are grateful to David Harrison for many helpful discussions and on-going support of this work. We thank Karthikeyani Paranthaman for zebrafish husbandry, Nicola Grant for artwork, Phillipe Gautier (for figure S4), and Nick Temperley and John Maule for technical assistance. We are grateful to Ian Jackson, Veronica van Heyningen, Nick Hastie, Corey Nislow, Lea Harrington, Robert Kelsh and Chris Norbury for helpful discussions and critical reading of the manuscript. This work was funded by the Medical Research Scotland (H.I., E.E.P.), National Institutes of Health (J.D.G.), the European Research Council (M.T.), the Canadian Institutes for Health Research Operating Grant MOP-79488 (M.T.), the Scottish Universities Life Sciences Alliance (M.T.), a Royal Society Wolfson Award (M.T.), the Wellcome Trust (E.E.P.), and an MRC Career Development Award (E.E.P.). Deposited in PMC for release after 6 months.

#### COMPETING INTERESTS

The authors declare no financial, personal or professional associations that interfere with the objectivity of this study.

#### AUTHOR CONTRIBUTIONS

H.I. and M.S. conceived, designed and performed experiments, and J.W., C.A., Z.Z., M.S., E.M. and E.E.P. performed experiments and analyzed data. S.D., J.G. and R.M. contributed to experimental design and provided reagents. M.T. and E.E.P. conceived and designed experiments, and wrote the paper.

#### SUPPLEMENTARY MATERIAL

Supplementary material for this article is available at <http://dmm.biologists.org/lookup/suppl/doi:10.1242/dmm.005769/-DC1>

Received 2 April 2010; Accepted 27 May 2010.

#### REFERENCES

- Anastasaki, C., Estep, A. L., Marais, R., Rauen, K. A. and Patton, E. E. (2009). Kinase-activating and kinase-impaired cardio-facio-cutaneous syndrome alleles have activity during zebrafish development and are sensitive to small molecule inhibitors. *Hum. Mol. Genet.* **18**, 2543-2554.
- Boone, C., Bussey, H. and Andrews, B. J. (2007). Exploring genetic interactions and networks with yeast. *Nat. Rev. Genet.* **8**, 437-449.
- Cheadle, C., Vawter, M. P., Freed, W. J. and Becker, K. G. (2003). Analysis of microarray data using Z score transformation. *J. Mol. Diagn.* **5**, 73-81.
- Chin, L., Garraway, L. A. and Fisher, D. E. (2006). Malignant melanoma: genetics and therapeutics in the genomic era. *Genes Dev.* **20**, 2149-2182.
- Cook, M. A., Chan, C. K., Jorgensen, P., Ketela, T., So, D., Tyers, M. and Ho, C. Y. (2008). Systematic validation and atomic force microscopy of non-covalent short oligonucleotide barcode microarrays. *PLoS One* **3**, e1546.
- Danks, D. M., Campbell, P. E., Walker-Smith, J., Stevens, B. J., Gillespie, J. M., Blomfield, J. and Turner, B. (1972). Menkes' kinky-hair syndrome. *Lancet* **1**, 1100-1102.
- Davies, S. P., Reddy, H., Caivano, M. and Cohen, P. (2000). Specificity and mechanism of action of some commonly used protein kinase inhibitors. *Biochem. J.* **351**, 95-105.
- De Freitas, J., Wintz, H., Kim, J. H., Poynton, H., Fox, T. and Vulpe, C. (2003). Yeast, a model organism for iron and copper metabolism studies. *Biomaterials* **16**, 185-197.
- Dell'Angelica, E. C. (2009). AP-3-dependent trafficking and disease: the first decade. *Curr. Opin. Cell Biol.* **21**, 552-559.
- Ericson, E., Gebbia, M., Heisler, L. E., Wildenhain, J., Tyers, M., Giaever, G. and Nislow, C. (2008). Off-target effects of psychoactive drugs revealed by genome-wide assays in yeast. *PLoS Genet.* **4**, e1000151.
- Geissler, S., Siegers, K. and Schiebel, E. (1998). A novel protein complex promoting formation of functional alpha- and gamma-tubulin. *EMBO J.* **17**, 952-966.
- Giaever, G., Chu, A. M., Ni, L., Connelly, C., Riles, L., Veronneau, S., Dow, S., Lucau-Danila, A., Anderson, K., Andre, B. et al. (2002). Functional profiling of the *Saccharomyces cerevisiae* genome. *Nature* **418**, 387-391.
- Gonzalez, M., Reyes-Jara, A., Suazo, M., Jo, W. J. and Vulpe, C. (2008). Expression of copper-related genes in response to copper load. *Am. J. Clin. Nutr.* **88**, 830S-834S.
- Grzmil, M., Whiting, D., Maule, J., Anastasaki, C., Amatruda, J. F., Kelsh, R. N., Norbury, C. J. and Patton, E. E. (2007). The INT6 cancer gene and MEK signaling pathways converge during zebrafish development. *PLoS One* **2**, e959.
- Hartwell, L. H., Szankasi, P., Roberts, C. J., Murray, A. W. and Friend, S. H. (1997). Integrating genetic approaches into the discovery of anticancer drugs. *Science* **278**, 1064-1068.
- Hawkins, T. A., Cavodeassi, F., Erdelyi, F., Szabo, G. and Lele, Z. (2008). The small molecule Mek1/2 inhibitor U0126 disrupts the chordamesoderm to notochord transition in zebrafish. *BMC Dev. Biol.* **8**, 42.
- Hillenmeyer, M. E., Fung, E., Wildenhain, J., Pierce, S. E., Hoon, S., Lee, W., Proctor, M., St Onge, R. P., Tyers, M., Koller, D. et al. (2008). The chemical genomic portrait of yeast: uncovering a phenotype for all genes. *Science* **320**, 362-365.
- Howell, G. J., Holloway, Z. G., Cobbald, C., Monaco, A. P. and Ponnambalam, S. (2006). Cell biology of membrane trafficking in human disease. *Int. Rev. Cytol.* **252**, 1-69.
- Hultman, K. A. and Johnson, S. L. (2010). Differential contribution of direct-developing and stem cell-derived melanocytes to the zebrafish larval pigment pattern. *Dev. Biol.* **337**, 425-431.
- Islinger, M., Li, K. W., Seitz, J., Volk, A. and Luers, G. H. (2009). Hitchhiking of Cu/Zn superoxide dismutase to peroxisomes-evidence for a natural piggyback import mechanism in mammals. *Traffic* **10**, 1711-1721.
- Jo, W. J., Loguinov, A., Chang, M., Wintz, H., Nislow, C., Arkin, A. P., Giaever, G. and Vulpe, C. D. (2008). Identification of genes involved in the toxic response of *Saccharomyces cerevisiae* against iron and copper overload by parallel analysis of deletion mutants. *Toxicol. Sci.* **101**, 140-151.
- Jo, W. J., Kim, J. H., Oh, E., Jaramillo, D., Holman, P., Loguinov, A. V., Arkin, A. P., Nislow, C., Giaever, G. and Vulpe, C. D. (2009). Novel insights into iron metabolism by integrating deletome and transcriptome analysis in an iron deficiency model of the yeast *Saccharomyces cerevisiae*. *BMC Genomics* **10**, 130.
- Keiser, M. J., Setola, V., Irwin, J. J., Laggner, C., Abbas, A. I., Hufeisen, S. J., Jensen, N. H., Kuijter, M. B., Matos, R. C., Tran, T. B. et al. (2009). Predicting new molecular targets for known drugs. *Nature* **462**, 175-181.
- Kumar, N. (2006). Copper deficiency myelopathy (human swayback). *Mayo Clin. Proc.* **81**, 1371-1384.
- Kuo, H. C., Moore, J. D. and Krebs, J. E. (2005). Histone H2A and Spt10 cooperate to regulate induction and autoregulation of the CUP1 metallothionein. *J. Biol. Chem.* **280**, 104-111.
- Liliom, K., Wagner, G., Kovacs, J., Comin, B., Cascante, M., Orosz, F. and Ovadi, J. (1999). Combined enhancement of microtubule assembly and glucose metabolism in neuronal systems in vitro: decreased sensitivity to copper toxicity. *Biochem. Biophys. Res. Commun.* **264**, 605-610.
- Liliom, K., Wagner, G., Pacz, A., Cascante, M., Kovacs, J. and Ovadi, J. (2000). Organization-dependent effects of toxic bivalent ions microtubule assembly and glycolysis. *Eur. J. Biochem.* **267**, 4731-4739.
- Liu, D., Xue, P., Meng, Q., Zou, J., Gu, J. and Jiang, W. (2009). Pb/Cu effects on the organization of microtubule cytoskeleton in interphase and mitotic cells of *Allium sativum* L. *Plant Cell Rep.* **28**, 695-702.
- Lum, P. Y., Armour, C. D., Stepanians, S. B., Cavet, G., Wolf, M. K., Butler, J. S., Hinshaw, J. C., Garnier, P., Prestwich, G. D., Leonardson, A. et al. (2004). Discovering modes of action for therapeutic compounds using a genome-wide screen of yeast heterozygotes. *Cell* **116**, 121-137.
- Madsen, E. and Gitlin, J. D. (2007a). Copper and iron disorders of the brain. *Annu. Rev. Neurosci.* **30**, 317-337.
- Madsen, E. and Gitlin, J. D. (2007b). Copper deficiency. *Curr. Opin. Gastroenterol.* **23**, 187-192.
- Madsen, E. C. and Gitlin, J. D. (2008). Zebrafish mutants calamity and catastrophe define critical pathways of gene-nutrient interactions in developmental copper metabolism. *PLoS Genet.* **4**, e1000261.
- Manolio, T. A., Collins, F. S., Cox, N. J., Goldstein, D. B., Hindorf, L. A., Hunter, D. J., McCarthy, M. I., Ramos, E. M., Cardon, L. R., Chakravarti, A. et al. (2009). Finding the missing heritability of complex diseases. *Nature* **461**, 747-753.
- Mendelsohn, B. A., Yin, C., Johnson, S. L., Wilm, T. P., Solnica-Krezel, L. and Gitlin, J. D. (2006). Atp7a determines a hierarchy of copper metabolism essential for notochord development. *Cell Metab.* **4**, 155-162.
- Montpetit, A., Cote, S., Brusteine, E., Drouin, C. A., Lapointe, L., Boudreau, M., Meloche, C., Drouin, R., Hudson, T. J., Drapeau, P. et al. (2008). Disruption of AP1S1, causing a novel neurocutaneous syndrome, perturbs development of the skin and spinal cord. *PLoS Genet.* **4**, e1000296.
- Nawaz, M., Manzi, C. and Krumschnabel, G. (2005). In vitro toxicity of copper, cadmium, and chromium to isolated hepatocytes from carp, *Cyprinus carpio* L. *Bull. Environ. Contam. Toxicol.* **75**, 652-661.

- Parsons, A. B., Brost, R. L., Ding, H., Li, Z., Zhang, C., Sheikh, B., Brown, G. W., Kane, P. M., Hughes, T. R. and Boone, C.** (2004). Integration of chemical-genetic and genetic interaction data links bioactive compounds to cellular target pathways. *Nat. Biotechnol.* **22**, 62-69.
- Parsons, A. B., Lopez, A., Givoni, I. E., Williams, D. E., Gray, C. A., Porter, J., Chua, G., Sopko, R., Brost, R. L., Ho, C. H. et al.** (2006). Exploring the mode-of-action of bioactive compounds by chemical-genetic profiling in yeast. *Cell* **126**, 611-625.
- Peterson, R. T.** (2008). Chemical biology and the limits of reductionism. *Nat. Chem. Biol.* **4**, 635-638.
- Petris, M. J., Strausak, D. and Mercer, J. F.** (2000). The Menkes copper transporter is required for the activation of tyrosinase. *Hum. Mol. Genet.* **9**, 2845-2851.
- Pratils, C. A., Taylor, B. S., Ye, Q., Viale, A., Sander, C., Solit, D. B. and Rosen, N.** (2009). (V600E)BRAF is associated with disabled feedback inhibition of RAF-MEK signaling and elevated transcriptional output of the pathway. *Proc. Natl. Acad. Sci USA* **106**, 4519-4524.
- Pribyl, P., Cepak, V. and Zachleder, V.** (2008). Cytoskeletal alterations in interphase cells of the green alga *Spirogyra decimina* in response to heavy metals exposure: II. The effect of aluminium, nickel and copper. *Toxicol. Vitro* **22**, 1160-1168.
- Quackenbush, J.** (2002). Microarray data normalization and transformation. *Nat. Genet.* **32**, 496-501.
- Rae, T. D., Schmidt, P. J., Pufahl, R. A., Culotta, V. C. and O'Halloran, T. V.** (1999). Undetectable intracellular free copper: the requirement of a copper chaperone for superoxide dismutase. *Science* **284**, 805-808.
- Raposo, G. and Marks, M. S.** (2007). Melanosomes-dark organelles enlighten endosomal membrane transport. *Nat. Rev. Mol. Cell Biol.* **8**, 786-797.
- Rawls, J. F. and Johnson, S. L.** (2000). Zebrafish kit mutation reveals primary and secondary regulation of melanocyte development during fin stripe regeneration. *Development* **127**, 3715-3724.
- Rustici, G., van Bakel, H., Lackner, D. H., Holstege, F. C., Wijnenga, C., Bahler, J. and Brazma, A.** (2007). Global transcriptional responses of fission and budding yeast to changes in copper and iron levels: a comparative study. *Genome Biol.* **8**, R73.
- Sannt, O., Pfirrmann, T., Braun, B., Juretschke, J., Kimmig, P., Scheel, H., Hofmann, K., Thumm, M. and Wolf, D. H.** (2008). The yeast GID complex, a novel ubiquitin ligase (E3) involved in the regulation of carbohydrate metabolism. *Mol. Biol. Cell* **19**, 3323-3333.
- Sebolt-Leopold, J. S.** (2008). Advances in the development of cancer therapeutics directed against the RAS-mitogen-activated protein kinase pathway. *Clin. Cancer Res.* **14**, 3651-3656.
- Setty, S. R., Tenza, D., Sviderskaya, E. V., Bennett, D. C., Raposo, G. and Marks, M. S.** (2008). Cell-specific ATP7A transport sustains copper-dependent tyrosinase activity in melanosomes. *Nature* **454**, 1142-1146.
- Tan, C. S., Bodenmiller, B., Pasculescu, A., Jovanovic, M., Hengartner, M. O., Jorgensen, C., Bader, G. D., Aebersold, R., Pawson, T. and Lindig, R.** (2009). Comparative analysis reveals conserved protein phosphorylation networks implicated in multiple diseases. *Sci. Signal.* **2**, ra39.
- Thiele, D. J. and Gitlin, J. D.** (2008). Assembling the pieces. *Nat. Chem. Biol.* **4**, 145-147.
- Titorenko, V. I. and Mullen, R. T.** (2006). Peroxisome biogenesis: the peroxisomal endomembrane system and the role of the ER. *J. Cell Biol.* **174**, 11-17.
- van Bakel, H., Strengman, E., Wijnenga, C. and Holstege, F. C.** (2005). Gene expression profiling and phenotype analyses of *S. cerevisiae* in response to changing copper reveals six genes with new roles in copper and iron metabolism. *Physiol. Genomics* **22**, 356-367.
- Wallin, M., Larsson, H. and Edstrom, A.** (1977). Tubulin sulfhydryl groups and polymerization in vitro. Effects of di- and trivalent cations. *Exp. Cell Res.* **107**, 219-225.
- Wanders, R. J. and Waterham, H. R.** (2005). Peroxisomal disorders I: biochemistry and genetics of peroxisome biogenesis disorders. *Clin. Genet.* **67**, 107-133.
- Wei, M. L.** (2006). Hermansky-Pudlak syndrome: a disease of protein trafficking and organelle function. *Pigment Cell Res.* **19**, 19-42.
- Westerfield, M.** (2000). *The Zebrafish Book. A Guide for the Laboratory use of Zebrafish (Danio rerio)*. Eugene: University of Oregon Press.
- Winzler, E. A., Shoemaker, D. D., Astromoff, A., Liang, H., Anderson, K., Andre, B., Bangham, R., Benito, R., Boeke, J. D., Bussey, H. et al.** (1999). Functional characterization of the *S. cerevisiae* genome by gene deletion and parallel analysis. *Science* **285**, 901-906.
- Yu, L., Lopez, A., Anafloos, A., El Bali, B., Hamal, A., Ericson, E., Heisler, L. E., McQuibban, A., Giaever, G., Nislow, C. et al.** (2008). Chemical-genetic profiling of imidazo[1,2-a]pyridines and -pyrimidines reveals target pathways conserved between yeast and human cells. *PLoS Genet.* **4**, e1000284.
- Yuan, D. S., Dancis, A. and Klausner, R. D.** (1997). Restriction of copper export in *Saccharomyces cerevisiae* to a late Golgi or post-Golgi compartment in the secretory pathway. *J. Biol. Chem.* **272**, 25787-25793.
- Zilberman, D., Coleman-Derr, D., Ballinger, T. and Henikoff, S.** (2008). Histone H2A.Z and DNA methylation are mutually antagonistic chromatin marks. *Nature* **456**, 125-129.
- Zon, L. I. and Peterson, R. T.** (2005). In vivo drug discovery in the zebrafish. *Nat. Rev. Drug Discov.* **4**, 35-44.

# Cross-species discovery of syncretic drug combinations that potentiate the antifungal fluconazole

Michaela Spitzer<sup>1,4</sup>, Emma Griffiths<sup>2,3,4</sup>, Kim M Blakely<sup>2</sup>, Jan Wildenhain<sup>1</sup>, Linda Ejim<sup>2</sup>, Laura Rossi<sup>2</sup>, Gianfranco De Pascale<sup>2</sup>, Jasna Curak<sup>2</sup>, Eric Brown<sup>2</sup>, Mike Tyers<sup>1,\*</sup> and Gerard D Wright<sup>2,\*</sup>

<sup>1</sup> Wellcome Trust Centre for Cell Biology, School of Biological Sciences, University of Edinburgh, Edinburgh, UK; <sup>2</sup> Michael G. DeGroot Institute for Infectious Disease Research and the Department of Biochemistry and Biomedical Sciences, McMaster University, Hamilton, Ontario, Canada and <sup>3</sup> Michael Smith Laboratories, University of British Columbia, Vancouver, British Columbia, Canada

<sup>4</sup> These authors contributed equally to this work

\* Corresponding authors. M Tyers, Wellcome Trust Centre for Cell Biology, School of Biological Sciences, University of Edinburgh, Room 307 Darwin Bldg, King's Buildings, Mayfield Road, Edinburgh EH9 3JR, UK. Tel.: +44 131 650 7027; Fax: +44 131 650 5376; E-mail: m.tyers@ed.ac.uk or GD Wright, Michael G. DeGroot Institute for Infectious Disease Research and the Department of Biochemistry and Biomedical Sciences, McMaster University, Hamilton, Ontario, Canada L8N 3Z5. Tel.: +1 905 525 9140/ext. 20230; Fax: +1 905 528 5330; E-mail: wrightge@mcmaster.ca

Received 11.1.11; accepted 26.4.11

**Resistance to widely used fungistatic drugs, particularly to the ergosterol biosynthesis inhibitor fluconazole, threatens millions of immunocompromised patients susceptible to invasive fungal infections. The dense network structure of synthetic lethal genetic interactions in yeast suggests that combinatorial network inhibition may afford increased drug efficacy and specificity. We carried out systematic screens with a bioactive library enriched for off-patent drugs to identify compounds that potentiate fluconazole action in pathogenic *Candida* and *Cryptococcus* strains and the model yeast *Saccharomyces*. Many compounds exhibited species- or genus-specific synergism, and often improved fluconazole from fungistatic to fungicidal activity. Mode of action studies revealed two classes of synergistic compound, which either perturbed membrane permeability or inhibited sphingolipid biosynthesis. Synergistic drug interactions were rationalized by global genetic interaction networks and, notably, higher order drug combinations further potentiated the activity of fluconazole. Synergistic combinations were active against fluconazole-resistant clinical isolates and an *in vivo* model of *Cryptococcus* infection. The systematic repurposing of approved drugs against a spectrum of pathogens thus identifies network vulnerabilities that may be exploited to increase the activity and repertoire of antifungal agents.**

*Molecular Systems Biology* 7: 499; published online 21 June 2011; doi:10.1038/msb.2011.31

*Subject Categories:* microbiology & pathogens

*Keywords:* antifungal; combination; pathogen; resistance; synergism

This is an open-access article distributed under the terms of the Creative Commons Attribution Noncommercial Share Alike 3.0 Unported License, which allows readers to alter, transform, or build upon the article and then distribute the resulting work under the same or similar license to this one. The work must be attributed back to the original author and commercial use is not permitted without specific permission.

## Introduction

The recent increase in fungal infection rates presents a serious clinical challenge (Arendrup *et al.*, 2009; Gullo, 2009; Shorr *et al.*, 2009). Immune-suppressed individuals, including transplant, cancer chemotherapy and HIV-infected patients, often succumb to opportunistic fungal pathogens from the genera *Candida*, *Cryptococcus*, *Aspergillus* and others (Groll *et al.*, 1996; Baddley *et al.*, 2001; Clark and Hajjeh, 2002; Richardson and Warnock, 2003). Unlike bacterial infections that can be treated with multiple antibiotic classes, therapeutic options for fungal infections are limited. The polyene amphotericin B, discovered in 1955, remains a front line fungicidal drug; however, amphotericin B non-specifically disrupts cell membrane integrity,

with concomitant severe patient toxicity. Synthetic azole antifungals such as fluconazole were introduced 40 years ago and inhibit lanosterol 14 $\alpha$ -demethylase, the gene product of *ERG11*, an essential cytochrome P450 enzyme in the ergosterol biosynthetic pathway (Groll *et al.*, 1998; Revankar *et al.*, 2004). Fluconazole binds to the heme Fe(III) of Erg11, resulting in depletion of ergosterol, the accumulation of C-14 methyl sterols and cell membrane disruption. The crossreactivity of azoles toward human P450 enzymes also results in toxicity and, moreover, clinical resistance is prevalent (Cannon *et al.*, 2009; Marie and White, 2009). Finally, the echinocandins, which include caspofungin, micafungin and anidulafungin, were introduced 10 years ago and inhibit the cell wall biosynthesis enzyme  $\beta$ -(1,3)-D-glucan synthase; however, these agents have a

restricted antifungal spectrum (Sucher *et al*, 2009). The dearth of selective agents and emerging patterns of clinical resistance demand new antifungal strategies.

A primary challenge in antifungal drug discovery is the paucity of fungal-specific molecular targets that are essential for cell growth, due to the conserved biochemical and molecular biological networks of all eukaryotes. This problem is exacerbated by the observation that many essential yeast genes can provide sufficient function at a fraction of wild-type dosage (Yan *et al*, 2009). Although only ~1100 of the ~6000 genes in yeast are essential under nutrient-rich growth conditions (Winzeler *et al*, 1999), almost all genes become essential in specific genetic backgrounds in which another non-essential gene has been deleted or otherwise attenuated, an effect termed synthetic lethality (Tong *et al*, 2001). Genome-scale surveys suggest that over 200 000 binary synthetic lethal gene combinations dominate the yeast genetic landscape (Costanzo *et al*, 2010). The genetic buffering phenomenon is also manifest as a phalanx of differential chemical-genetic interactions in the presence of sublethal doses of bioactive compounds (Hillenmeyer *et al*, 2008). These observations illuminate the inherent redundancy of genetic networks, and frame the problem of interdigitating network functions with single agent therapeutics (Hopkins, 2008).

This genetic network organization suggests that judicious combinations of small molecule inhibitors of both essential and non-essential targets may elicit additive or synergistic effects on cell growth (Sharom *et al*, 2004; Agoston *et al*, 2005; Fitzgerald *et al*, 2006; Lehar *et al*, 2007, 2008; Hopkins, 2008). Indeed, *ad hoc* combinations of anti-infective drugs are frequently used to treat fungal infections (Eliopoulos and Moellering, 1991; Johnson and Perfect, 2010). However, this chance approach fails to exploit richness of the chemical-genetic landscape (Sharom *et al*, 2004; Hopkins, 2008; Lehar *et al*, 2008). Instead, unbiased screens for synergistic enhancers of a specific bioactivity that are not themselves active, sometimes termed syncretic combinations, are needed to fully explore chemical space (Keith *et al*, 2005). Compounds that enhance the activity of known agents in model yeast and cancer cell line systems have been identified both by focused small molecule library screens (Borisy *et al*, 2003; Zhang *et al*, 2007; Zhai *et al*, 2010) and by computational methods (Lehar *et al*, 2007; Nelander *et al*, 2008; Jansen *et al*, 2009; Zinner *et al*, 2009). Furthermore, direct tests of synergistic compounds have successfully yielded combinations that are active against pathogenic fungi, including the combination of fluconazole with chemical inhibitors of Hsp90, calcineurin or ARF (Cowen *et al*, 2009; Singh *et al*, 2009; Epp *et al*, 2010) and the antibiotic polymyxin B (Zhai *et al*, 2010).

To extend the strategy of chemical synthetic lethality to clinically relevant fungal pathogens, we interrogated a focused bioactive library of known drugs for synergistic enhancers of the fungistatic drug fluconazole in systematic screens against *Candida albicans*, *Cryptococcus neoformans* and *Cryptococcus gattii*, as well as the genetically tractable budding yeast *Saccharomyces cerevisiae*. Compounds not previously recognized in the clinic as antifungal agents caused potent growth inhibition in conjunction with fluconazole, often in a genus- or species-specific manner. Selected combinations were characterized for mechanism of action and shown to be active against fluconazole-

resistant isolates and efficacious in an *in vivo* infection model. The combinatorial redeployment of known drugs defines a powerful antifungal strategy and establishes a number of potential lead combinations for future clinical assessment.

## Results

### Systematic antifungal potentiation screens in model and pathogenic fungi

Cell-based high-throughput screens were performed on a panel of four fungal strains to identify small molecules that potentiate fluconazole across a range of genera and species. The human pathogens *C. neoformans* (H99), *C. gattii* (R265) and *C. albicans* (Caf2-1) as well as the model fungus *S. cerevisiae* (BY4741) were screened in duplicate against the Prestwick library, which consists of 1120 off-patent drugs and other bioactive agents (<http://www.prestwickchemical.com>). To identify compounds that potentiate the effect of fluconazole, yet have minimal antifungal activity on their own, each screen was performed in the presence and absence of 0.5 minimal inhibitory concentration (MIC) of fluconazole at a single compound concentration of 30  $\mu$ M. Residual activity was calculated for each compound and all data were normalized for plate- and row/column-specific effects (Supplementary Figure S1; see Supplementary Table S1 for screen data). Hits were determined using median absolute deviation (MAD) statistics. By this criterion, 43 compounds were active against *S. cerevisiae*, 30 against *C. albicans*, 70 against *C. neoformans* and 91 against *C. gattii* (Figure 1A and B).

The set of 148 compounds that potentiated the antifungal action of fluconazole in one or more of the screens (Supplementary Figure S2) was structurally diverse and represented a broad range of different therapeutic activities, including antiparasitics, cardiovascular protectives, dermatologicals, genitourinary tract anti-infectives, hormone modulators and a variety of neuroleptic drugs. Notably, 15 of the 17 tricyclic phenothiazine/thioxanthene antipsychotics present in the Prestwick library exhibited strong interactions with fluconazole against *C. gattii* and *C. neoformans* (Figure 1C). Derivatives of tricyclic phenothiazines inhibit fatty acid synthesis and disrupt lipid trafficking (Li *et al*, 2008).

A striking number of hits were species or genus specific (Figure 1B). Six compounds were hits in all screens: (i) the antidepressant sertraline (Zoloft<sup>®</sup>); (ii) the monoamine oxygenase inhibitor pirlindole, also known to have antidepressant activity; (iii) the allylamine antifungal naftifine; (iv) the antibiotic prodrug pivampicillin; (v) the anti-nausea drug thiethylperazine (Torecan<sup>®</sup>); and (vi) the antipsychotic drug zuclopenthixol. The latter two compounds are members of the large family of phenothiazines that have antipsychotic and other central nervous system (CNS) activities.

### Synergy assessment and fungicidal activity

To determine whether hit compounds acted in a synergistic or additive manner with fluconazole, we selected 12 of the 148 hits (albendazole, azaperone, clofazimine, clomiphene, L-cycloserine, kawain, lynestrolol, mitoxantrone, sertraline, suloctidil, tamoxifen and trifluoperazine) for detailed studies

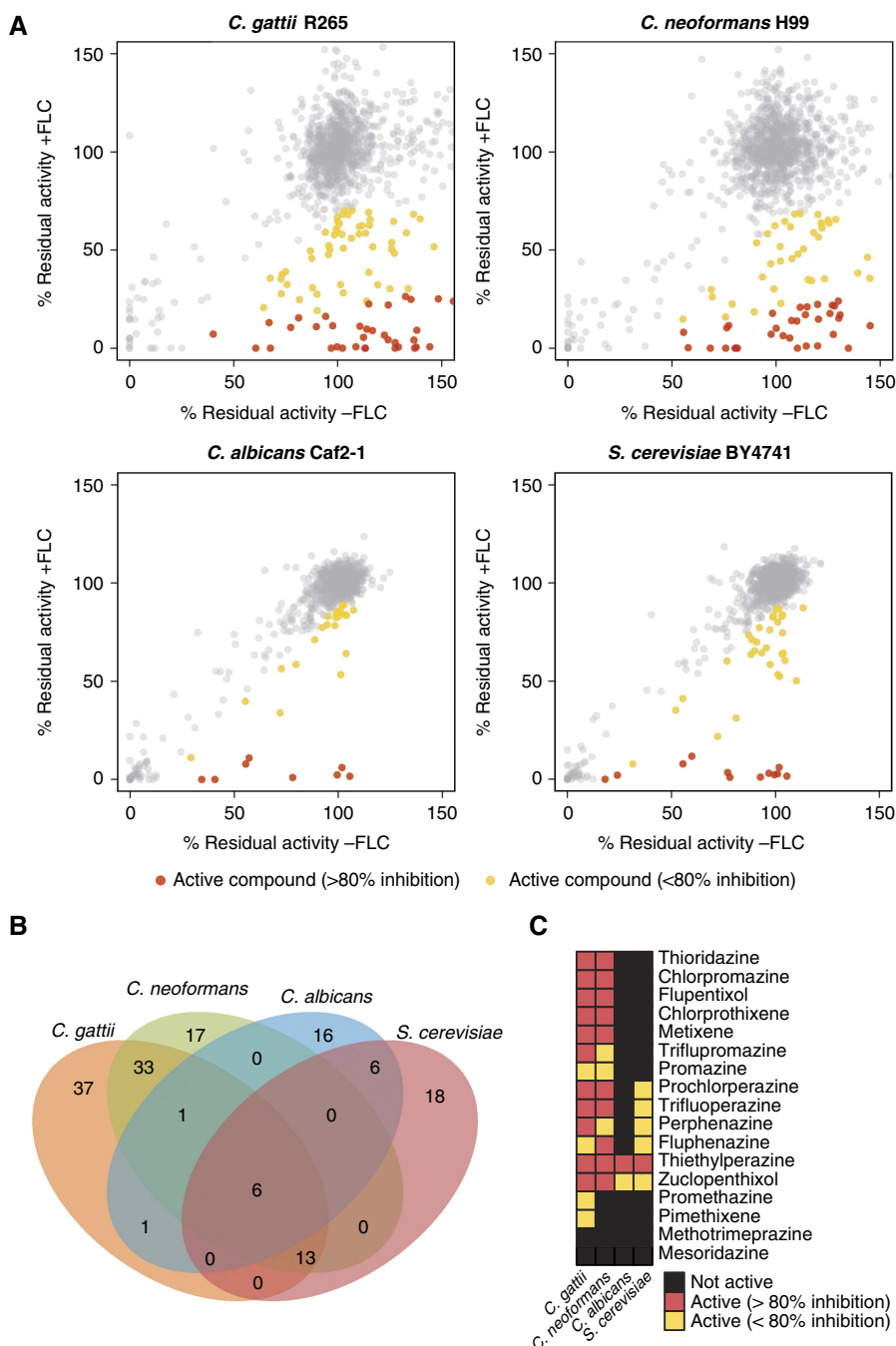


**Figure 1** Unbiased screens for bioactive compounds that potentiate the antifungal activity of fluconazole. **(A)** Scatter plots for Prestwick library screens for four fungal species. Growth inhibition caused by compounds in the absence (x axis) and presence of fluconazole (y axis) is represented by residual activity after treatment. Yellow and red filled circles indicate compounds that were classified as active (2 median absolute deviations below the diagonal). Compounds that inhibited growth in the presence of fluconazole by at least 80% compared with the effect of that compound alone are highlighted in red; FLC, fluconazole. **(B)** Overlap of hits between different fungal species. **(C)** Activity of 17 phenothiazine/thioxathene compounds in different fungal species.

in all four fungal species. We based this selection on an analysis of distinct chemical class, with one or two representative structures from families of similar agents that emerged in the screen, commercial availability of compound, therapeutic importance, and known mode of action (Supplementary Figure S3). These criteria yielded a tractable number of hit compounds for detailed downstream analysis. We also tested five known antifungal drugs, both as positive controls and to

explore other potential interactions with fluconazole: amphotericin B, the ergosterol biosynthesis inhibitors ketoconazole, terbinafine (an allylamine analog of naftifine used in the clinic) and fenpropidin (an agricultural fungicide), and the echinocandin caspofungin. Dose-dependent MIC values for these 17 compounds were determined for each of the four species (Supplementary Table S2). The interaction of each compound with fluconazole was assessed by standard con-

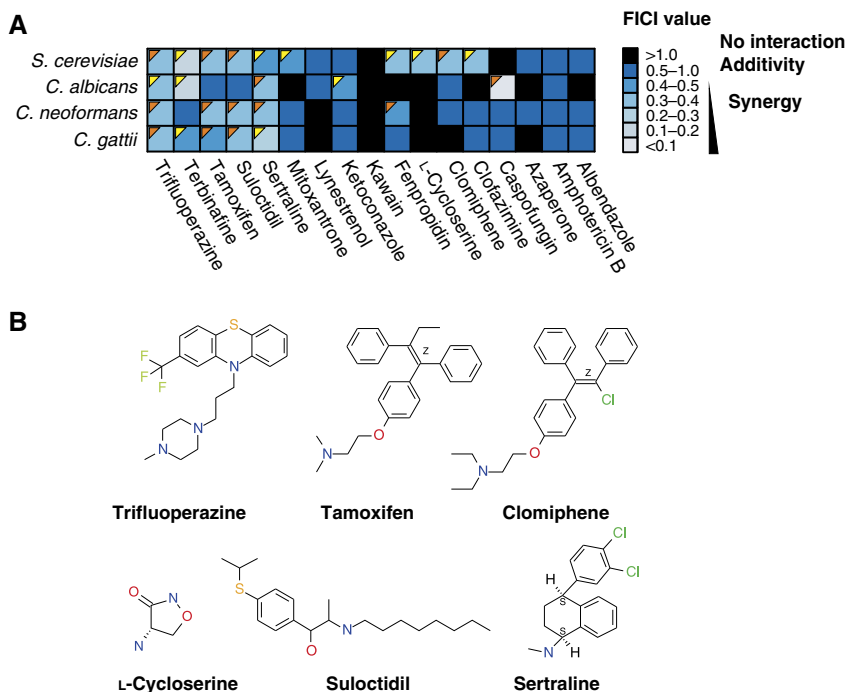


**Figure 2** Synergistic drug interactions with fluconazole. **(A)** Heat map of drug interactions with fluconazole in each species. Dark blue indicates additive effects (FICI of 0.5–1); lighter shades of blue represent synergy (FICI <0.5). Orange triangles indicate fungicidal drug combinations; yellow triangles indicate fungistatic drug combinations. **(B)** Chemical structures of the six drugs chosen for detailed mode of action studies. Source data is available for this figure at [www.nature.com/msb](http://www.nature.com/msb).

centration matrix (checkerboard) analysis (Figure 2A; Supplementary Table S3). Data were quantified by calculation of the fractional inhibitory concentration index (FICI), the accepted method for drug interactions in infectious disease (Eliopoulos and Moellering, 1991; Odds, 2003). Only two compounds, sertraline and trifluoperazine, exhibited synergy with fluconazole against all four fungal species. A number of synergizers exerted effects exclusively on a particular species: *S. cerevisiae* was uniquely susceptible to four different compounds in the presence of fluconazole (clofazimine, clomiphene, L-cycloserine and mitoxantrone), while only *C. albicans* was susceptible to ketoconazole or caspofungin in combination with fluconazole. Neither *Cryptococcus* species exhibited any unique synergistic susceptibilities. Most hits from the screens were confirmed as synergistic with fluconazole, except for albendazole, azaperone and kawain in *S. cerevisiae*, and azaperone, L-cycloserine and lynestrenol in *C. albicans* (Supplementary Figure S4). Quantification of interactions at different drug concentrations revealed some additional synergies with fluconazole: trifluoperazine exhibited synergy against *C. albicans*, tamoxifen against *C. gattii* and *C. neoformans*, and suloctidil against *C. neoformans* and *S. cerevisiae* (Supplementary Figure S4). Based on the detailed analysis of these 12 compounds, the high-throughput screens proved a reliable means to identify synergistic drug interactions, with an estimated false positive rate of 0.20 and a false negative rate of 0.28. Importantly, and in contrast to the merely fungistatic effect of fluconazole alone, several combinations of fluconazole and different synergistic compounds were fungicidal, often in a species-dependent manner (Figure 2A). For example, trifluoperazine exhibited synergy with fluconazole and was fungicidal in all species with the exception of *C. albicans*.

## Chemical–genetic profiles of synergistic combinations

We explored the molecular basis for the synergy of trifluoperazine, tamoxifen, clomiphene, sertraline, suloctidil and L-cycloserine with fluconazole (Figure 2B), using established genome-wide methods in *S. cerevisiae* to identify gene deletion strains that are sensitive to drug treatment (Giaever *et al*, 1999; Parsons *et al*, 2006; Hillenmeyer *et al*, 2008). Genome-wide pools of deletion strains were grown in the presence of drugs, genomic DNA isolated from drug-treated and control cultures, and barcode sequence tags amplified and hybridized to barcode microarrays (Cook *et al*, 2008).

First, we profiled compound action in haplo-insufficiency screens, in which the ~1000 deletion strains heterozygous for essential genes were tested for drug sensitivity to identify candidate drug targets (Giaever *et al*, 1999). As expected, deletion of one copy of *ERG11* conferred sensitivity to fluconazole (Figure 3A; Supplementary Figure S5). Deletion of one copy of either *LCB1* or *LCB2*, which encode subunits of the enzyme serine palmitoyltransferase that catalyzes the committed step of sphingolipid biosynthesis, caused sensitivity to L-cycloserine (Figure 3A; Supplementary Figure S5). In yeast membrane extracts, high concentrations of L-cycloserine (1 mM) partially inhibit serine palmitoyltransferase (Pinto *et al*, 1992). All five remaining compounds—trifluoperazine, tamoxifen, clomiphene, sertraline and suloctidil (referred to as the membrane active group)—conferred sensitivity to loss of one copy of the *NEO1* gene (Figure 3A; Supplementary Figure S5), which encodes an essential aminophospholipid translocase required for membrane trafficking and vacuolar biogenesis. Deletion of the ortholog of *NEO1* in *C. neoformans* (*APT1*) has recently been shown to result in hypersensitivity to amphotericin B and fluconazole, as well as

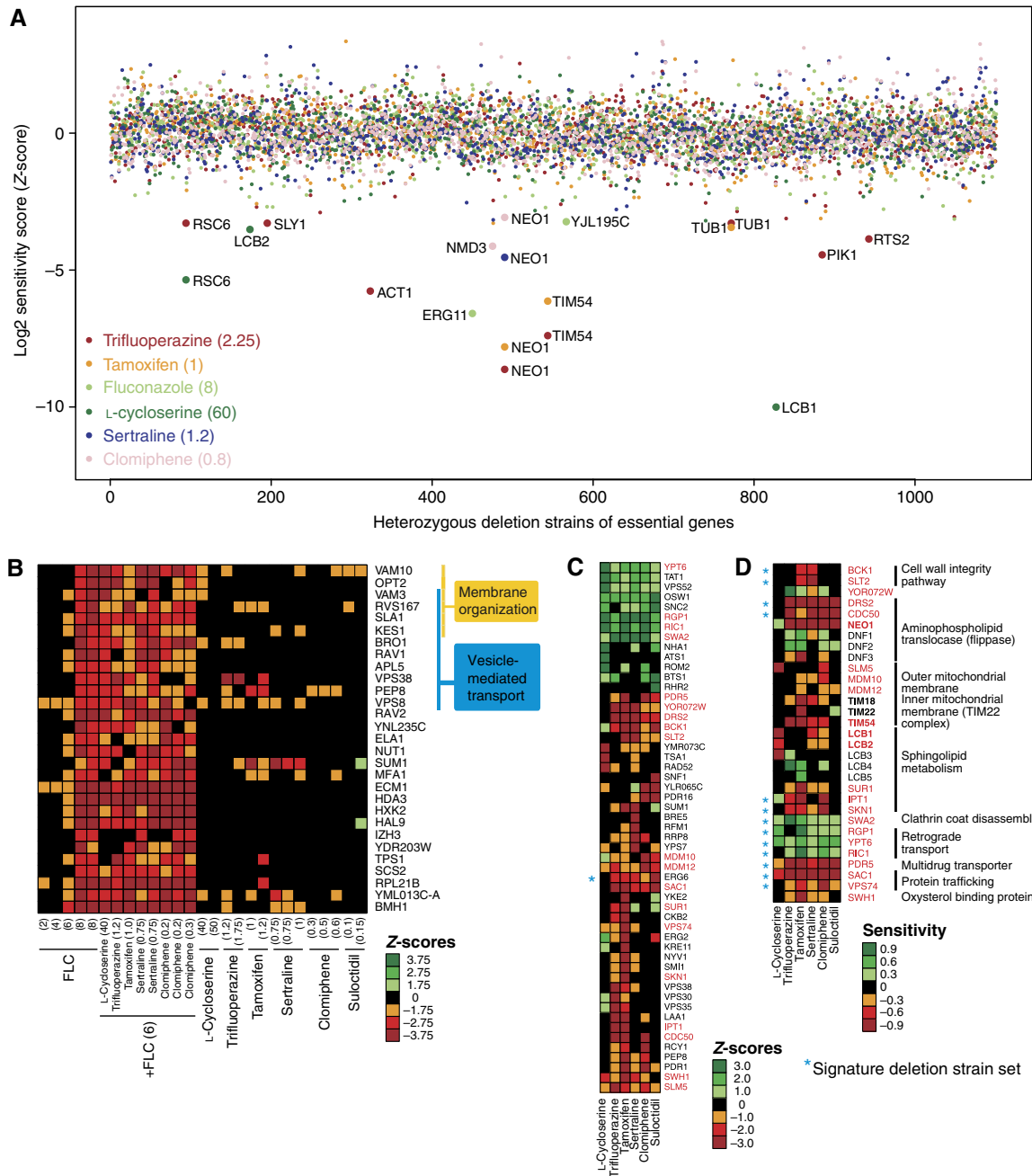


**Figure 3** Chemical–genetic interactions of six synergistic drugs. **(A)** Sensitivity of heterozygous essential deletion strains to five different synergistic drugs and fluconazole, as assessed by barcode microarray hybridization. **(B)** Core set of haploid deletion strains that are sensitive to fluconazole, as assessed by barcode microarray hybridization. Several concentrations of fluconazole were tested to correlate the signature with MIC. The effect of the six synergistic drugs on the core fluconazole profile was examined in the presence or absence of a threshold concentration of fluconazole (6  $\mu\text{g}/\text{ml}$ ). Genes implicated in membrane organization and vesicle-mediated transport are indicated. **(C)** Main cluster of haploid deletion strain sensitivities to the six synergistic drugs in the absence of fluconazole, as assessed by barcode microarray hybridization. Strains that have a Z-score more significant than  $\pm 3$  for at least one of the drugs in duplicate profiles are shown. Gene names in red indicate deletion strains that were chosen for verification by quantitative growth curve assays. **(D)** Log-ratio scores calculated from individual growth curve assays to confirm chemical–genetic interactions of the six synergistic drugs. Gene names in bold indicate heterozygous deletion strains for essential genes. Values in parentheses indicate drug concentration in  $\mu\text{g}/\text{ml}$ . Negative Z-scores and log-ratios indicate sensitivity of a strain to a given drug, whereas positive scores represent resistance. Asterisks indicate 14 deletion strains that comprise the core signature set for membrane active compounds. Source data is available for this figure at [www.nature.com/msb](http://www.nature.com/msb).

attenuated virulence (Hu and Kronstad, 2010). In addition, deletion of one copy of *TIM54*, a translocase of the inner mitochondrial membrane, confers sensitivity to tamoxifen and trifluoperazine (Figure 3A), consistent with the potential membrane targets of these drugs.

We then generated haploid chemical–genetic profiles for the synergistic compounds individually and in combination with fluconazole (Supplementary Figure S6). This profiling method reveals genes that buffer against drug toxicity and can identify compounds with similar bioactivities based on shared chemical–



genetic interaction profiles (Hillenmeyer *et al*, 2008). Strains deleted for genes that function in vesicle-mediated transport and membrane organization were sensitive to fluconazole alone (Figure 3B). For drug combinations, we chose a concentration of fluconazole (6 µg/ml) that caused ~20% growth inhibition compared with control and thereby minimized the selection against fluconazole-sensitive strains. Importantly, the syncretic drugs alone did not impair the growth of fluconazole-sensitive deletion strains (Figure 3B; Supplementary Figure S5), but significantly sensitized cells to low doses of fluconazole (Supplementary Table S4). To explore the potential mechanism of this sensitization further, we examined the chemical–genetic profiles of single compounds (Figure 3C; Supplementary Figure S7; Supplementary Table S5). The membrane active group of trifluoperazine, tamoxifen, clomiphene, sertraline and suloctidil caused growth inhibition of a core set of deletion strains that included genes that encode the post-Golgi-associated aminophospholipid translocase (flippase) Drs2 and its activating subunit Cdc50, the ergosterol biosynthesis enzyme Erg6, the protein trafficking factors Sac1 and Vps74, the mitochondrial outer membrane import factors Mdm10 and Mdm12, and the cell wall integrity MAPK kinase Slt2 and its upstream activating kinase Bck1. A number of genes implicated in downstream steps of sphingolipid metabolism, including *IPT1*, *SUR1*, *SKN1*, *YPK1* and *SWH1*, were also required for cell survival in the presence of the membrane active compounds. Notably, strains disrupted for non-essential genes implicated in uncoating of clathrin vesicles (*SWA2*) and retrograde transport to the cis-Golgi network (*YPT6*, *RGP1*, *RIC1* and *VPS52*) were resistant to all six fluconazole synergizers, suggesting that altered vesicle trafficking may compensate for membrane perturbation and/or Erg11 inhibition.

We confirmed the chemical–genetic interactions between these haploid deletion strains and each drug using quantitative growth curve assays (Figure 3D). We also assessed strains that were heterozygous for *ERG11*, *NEO1*, *LCB1* and *LCB2* as well as *TIM18* and *TIM22*, which function in a complex with *TIM54*. In addition, we included haploid deletion strains for *DNF1/2/3*, the other three flippases in *S. cerevisiae*, and *LCB3/4/5*, which function downstream of *LCB1/2*. The quantitative growth curves corroborated the barcode microarray results, with the exception of the dubious ORF *YOR072W*. The range of drug concentrations tested in the growth curve assays revealed additional chemical–genetic interactions, such as *TIM18*, which were not recovered at the single drug concentrations used in the barcode profiles.

The results of these genome-wide chemical–genetic screens point to two related modes of action for the syncretic combinations tested. Trifluoperazine, tamoxifen, clomiphene, sertraline and suloctidil appear to cause general perturbation of membrane, vesicle trafficking and lipid biosynthesis functions, whereas L-cycloserine preferentially interferes with an early step in sphingolipid biosynthesis, consistent with its proposed mechanism of action (Pinto *et al*, 1992). To test the latter hypothesis, we examined the effects of myriocin, another known inhibitor of the first step of the sphingolipid biosynthesis pathway (Miyake *et al*, 1995), and found that it also potentiated the inhibition of cell growth by fluconazole (FICI=0.625).

## Cell biological effects of synergistic combinations

We assessed the effects of trifluoperazine, tamoxifen, sertraline and L-cycloserine alone and in combination with fluconazole on *S. cerevisiae* cell physiology. The diagnostic fluorescent dyes Calcofluor White, FM4-64 and Mitotracker Green were used to visualize cell wall and bud scars, vacuolar membranes and mitochondria, respectively. For each reporter dye, fluconazole produced staining patterns that were similar to solvent controls. In contrast, treatment with trifluoperazine, tamoxifen, clomiphene and sertraline caused a drastic loss of localization and strong intracellular accumulation of each dye (Figure 4A; Supplementary Figure S8). In particular, the disruption of vacuolar structure revealed by FM4-64 staining suggested severe loss of cell membrane integrity. Consistent with its different genetic target profile, treatment with L-cycloserine had no observable effects on the localization of any of the dyes (Figure 4B).

Lethal perturbation of the membrane and/or cell wall can often be rescued by osmotic stabilization. Sorbitol (1 M) effectively suppressed the syncretic growth inhibitory effects of trifluoperazine, tamoxifen, clomiphene, sertraline and suloctidil, again supporting a common membrane perturbation mechanism for these compounds, but had no such protective effect on cells treated with L-cycloserine and fluconazole (Figure 4C). These cell biological results affirm the different mechanisms of action of the two compound classes.

## Integration of chemical–gene interactions with genetic interaction networks

A primary challenge in the discovery of synergistic drug combinations is the vast number of possible combinations of drug pairs (Sharom *et al*, 2004; Hopkins, 2008; Lehar *et al*, 2008). Integration of drug-induced gene expression profiles (Lum *et al*, 2004) and chemical–genetic profiles (Hillenmeyer *et al*, 2008) with comprehensive genetic interaction networks (Costanzo *et al*, 2010) can allow computational prediction of synergistic drug pairs (Lehar *et al*, 2007; Nelander *et al*, 2008; Jansen *et al*, 2009). To assess whether the individual profiles of fluconazole and each of the syncretic drugs could rationalize drug interactions, we integrated the chemical–genetic profiles generated above for each syncretic compound with a global genetic interaction network composed of both high-throughput (HTP) and low-throughput (LTP) data compiled from the primary literature (Breitkreutz *et al*, 2008; Costanzo *et al*, 2010). Deletion strains that were sensitive to treatment with single drugs were used to assess the number of genetic interactions linked to the chemical–genetic space (CGS) of fluconazole and each of the synergizers. A core set of haploid deletion strains affected by the membrane active group of compounds, referred to as the signature strain set (Figure 3D), exhibited many genetic interactions with the top 50 fluconazole-sensitive strains (Figure 5A). The top 50 most sensitive deletion strains for each individual drug (*Z*-scores above ~2.0) also showed many genetic interactions with the fluconazole profile. We tested the significance of the genetic connections between the profiles using simulations of genetic interactions shared between randomly chosen gene sets of a specific size, based on the known chemical sensitivities of 1143

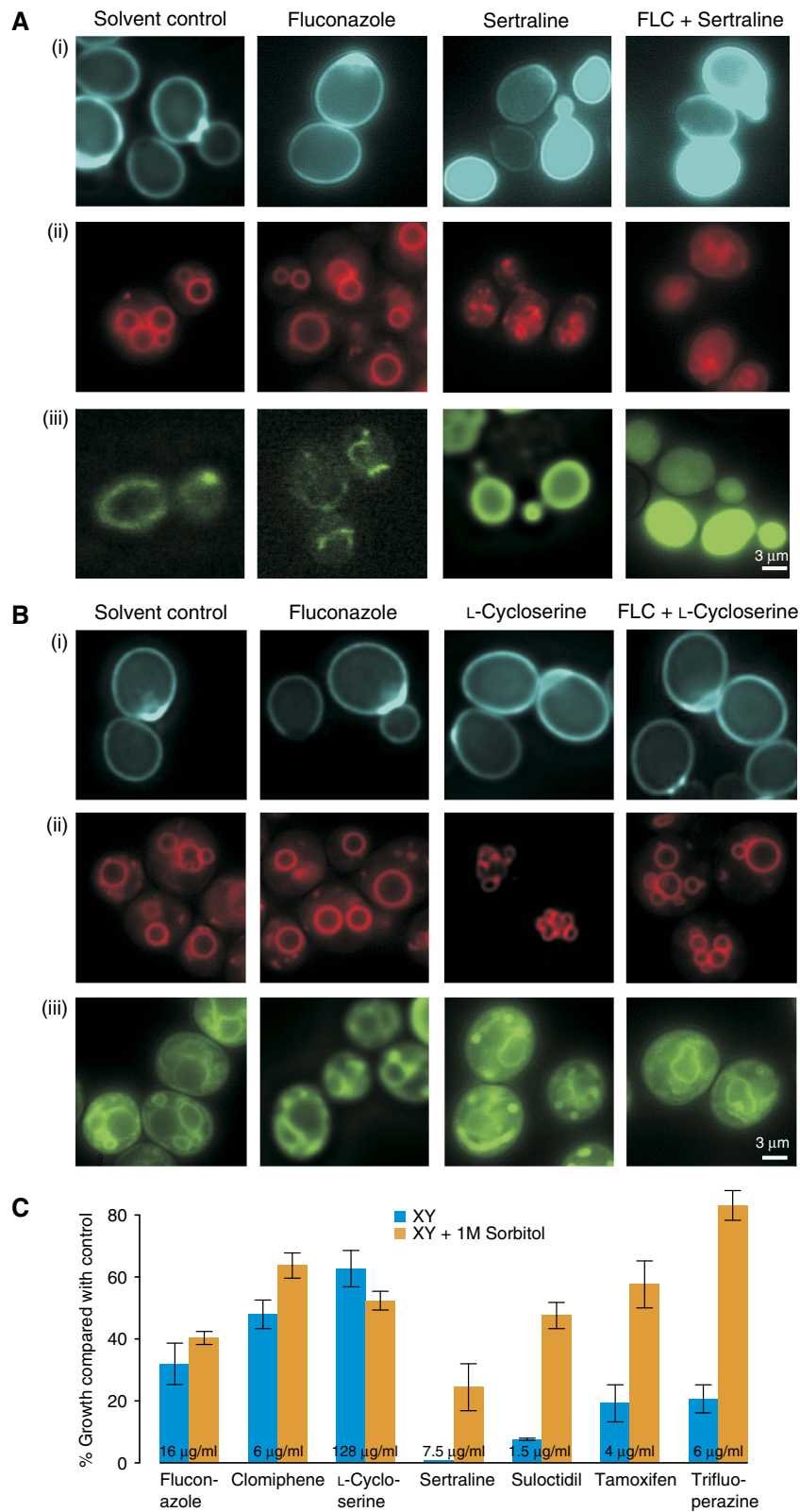


**Figure 4** Effects of syncretic drugs on membrane integrity. A wild-type *S. cerevisiae* strain was grown in the presence of the indicated drugs and stained with (i) Calcofluor White M2R, (ii) FM4-64 and (iii) Mitotracker Green FM, and imaged by fluorescence microscopy. **(A)** Sertraline (128 μg/ml) in the presence and absence of fluconazole (64 μg/ml). **(B)** L-Cycloserine (128 μg/ml) in the presence and absence of fluconazole (128 μg/ml). **(C)** Growth of wild-type *S. cerevisiae* compared with control wells in the presence of the indicated drugs with and without 1 M sorbitol. The mean of four independent measurements is shown; error bars represent standard error. Source data is available for this figure at [www.nature.com/msb](http://www.nature.com/msb).

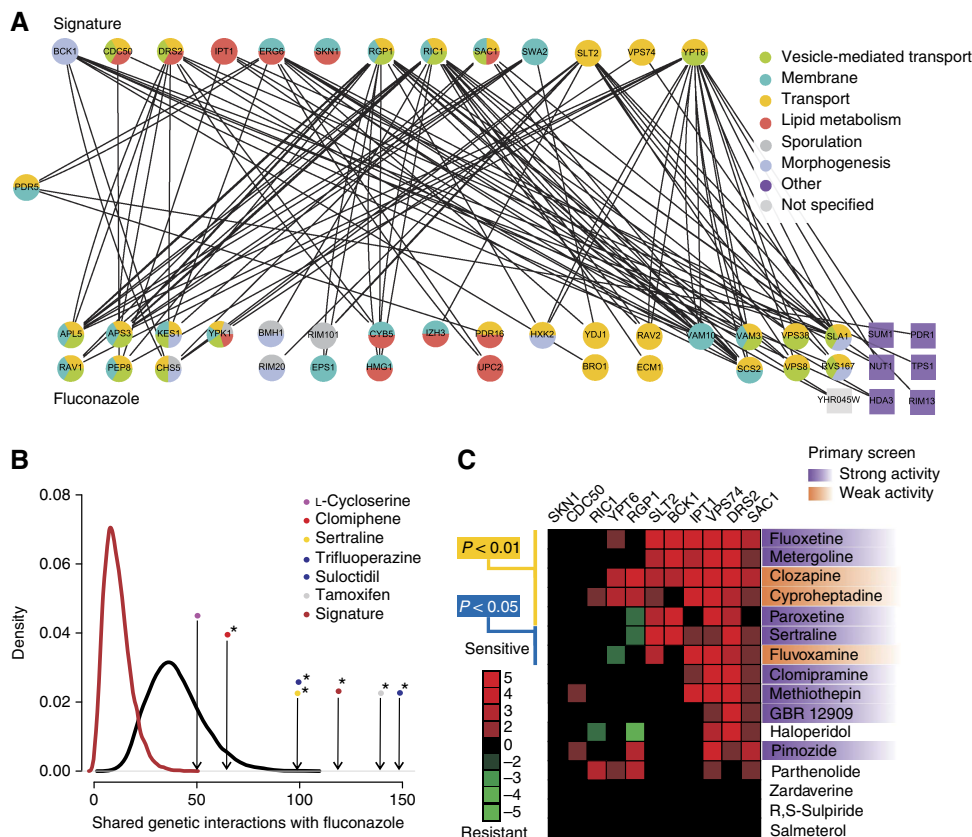


**Figure 5** Rationalization of synergistic interactions by integration of chemical–genetic and genetic interaction networks. **(A)** Bipartite graph of genetic interactions between top 50 chemical–genetic interactors of fluconazole and the signature deletion strains sensitive to the five membrane active compounds. As *PDR5* was a member of both sets, it is positioned midway between the two sets. Enriched Gene Ontology (GO) SLIM biological processes are indicated (adjusted  $P$ -value  $< 0.05$ ). GO enrichment was calculated and visualized using GOLORIZE (Garcia *et al*, 2007). **(B)** Chemical–genetic space (CGS) simulation with the 50 most sensitive deletion strains for each of the synergistic drugs as well as the signature deletion strain set. Arrows indicate the number of actual genetic interactions for the different drugs; black curve represents the background distribution of genetic interactions between two random sample sets of 50 non-essential deletion strains chosen from 1143 strains that respond to a variety of different chemicals and drugs (Hillenmeyer *et al*, 2008); dark red curve depicts the same background distribution except that the second sample set was chosen to match the size of signature deletion set. Asterisks indicate a  $P$ -value  $< 0.05$ . **(C)** Drug sensitivity of 11 of the 14 signature deletion strains identified in this study for 16 previously profiled psychiatric drugs present in the Prestwick library (Ericson *et al*, 2008). Strong activity refers to compounds that were hits in the primary screens, that is, at least 2 MAD away from the diagonal, whereas weak activity refers to compounds that showed at least 20% growth inhibition and were  $> 1$  MAD away from the diagonal. Source data is available for this figure at [www.nature.com/msb](http://www.nature.com/msb).

non-essential deletion strains that respond to various drug treatments (Hillenmeyer *et al*, 2008). The signature deletion set shared by the membrane active group was significantly enriched for genetic interactions with fluconazole-sensitive deletion strains ( $P$ -value  $< 10^{-7}$ ). The individual profiles for tamoxifen, trifluoperazine, clomiphene, sertraline and sulcetidil also showed a significant enrichment of genetic interactions with the fluconazole-sensitive strain profile (all  $P$ -values  $< 0.05$ ), whereas L-cycloserine did not (Figure 5B; Supplementary Table S6). As a more conservative measure of pathway separation (Kelley and Ideker, 2005), we applied a parallel pathway permutation (PPP) test, in which the chemical–genetic interactors of fluconazole and each of the synergistic drugs were pooled and randomly assigned to two groups (Supplementary Figure S9). By this stringent method, the signature deletion set and the top 50 most sensitive deletion strains from the trifluoperazine profile also exhibited significant enrichment (both  $P$ -values  $< 0.05$ ; Supplementary Figure S9; Supplementary Table S6). The genetic interactions that link the chemogenomic profiles of synergistic compound pairs thus provide a rational basis for synergism.

To assess the predictive power of the signature deletion set derived from the membrane active compounds, we retrospectively analyzed chemical–genetic profiles for 81 psychoactive drugs known to impair yeast growth (Ericson *et al*, 2008). Of this set, 16 compounds were represented in the Prestwick library, 7 of which were predicted to synergize with fluconazole based on their effect on deletion strains in the signature set. In our primary screens against the four fungal species, four of these seven compounds were indeed hits in our screen, while the other three compounds showed weak activity (Figure 5C; Supplementary Table S1). These results demonstrate that chemical–genetic interaction profiles can predict synergistic drug combinations.

### Species-specific effects of ergosterol pathway inhibition

As the psychiatric drugs trifluoperazine and sertraline exhibited synergy with fluconazole against each fungal species, we tested whether other ergosterol biosynthesis

**Table I** Combinations of syncretic drugs exhibit species-specific synergism and higher order interactions with fluconazole

	Terbinafine Trifluoperazine		Terbinafine Sertraline		Ketoconazole Trifluoperazine		Ketoconazole Sertraline	
(A) FICI values for drug combinations in different fungal species								
<i>C. neoformans</i> (H99)	2		0.75		0.25		0.38	
<i>C. albicans</i> (Caf2-1)	2		0.5		0.38		0.16	
<i>S. cerevisiae</i> (BY4741)	0.38		0.52		0.38		0.31	
	Sert (32)	Sert (64)	Tri	Tri + FLC (4)	Tam	Tam + FLC (4)	Suloc	Suloc + FLC (4)
(B) FICI values for double and triple drug combinations in <i>S. cerevisiae</i>								
Trifluoperazine	0.38	0.50						
Tamoxifen	0.50	0.63	0.50	0.75				
Sulocidil	1.25	1.50	2.00	0.56	1.00	0.75		
L-Cycloserine	1.25	0.63	1.00	2.00	1.00	0.52	2.00	0.31

(A) FICIs from combination matrix analysis of sertraline, trifluoperazine, with the ergosterol inhibitors terbinafine and ketoconazole in different species. (B) FICIs from combination matrix analysis of syncretic drugs and higher order combinations. Trifluoperazine (Tri), tamoxifen (Tam), sulocidil (Suloc) and L-cycloserine were combined as indicated, in the presence or absence of 1/8 MIC fluconazole (4 µg/ml) and assayed for growth inhibition of a *S. cerevisiae* strain (BY4741). FICI values <0.5 indicate synergy, values between 0.5 and 1 indicate additivity and values >1 indicate no interaction. Drug concentrations are given in µg/ml.

inhibitors might exhibit synergy with these compounds. We assessed interactions with ketoconazole, an imidazole inhibitor of *ERG11*, and terbinafine, an inhibitor of the Erg1 squalene epoxidase in *Cryptococcus*, *Candida* and *Saccharomyces*. Ketoconazole was synergistic with both psychiatric drugs in all fungal species, whereas terbinafine showed synergies with sertraline in *Candida* and *Saccharomyces* but not in *Cryptococcus*, and synergized with trifluoperazine only in *Saccharomyces* (Table IA). These findings suggest that while mechanisms of synergy are conserved between different inhibitors of the same enzymes/pathways, species-specific differences readily emerge with different compounds, likely due to subtle differences in genetic network structure (Kuo *et al*, 2010).

### Higher order combinations of synergizers

Compounds that act in an identical manner are in principle expected not to exhibit synergy but instead should show only additive dosage effects. We examined pairwise combinations within four members of the membrane active group (sertraline, trifluoperazine, sulocidil and tamoxifen), as well as with the sphingolipid-selective synergizer L-cycloserine (Table IB). Despite their partially overlapping genetic profiles, synergistic interactions in *S. cerevisiae* were observed between tamoxifen and trifluoperazine (FICI=0.5), sertraline and trifluoperazine (FICI=0.4) and sertraline and tamoxifen (FICI=0.5). These synergies suggested that in addition to the core effects on membrane permeability, each compound likely elicits one or more specific effects that contribute to overall mechanism of action, and that combining these effects results in further synergism. This observation predicted that higher order combinations between synergizers might lead to even stronger growth inhibition. When compound pairs were tested in the presence of fluconazole in three-way combinations, fungal growth was often potently inhibited (Table IB). Titration of fluconazole concentrations revealed exquisite sensitivity to the sulocidil/trifluoperazine, L-cycloserine/sulocidil and L-cycloserine/tamoxifen combinations in the presence of just 1/8 MIC fluconazole (Table IB). The L-cycloserine/sulocidil pair exhibited the most potent synergy with fluconazole

with an FICI of 0.31. These results demonstrate that it is possible to incrementally build higher order synergistic combinations based on the subtly different properties of individual synergizers, even within in the same class.

### In vivo synergy in an insect model of infection

The caterpillar of the greater wax moth *Galleria mellonella* is a validated *in vivo* infection model for study of Cryptococcal virulence, host immune responses to infection and the effects of antifungal compounds (Mylonakis *et al*, 2005; Scully and Bidochka, 2006; Cowen *et al*, 2009). We assessed the effect of a synergistic drug combination on the survival rate of *G. mellonella* infected with *C. neoformans* because of the prevalence of this virulent pathogen in immune-suppressed individuals. *G. mellonella* was inoculated with *C. neoformans* H99 and subsequently treated with fluconazole and sertraline, individually and in combination. The synergistic action of fluconazole and sertraline was evident in *G. mellonella* survival rates when compared with either drug alone (Figure 6A and B). Survival increased by 40% when treated with fluconazole and sertraline in combination, with an overall 60% survival rate after seven days of infection ( $P < 0.02$  for fluconazole versus fluconazole/sertraline). These results demonstrate that potentiators of fluconazole activity identified *in vitro* exhibit comparable activity in an animal model of infection.

### Synergistic activity against fluconazole-resistant *Candida* isolates

To address whether syncretic compounds can act on clinically resistant strains, we investigated whether the combination of fluconazole and sertraline is effective against fluconazole-resistant clinical isolates of *C. albicans* (F-07-2007, F-01-2008), *C. glabrata* and a resistant control strain *C. parapsilosis* (ATCC 22019). Sertraline increased the susceptibility of resistant strains to fluconazole by up to 32-fold (Figure 6C and D; Supplementary Table S7). In the presence of sertraline, fluconazole MIC values ranged from 2 to 8 µg/ml, comparable to wild-type (Caf2-1, MIC=8 µg/ml) and drug pump-deficient

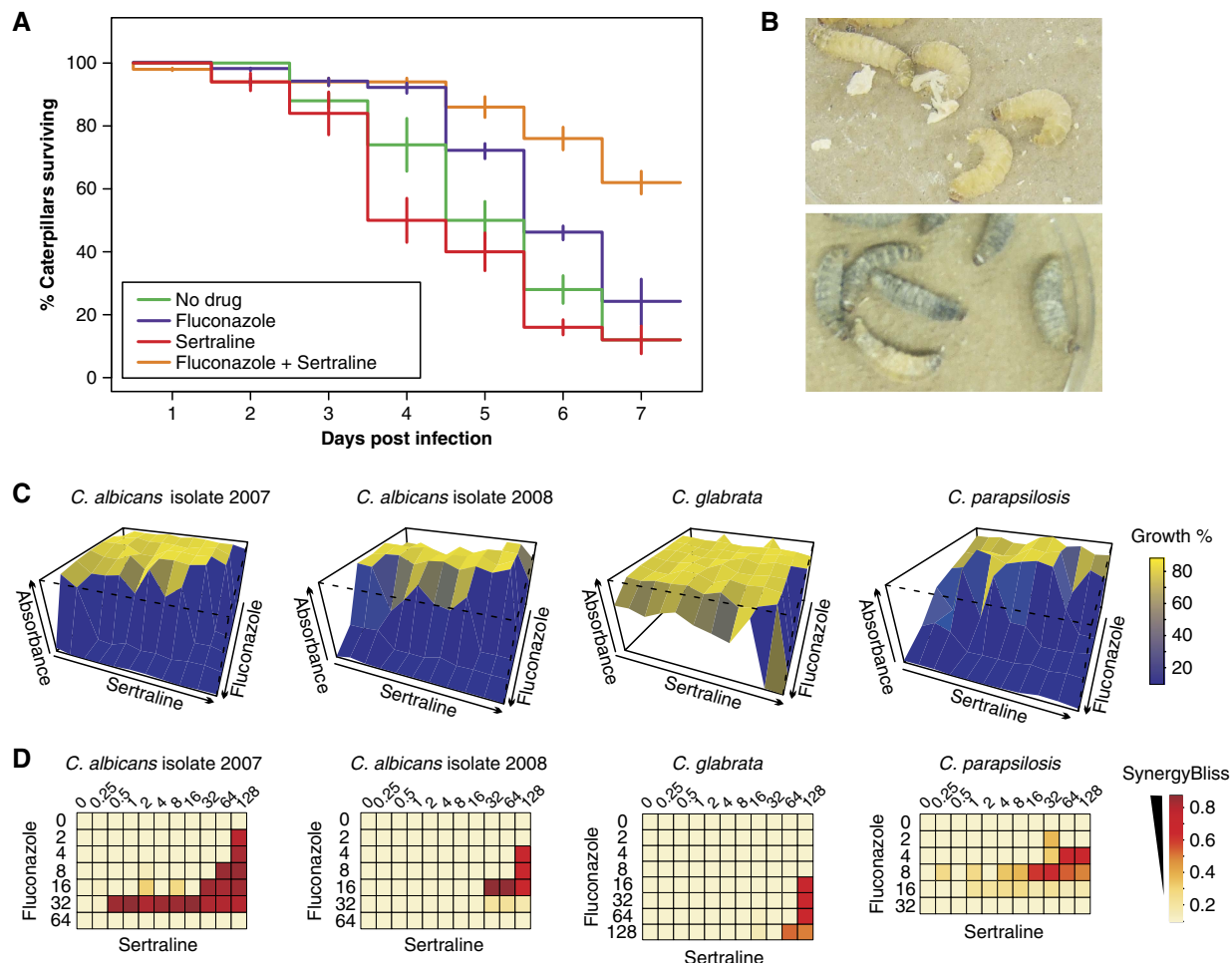


**Figure 6** Synergistic activity of sertraline and fluconazole in an *in vivo* infection model and against clinical isolates. **(A)** *G. mellonella* caterpillars were injected with  $8 \times 10^3$  cfu *C. neoformans* H99 on day 0 and drugs alone or in combination (1  $\mu$ g fluconazole; 26  $\mu$ g sertraline) on the first day and incubated for 1 week at 37 °C. Values are mean of three independent experiments; error bars indicate standard deviation of the mean. **(B)** Uninfected *G. mellonella* caterpillars (top); melanization of infected *G. mellonella* caterpillars without drug treatment (bottom). **(C)** Combination matrix assays against drug-resistant *Candida* strains. Residual growth was plotted as a function of combinations of two-fold dilutions of each drug. **(D)** Bliss synergy analysis for combination assays shown in panel **(C)**. The apparent absence of synergy at the highest fluconazole concentrations for *C. albicans* and *C. parapsilosis* is due to growth inhibition caused by fluconazole alone. Drug concentrations are in  $\mu$ g/ml. Source data is available for this figure at [www.nature.com/msb](http://www.nature.com/msb).

(MIC=2  $\mu$ g/ml) strains of *C. albicans*. The sertraline/fluconazole combination was synergistic in both *C. albicans* clinical isolates as well as the *C. parapsilosis* reference strain, but not in the *C. glabrata* strain. As noted above, this differential sensitivity may indicate strain-specific drug effects, or different mechanisms of drug resistance (Kuo *et al*, 2010). We conclude that synergistic activities in reference laboratory strains can be transposed to drug-resistant pathogens derived from clinical environments.

## Discussion

### Systematic screens for syncretic combinations reveal new antifungal chemical space

The combination of known antifungal agents is an established therapeutic tactic in infectious disease control (Johnson and Perfect, 2010). Here, we show that antifungal chemical space can be systematically expanded through the combination of

a known antifungal drug with other bioactive compounds that do not have antifungal activity *per se*, including off-patent drugs previously approved for other indications. Novel syncretic drug combinations were readily identified in systematic screens against different fungal pathogens in the presence of subtherapeutic concentrations of fluconazole. These chemically diverse drug hits derive from a broad spectrum of human therapeutic areas that otherwise would not have been explored by infectious disease clinicians. Although hits from screens for fluconazole potentiation in the *S. cerevisiae* model system can be transposed to pathogenic fungi (Borisy *et al*, 2003; Zhang *et al*, 2007; Jansen *et al*, 2009; Epp *et al*, 2010), our primary screen data reveals considerable species specificity that by definition cannot be predicted from model organism drug-gene interactions. Indeed, in our primary screen, while 58% (25/43) of hits against *S. cerevisiae* exhibited synergistic activity against one or more fungal pathogens, only 19% (25/130) of the total hits against

pathogenic species were detected in *S. cerevisiae*. This observation underscores the need to undertake primary screens in the pathogen of interest.

Many syncretic combinations exhibited fungicidal activity, a highly desirable feature for neutropenic or otherwise immune-compromised patients. The fungicidal combination of fluconazole and the antidepressant sertraline (Zoloft<sup>®</sup>) was effective against all species tested, including drug-resistant clinical isolates of *Candida*, and in an *in vivo* insect model of *C. neoformans* infection. Therapeutic intervention for fungal infections of the CNS is a particular clinical challenge because of the stringent requirement to breach the blood brain barrier. The fact that sertraline targets serotonin receptors in the CNS suggests that the sertraline-fluconazole combination may be effective in the treatment of fungal meningitis.

### Molecular mechanisms and prediction of drug synergism

Genome-wide chemical-genetic profiles of a selected set of six fungicidal synergizers revealed two different patterns of synergy. Five compounds—trifluoperazine, tamoxifen, clomiphen, sertraline and suloctidil—elicited genetic sensitivities and cell biological phenotypes associated with a loss of membrane integrity. The membrane perturbation caused by these compounds may increase susceptibility to accumulation of ergosterol pathway intermediates, impair fluconazole export by drug efflux pumps and/or impair import of exogenous ergosterol (Kuo *et al*, 2010). It is also possible that the synergizers affect active import of azoles through altered localization of drug transporters or general membrane perturbation (Mansfield *et al*, 2010). Notably, all five membrane active compounds are cationic amphiphilic drugs (CADs) that intercalate preferentially into one side of the lipid bilayer, thereby causing membrane expansion and cell wall stress (Sheetz and Singer, 1974), consistent with the observed chemical-genetic interactions with *NEO1*, *DRS2*, *SLT2* and *BCK1*. Moreover, genetic resistance to CADs is conferred by perturbation of vesicular membrane biogenesis and/or trafficking (Rainey *et al*, 2010). The synthetic lethal genetic interactions that occur between strains in the fluconazole and membrane active chemical-genetic profiles retrospectively predicted the synergistic effects of other hits in our primary screens. Moreover, when combined with another source of chemical-genetic interaction data (Ericson *et al*, 2008), the membrane active signature strain set correctly identified further synergistic hits in our primary screen data. In addition, the genetic interaction profile of L-cycloserine correctly predicted a novel synergistic interaction between the sphingolipid biosynthesis inhibitor myriocin and fluconazole. The potentiation of fluconazole activity by CADs and/or inhibition of sphingolipid biosynthesis may allow new general approaches to antifungal therapy in the clinic. As genetic and chemical-genetic space is elaborated, mechanism-based predictive approaches should become a powerful means of identifying new synergistic combinations.

### Species-specific syncretic effects

We observed many genus- and species-specific syncretic interactions, which reflects differences in the genetic networks that dictate cellular responses to each compound (Perlstein

*et al*, 2007). Since divergence from a common ancestor over 100 million years ago, different pathogenic species have adapted to particular host environments. For example, genetic plasticity of the fungal mating-type locus affects survival in mammalian hosts (Nielsen and Heitman, 2007). Developmental system drift (True and Haag, 2001) can also affect drug susceptibility, as shown by the differential effects of nikkomyacin Z on chitin synthase paralogs in *Saccharomyces* and *Candida* (Gaughran *et al*, 1994; Sudoh *et al*, 2000). Marked differences in the transcriptional response of *Saccharomyces*, *Candida* and *Kluyveromyces* to fluconazole treatment underscore the quite distinct mechanisms whereby different species can respond to the same drug (Kuo *et al*, 2010). More generally, species differences in the response to chemical perturbation may reflect the evolutionary plasticity of genetic interaction networks (Kapitzky *et al*, 2010). Species-selective antifungal combinations may afford a means to both increase efficacy and decrease host toxicity. Systematic analysis of drug–drug interactions may also provide a means to classify and predict drug mechanism of action (Yeh *et al*, 2006; Hopkins, 2008).

### Higher order drug–drug interactions

The densely connected structure of genetic networks predicts that it should be possible to devise higher order drug combinations with greater selectivity and potency (Sharom *et al*, 2004; Agoston *et al*, 2005; Lehar *et al*, 2007). That is, compounds that target multiple genetically redundant parallel pathways may exhibit *n*-way synergies. In an initial elaboration of this concept, we found that the combination of a non-synergistic pair (suloctidil and L-cycloserine, drawn from the membrane active and sphingolipid target classes, respectively) with a low dose of fluconazole resulted in a highly potent three-way synergism. Somewhat unexpectedly given their shared core genetic profiles, pairwise tests of four compounds in the membrane active class also revealed synergistic interactions in the absence of fluconazole. This type of drug–drug interaction, which has been observed previously with bacteria and yeast (Yeh *et al*, 2006; Jansen *et al*, 2009), suggests that, aside from the common core profile, each drug must have additional specific targets that contribute to overall synergism. The complex genetic profiles of each drug reflect effects on primary and secondary targets in the cell, drug metabolism and detoxification, and genetic feedback between different network elements (Sharom *et al*, 2004; Kitano, 2007; Lehar *et al*, 2008). Other documented interactions between fluconazole, reactive oxygen species, Hsp90, calcium metabolism and vesicle trafficking may contribute to these complex interactions (Cowen *et al*, 2009; Xu *et al*, 2009; Epp *et al*, 2010; Gamarra *et al*, 2010). We note that although shared drug profiles have been suggested to be predictive of synergistic interactions (Jansen *et al*, 2009), in many instances this is not the case (Yeh *et al*, 2006). Even drugs with well-documented mechanisms of action can have substantially different genetic interaction profiles compared with their presumptive targets. For example, although the genetic interaction profiles of fluconazole and its known target *ERG11* exhibit significant overlap, more than half of the interactions are not shared (Parsons *et al*, 2004). Recently, it has been shown that drug combinations can exhibit remarkably selective but unpredict-

able effects on the abundance of many different proteins (Geva-Zatorsky *et al*, 2010).

## Therapeutic implications

The benefits of combinatorial anti-infective therapies include a decrease in the rate of selection of resistant strains, a lower required dosage of individual drugs, a decrease in host toxicity and enhanced antimicrobial activity (Sharom *et al*, 2004; Hopkins, 2008; Lehar *et al*, 2008). As shown in this study and elsewhere (Zhang *et al*, 2007; Jansen *et al*, 2009; Epp *et al*, 2010), syncretic combinations of drugs with improved antifungal properties can be readily identified in both model fungal species and highly pathogenic clinical isolates. Importantly, while it is a potential concern that undesirable side effects may arise from drug combinations, as occurs for example with known contraindicated drugs, it has recently been shown that synergistic combinations usually yield enhanced selectivity without adverse side effects (Lehar *et al*, 2009). As noted above, these benefits may include improved activity in therapeutically recalcitrant tissues, such as the CNS. These combinatorial principles apply equally to viral and bacterial pathogens, cancer and other genetic diseases (Borisov *et al*, 2003; Fitzgerald *et al*, 2006; Hopkins, 2008; Lehar *et al*, 2009).

## Materials and methods

### Chemicals, high-throughput screens and MIC determination

Fluconazole was purchased from Sandoz (Quebec, Canada). All other compounds were obtained from Sigma (St Louis) or Prestwick Chemicals (Illkirch, France). The Prestwick Chemical library was screened in duplicate in the presence and absence of 1/2 MIC fluconazole at a final concentration of 30  $\mu$ M in 384-well flat bottom microtitre plates. OD<sub>600</sub> was determined after 48 h at 30 or 37°C. MIC determinations were based on Clinical and Laboratory Standards Institute (CLSI) protocols (Eliopoulos and Moellering, 1991; Odds, 2003), with the exception that yeast SC medium was used instead of mammalian cell RPMI 1640 medium. Overnight cultures in synthetic complete media (SC: 0.67% Difco™ yeast nitrogen base w/o amino acids, 0.08% amino acid add back and 2% glucose) were diluted in 0.85% NaCl to an OD<sub>530</sub> of 0.11, followed by a 1:100 dilution in 0.85% NaCl, and a final 1:20 dilution in SC media. Two-fold dilution series (0–128  $\mu$ g/ml) of fluconazole and other antifungal drugs were added to 200  $\mu$ l of diluted culture in 96-well plates and OD<sub>600</sub> determined after 48 h at 30 or 37°C. For fluconazole, MIC was set at the lowest concentration that caused 80% reduction in growth, corresponding to two on the azole MIC numerical scale. For other drugs, MIC was set as the lowest concentration that yielded no growth.

Time kill MIC assays were performed at six different concentrations of compound and fluconazole (fluconazole at MIC, fluconazole at 1/4 MIC, compound at MIC, compound at 1/4 MIC, both fluconazole and compound at MIC, and both fluconazole and compound at 1/4 MIC). At 0, 24 and 48 h dilutions from each well were spotted on an SC agar plate, incubated for 48 h and colony counts determined. A fungicidal effect was defined as > 3log<sub>10</sub> (99.9% killing) reduction in CFU/ml at synergistic concentrations after 24 h incubation.

### Synergy matrix assays

Fluconazole and syncretic compounds were two-fold serially diluted across the rows and columns of a 96-well plate (0–128  $\mu$ g/ml; for daunorubicin HCl, terbinafine, trifluoperazine dihydrochloride and ellipticine dilutions were from 0–64  $\mu$ g/ml), incubated with fungal

cultures and OD<sub>600</sub> determined after 48 h. The FIC index of each drug combination was determined by adding the individual FIC values, as calculated by standard CLSI protocols (Eliopoulos and Moellering, 1991; Odds, 2003). To probe chemical interactions between sertraline, trifluoperazine, L-cycloserine, sulcotidil and tamoxifen, checkerboard assays were carried out between these five compounds in the absence and presence of 1/2 and 1/8 MIC fluconazole (16 and 4  $\mu$ g/ml, respectively).

### Chemical–genetic profiles and secondary assays

*S. cerevisiae* deletion collections (*MATa* haploid and heterozygous essential deletion strains) were obtained from Research Genetics (Germany). Compounds were screened at a concentration that caused ~30% growth inhibition at a final DMSO concentration of 0.2% (Giaever *et al*, 1999). Deletion pools were grown for 10 generations, gDNA extracted and barcode tags amplified with fluorescently labeled UP and DN primers, followed by hybridization of PCR products to spotted barcode microarrays (Cook *et al*, 2008). Arrays were scanned on a GenePix 4200AL and analyzed with GenePix Pro 6.0 software. Data sets are available at ArrayExpress (E-MTAB-394). Chemical–genetic interactions were confirmed in quantitative growth assays at 30°C with continuous shaking at 564 r.p.m. on a Sunrise shaker/reader (Tecan); OD<sub>600</sub> readings were taken every 15 min and values at the end of logarithmic phase used to calculate the log ratio between deletion and wild-type strains. For sorbitol rescue, wild-type strains were grown in the presence of indicated compounds and 1 M sorbitol. For microscopy, cells were embedded in 1% low melt agarose and stained with Calcofluor White M2R (Sigma), Mitotracker Green FM (Molecular Probes) or FM4-64 (Molecular Probes) and imaged at  $\times$  100 on a Leica DMI 6000 B microscope with a Hamamatsu Orca ER-AG camera and Volocity 4 software. Images were deconvolved using AutoDeblur Gold CWF using 2-D blind deconvolution and 10 iterations per image.

### Computational analysis of gene–drug network interactions

The 50 most sensitive deletion strains from duplicate chemical–genetic profiles for clomiphen, L-cycloserine, sertraline, sulcotidil, tamoxifen and trifluoperazine were tested against the top 50 fluconazole-sensitive deletion strains (from replicate arrays at 8  $\mu$ M). Shared genetic interactions between the sets of deletion strains were determined based on genetic interaction data obtained from BioGRID (Breitkreutz *et al*, 2008; BIOGRID release 2.62, <http://www.thebiogrid.org>). Visualization of bipartite graphs and simulations was performed with an online tool available at [http://tyerslab.bio.ed.ac.uk/tools/genelookup\\_bipartite.php](http://tyerslab.bio.ed.ac.uk/tools/genelookup_bipartite.php). Simulations based on CGS were derived from 1143 non-essential deletion strains that respond to various drug treatments (Hillenmeyer *et al*, 2008). For each drug pair, control gene sets of the same size were picked at random and the number of genetic interactions counted to generate a background distribution of the number of interactions that would occur by chance, based on the compiled genetic interaction data. This distribution was used to calculate the *P*-value for each drug pair. For PPP, the chemical–genetic interactors of fluconazole and each of the synergistic drugs were pooled, randomly assigned to two groups and genetic interactions counted to obtain a background distribution for each drug pair. The definition of the signature deletion strain set was based on confirmatory quantitative growth curve assays (Figure 3D). For both the CGS and PPP methods, 10 000 simulations were conducted for each drug pair. To predict potential synergistic candidates based on overlap with published chemical–genetic profiles (Ericson *et al*, 2008), we used a binary data matrix based on a Z-score cutoff of  $\pm$ 3. The significance of enrichment was calculated based on the number of genes that overlapped with the signature strain set; a subset of 4 out of 11 genes was significant with a *P*-value < 0.05.

### Insect larvae assays

Ten weight matched (250–400 mg/worm) *G. mellonella* caterpillars per dish were inoculated with *C. neoformans* H99 and subsequently

injected with different combinations of compound, fluconazole and/or control solutions (Mylonakis *et al*, 2005). Over a 7-day period, caterpillars were examined visually for discoloration due to melanization and for failure to respond to touch as an inviability end point.

## Supplementary information

Supplementary information is available at the *Molecular Systems Biology* website ([www.nature.com/msb](http://www.nature.com/msb)).

## Acknowledgements

We thank J Blanchard and C Murphy for helpful discussions on small molecule screens, L Scully for advice on the *G. mellonella* infection model, JW Kronstad for the *C. neoformans* H99 and *C. gattii* R265 strains, M Whiteway for the *C. albicans* Caf-2 strain and D Yamamura for the fluconazole-resistant *C. glabrata*, *C. parapsilosis* and *C. albicans* clinical isolates. This research was supported by the Canada Research Chair program (EDB, GDW), a Royal Society Wolfson Research Merit Award (MT), a Scottish Universities Life Sciences Alliance Research Chair (MT), and by grants from the Canadian Institutes for Health Research (FRN79488 to GDW and MT) and the European Research Council (2007-223411 to MT).

*Author contributions:* EG, MS, KMB, JW, GDP, MT and GDW designed experiments; EG, KMB, LE and LR performed chemical screens; MS performed genome-wide genetic profiles and growth curves; GDP, JC and LR performed microscopy; EG, MS and JW performed data analysis; EG, MS, JW, MT and GDW wrote the manuscript.

## Conflict of interest

The authors declare that they have no conflict of interest.

## References

Agoston V, Csermely P, Pongor S (2005) Multiple weak hits confuse complex systems: a transcriptional regulatory network as an example. *Phys Rev E Stat Nonlin Soft Matter Phys* **71**: 051909

Arendrup MC, Fisher BT, Zaoutis TE (2009) Invasive fungal infections in the paediatric and neonatal population: diagnostics and management issues. *Clin Microbiol Infect* **15**: 613–624

Baddley JW, Stroud TP, Salzman D, Pappas PG (2001) Invasive mold infections in allogeneic bone marrow transplant recipients. *Clin Infect Dis* **32**: 1319–1324

Borisy AA, Elliott PJ, Hurst NW, Lee MS, Lehar J, Price ER, Serbedzija G, Zimmermann GR, Foley MA, Stockwell BR, Keith CT (2003) Systematic discovery of multicomponent therapeutics. *Proc Natl Acad Sci USA* **100**: 7977–7982

Breitkreutz BJ, Stark C, Reguly T, Boucher L, Breitkreutz A, Livstone M, Oughtred R, Lackner DH, Bahler J, Wood V, Dolinski K, Tyers M (2008) The BioGRID Interaction Database: 2008 update. *Nucleic Acids Res* **36**: D637–D640

Cannon RD, Lamping E, Holmes AR, Niimi K, Baret PV, Keniya MV, Tanabe K, Niimi M, Goffeau A, Monk BC (2009) Efflux-mediated antifungal drug resistance. *Clin Microbiol Rev* **22**: 291–321

Clark TA, Hajjeh RA (2002) Recent trends in the epidemiology of invasive mycoses. *Curr Opin Infect Dis* **15**: 569–574

Cook MA, Chan CK, Jorgensen P, Ketela T, So D, Tyers M, Ho CY (2008) Systematic validation and atomic force microscopy of non-covalent short oligonucleotide barcode microarrays. *PLoS One* **3**: e1546

Costanzo M, Baryshnikova A, Bellay J, Kim Y, Spear ED, Sevier CS, Ding H, Koh JL, Toufighi K, Mostafavi S, Prinz J, St Onge RP, VanderSluis B, Makhnevych T, Vizeacoumar FJ, Alizadeh S, Bahr S, Brost RL, Chen Y, Cokol M *et al* (2010) The genetic landscape of a cell. *Science* **327**: 425–431

Cowen LE, Singh SD, Kohler JR, Collins C, Zaas AK, Schell WA, Aziz H, Mylonakis E, Perfect JR, Whitesell L, Lindquist S (2009) Harnessing Hsp90 function as a powerful, broadly effective therapeutic strategy for fungal infectious disease. *Proc Natl Acad Sci USA* **106**: 2818–2823

Eliopoulos GM, Moellering RC (1991) *Antimicrobial Combinations*. Baltimore: Williams and Wilkins

Epp E, Vanier G, Harcus D, Lee AY, Jansen G, Hallett M, Sheppard DC, Thomas DY, Munro CA, Mullick A, Whiteway M (2010) Reverse genetics in *Candida albicans* predicts ARF cycling is essential for drug resistance and virulence. *PLoS Pathog* **6**: e1000753

Ericson E, Gebbia M, Heisler LE, Wildenhain J, Tyers M, Giaever G, Nislow C (2008) Off-target effects of psychoactive drugs revealed by genome-wide assays in yeast. *PLoS Genet* **4**: e1000151

Fitzgerald JB, Schoeberl B, Nielsen UB, Sorger PK (2006) Systems biology and combination therapy in the quest for clinical efficacy. *Nat Chem Biol* **2**: 458–466

Gamarra S, Rocha EM, Zhang YQ, Park S, Rao R, Perlin DS (2010) Mechanism of the synergistic effect of amiodarone and fluconazole in *Candida albicans*. *Antimicrob Agents Chemother* **54**: 1753–1761

Garcia O, Saveanu C, Cline M, Fromont-Racine M, Jacquier A, Schwikowski B, Aittokallio T (2007) Golorize: a Cytoscape plug-in for network visualization with Gene Ontology-based layout and coloring. *Bioinformatics* **23**: 394–396

Gaughran JP, Lai MH, Kirsch DR, Silverman SJ (1994) Nikkomycin Z is a specific inhibitor of *Saccharomyces cerevisiae* chitin synthase isozyme Chs3 *in vitro* and *in vivo*. *J Bacteriol* **176**: 5857–5860

Geva-Zatorsky N, Dekel E, Cohen AA, Danon T, Cohen L, Alon U (2010) Protein dynamics in drug combinations: a linear superposition of individual-drug responses. *Cell* **140**: 643–651

Giaever G, Shoemaker DD, Jones TW, Liang H, Winzler EA, Astromoff A, Davis RW (1999) Genomic profiling of drug sensitivities via induced haploinsufficiency. *Nat Genet* **21**: 278–283

Groll AH, De Lucca AJ, Walsh TJ (1998) Emerging targets for the development of novel antifungal therapeutics. *Trends Microbiol* **6**: 117–124

Groll AH, Shah PM, Mentzel C, Schneider M, Just-Nuebling G, Huebner K (1996) Trends in the postmortem epidemiology of invasive fungal infections at a university hospital. *J Infect* **33**: 23–32

Gullo A (2009) Invasive fungal infections: the challenge continues. *Drugs* **69**(Suppl 1): 65–73

Hillenmeyer ME, Fung E, Wildenhain J, Pierce SE, Hoon S, Lee W, Proctor M, St Onge RP, Tyers M, Koller D, Altman RB, Davis RW, Nislow C, Giaever G (2008) The chemical genomic portrait of yeast: uncovering a phenotype for all genes. *Science* **320**: 362–365

Hopkins AL (2008) Network pharmacology: the next paradigm in drug discovery. *Nat Chem Biol* **4**: 682–690

Hu G, Kronstad JW (2010) A putative P-type ATPase, Apt1, is involved in stress tolerance and virulence in *Cryptococcus neoformans*. *Eukaryot Cell* **9**: 74–83

Jansen G, Lee AY, Epp E, Fredette A, Surprenant J, Harcus D, Scott M, Tan E, Nishimura T, Whiteway M, Hallett M, Thomas DY (2009) Chemogenomic profiling predicts antifungal synergies. *Mol Syst Biol* **5**: 338

Johnson MD, Perfect JR (2010) Use of antifungal combination therapy: agents, order, and timing. *Curr Fungal Infect Rep* **4**: 87–95

Kapitzky L, Beltrao P, Berens TJ, Gassner N, Zhou C, Wuster A, Wu J, Babu MM, Elledge SJ, Toczyski D, Lokey RS, Krogan NJ (2010) Cross-species chemogenomic profiling reveals evolutionarily conserved drug mode of action. *Mol Syst Biol* **6**: 451

Keith CT, Borisy AA, Stockwell BR (2005) Multicomponent therapeutics for networked systems. *Nat Rev Drug Discov* **4**: 71–78

Kelley R, Ideker T (2005) Systematic interpretation of genetic interactions using protein networks. *Nat Biotechnol* **23**: 561–566

Kitano H (2007) A robustness-based approach to systems-oriented drug design. *Nat Rev Drug Discov* **6**: 202–210

Kuo D, Tan K, Zinman G, Ravasi T, Bar-Joseph Z, Ideker T (2010) Evolutionary divergence in the fungal response to fluconazole revealed by soft clustering. *Genome Biol* **11**: R77



- Lehar J, Krueger AS, Avery W, Heilbut AM, Johansen LM, Price ER, Rickles RJ, Short III GF, Staunton JE, Jin X, Lee MS, Zimmermann GR, Borisy AA (2009) Synergistic drug combinations tend to improve therapeutically relevant selectivity. *Nat Biotechnol* **27**: 659–666
- Lehar J, Stockwell BR, Giaever G, Nislow C (2008) Combination chemical genetics. *Nat Chem Biol* **4**: 674–681
- Lehar J, Zimmermann GR, Krueger AS, Molnar RA, Ledell JT, Heilbut AM, Short III GF, Giusti LC, Nolan GP, Magid OA, Lee MS, Borisy AA, Stockwell BR, Keith CT (2007) Chemical combination effects predict connectivity in biological systems. *Mol Syst Biol* **3**: 80
- Li H, Black PN, Chokshi A, Sandoval-Alvarez A, Vatsyayan R, Sealls W, DiRusso CC (2008) High-throughput screening for fatty acid uptake inhibitors in humanized yeast identifies atypical antipsychotic drugs that cause dyslipidemias. *J Lipid Res* **49**: 230–244
- Lum PY, Armour CD, Stepaniants SB, Cavet G, Wolf MK, Butler JS, Hinshaw JC, Garnier P, Prestwich GD, Leonardson A, Garrett-Engele P, Rush CM, Bard M, Schimmack G, Phillips JW, Roberts CJ, Shoemaker DD (2004) Discovering modes of action for therapeutic compounds using a genome-wide screen of yeast heterozygotes. *Cell* **116**: 121–137
- Mansfield BE, Oltean HN, Oliver BG, Hoot SJ, Leyde SE, Hedstrom L, White TC (2010) Azole drugs are imported by facilitated diffusion in *Candida albicans* and other pathogenic fungi. *PLoS Pathog* **6**: e1001126
- Marie C, White TC (2009) Genetic basis of antifungal drug resistance. *Curr Fungal Infect Rep* **3**: 163–169
- Miyake Y, Kozutsumi Y, Nakamura S, Fujita T, Kawasaki T (1995) Serine palmitoyltransferase is the primary target of a sphingosine-like immunosuppressant, ISP-1/myriocin. *Biochem Biophys Res Commun* **211**: 396–403
- Mylonakis E, Moreno R, El Khoury JB, Idnurm A, Heitman J, Calderwood SB, Ausubel FM, Diener A (2005) *Galleria mellonella* as a model system to study *Cryptococcus neoformans* pathogenesis. *Infect Immun* **73**: 3842–3850
- Nelander S, Wang W, Nilsson B, She QB, Pratilas C, Rosen N, Gennemark P, Sander C (2008) Models from experiments: combinatorial drug perturbations of cancer cells. *Mol Syst Biol* **4**: 216
- Nielsen K, Heitman J (2007) Sex and virulence of human pathogenic fungi. *Adv Genet* **57**: 143–173
- Odds FC (2003) Synergy, antagonism, and what the checkerboard puts between them. *J Antimicrob Chemother* **52**: 1
- Parsons AB, Brost RL, Ding H, Li Z, Zhang C, Sheikh B, Brown GW, Kane PM, Hughes TR, Boone C (2004) Integration of chemical-genetic and genetic interaction data links bioactive compounds to cellular target pathways. *Nat Biotechnol* **22**: 62–69
- Parsons AB, Lopez A, Givoni IE, Williams DE, Gray CA, Porter J, Chua G, Sopko R, Brost RL, Ho CH, Wang J, Ketela T, Brenner C, Brill JA, Fernandez GE, Lorenz TC, Payne GS, Ishihara S, Ohya Y, Andrews B *et al* (2006) Exploring the mode-of-action of bioactive compounds by chemical-genetic profiling in yeast. *Cell* **126**: 611–625
- Perlstein EO, Ruderfer DM, Roberts DC, Schreiber SL, Kruglyak L (2007) Genetic basis of individual differences in the response to small-molecule drugs in yeast. *Nat Genet* **39**: 496–502
- Pinto WJ, Wells GW, Lester RL (1992) Characterization of enzymatic synthesis of sphingolipid long-chain bases in *Saccharomyces cerevisiae*: mutant strains exhibiting long-chain-base auxotrophy are deficient in serine palmitoyltransferase activity. *J Bacteriol* **174**: 2575–2581
- Rainey MM, Korostyshevsky D, Lee S, Perlstein EO (2010) The antidepressant sertraline targets intracellular vesiculogenic membranes in yeast. *Genetics* **185**: 1221–1233
- Revankar SG, Fu J, Rinaldi MG, Kelly SL, Kelly DE, Lamb DC, Keller SM, Wickes BL (2004) Cloning and characterization of the lanosterol 14 $\alpha$ -demethylase (*ERG11*) gene in *Cryptococcus neoformans*. *Biochem Biophys Res Commun* **324**: 719–728
- Richardson M, Warnock D (2003) *Fungal Infection: Diagnosis and Management*. Oxford: Blackwell Publishing
- Scully LR, Bidochka MJ (2006) The host acts as a genetic bottleneck during serial infections: an insect-fungal model system. *Curr Genet* **50**: 335–345
- Sharom JR, Bellows DS, Tyers M (2004) From large networks to small molecules. *Curr Opin Chem Biol* **8**: 81–90
- Sheetz MP, Singer SJ (1974) Biological membranes as bilayer couples. A molecular mechanism of drug-erythrocyte interactions. *Proc Natl Acad Sci USA* **71**: 4457–4461
- Shorr AF, Tabak YP, Johannes RS, Sun X, Spalding J, Kollef MH (2009) Candidemia on presentation to the hospital: development and validation of a risk score. *Crit Care* **13**: R156
- Singh SD, Robbins N, Zaas AK, Schell WA, Perfect JR, Cowen LE (2009) Hsp90 governs echinocandin resistance in the pathogenic yeast *Candida albicans* via calcineurin. *PLoS Pathog* **5**: e1000532
- Sucher AJ, Chahine EB, Balcer HE (2009) Echinocandins: the newest class of antifungals. *Ann Pharmacother* **43**: 1647–1657
- Sudoh M, Yamazaki T, Masubuchi K, Taniguchi M, Shimma N, Arisawa M, Yamada-Okabe H (2000) Identification of a novel inhibitor specific to the fungal chitin synthase. Inhibition of chitin synthase 1 arrests the cell growth, but inhibition of chitin synthase 1 and 2 is lethal in the pathogenic fungus *Candida albicans*. *J Biol Chem* **275**: 32901–32905
- Tong AH, Evangelista M, Parsons AB, Xu H, Bader GD, Page N, Robinson M, Raghibzadeh S, Hogue CW, Bussey H, Andrews B, Tyers M, Boone C (2001) Systematic genetic analysis with ordered arrays of yeast deletion mutants. *Science* **294**: 2364–2368
- True JR, Haag ES (2001) Developmental system drift and flexibility in evolutionary trajectories. *Evol Dev* **3**: 109–119
- Winzeler EA, Shoemaker DD, Astromoff A, Liang H, Anderson K, Andre B, Bangham R, Benito R, Boeke JD, Bussey H, Chu AM, Connelly C, Davis K, Dietrich F, Dow SW, El Bakkoury M, Foury F, Friend SH, Gentalen E, Giaever G *et al* (1999) Functional characterization of the *S. cerevisiae* genome by gene deletion and parallel analysis. *Science* **285**: 901–906
- Xu Y, Wang Y, Yan L, Liang RM, Dai BD, Tang RJ, Gao PH, Jiang YY (2009) Proteomic analysis reveals a synergistic mechanism of fluconazole and berberine against fluconazole-resistant *Candida albicans*: endogenous ROS augmentation. *J Proteome Res* **8**: 5296–5304
- Yan Z, Berbenetz NM, Giaever G, Nislow C (2009) Precise gene-dose alleles for chemical genetics. *Genetics* **182**: 623–626
- Yeh P, Tschumi AI, Kishony R (2006) Functional classification of drugs by properties of their pairwise interactions. *Nat Genet* **38**: 489–494
- Zhai B, Zhou H, Yang L, Zhang J, Jung K, Giam CZ, Xiang X, Lin X (2010) Polymyxin B, in combination with fluconazole, exerts a potent fungicidal effect. *J Antimicrob Chemother* **65**: 931–938
- Zhang L, Yan K, Zhang Y, Huang R, Bian J, Zheng C, Sun H, Chen Z, Sun N, An R, Min F, Zhao W, Zhuo Y, You J, Song Y, Yu Z, Liu Z, Yang K, Gao H, Dai H *et al* (2007) High-throughput synergy screening identifies microbial metabolites as combination agents for the treatment of fungal infections. *Proc Natl Acad Sci USA* **104**: 4606–4611
- Zinner RG, Barrett BL, Popova E, Damien P, Volgin AY, Gelovani JG, Lotan R, Tran HT, Pisano C, Mills GB, Mao L, Hong WK, Lippman SM, Miller JH (2009) Algorithmic guided screening of drug combinations of arbitrary size for activity against cancer cells. *Mol Cancer Ther* **8**: 521–532



*Molecular Systems Biology* is an open-access journal published by *European Molecular Biology Organization* and *Nature Publishing Group*. This work is licensed under a Creative Commons Attribution-NonCommercial-Share Alike 3.0 Unported License.